# The (un)SAFE and RISK(y) sides of Doxorubicin-induced cardiotoxicity

Toni Leigh Goldswain

*Thesis presented in partial fulfilment of the requirements for the degree of Master of Science (Physiological Sciences) in the Faculty of Science at Stellenbosch University*

Supervisor: Dr BJN Sishi
Co-supervisor: Dr L Lacerda

December 2014

*The financial assistance of the National Research Foundation (NRF) towards this research is hereby acknowledged. Opinions expressed and conclusions arrived at, are those of the author and are not necessarily to be attributed to the NRF*

# Declaration

By submitting this thesis electronically, I declare that the entirety of the work contained therein is my own, original work, that I am the sole author thereof (save to the extent explicitly otherwise stated), that reproduction and publication thereof by Stellenbosch University will not infringe any third party rights and that I have not previously in its entirety or in part submitted it for obtaining any qualification.

December 2014

# SUMMARY


## Introduction

The discovery of Doxorubicin in the 1960s has drastically improved the survival rates of cancer patients, however, its success is limited by dose-dependent cardiotoxicity. While much of the literature has focused on acute cardiotoxicity which is minor and generally reversible, chronic cardiotoxicity poses a serious threat to cancer survivors since it can lead to dilative cardiomyopathy, congestive heart failure and even death. The mechanisms that contribute to cardiotoxicity are still a matter of controversy, however, oxidative stress-induced myocardial damage and apoptosis are thought to be the major role players. Reperfusion injury, also characterized by oxidative stress and apoptosis, occurs as a result of restoring blood flow to an ischemic heart. Fortunately, pre- and post-conditioning are techniques employed to minimize this damage and are thought to do so by activating the reperfusion injury salvage kinase (RISK) and survivor activating factor enhancement (SAFE) pathways. The RISK pathway involves the pro-survival kinases, Erk1/2 and Akt, while the SAFE pathway, triggered by TNF-α, involves Jak2 and STAT3. Since both reperfusion injury and Doxorubicin-induced cardiotoxicity share similar characteristics, this study aimed to determine whether the RISK and SAFE pathways are activated in response to long-term Doxorubicin treatment. Furthermore, this study aimed to determine whether TNF-α is produced during treatment, since its role in Doxorubicin-induced cardiotoxicity is still relatively unknown.

## Methods

H9c2 cardiomyocytes and differentiated C2C12 myotubes were treated daily with increasing concentrations of Doxorubicin for a total of 120 hours. Cell viability, apoptosis and necrosis were assessed using the MTT, Caspase-Glo® 3/7 and lactate dehydrogenase assays respectively. TNF-α production was measured using Quantikine® ELISA kits and various assays were used to assess oxidative stress, anti-oxidant capacity and anti-oxidant status. The protein expression of the RISK and SAFE pathways were analysed by western blotting using both phospho-specific and total antibodies.

## Results and Discussion

Treatment with Doxorubicin caused a time- and dose-dependent decrease in cell viability in both cell lines and this was accompanied by an increase in apoptosis. In the H9c2 cardiomyocytes, treatment with 0.2 μM Doxorubicin yielded significant levels of TNF-α after 120 hours and we can speculate that these low levels partially protected the cells from the toxic effects of Doxorubicin by activating the

SAFE pathway, since both Jak2 and STAT3 were phosphorylated at this concentration. Treatment with 1 μM Doxorubicin caused a larger and biphasic pattern of TNF-α release, which may have then contributed to the decrease in cell viability, since the SAFE pathway was not activated at this concentration. Akt was phosphorylated during the first 72 hours of treatment with the low dose of Doxorubicin, but chronic treatment prevented this phosphorylation. While Erk1/2 was not phosphorylated at all at the low dose of Doxorubicin, neither Akt nor Erk1/2 was phosphorylated at the high dose and their inhibition may contribute to the cardiotoxic effects of Doxorubicin. In the C2C12 myotubes, a significant amount of TNF-α was produced after 120 hours of treatment with the low dose of Doxorubicin. Treatment with the high dose of Doxorubicin induced significant TNF-α production at every time point. While STAT3 was phosphorylated at the serine residue after treatment with the low dose of Doxorubicin, treatment with the high dose induced phosphorylation at the tyrosine residue in a time-dependent manner. p-Jak2 expression was significantly down-regulated at both concentrations of Doxorubicin, suggesting that STAT3 proteins can by-pass activation by Jak2. The Erk1/2 leg of the RISK pathway was also not activated for the majority of the treatment period, however, p-Akt expression was increased at the low concentration of Doxorubicin relative to total Akt expression.

**Conclusion**

These observations indicate that treatment with Doxorubicin causes a severe, dose-dependent loss in viability which is likely to mediated by high concentrations of TNF-α (induced by high concentrations of Doxorubicin) and down-regulation of protective signaling pathways. TNF-α may confer partial protection at low concentrations by activating the SAFE pathway. However, activation of the SAFE pathway could not provide sufficient protection from Doxorubicin, most probably because the RISK pathway was not simultaneously activated. Our results also clearly highlight the differences between acute and chronic treatment since a single high dose of Doxorubicin produced vastly different responses to cumulative treatment with a low dose. Before one can extrapolate these results into the clinical setting, further research is required to provide a better understanding of the RISK and SAFE pathways and whether stimulation thereof will provide a protective effect. In addition, although our study has shown that TNF-α is produced in response to Doxorubicin treatment, its true role, whether beneficial or detrimental, remains to be determined.

# OPSOMMING

**Inleiding**

Die ontdekking van Doksorubisien (DOKS) in die 1960's het die oorlewingsyfer van kankerpasiënte drasties verhoog, maar DOKS-gebruik gaan egter ook gepaard met dosis-afhanklike kardiotoksisiteit. Terwyl die literatuur grootliks fokus op akute kardiotoksisiteit, wat minimaal en algemeen omkeerbaar is, hou kroniese kardiotoksisiteit 'n ernistige bedreiging vir kankeroorlewendes in, aangesien dit kan lei tot dilatiewe kardiomiopatie, kongestiewe hartversaking, en selfs dood. Die spesfikieke meganismes wat bydrae tot kardiotoksisiteit is tans steeds onbekend, maar oksidatiewe stres-geinduseerde miokardiale skade en apoptose word beskou as hoof bydraende faktore. Reperfussie skade, ook gekaraktiseer deur die teenwoordigheid van oksidatiewe stres en apoptose, kom voor as gevolg van die herstel van bloedtoevoer na 'n isgemiese hart. Om die skade te minimaliseer word voor- en na-kondisionerings tegnieke geïmplimenteer wat die RSHK (Reperfussie Skade Herwinnings Kinase) en OAFV (Oorlewerings Aktiverings Faktor Versterkings)-weë aktiveer. Die RSHK weg maak gebruik van pro-oorlewings kinases Erk1/2 en Akt, terwyl die TNF-α geaktiveerde OAFV weg Jak2 en STAT3 betrek. Aangesien beide reperfussie skade en DOKS-geinduseerde kardiotoksisiteit soortgelyke eienskappe deel, is die doel van hierdie studie om vas te stel of die RSHK en OAFV-weë geaktiveer word in langtermyn DOKS behandeling. Boonop is nog 'n doel van hierdie studie om vas te stel of TNF-α geproduseer word tydens behandeling, aangesien die rol daarvan in DOKS-geinduseerde kardiotoksisiteit steeds onbekend is.

**Metodes**

H9c2 kardiomiosiet en gedifferensieerde C2C12 miobuise was daagliks behandel met toenemende konsentrasies van Dox vir 120 ure. Die effekte van DOKS op sel lewensvatbaarheid, apoptose en nekrose is onderskeidelik ondersoek deur middel van die MTT, Caspase-Glo® 3/7 en LDH toetse. TNF-α produksie is bepaal deur van die Quantikine® toets gebruik te maak, en verskeie metodes is gebuik om die oksidatiewe stres, anti-oksidantkapasiteit en anti-oksidantstatus te bepaal. Die proteïenuitdrukking van die RSHK (Erk1/2 en Akt) en OAFV (Jak2 en STAT3) weë was ontleed deur middel van westerse afklattingstegniek deur van beide fosfospesifieke en totale teenliggaampies gebruik te maak.

**Resultate en Bespreking**

Behandeling met DOKS het ‘n tyd en dosis-afhanklike afname in sel lewensvatbaarheid in beide sellyne veroorsaak, wat gepaard gegaan het met ‘n toename in apoptose. In die H9c2 kardiomiosiete, het ‘n lae DOKS dosisbehandeling (0.2 μM) betekenisvolle vlakke van TNF-α na 120 uur opgelewer en ons kan spekuleer dat hierdie lae vlakke gedeeltelik die selle van die toksiese effekte van DOKS deur die aktivering van die OAFV weg beskerm het omrede beide Jak2 en STAT3 by hierdie konsentrasie gefosforileer is. Die hoë DOKS dosis (1 μM) het ‘n groter en bifasiese patroon van TNF-α vrystelling vertoon, wat kon bydra tot die DOKS-geinduseerde afname in sel lewensvatbaarheid. Akt is gedurende die eerste 72 uur van behandeling gefosforileer met die lae DOKS dosis, maar kroniese behandeling het hierdie fosforilering verhoed. Terwyl Erk1/2 glad nie gefosforileer is by die lae DOKS dosis nie, is nie Akt of Erk1/2 by die hoë dosis gefosforileer nie, en kan hierdie inhibering bydrae tot die kardiotoksiese effekte van DOKS. In die C2C12 miobuise, is ‘n betekenisvolle hoeveelheid TNF-α na 120 uur van behandeling geproduseer by die lae DOKS dosis. Behandeling met die hoë DOKS dosis het betekenisvolle TNF-α produksie geinduseer by elke tydspunt. Terwyl STAT3 gefosforileer is by die serienresidu na behandeling met die lae DOKS dosis, het behandeling met die hoë dosis fosforilering by die tirosienresidu op ’n tydsafhanklike wyse plaasgevind. p-Jak2 uitdrukking was betekenisvol verminder by beide DOKS konsentrasies, wat aanduidend is dat die STAT3 proteïene nie geaktiveer hoef te word deur Jak2 nie. Die Erk1/2 been van die RSHK weg is ook nie geaktiveer gedurende die oorhoofse behandelingstydperk nie, alhoewel, p-Akt wel uitgedruk is by die lae konsentrasie van DOKS relatief tot die totale Akt uitdrukking.

**Gevolgtrekkings**

Die resultate van hierdie studie toon dat DOKS-behandeling tot ‘n dosis-afhanklike verlies in sel lewensvatbaarheid lei. Hierdie effek word waarskynlik bemiddel deur die teenwoordigheid van hoë konsentrasies TNF-α, en ook die afregulering van die beskermende seinweë. TNF-α kan moontlik gedeeltelike beskerming bied by lae konsentrasies deur aktivering van die OAFV weg. Die aktivering van die OAFV weg kon egter nie voldoende beskerming teen DOKS bied nie; moontlik as gevolg van die afwesigheid van die gelyktydige RSHK weg aktivering. Ons resultate vertoon die verskille tussen die akute en kronies behandeling aangesien ‘n enkele hoë-dosis van DOKS, in vergelyking met ‘n kumulatiewe lae-dosis, grootliks verskillende resultate opgelewer het. Voordat hierdie resultate klinies verder ondersoek kan word is verdere navorsing nodig om TNF-α en die RSHK en OAFV-weë beter te verstaan, en om vas te stel of stimulering van hierdie seinoordragpaaie ‘n beskermende effek teweeg sal bring.

To those who have yet to learn…

I pray that you will be given the opportunity to be educated, for it holds a power that no one can take away and fuels a fire deep within you to always desire to know more.

"Education is the most powerful weapon which you can use to change the world"

**NELSON MANDELA**

# ACKOWLEDGEMENTS

I am sincerely grateful to the following people as I could not have completed this study without them.

**Dr Balindiwe Sishi** (my supervisor): There are actually no words that could describe how grateful I am for all that you have done over the last two years. Thank you for your unconditional willingness to teach, guide and support. You are not only a role model as a supervisor, but also as a friend. Thank you for also having fun with us when the work was over.

**Dr Lydia Lacerda** (my co-supervisor): Thank you for always offering your knowledge so freely and for being so willing to help without hesitation. Your wisdom is truly inspiring. If I can be half the scientist you are, then I will be happy. Your warm, cheerful presence in the department was felt every day.

**My parents:** Thank you for my education; not just the two years of masters but for my whole school career. I am who I am because of you. Thank you for always supporting me and for being so eager to know what I am doing in the lab every day.

**Colleagues:** Thank you for your knowledge, your skills and your expertise.

**Caleigh Opperman**: Thank you for your time, your skills, your advice and your friendship. I appreciate the time you spent helping me do monotonous experiments; you made doing Bradford's and Westerns that much more bearable. Thank you for ensuring that we laughed every day.

**Morné Mortimer:** Thank you for always answering my questions, helping me when I'm stuck and teaching me everything you know. I know that at times I was a pain because you had your own thesis to worry about, so I am really grateful that you took the time to help me. Thank you for always caring for me and for always being on my side.

**Disease Signaling Group:** Thank you for your input over the years, your suggestions, your critique and your friendship. Not a single meeting went by without hysterical laughter.

**Oxidative Stress Department at CPUT:** Thank you for being so willing to teach us new techniques even though you had your own work to do. I appreciate it so much.

**The NRF and the MRC:** Thank you for the financial support which allowed me to complete my masters. Without it I would not have had the opportunity to do this study.

# ABBREVIATIONS

| | |
|---|---|
| **·OH** | Hydroxyl |
| **AA** | Antibiotic antimycotic |
| **AAPH** | 2,2'-azobis (2-methylpropionamidine) dihydrochloride |
| **AIF** | Apoptosis inducing factor |
| **ANOVA** | Analysis of variance |
| **Apaf-1** | Apoptotic protease activating factor 1 |
| **ATP** | Adenosine triphosphate |
| **AUC** | Area under the curve |
| **BHT** | Butylated hydroxytoluene |
| **$Ca^{2+}$** | Calcium |
| **CHF** | Congestive heart failure |
| **CVD** | Cardiovascular disease |
| **Cyt c** | Cytochrome c |
| **DMEM** | Dulbecco's Modified Eagles Medium |
| **DNR** | Daunorubicin |
| **DOX** | Doxorubicin |
| **DTNB** | 5,5' dithiobis-(2-nitrobenzoic acid) |
| **DXZ** | Dexrazoxane |
| **EDTA** | Ethylenediaminetetraacetic acid |
| **EGF-3** | Epidermal growth factor-3 |
| **ELISA** | Enzyme-linked immunosorbent assay |
| **ERK** | Extracellular signal-related kinases |
| **EtOH** | Ethanol |
| **FADD** | Fas-Associated protein with Death Domain |
| **FBS** | Fetal bovine serum |
| **$Fe^{2+}$** | ferrous iron |
| **GAPDH** | Glyceraldehyde 3-phosphate dehydrogenase |
| **GIK** | Glucose insulin potassium |
| **GR** | Glutathione reductase |
| **GSH** | Glutathione (reduced) |
| **GSH-Px1** | Glutathione peroxidase 1 |
| **GSSG** | Glutathione disulphide (oxidized) |
| **$H_2O_2$** | Hydrogen peroxide |
| **HCL** | Hydrochloric acid |
| **HS** | Horse serum |
| **IAPs** | Inhibitors of apoptosis |
| **IGF-1** | Insulin-like growth factor 1 |
| **IL-6** | Interleukin 6 |
| **iNOS** | Inducible nitric oxide synthase |
| **IR** | Ischemia reperfusion |
| **JAK** | Janus kinase |
| **LDH** | Lactate dehydrogenase |
| **M2VP** | 1-methyl-2-vinyl-pyridium trifluoromethane sulfonate |
| **MAPK** | Mitogen-activated protein kinase |
| **MDA** | Malondialdehyde |
| **MI** | Myocardial infarction |
| **MnSOD** | Manganese superoxide dismutase |
| **mPTP** | Mitochondrial permeability transition pore |
| **mRNA** | Messenger ribonucleic acid |
| **MTC** | Mitochondria |

| | |
|---|---|
| **MTT** | 3-(4,5-dimethylthiazol-2-yl)-2,5-diphenyltetrazolium bromide) |
| **$Na_3PO_4$** | Trisodium phosphate |
| **NAC** | N-acetylcysteine |
| **NaCl** | Sodium chloride |
| **NaF** | Sodium fluoride |
| **NaOH** | Sodium hydroxide |
| **NFκB** | Nuclear factor kappa-light-chain-enhancer of activated B cells |
| **NO** | Nitric oxide |
| **$O_2^{\cdot-}$** | Superoxide |
| **ORAC** | Oxygen radical absorbance capacity |
| **P90RSK** | p90 ribosomal S6 kinase |
| **PBS** | Phosphate buffered saline |
| **$PGE_2$** | Prostaglandin E2 |
| **PI3-K** | Phosphoinositide 3-kinase |
| **PMSF** | Phenylmethanesulfonyl fluoride |
| **PVDF** | Polyvinylidene fluoride |
| **RIPA** | Radioimmunoprecipitation assay |
| **RISK** | Reperfusion injury salvage kinase |
| **RNA** | Ribonucleic acid |
| **ROS** | Reactive oxygen species |
| **SAFE** | Survivor activating factor enhancement |
| **SBTI** | Soybean trypsin inhibitor |
| **SDS** | Sodium dodecyl sulphate |
| **SDS-PAGE** | Sodium dodecyl sulphate polyacrylamide gel electrophoresis |
| **$Ser^{15}$** | Phosphorylation on serine 15 |
| **$Ser^{727}$** | Phosphorylation on serine 727 |
| **SH2** | Src-homology-2 |
| **SOD** | Superoxide dismutase |
| **SR** | Sarcoplasmic reticulum |
| **STAT** | Signal transducer and activator of transcription 3 |
| **TBA** | Thiobarbituric acid |
| **TBARS** | Thiobarbituric acid reactive substances |
| **t-BID** | Truncated Bid |
| **TBS-T** | Tris buffered saline with Tween |
| **TMB** | 3,3',5,5'-Tetramethylbenzidine |
| **TNFR1** | Tumor necrosis factor receptor 1 |
| **TNFR2** | Tumor necrosis factor receptor 2 |
| **TNF-α** | Tumor necrosis factor alpha |
| **TRADD** | TNFR1 associated death domain protein |
| **TRAF-2** | TNF receptor-associated factor 2 |
| **Tris-HCL** | Tris-Hydrochloric acid |
| **$Tyr^{705}$** | Phosphorylation on tyrosine 705 |

# UNITS

| | |
|---|---|
| **g** | gram |
| **mg** | milligram |
| **kg** | kilogram |
| **mM** | millimolar |
| **µM** | micromolar |
| **nM** | nanomolar |
| **M** | molar |
| **nm** | nanometer |
| **L** | litre |
| **mL** | millilitre |
| **µL** | microlitre |
| **g/mL** | gram per milliliter |
| **mg/mL** | milligram per milliliter |
| **ng/mL** | nanogram per milliliter |
| **pg/mL** | picogram per milliliter |
| **mg/m$^2$** | milligram per metre squared |
| **mg/kg** | milligram per kilogram |
| **µg/kg** | microgram per kilogram |
| **° C** | degrees Celsius |
| **%** | percentage |

# LIST OF TABLES

# LIST OF FIGURES

# TABLE OF CONTENTS

# CHAPTER 1

## 1.1 Doxorubicin and its Discovery

Cancer is a major global health concern (Siegel *et al*., 2014) with an estimated 12.7 million new cases and 7.6 million deaths worldwide in 2008 (Ferlay *et al*., 2010). Interestingly, 56% of these cancer cases and 63% of cancer deaths occurred in the less developed nations of the world (Ferlay *et al*., 2010). In South Africa, the incidence of breast cancer particularly is on par with worldwide statistics; however, because the last report by the National Cancer Registry was done in 2005, the true incidence of cancer in our country is likely to be underestimated (Vorobiof *et al*., 2001). Anthracyclines are rated amongst the best anti-cancer drugs ever developed (Barrett-Lee *et al*., 2009; Minotti *et al*., 2004a) due to their wide spectrum of activity against virtually all human cancers (Cortés-Funes and Coronado, 2007). Doxorubicin (DOX) and Daunorubicin (DNR) were the first anthracyclines to be discovered and were isolated from *Streptomyces peucetius* in the early 1960s (Minotti *et al*., 2004a). The chemical structure of DOX and DNR are almost identical (Figure 1.1), both containing aglyconic and sugar moieties (Minotti *et al*., 2004b). The aglycone, known as doxorubicinone, consists of a tetracyclic ring (A – D) containing adjacent quinone-hydroquinone moieties in rings B and C, while the sugar moiety, known as daunosamine, is attached to carbon number 7 by a glycosidic bond (Sies and Packer, 2004). The only difference between the two is that DOX terminates with a primary alcohol whereas DNR terminates with a methyl group (Minotti *et al*., 2004a). Although small, this difference plays an important role on the spectrum of action of these two drugs.

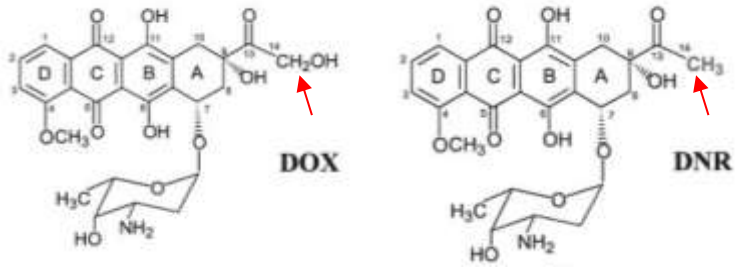


**Figure 1.1: Chemical structure of DOX (Doxorubicin) and DNR (Daunorubicin).** The chemical structures illustrated above indicate the aglyconic tetrapeptide rings (A – D) and the sugar moiety at C7 in both DOX and DNR. However, the side chains of the two molecules differ, with the side chain (indicated by an arrow) of DOX terminating in an alcohol and the side chain of DNR terminating in a methyl group. Adapted from Minotti *et al*., (2004a).

While DNR is used primarily for the treatment of myeloblastic and lymphoblastic leukemias, DOX is used to treat several human malignancies including breast cancer (Minotti *et al*., 2004a; Vander Heide and L'Ecuyer, 2007), solid tumours of the bile duct, oesophagus and liver (Di Marco *et al*., 1969; Gewirtz, 1999), soft tissue sarcomas, osteosarcomas and the more aggressive lymphomas (Gewirtz, 1999; Minotti *et al*., 2004a; Takemura and Fujiwara, 2007). The introduction of anthracyclines such as DOX to chemotherapeutic regimens has been one of the great successes of oncology. This is particularly evident in childhood cancers where the 5-year survival rate increased from approximately 30% in the 1960s to 70-80% today (Gatta *et al*., 2002; Vander Heide and L'Ecuyer, 2007). Despite being more than 50 years old, DOX remains an integral part of the chemotherapeutic regimens used today (Weiss, 1992).

Even though DOX has been used for the last five decades, the mechanisms of action against cancer cells are not yet fully understood (Eom *et al*., 2005; Gewirtz, 1999; Minotti *et al*., 2004a; Swift *et al*., 2006) Despite being a controversial subject, several mechanisms have been proposed: **i**) DNA intercalation, thereby preventing the biosynthesis of macromolecules; **ii**) DNA damage through inhibition of topoisomerase II; **iii**) DNA binding and alkylation; **iv**) interference with DNA unwinding, strand separation and helicase activity; **v**) DNA cross-linking; **vi**) direct membrane effects; **vii**) generation of free radicals leading to lipid peroxidation and **viii**) apoptosis as an end result of the above mentioned events (Gewirtz, 1999).

In order to evaluate the mechanisms by which DOX works, one must first consider the clinical concentrations of the drug that are observed in patients undergoing treatment. During a single administration of between 15 - 90 mg/m$^2$, the peak plasma concentration detected was 5 µM (Greene *et al*., 1983), while the minimum was 0.3 µM (Gewirtz, 1999). Generally, plasma concentrations lie between 1 – 2 µM but decline within an hour to a steady-state of 25 – 250 nM (Muller *et al*., 1993). However, many *in vitro* experiments that have been reported in the literature have made use of DOX concentrations that are too high compared to peak and steady-state concentrations observed in patients. It has therefore been suggested that caution must be taken when evaluating cell studies that have used concentrations of DOX greater than 1 – 2 µM (Minotti *et al*., 2004a). Bearing this in mind, it is important to realize that even though these studies may highlight the *potential* mechanisms of DOX's actions, they are unlikely to indicate the mechanisms associated with clinical concentrations of the drug (Gewirtz, 1999).

## 1.2 Proposed Mechanisms of Action

### 1.2.1 Inhibiting the Biosynthesis of Macromolecules

Some of the earliest studies on the mechanisms of DOX reported its ability to inhibit the biosynthesis of both DNA and RNA (Kim and Kim, 1972; Meriwether and Bachur, 1972), possibly by intercalating with DNA and inhibiting DNA polymerase. DOX is taken up into the nucleus very rapidly, where it binds with a high affinity to DNA through intercalation between base pairs (Cutts *et al*., 2005). Kim and Kim (1972) have shown significant inhibition of DNA synthesis in HeLa cells at concentrations as low as 0.02 mM DOX, however, several other studies have failed to detect any inhibition at the lower ranges of DOX (Gewirtz, 1999). For example, Meriwether and Bachur, (1972) reported that at least 2 µM DOX is required to inhibit DNA and RNA synthesis in a leukemic cell line.

### 1.2.2 Inhibition of Topoisomerase II

Topoisomerases are important enzymes that mediate DNA unwinding for transcription and DNA replication (Swift *et al*., 2006). They modify DNA topology without changing DNA sequence and/or structure (Minotti *et al*., 2004a). Topoisomerases cause single- or double-stranded breaks in DNA that are resealed once the conformation of the double helix has been changed (Minotti *et al*., 2004a). Shortly after the discovery of DOX, studies by Ross *et al*. (1978) reported the induction of strand breaks in both single- and double-stranded DNA which were gradually and incompletely repaired once DOX was removed from the cells. Ten years later, numerous studies identified topoisomerase II as one of the main target sites for DOX, which then became known as a "topoisomerase II poison" (Burden and Osheroff, 1998; Cutts *et al*., 2005). Unlike other enzyme-targeting drugs, DOX does not kill cancer cells by inhibiting the catalytic activity of topoisomerase. Instead, DOX stabilizes a reaction intermediate in which strands of DNA are cut and linked to the tyrosine residue of topoisomerase II, and by doing so, prevents resealing of the DNA (Chen *et al*., 2007). The subunits of the enzyme remain locked onto the 5' end of the DNA molecule after the cleavage reaction is complete (Gewirtz, 1999; Minotti *et al*., 2004a). DOX therefore 'poisons' topoisomerase by increasing the concentration of DNA cleavage complexes, resulting in double-stranded DNA breaks (Burden and Osheroff, 1998). This DNA damage results in growth arrest at the G1 and G2 phase, as well as programmed cell death (Chen *et al*.,

2007). The formation and stability of the DOX-DNA-topoisomerase complex ultimately relies on the structure of the anthracycline since the planar ring system of DOX is important for its intercalation into DNA as rings B and C overlap with adjacent base pairs, and ring D passes through the site of intercalation (Minotti *et al*., 2004a). However, the idea that topoisomerase enzymes are the primary targets during DOX-induced cytotoxicity is now being rejected, as this phenomenon is not observed at clinical concentrations of the drug. Although it is possible that inhibition of topoisomerase II does contribute to the mechanism of action of DOX, other mechanisms may play more important roles at clinically relevant concentrations (Cullinane *et al*., 2000; Cutts *et al*., 2005).

### 1.2.3 DNA Adduct Formation and DNA Cross-linking

Anthracyclines are known to form covalent bonds with DNA, however, even though there are very early studies reporting the formation of DOX-DNA adducts, it was not until 1990 that the specific adduct sites were revealed (Cutts *et al*., 2005). Two types of covalent bonding exist, namely unstable drug-DNA adducts and more stable drug-DNA cross-links (Minotti *et al*., 2004a). Studies by Phillips *et al.* (1989) have described the formation of DNA adducts in both single- and double-stranded DNA following treatment with 10 µM DOX. It was hypothesized that DOX binds to DNA via a quinone methide intermediate, formed when the semiquinone produced during redox cycling is reduced even further (Cullinane and Phillips, 1990). Cummings *et al*. (1992) also reported the chemically activated binding of DOX to DNA at concentrations of 50 µM and 1 mM. Others have explored the possibility that DOX-DNA binding may cause DNA cross links, but such studies have again been performed at elevated drug concentrations that are not achievable in patients (Cullinane and Phillips, 1990). These studies therefore provide little pathophysiological relevance.

*In vitro* studies have shown that the rate of formation of DNA adducts is the same as the rate of formation of DNA cross-links, suggesting that adduct formation and DNA cross-links are one and the same (Cullinane *et al*., 2000). It has been shown that DOX-DNA adducts are formed almost solely at guanine-cytosine-rich (GC) regions (Phillips *et al.*, 1989), an interaction that is stabilised by bonds mediated by cellular formaldehyde. Formaldehydes are produced in free radical reactions using carbon sources such as lipids (Yang *et al*., 2014). This reaction involves the formation of a covalent bond on one side of a DNA strand and a hydrogen bond on the other

side of the DNA strand (between DOX and guanine) resulting in a mono-adduct (Cullinane *et al*., 2000). This mono-adduct is then stabilized by hydrogen bonds between the intercalated DOX and the guanine on the opposite strand of DNA, producing a virtual DNA cross-link (Cullinane *et al*., 2000). The structure of the DOX-DNA adduct has now been determined using 2-dimensional nuclear magnetic resonance spectroscopy, which has confirmed that DOX intercalates alongside GC sequences (Cullinane *et al*., 2000).

### 1.2.4 Interference with Strand Separation and DNA Helicase

Studies by Gewirtz (1999) have shown that low concentrations (0.05, 0.1 and 0.5 µM) of DOX interfere with the unwinding of DNA in MCF-7 breast cancer cells. This result may possibly be related to the DNA cross-linking described previously, however, the concentration of DOX used in this study was twice as low as those found to cause DNA cross-linking. Alternatively, DOX may interfere with DNA unwinding at the level of the helicases. Since binding of DOX to GC sites increases overall DNA duplex stability, helicases are unable to separate DNA strands and hence their action is prevented (Bachur *et al*., 1993). Importantly, the concentrations of DOX required to block helicase activity fall within a clinically relevant range (0.4 µM) (Bachur *et al*., 1993).

### 1.2.5 The Free Radical Hypothesis

It is well documented that under suitable conditions, the chemical structure of DOX allows for the production of reactive oxygen species (ROS) (Singal and Iliskovic, 1998; Zhang *et al*., 2009). A one-electron reduction of the C ring of DOX results in the formation of a semiquinone free radical which, following a reaction with oxygen, produces superoxides, peroxides and hydroxyl radicals (Montaigne *et al*., 2012; Olson *et al*., 1981; Sinha, 1989). Electrons are then donated back to DOX whose structure is regenerated (Keizer *et al*., 1990). This process is known as "redox cycling" (Figure 1.2) and is particularly damaging as only a small amount of DOX is required to produce large amounts of superoxide radicals (Keizer *et al*., 1990; Montaigne *et al*., 2012). The semiquinone free radicals generated by DOX are known to cause cleavage and degradation of DNA. Due to the quinone moiety in its structure, DOX acts as an electron acceptor in a reaction facilitated by enzymes such as P450 reductase, NADH dehydrogenase and xanthine oxidase (Keizer *et al*., 1990; Sinha, 1989), suggesting that redox-cycling of DOX can

take place within the cytoplasm, mitochondria, endoplasmic reticulum (Doroshow, 1983) and nucleus *(*Bachur *et al*., 1982). Whether these free radicals are produced at clinical concentrations of DOX and at normal oxygen tension are questions that still remain unanswered (Gewirtz, 1999). When clinically relevant concentrations of DOX were used, there was a lag between administration of DOX and the detection of free radicals. This may be because free radicals are produced as a delayed response to cellular disturbances, or simply because the current methods for the detection of free radicals lack sensitivity (Minotti *et al*., 2004a).

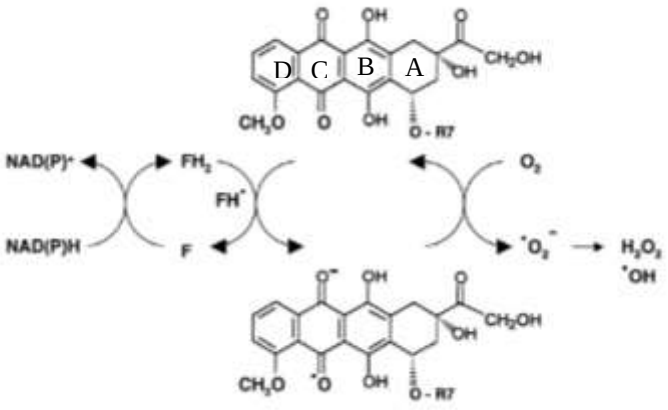


**Figure 1.2: Reactive oxygen species are generated through "redox cycling" of DOX.** A one-electron reduction of ring C produces a semiquinone free radical. Adapted from Takemura & Fujiwara (2007).

Free radicals are also generated through interactions between DOX and iron, since a one-electron reduction of DOX causes the release of iron from intracellular stores (Minotti *et al*., 2004a). Binding of DOX to the iron results in a 3: 1 drug-iron complex that converts superoxide ($O_2^{\bullet-}$) and hydrogen peroxide ($H_2O_2$) into more potent hydroxyl radicals ($^{\bullet}OH$) (Olson and Mushlin, 1990). $^{\bullet}OH$ radicals were observed to cause DNA damage in a cytochrome P450 reductase-based system following treatment with 100 µM DOX (Feinstein *et al*., 1993). Utilizing both an enzyme- and cell-free system Eliot *et al*. (1984) reported iron-mediated damage to DNA, as well as the generation of $^{\bullet}OH$ radicals, using 10 – 30 µM of DOX. Others have reported that the minimum concentration of DOX necessary for the detection of ROS after 4 hours is 4 µM, again far exceeding that which is obtained in a patient (Ubezio and Civoli, 1994). These findings emphasize the need for more sensitive methods in determining the levels of ROS at clinically relevant concentrations of DOX. However, studies have indicated that free radical release and subsequent damage to the cell may only occur at higher concentrations of DOX, while damage

caused by topoisomerase II inhibition occurs at lower concentrations of the drug (Fornari *et al*., 1994).

DOX-induced generation of free radicals is likely to lead to lipid peroxidation of the cell membrane. When free radicals are produced close to cell membranes, $^{\bullet}$OH radicals attack the fatty acids within the membrane, generating a carbon-centered free radical (Horenstein *et al*., 2000). Carbon-centered free radicals then react with oxygen to form peroxyl radicals which in turn form lipid hydroperoxides that increase membrane permeability. Lipid hydroperoxides can also form toxic byproducts such as malondialdehyde (MDA) which can damage membrane proteins and render membrane-bound enzymes inactive (Horenstein *et al*., 2000). MDA is a mutagen in human and bacterial cells and carcinogenic in rats and causes large insertions and deletions of DNA at GC-rich regions (Niedernhofer *et al*., 2003) Studies assessing lipid peroxidation have been carried out under non-physiological conditions and at elevated concentrations of DOX, conditions which alone will promote oxidative stress (Gewirtz, 1999). Although a handful of studies have used clinically relevant concentrations of DOX while assessing lipid peroxidation, the levels of lipid peroxidation did not change significantly over the concentration range, suggesting that lipid peroxidation is unlikely to play a major role in the cytotoxic action of DOX (Gewirtz, 1999).

Glutathione (GSH) reduces harmful peroxides into less harmful alcohols in the presence of glutathione peroxidase-1 (GSH-Px1) and in doing so becomes oxidized to glutathione disulphide (GSSG). GSSG is then recycled back into GSH in the presence of glutathione reductase and NADPH (Olson *et al*., 1981). GSH is abundant in the cytosol, nucleus and mitochondria, highlighting the importance of this antioxidant within a cell (Valko *et al*., 2007). GSH protects against oxidative stress by **i)** assisting detoxifying enzymes such as GSH-Px1, **ii)** participating in amino acid transport through the plasma membrane, **iii)** scavenging hydroxyl radicals and detoxifying hydrogen and lipid peroxides and **iv)** regenerating the most important antioxidants back to their active forms (Masella *et al*., 2005). Unfortunately, however, treatment with DOX can deplete endogenous GSH and inhibit GSH-Px1 (Mukherjee *et al*., 2003; Siveski-Iliskovic *et al*., 1994)

## 1.3 Doxorubicin and the Heart

The heart is a truly remarkable organ. However, unlike other cell types, cardiomyocytes are unable to undergo cellular repair (Ewer and Ewer, 2010). Nevertheless, the heart still has the capacity to increase cardiac output during exercise, survive the loss of myocytes through insults such as myocardial infarction (MI) and undergo lifetime stressors like hypertension (Ewer and Ewer, 2010). According to the latest American Heart Association statistics, approximately 83.6 million (1 in 3) adult Americans suffer from at least one type of cardiovascular disease (CVD) (Go *et al*., 2013). Of this population, 15.4 million suffer from coronary heart disease including MI, angina, heart failure and stroke (Go *et al*., 2013). Sadly, it is projected that by 2030, 40.8% of the American population will have some form of CVD (Go *et al*., 2013). Like CVD, cancer affects millions of people worldwide and its incidence increases with advancing age (Ewer and Ewer, 2010; Gustafsson and Gottlieb, 2003). Although many forms of cancer do metastasize to the heart, cancer therapies as a risk factor for aggravating underlying heart disease or initiating *de novo* heart conditions did not become a major concern until the early 1970s (Ewer and Ewer, 2010). Despite this, anthracyclines have enabled oncologists to effectively control malignancies, however, the cardiac problems associated with these drugs were not anticipated.

## 1.4 Doxorubicin-induced cardiotoxicity

Despite its widespread use and clinical efficacy, the success of DOX is limited by cardiotoxicity. One of the most well documented shortcomings of DOX is cumulative, dose-dependent, myocardial damage which can lead to dilative cardiomyopathy, congestive heart failure (CHF) (Mercuro *et al*., 2007; Swain *et al*., 2003), a reduced quality of life or even death (Mercuro *et al*., 2007). It is estimated that nearly two million Americans are at risk of developing cardiotoxicity after treatment with DOX (Gianni *et al*., 2008). Although much of the literature has focused on the resulting cardiomyopathy, this condition is one of many. The effects on vasculature can result in ischemia or changes in blood pressure and within the pericardium there may be imbalances in fluid equilibrium, pericardial swelling, as well as an increased risk of arrhythmias (Ewer and Ewer, 2010). Furthermore, all of the above mentioned conditions may be further exacerbated by the cancer itself, possibly through the inflammatory response (Ewer and Ewer, 2010).

Cardiotoxicity, defined as a broad range of adverse effects on heart function induced by therapeutic molecules (Montaigne *et al*., 2012), went undetected in the pre-clinical animal studies and was only documented during early clinical trials. In the late 1970s, clinical studies showed convincing evidence that the cardiac disturbances observed during treatment were directly related to repeated administration of DOX (Šimùnek *et al*. 2009). In a retrospective analysis, Von Hoff *et al*. (1979) identified that the total cumulative dose of DOX is a major risk factor for heart failure (Figure 1.3). In addition, it was observed that increasing age and previous or simultaneous radiation therapy (Bristow *et al*., 1978) or chemotherapy (Minow *et al*., 1977) were associated with an increased risk of DOX-induced CHF. Since DOX-induced cardiotoxicity is dose-dependent (Unverferth *et al*., 1983; Vander Heide and L'Ecuyer, 2007), the incidence of developing CHF is 3% when the cumulative dose exceeds 400 mg/m$^2$ of body surface area (Von Hoff *et al*., 1979). This incidence rises to 7% when the dose is 551 – 600 mg/m$^2$ and increases to 18% at doses exceeding 601 mg/m$^2$ (Von Hoff *et al*., 1979), however, other studies indicate that these incidences are in fact under-estimated. Swain *et al*., (2003) observed a 5% risk at a cumulative dose of 400 mg/m$^2$, 26% at 550 mg/m$^2$ and 48% at 700 mg/m$^2$. Interestingly, of 630 patients taking part in this retrospective analysis, 5.1% developed DOX-induced CHF (Swain *et al*., 2003). Patients who had shown no symptoms at the time of remission all had a significantly higher incidence of cardiovascular complications four to twenty years after the last treatment (Singal *et al*., 1997). Moreover, it has previously been estimated that the risk of death from cardiac events associated with the use of DOX was 8.2 fold higher than that of the normal population, even 25 years treatment (Lipshultz *et al*., 2004). DOX-induced cardiotoxicity carries a poor prognosis since it has proven to be lethal in 60% of patients (Von Hoff *et al*., 1979).

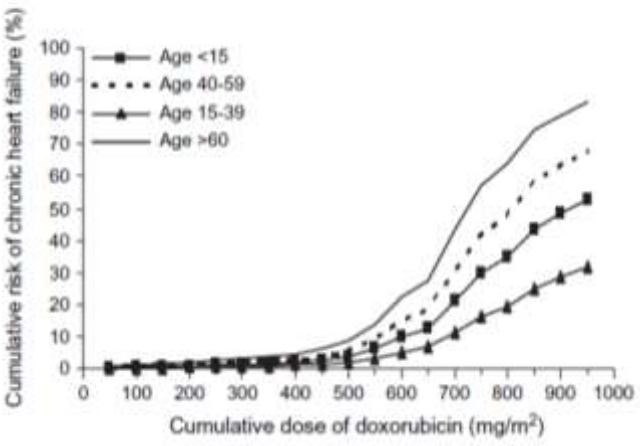


**Figure 1.3: Cumulative risk of DOX-induced heart failure.** Following exposure to cumulative doses of DOX once every 3 weeks, the risk of developing chronic heart failure increases in a proportional manner. The graph shown above further categorizes this risk according to age. Image obtained from Barrett-Lee *et al.*, (2009).

Cumulative, dose-dependent, DOX-induced cardiotoxicity implies that irreversible damage occurs to the heart with each additional administration of the drug. The second administration thus further suppresses the already damaged heart, leading to cardiomyocyte death (Barrett-Lee *et al*., 2009; Chen *et al*., 2007). Since the heart has a limited capacity for regeneration (Chen *et al*., 2007), incremental administrations of DOX compromise the heart even further until it can no longer meet the body's demands. When the heart's compensatory mechanisms become overwhelmed, heart failure develops and with any additional drug exposure, death may follow (Ewer and Ewer, 2010).

### 1.4.1 Classification of cardiotoxicity

Anthracycline-induced cardiotoxicity has been classified into 4 different types: **i)** "acute" cardiotoxicity occurs during or immediately after anthracycline administration and usually occurs when the drug is administered as a bolus or via rapid intravenous infusion (Montaigne *et al*., 2012; Šimùnek *et al*., 2009). Acute cardiotoxicity is generally minor and reversible and typically leads to vasodilatation, hypotension and disturbances in cardiac rhythm (tachycardia) (Lefrak *et al*., 1973). Acute myocardial injury can usually be detected by elevated levels of cardiac troponin I (Barrett-Lee *et al*., 2009), which also predicts the future development of left ventricular contractile dysfunction and its severity (Cardinale *et al*., 2002) **ii)** "Subchronic"

cardiotoxicity is extremely rare and presents itself as pericarditis-myocarditis syndrome within 1 – 3 days after treatment **iii)** "Early chronic" cardiotoxicity develops weeks to months after the completion of chemotherapy and is characterised by dilated cardiomyopathy, left ventricular contractile dysfunction and CHF (Šimùnek *et al*., 2009). Histopathological changes are distinctive and consist of dilation of the sarcoplasmic reticulum of myocytes, cytoplasmic vacuolization, mitochondrial swelling (Figure 1.4A) and loss of myofibres (Figure 1.4B) (Chen *et al*., 2007; Lefrak *et al*., 2006; Minotti *et al*., 2004a; Šimùnek *et al*., 2009). These morphological characteristics are also seen in experimental models using rats (Weinberg and Singal, 1987), mice (Lambertenghi-Deliliers *et al*., 1976) and rabbits (Olson *et al*., 1974), indicating that the final morphological damage is species-independent.

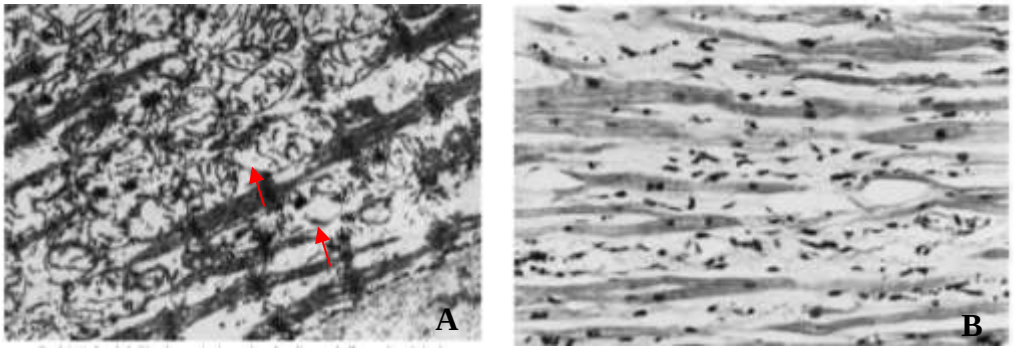


**Figure 1.4A and B: Case report of DOX-induced cardiotoxicity in 1971. (A)** The remaining myofibres exhibit widened, disrupted Z-lines which are separated by swollen mitochondria (arrows) (30 000x). **(B)** Image clearly shows considerable loss in the number of muscle fibers and an increase in the amount of interstitial tissue (300x). Image obtained from Lefrak *et al*., (2006).

Finally, **iv)** "delayed" or "late-onset chronic" cardiotoxicity was first described in the 1990s and is typically seen amongst survivors of childhood cancers, decades after the completion of treatment (Lipshultz *et al*., 1991). A study in 2006 showed that 30-year childhood cancer survivors had a 15-, 10- and 9-fold higher risk of heart failure, other CVDs and stroke, respectively (Oeffinger *et al*., 2006). The Childhood Cancer Survival Study showed that 30 years after treatment, the incidence for chronic health complications was as high as 73%, with 42% of these patients suffering from disabling, life threatening conditions (Oeffinger *et al*., 2006). Some of the characteristics associated with chronic DOX-induced cardiotoxicity include a significant drop in blood pressure, an elevated heart rate, a decrease in ejection fraction and ultimately heart

failure (Lefrak *et al*., 1973). Yi *et al*., (2006) demonstrated that seven out of nine mice died during the first six weeks after the last DOX injection, similar to what is observed in humans who succumb to heart failure months or years after the end of their chemotherapy.

Acute cardiotoxicity is not a considered a major clinical problem as it usually resolves shortly after an infusion, however, the chronic forms of cardiotoxicity are serious and drastically affect the morbidity and mortality of patients requiring long-term therapy (Šimùnek *et al*., 2009). In addition to the cumulative dose of DOX aiding in the development of cardiotoxicity, other important risk factors include age at treatment (both low and high), long-standing hypertension, pre-existing cardiac abnormalities, previous chemotherapy and a history of cardiac disease (Zuppinger *et al*., 2007). In an effort to demonstrate the dangers of DOX, Lefrak *et al*., (2006) indicated that 11 out of 399 advanced-stage cancer patients receiving DOX developed sudden onset CHF. Furthermore, these patients had no prior history of cardiac disease. Eight of these eleven patients died within three weeks of the first symptoms. What should have been a highly promising drug now adds to the already cumbersome burden of CVD and cancer.

When evaluating papers on anthracycline cardiotoxicity, it is important to take the different experimental conditions into consideration. Clearly, the best and most appropriate data would be that obtained from human patients, however, human myocardial biopsy samples are extremely difficult to obtain. In addition, patients are treated with different multidrug regimens and thus their biopsies may be very heterogeneous. It is thus necessary to make use of experimental models in order gain insight into the molecular mechanisms of anthracycline cardiotoxicity. One of the simplest models involves the cell culture of primary neonatal or adult rat cardiomyocytes. It has also become widely accepted to make use of cardiomyocyte-derived cell lines, particularly H9c2 rat embryonic cardiomyoblasts (L'Ecuyer *et al*., 2001). *Ex vivo* studies make use of isolated atria, papillary muscles or whole hearts for perfusions, whereas *in vivo* studies, commonly using mice, rats, rabbits, pigs and dogs, allow for repeated administration of anthracyclines to simulate chronic cardiotoxicity (Šimùnek *et al*., 2009).

## 1.5 Mechanisms of Doxorubicin-induced Cardiotoxicity

### 1.5.1 Doxorubicin and Free Radicals

The two main mechanisms for DOX-induced cardiotoxicity that have been proposed are: **i)** damage to membranes by DOX-generated free radicals and **ii)** DNA uncoiling due to DOX-DNA binding (Unverferth *et al*., 1983). Other mechanisms include inhibition of DNA and protein synthesis (Monti *et al*., 1995), mitochondrial abnormalities, changes in sarcolemmal calcium ($Ca^{2+}$) homeostasis (Olson *et al*., 1974; Singal and Pierce, 1986) and imbalances in myocardial electrolytes (Olson *et al*., 1974). It is well documented that DOX-induced cardiotoxicity is associated with the generation of oxygen-derived free radicals, unstable chemical species containing unpaired electrons (Olson *et al*., 1981). Supporting this theory are studies making use of free radical scavengers such as α-tocopherol, among others, which protected mice against DOX-induced cardiotoxicity while still allowing DOX to inhibit the synthesis of DNA in the tumor (Myers *et al*., 1977). Other studies have shown that transgenic mice over-expressing superoxide dismutase (SOD) in their cardiac mitochondria are protected from DOX-induced cardiotoxicity following treatment with clinically relevant doses (Yen *et al*., 1996).

The enzymatic pathway for the production of free radicals involves the mitochondria (Vander Heide and L'Ecuyer, 2007). DOX has a high affinity for cardiolipin, a phospholipid that is richly embedded in the inner mitochondrial membrane. DOX therefore targets the mitochondria where it accumulates over time (Childs *et al*., 2002). Intracellular concentrations of DOX have been reported to be 10 times that of extracellular concentrations. In other words, when plasma concentrations are between 0.5 – 1 µM, the concentration within the mitochondria is approximately 50 – 100 µM (Kalyanaraman *et al*., 2002). NADH dehydrogenase, present within the mitochondria, converts DOX into a semiquinone which, following redox cycling, produces $O_2^{\bullet-}$ and $H_2O_2$. *In vitro* studies have demonstrated that $O_2^{\bullet-}$, a product of DOX redox cycling, is small enough to enter ferritin transprotein channels and reduce the iron core of ferritin, releasing iron in the ferrous ($Fe^{2+}$) form and $H_2O_2$. $Fe^{2+}$ and $H_2O_2$ combine to generate a more potent perferryl iron or $^{\bullet}OH$ (Kalyanaraman *et al*., 2002). It is therefore suggested that $O_2^{\bullet-}$, $H_2O_2$, iron, $^{\bullet}OH$ and $Ca^{2+}$ are also responsible for the cardiotoxic effects of DOX, causing damage by inhibiting important proteins and enzymes involved in the mitochondrial respiratory chain

(Singal and Panagia, 1984). Interestingly, while semiquinones in liver microsomes prefer to react with oxygen producing relatively harmless superoxide radicals, semiquinones formed in the mitochondria of the heart preferentially react with $H_2O_2$ to produce highly reactive $^{\bullet}OH$ (Nohl and Jordan, 1983).

Following treatment with DOX, cardiomyocytes also undergo apoptosis in response to redox cycling and the formation of $O_2^{\bullet-}$ and $H_2O_2$ (Gustafsson and Gottlieb, 2003). Apoptosis however, can be attenuated when the cells are treated with cell-permeable free radical scavengers (Minotti *et al*., 2004a). Since apoptosis can be prevented by treatment with free radical scavengers and iron chelators, the apoptotic effects of $O_2^{\bullet-}$ and $H_2O_2$ are thought to be mediated by a cellular store of low molecular weight iron (Sawyer *et al*., 1999). However, one question still remains: how are pools of intracellular iron formed considering that cells have minimal free iron available for free radical reactions? One possibility is that prior to apoptosis, cardiomyocytes undergo extensive disruptions in iron homeostasis, resulting in iron release from intracellular stores (Minotti *et al*., 2004a).

### 1.5.2 Apoptosis

While the mechanisms of DOX cytotoxicity and DOX-induced cardiotoxicity may share similarities, it is important to note that the responses of different cell types, namely cardiac and cancer, to these mechanisms, are likely to be very different. Until recently, apoptosis was disregarded as a major mechanism for cardiotoxicity, but recent research has altered this picture. Apoptosis is a tightly regulated suicide program that is characterized by chromatin condensation, DNA fragmentation, membrane blebbing and cell shrinkage (Gustafsson and Gottlieb, 2003; Zhang *et al*., 2009). A handful of researchers have reported the induction of apoptosis at drug concentrations of between 0.05 and 10 µM, while others have demonstrated that the cell death observed at elevated concentrations of the drug is not due to apoptosis, but more likely due to necrosis (Chen *et al*., 2007). Necrosis, in contrast to apoptosis, is an uncontrolled, irreversible process that is characterized by cell swelling and membrane disruption (Gustafsson and Gottlieb, 2003). DOX-induced cardiotoxicity may be caused by the activation of *p*53 in response to DNA damage in the heart (Liu *et al.*, 2008). *p*53 is a tumor suppressor protein which, once activated, is phosphorylated at serine[15]. *p*53 then translocates to the nucleus where it upregulates the

expression of genes associated with cell cycle arrest, DNA repair and apoptosis. A study by Liu *et al*., (2008) showed that DOX causes a time-dependent increase in *p*53, by up to 9-fold, when compared to control cells.

Apoptosis can occur via two pathways: the intrinsic (mitochondrial) pathway and the extrinsic (death receptor) pathway (Figure 1.5) (Gustafsson and Gottlieb, 2003). In the extrinsic pathway, appropriate ligands bind to cell membrane receptors from the tumor necrosis factor (TNF) superfamily. These death receptors contain death domains that are critical for their pro-apoptotic function (Chinnaiyan *et al*., 1995). Following ligand binding, death receptors such as Fas and tumor necrosis factor receptor 1 (TNFR1) form a homotrimeric complex that recruits adaptor proteins like FADD (Fas-associated death domain) and TRADD (TNFR-associated death domain) (Tolosa *et al*., 2005). Studies of DOX-induced cardiotoxicity have reported over-expression of Fas, but it's down-regulation can reduce apoptosis in cardiomyocytes (Nakamura *et al.*, 2000). Cardiomyocytes exhibit functional TNF receptors and undergo apoptosis following treatment with relatively high concentrations of TNF-alpha (TNF-α) (Krown *et al*., 1996), however, on the other hand, studies have suggested that TNF-α may play a cardio-protective role at certain concentrations (Gustafsson and Gottlieb, 2003).

Treatment with DOX increases oxidative stress and disrupts calcium homeostasis within the cell (Zhang *et al*., 2009). ROS raises calcium levels by promoting its release from the sarcoplasmic reticulum. This in turn creates a vicious cycle where elevated $Ca^{2+}$ levels then increase ROS production through $Ca^{2+}$-sensitive ROS-producing enzymes (Zhang *et al*., 2009). Since the mitochondria are situated in close proximity to the $Ca^{2+}$-release site, they are exposed to large quantities of $Ca^{2+}$. The overwhelming levels of ROS, together with elevated levels of $Ca^{2+}$ beyond the threshold, trigger the opening of the mitochondrial permeability transition pore (mPTP). This causes a loss in mitochondrial membrane potential and ultimately the release of cytochrome c (Zhang *et al*., 2009). Cytochrome c, located in the inner mitochondrial membrane, (Chen *et al*., 2007; Childs *et al*., 2002) forms part of the intrinsic apoptotic pathway.

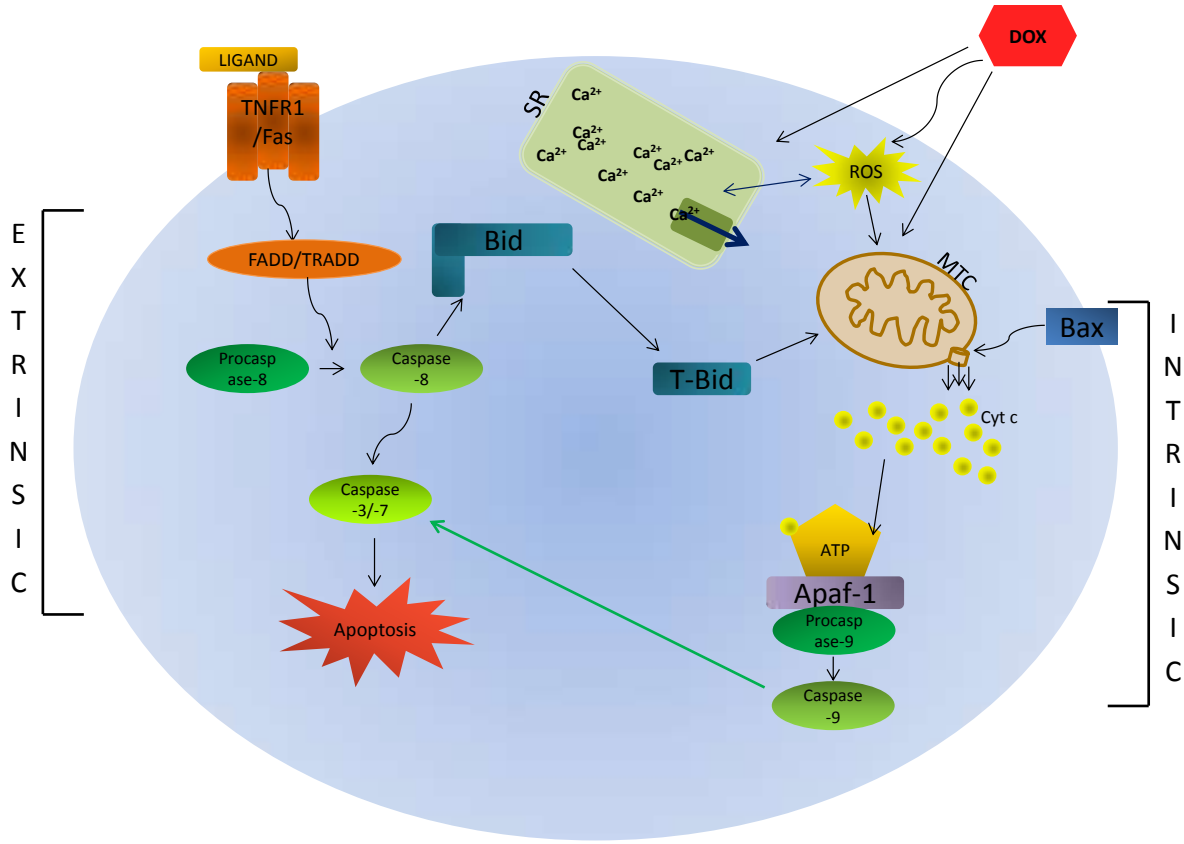


**Figure 1.5: Schematic representation of the intrinsic and extrinsic apoptotic pathways.** The extrinsic pathway involves the death receptors Fas and TNFR1. Ligand binding (such as DOX-induced TNF-α) triggers this pathway which results in the activation of caspase-8 which subsequently activates caspase-3 and -7. The intrinsic pathway is activated in response to oxidative stress. An increase in ROS releases cytochrome c from the mitochondria. An apoptosome is then formed which activates caspase-3. Both pathways result in apoptosis. Abbreviations: SR, sarcoplasmic reticulum, MTC, mitochondria, Cyt c, cytochrome c.

It is well known that mitochondria are abundant in the myocardium and are able to detect several cellular stress signals including a loss of growth factors, hypoxia, oxidative stress as well as changes in calcium homeostasis (Gustafsson and Gottlieb, 2003). In response to these signals, mitochondria then release various pro-apoptotic factors such as cytochrome c, apoptosis-inducing factor (AIF), Smac/Diablo and pro-caspases into the cytosol. Caspases are a family of proteases that cleave pro-survival molecules and structural proteins (Gustafsson and Gottlieb, 2003). They are present in a cell as inactive procaspases and are activated through cleavage at a specific site in response to apoptotic stimuli. Activation of the death receptor pathway results in activation of caspase-8 (an initiator caspase) which is able to activate downstream caspases,

thereby triggering apoptosis (Hirata *et al*., 1998). Cytochrome c forms a complex with Apaf-1, adenosine triphosphate (ATP), and pro-caspase 9 (an initiator caspase), known as an apoptosome, which activates caspase-3 or -7 (effector caspases), culminating in apoptosis (Chen *et al*., 2007).

Bax, a pro-apoptotic protein, can further aid in cytochrome c release by integrating itself into the inner mitochondrial membrane and facilitating the opening of the mPTP. Free radicals, particularly $H_2O_2$ produced during redox cycling, actively participate in the induction of cytochrome c releasing via the opening of the mPTP (Minotti *et al*., 2004a). This causes DNA fragmentation, with the end result being apoptosis (Chen *et al*., 2007). Accumulating research points to cross-talk between the extrinsic and intrinsic apoptotic pathways as evidenced by the ability of caspase-8 to cleave Bid (pro-apoptotic) to truncated Bid (t-Bid), which then translocates to the mitochondria where it stimulates the release of cytochrome c (Li *et al*., 1998). Based on the above, DOX induced apoptosis is essential for the elimination of cancerous cells, but equally important is its detrimental role during cardiotoxicity (Kalyanaraman *et al*., 2002).

The topic of DOX-induced apoptosis *in vivo* remains a controversial one, despite solid evidence of apoptosis *in vitro.* Myocardial apoptosis has previously been reported in animal studies simulating DOX-induced cardiotoxicity, however, all markers of apoptosis declined to baseline before completion of the treatment period (Arola *et al*., 2000). Other studies have observed apoptosis at 4 days post treatment, a decline between days 10 and 16 and again a peak at 21 days after the last DOX injection (Kumar *et al*., 2001). These results suggest that there may be a period of apoptotic silence while DOX-induced cardiomyopathy develops. Clinically, evidence of myocardial apoptosis has been demonstrated hours after treatment with DOX where endomyocardial biopsies indicated mitochondrial swelling and chromatin condensation, both characteristic of apoptotic cell death (Unverferth *et al*., 1983).

## 1.6 Why the heart?

One of the reasons why cardiomyocytes are more susceptible to oxidative stress-induced apoptosis than other cell types is because cardiomyocytes contain low levels of anti-oxidant defenses such as catalase and SOD (Doroshow *et al*., 1980). Since organs such as the liver and the kidney generate free radicals during every day catabolism, they have much higher levels of

GSH than organs such as the heart which produces fewer free radicals (Doroshow *et al*., 1979). Furthermore, GSH-Px1 undergoes prolonged inactivation following treatment with DOX (Doroshow *et al*., 1980). When GSH-Px1 is inactive, an important defense mechanism is eliminated and apoptosis is induced (Minotti *et al*., 2004a). Moreover, DOX also causes a reduction in the activity and protein levels of cytosolic copper-zinc SOD. This is likely to be caused by an accumulation of damage at the transcriptional and translational level (Li *et al*., 2002).

As mentioned previously, cardiac cells are incredibly rich in mitochondria which makes them even more susceptible to ROS produced by these organelles (Keizer *et al*., 1990). Furthermore, DOX is known to have a high affinity for cardiolipin, a phospholipid found in the inner mitochondrial membrane (Schlame *et al*., 2000). Because of this property, DOX is likely to concentrate within cardiomyocytes, forming practically undissociable complexes with cardiolipin. This results in the inhibition of cytochrome c oxidase within the heart and impedes the flow of electrons through the respiratory chain (Gilliam *et al*., 2013; Schlame *et al*., 2000). Excess electrons can then be accepted by oxygen resulting in the production of free radicals (Schlame *et al*., 2000; Vander Heide and L'Ecuyer, 2007). Proteomic studies support this notion as significant changes to the subunits of complex one of the electron transport chain results in insufficient enzyme function of this complex (Štěrba *et al*., 2011).

## 1.7 Potential treatments

More than 500 anthracyclines have been synthesized in an attempt to improve cytotoxic action while simultaneously decrease the cardiotoxic side effects (Sinha, 1989). The results of such research have been disappointing and thus DOX remains the most widely used anthracycline today. Although there is currently no treatment for DOX-induced cardiotoxicity, clinicians instead aim to prevent existing cardiomyopathies from worsening. However, for patients who already exhibit end-stage heart failure, transplants remain their only option (Thomas *et al*., 2002). One of the approaches used to minimize DOX-induced cardiotoxicity is to decrease the peak concentration of DOX in the plasma (Singal *et al*., 1997) and limit the cumulative dose of DOX. This can be achieved by administering DOX concomitantly with other drugs such as Vincristine and Cisplatin in a drug "cocktail" in order to limit the total amount of DOX used

(Singal and Iliskovic, 1998). A recommended, cumulative dose of 500 mg/m$^2$ in a lifetime has also been established. This dose should only be exceeded under intensive cardiac monitoring and pharmacological cardioprotection (Šimùnek *et al*., 2009). A significant decrease in the incidence of cardiotoxicity has been observed when the drug is administered slowly over 6 – 96 hours, compared to a rapid infusion over 15 minutes (Legha *et al*., 1982; Torti *et al*., 1983). This method limits the peak levels of DOX and is associated with a lower risk of cardiotoxicity. However, slow infusions will increase hospital stays and add to the already high costs of chemotherapy.

Adult cardiomyocytes have a highly oxidative metabolism with limited oxidative defenses, therefore anthracycline-induced injury could be reduced by increasing these defenses. Unfortunately, the promising results observed in animal models following treatment with various anti-oxidants were not observed in the human patients suffering from DOX-induced cardiotoxicity in clinical trials. This may suggest that the experimental models and the type of anti-oxidants used may play a role in the effectiveness of the anti-oxidant at providing protection. It is also crucial to carefully optimize the dose of the anti-oxidants used in each model (Singal *et al*., 1997).

Unlike other antioxidants, melatonin is distributed in all subcellular compartments due to its solubility in both lipids and water, and can therefore enter cardiac cells to scavenge free radicals (Liu *et al*., 2002). It has been reported by Zhang *et al*., (2013) that melatonin treatment substantially reduced DOX-induced myocardial injury in rats and protected against lipid peroxidation in this model. Believed to be one of the most potent anti-oxidants, melatonin has been shown to inhibit necrosis and apoptosis during DOX-induced cardiotoxicity (Liu *et al*., 2002). One of the earliest anti-oxidants used to reduce cardiotoxicity was vitamin E, which was administered as an injection 24 hours prior to treatment with DOX. Vitamin E provided cardioprotection against DOX-induced cardiomyopathy and enhanced the antioxidant activity of the rat myocardium by increasing the activity of GSH-Px1 (Siveski-Iliskovic *et al*., 1994). However, subsequent research has shown that vitamin E only provides protection in acute models of cardiotoxicity and fails to offer protection during chronic cardiotoxicity (Mimnaugh *et al*., 1979). Similarly, in 1983, N-acetylcysteine (NAC) was highly effective in acute preclinical trials, but failed to show protection against chronic DOX-induced cardiotoxicity (Myers *et al*.,

1983). The poor results obtained whilst using antioxidants in human studies also suggests that cardiotoxicity is caused by more than just the generation of ROS (Takemura and Fujiwara, 2007).

Despite several decades of intense research, only one drug has been approved for use in the clinical setting as a pharmacological cardioprotective agent. Dexrazoxane (DXZ/ICRF-187) was discovered accidently during its pre-clinical testing as an anti-cancer agent (Herman *et al*., 1979). DXZ was repeatedly identified to protect the myocardium from all forms of anthracyclines in both animal and human models (Šimùnek *et al*., 2009). DXZ is an iron-chelating agent that also abolishes the DNA and mitochondrial damage induced by DOX (Xiang *et al*., 2009), without compromising the ability of anthracyclines to inhibit the growth of tumours (van Dalen *et al*., 2011). DXZ permeates the cell membrane, where it rapidly undergoes hydrolysis to its metal ion-binding form, ADR-925 (Xiang *et al*., 2009). In this manner, DXZ provides protection from anthracyclines by chelating free iron and iron bound in DOX-iron complexes, thus preventing the formation of DOX-induced ROS and damage to mitochondria (Hasinoff *et al*., 2003). Consequently, pools of free iron are reduced and iron bound to DOX is displaced from the complex. In animal models, treatment with DXZ significantly reduced the occurrence of cardiac lesions associated with cardiotoxic doses of DOX and resulted in a significant increase in the survival rate (Cvetković and Scott, 2005). Others have shown that DXZ is more effective when administered prior to, or simultaneously with DOX treatment, rather than after DOX treatment (Hasinoff *et al*., 2003). In human studies, DXZ has also provided significant cardioprotection during DOX treatment. In phase III trials, the incidence of DOX-induced cardiac events was only 0 – 15% in women with advanced breast cancer receiving DXZ, compared to 16 – 50% not receiving it (Swain *et al*., 1997). More specifically, DXZ significantly reduced the incidence of CHF from 8 – 27% in women not receiving DXZ, to 0 – 3% in women who were (Swain *et al*., 1997). Unfortunately, the success of DXZ is limited by severe myelosuppression (Curran *et al*., 1991).

## 1.8 Salvaging the heart from cardiotoxicity: what role does the RISK pathway play?

The deleterious effects of DOX-induced cardiotoxicity share many characteristics with ischemia-reperfusion injury, including the generation of ROS and apoptotic cell death (Frias *et al*., 2008). Following an acute coronary blockage with the risk of MI, cardiologists make use of reperfusion, a technique that is required to save the ischemic heart cells from dying. Although this procedure is beneficial, restoration of blood flow results in myocardial reperfusion injury, reducing the potential benefits of myocardial reperfusion (Yellon and Hausenloy, 2007). Within the first few minutes of restoring blood flow to the ischemic myocardium, a condition of oxidative stress arises (Zweier, 1988) as a result of elevated ROS production (Zhao, 2004). This burst of ROS causes myocardial injury and cardiomyocyte death. This phenomenon is known as the "oxygen paradox" since the reoxygenation of the ischemic myocardium is thought to generate a greater degree of damage than the ischemia itself (Hearse *et al*., 1973).

Due to the paradoxical nature of ischemia reperfusion, novel strategies to protect the heart from reperfusion injury have been developed; namely pre- and post-conditioning. Protection is achieved by repeatedly, but briefly, exposing the heart to conditions of ischemia, before or after the potentially lethal ischemic insult (Lecour, 2009a). This reduces oxidative stress, $Ca^{2+}$ overload and inflammation (Hausenloy, 2009). Both pre- and post-conditioning are believed to protect from reperfusion injury via the activation of the RISK pathway (Figure 1.6, chapter 1.9) (Hausenloy and Yellon, 2004). This pathway involves the activation of the pro-survival kinases Akt/PKB and Erk1/2 (extracellular signal-related kinase). Studies have demonstrated that the activation of these kinases by pre- and post-conditioning, whether mechanically or pharmacologically, at the onset of reperfusion, reduces infarct size by 40 – 50% (Hausenloy, 2009). Activation of the RISK pathway causes down-regulation of pro-apoptotic proteins and maintains the integrity of the mitochondria (Xiang *et al*., 2009). In the context of DOX-induced cardiotoxicity, damage to cardiomyocytes and cell death due to apoptosis are strongly believed to occur as a result of down-regulation of Akt and Erk1/2 both *in vitro* and *in vivo* (Lou *et al*., 2005).

### 1.8.1 Erk1/2

The mitogen-activated protein kinase (MAPK) pathway is initiated by G-protein coupled receptors, receptor tyrosine kinases and by stress stimuli (Sugden and Clerk, 1998). The two most well studied kinases involved in the MAPK cascade are Erk1 and Erk2 who are directly controlled by MEK1 and MEK2 of the MAPK family. All three members of the MAPK family are found to be activated during ischemia-reperfusion injury, as well as in samples obtained from humans with heart failure (Bueno and Molkentin, 2002). The activation of these MAPKs is thought to be mediated by an increase in oxidative stress (Lou *et al*., 2005).

Within the heart, Erk1/2 are potently and quickly activated by growth factors and are involved in cell survival, differentiation, proliferation and apoptosis following ischemia-reperfusion injury, oxidative stress and exposure to anthracyclines such as DOX (Bueno and Molkentin, 2002; Lips *et al*., 2004; Lou *et al*., 2005). Although the mechanism by which this occurs is not certain, it is believed to involve the inactivation of pro-apoptotic proteins (Hausenloy and Yellon, 2004) and antagonization of apoptosis (Lips *et al*., 2004). Activation of Erk1/2 may possibly activate the p90 ribosomal S6 kinase (p90RSK), which then phosphorylates Bad and promotes cell survival (Xiang *et al*., 2009). Additionally, Erk1/2 inhibits cytochrome c-induced activation of caspases (Hausenloy and Yellon, 2004).

Immunohistochemical analysis indicates that phospho-Erk1/2 (p-Erk1/2) translocates to the nucleus following activation by 1 µM DOX for up to 48 hours and this finding was confirmed by western blotting of nuclear fractions (Liu *et al*., 2008). However, it has been previously shown that phosphorylation of Erk1/2 was significantly decreased in a rat model of DOX-induced heart failure (Lou *et al*., 2005; Xiang *et al*., 2009), where the cumulative dose of DOX was 15 mg/kg, which may explain the increase in cell death following DOX treatment. In contrast, other studies have reported an increase in the level of p-Erk1/2 following acute treatment with DOX (Gharanei *et al*., 2013; Tang *et al.*, 2002) and thus highlights its role as a cell survival protein. Supporting evidence can be found with the inhibition of Erk1/2 which leads to exacerbated DOX-induced apoptosis and cytotoxicity after treatment with 20 nM DOX for 48 hours (Brantley-Finley *et al*., 2003).

These contradictory findings may suggest that the role played by these MAPKs is influenced by the cell-type, drug concentration, duration of exposure and the model of cardiotoxicity assessed (Fan and Chambers, 2001). Since p-Erk1/2 has been shown to play pro-apoptotic, anti-apoptotic and neutral roles, its function is clearly dependent on the context. Examples of this are summarized in table 1. Important comparisons can be made with regards to acute (Ichihara *et al*., 2007; Li *et al*., 2006) versus chronic (Lou *et al*., 2005; Xiang *et al*., 2009) models and to studies that made use of clinically relevant (Liu *et al*., 2008) versus clinically unattainable (Das *et al*., 2011) concentrations of DOX. In addition, Erk1/2 responses after treatment with DOX appears to be regulated differently depending on whether DOX is administered *in vivo* or *in vitro*, emphasizing the importance of the model being studied. Erk1/2 activation during ischemia reperfusion reduces the amount of reperfusion-injury-related apoptosis (Bueno and Molkentin, 2002), therefore, in a similar manner that activation of Erk1/2 during IR reduces reperfusion-injury-related apoptosis, it is highly plausible that activation of Erk1/2 during DOX treatment may protect the myocardium in our model of chronic DOX-induced cardiotoxicity

### 1.8.2 Akt

Akt is a serine/threonine kinase that promotes cell survival by modulating the pro-apoptotic function of anthracyclines (Chen *et al*., 2007). DOX-induced apoptosis of cardiomyocytes can be prevented through PI3-K/Akt signaling (Fukazawa *et al*., 2003). Akt is located in the cytosol in an inactive state and is activated in response to various growth factors, including insulin-like growth factor-1 (IGF-1), epidermal growth factor-3 (EGF-3) and interleukin-6 (IL-6) (Fukazawa *et al*., 2003) where it regulates cell survival, replication and apoptosis (Kim *et al*., 2008). IGF-1 attenuates apoptosis by activating PI3K/Akt signaling, which subsequently inhibits caspase-9 (Wu *et al*., 2000) as well as the pro-apoptotic protein Bad (Negoro *et al*., 2001). Evidence supporting the pro-survival properties of Akt has been demonstrated in patients receiving a GIK (glucose, insulin, potassium) cocktail during reperfusion. The presence of insulin in this cocktail stimulates Akt activation which is otherwise down-regulated during an ischemic insult. Activation of Akt subsequently reduces infarct size, preserves heart function, enhances contractility and increases glucose uptake during hypoxic conditions (Jonassen *et al*., 2001).

As with Erk1/2, Akt also inhibits cytochrome c-induced apoptosis through the suppression of the opening of the mPTP (Hausenloy and Yellon, 2004). It has recently been postulated that a

cumulative dose of 20 mg/kg DOX down-regulates Akt signaling *in vivo* (Fan *et al.*, 2008) and therefore interferes with the protective role that Akt may play in this context. This has been proven in studies making use of adenovirus-mediated delivery of a constitutively active Akt gene which protected the heart against DOX-induced cardiomyopathy (Taniyama and Walsh, 2002). Furthermore, inhibition of Akt results in increased apoptosis during DOX-induced cardiotoxicity, supporting the protective role that Akt plays (Zhao *et al*., 2004). Ichihara *et al*., (2007) observed that the levels of Akt are in fact elevated in mice following a single treatment with 15 mg/kg DOX (Ichihara *et al*., 2007) and it is believed to act as an endogenous, protective mechanism of the heart to defend against the toxic effects of this anthracycline (Gharanei *et al*., 2013; Ichihara *et al*., 2007). However, Gabrielson *et al*., (2007) observed that DOX-induced injury beyond an undefined threshold cannot be rescued by Akt. In fact, little is known about the effects of chronic Akt activation. Samples obtained from human patients with advanced heart failure displayed heightened Akt phosphorylation (Haq *et al*., 2001) which may suggest that prolonged Akt activation is not sufficient for long-term cardioprotection or that Akt may actually exert adverse effects after chronic stimulation (Nagoshi *et al*., 2005). Nevertheless, Akt is largely regarded as a pro-survival kinase and its effects during cardiotoxicity are likely to be beneficial. Table 1 summarizes some of the mixed findings regarding Akt signaling in DOX-induced cardiotoxicity, indicating the concentration and duration of DOX exposure. Within the context of DOX-induced cardiotoxicity, it is thus speculated that Akt is up-regulated in a time- and dose-dependent manner, to provide protection from the cardiotoxic side effects of DOX.

**Table 1:** Comparison of Erk1/2 and Akt responses following treatment with DOX in different models of cardiotoxicity

| Author | Model | [DOX] | Duration of treatment | Erk1/2 response | Akt response |
|---|---|---|---|---|---|
| Xiang *et al*., (2009) | Male Sprague-Dawley heart tissue | 2.5 mg/kg | Weekly for 6 weeks | ↓ | ↓ |
| Lou *et al*., (2005) | Male Sprague-Dawley heart tissue | 2.5 mg/kg | 6 doses over 2 weeks | ↓[1] | |
| Li *et al*., (2006) | C57BL/6J mice | 15 mg/kg | Single injection | ↓ | Unchanged |
| Gabrielson *et al*., (2007) | Female Sprague-Dawley heart tissue | 2.5 mg/kg | Weekly for 6 weeks | | ↑[2] |
| Gharanei *et al*., (2013) | Male Sprague-Dawley heart tissue following DOX perfusion | 1 µM | 120 minutes | ↑ | ↑ |
| Liu *et al*., (2008) | H9c2 rat embryonic cells | 1 µM | 1, 3, 6, 12, 24 and 48 hours | ↑ | |
| Ichihara *et al*., (2007) | C57BL/6J mice left ventricle | 15 mg/kg | Single injection | | ↑ |
| Das *et al*., (2011) | Male Swiss albino rats | 3 mg/kg | 3 doses over 4 days[3] | ↓ | ↓ |

[1] P-Erk1/2 increased initially to a maximum after 4 hours, but declined significantly at the heart failure stage
[2] Western blot analysis of p-Akt was performed 4 weeks after the last DOX injection
[3] The cumulative dose of 9 mg/kg is equivalent to 630 mg per 70 kg man which is above the clinical threshold. Analysis was performed on day 28.

## 1.9 The SAFE pathway

For more than 2500 years, physicians have observed similar characteristics in patients with CHF and in those with chronic inflammatory disorders (Ferrari, 1999) and in more recent research it has become evident that the progression of heart failure may be influenced by the expression of various cytokines (Seta *et al*., 1996). According to the "cytokine hypothesis", first proposed in the 1990s, the progression of heart failure is mediated by the cytokine cascade, which, following injury to the myocardium, exerts deleterious effects (Seta *et al*., 1996) in a state of chronic inflammation. Cytokines are a group of proteins with small molecular weights, secreted by cells in response to stimuli such as stress. Cytokines differ from hormones in that they are produced by several cell types and act over short distances, as opposed to hormones which are produced by specific cell types and act over longer distances (Seta *et al*., 1996) To date, two classes of cytokines have been identified: vasoconstrictor/anti-inflammatory cytokines (endothelin) and vasodepressor/pro-inflammatory cytokines such as IL-6 and TNF-α.

TNF-α is a pleiotropic, pro-inflammatory cytokine that signals through two receptors, TNFR1 (p55) and TNFR2 (p75) (Pfeffer, 2003). While the death domain of TNFR1 has been shown to be essential for apoptosis (Krown *et al.*, 1996), the function of TNFR2 is not well understood (Monden *et al*., 2007). Even though TNF-α's affinity for TNFR2 is five times higher than that of TNFR1, it is TNFR1 that is most active within the cell (Tartaglia and Goeddel, 1992). A TNF-α binding protein has also been identified in the mitochondria, suggesting the existence of a pathway that is able to deliver TNF-α directly to the mitochondria, by-passing the activation of the receptors (Ledgerwood *et al*., 1998). TNF-α is expressed as a 26 kDa transmembrane protein, from which a 17 kDa soluble subunit is cleaved (Bradley, 2008). Both the membrane-associated and soluble forms are active as homotrimers, although each may have distinct biological activities (Bradley, 2008). TNF-α was originally documented to induce apoptosis in tumor cells but it is now implicated in several cellular responses including inflammation, cell proliferation, survival, differentiation and cachexia (Ware, 2003).

Studies have shown that ventricular dysfunction and dilated cardiomyopathy are associated with elevated circulating TNF-α levels (Hegewisch *et al*., 1988), which may also extend to DOX-induced cardiotoxicity and how this drug causes injury to the heart. It is possible that TNF-α

contributes to DOX-induced cardiac injury through a local inflammatory response and cardiomyocyte apoptosis as it does after MI (Bryant *et al*., 1998; Krown *et al*., 1996; Schulz and Heusch, 2009). The mechanism of cytotoxicity is thought to be associated with the production of ROS (Busquets *et al*., 2003) since TNF-α can cause oxidative stress by increasing the activity of inducible nitric oxide synthase (iNOS) and the production of nitric oxide (NO) (Ferrari, 1999; Sugamori *et al*., 2002). Interestingly, neither TNF-α mRNA or protein is expressed in the heart under normal conditions, however, during times of stress, the heart is able to synthesize TNF-α mRNA and protein *de novo* (Bryant *et al*., 1998; Ferrari, 1999; Torre-Amione *et al*., 1996). DOX promotes the release of TNF-α from macrophages, and tumors themselves cause a further increase in TNF-α levels during DOX treatment (Shan *et al*., 1996). Since cardiac cells also have the ability to produce TNF-α, it is likely that TNF-α levels within the heart are much higher than in the surrounding tissue (Krown *et al*., 1996).

### 1.9.1 The dual roles of TNF-alpha

Several bodies of evidence demonstrate that the role TNF-α plays within the heart is a complicated one, since TNF-α can exert both beneficial and detrimental effects (Ferrari, 1999). A summary of these contrasting effects can be found in table 2. Several factors need to be considered when evaluating the role that TNF-α may play. Since TNF-α exerts such pleiotropic effects, its role is clearly dependent on the context and influenced by the duration and concentration of exposure.

Several studies have provided evidence to suggest that TNF-α plays a detrimental role. Long exposure to high levels of TNF-α can exert anti-angiogenic effects (Heba *et al*., 2001) and induce apoptosis and inflammation (Chiosi *et al*., 2007). Research by Krown *et al*., (1996) indicated that treatment with TNF-α for 18 hours caused significant apoptosis in rat cardiomyocytes. They reported a maximum apoptotic effect at 0.4 nM (68 pg/mL) TNF-α, where after apoptosis declined even though additional TNF-α was administered. This may be due to down-regulation of the TNF-α receptors by receptor-mediated endocytosis, reducing TNF-α responsiveness. This study further reported that the extent of TNF-α induced apoptosis is directly proportional to the concentration of the cytokine. Of more relevance is the fact that the concentrations of TNF-α used in this study are within the range found in the serum of patients suffering MI. Mohamed *et al*., (2004) reported that DOX causes an increase in serum TNF-α in rats and it has been

suggested that it is DOX-induced oxidative stress that causes this increase, since treatment with garlic, known for its antioxidant properties, reduced the expression of myocardial TNF-α (Mukherjee *et al*., 2003). Chiosi *et al*., (2007) exposed H9c2 cells to 1 µM DOX for 24 and 48 hours and observed a potent increase in apoptosis. Furthermore, co-treatment with 10 ng/mL TNF-α potentiated the DOX-induced apoptosis. Interestingly, TNF-α alone did not cause considerable apoptosis in their model, compared to control samples, suggesting a more beneficial role for TNF-α.

Low levels and short exposure to TNF-α may aid in an adaptive response to stress (Chiosi *et al*., 2007), promote angiogenesis (Heba *et al*., 2001) and reduce areas of infarction (Deuchar *et al*., 2007). Lecour *et al*., (2002) have further indicated a beneficial role of TNF-α in the context of ischemic pre-conditioning, where they reported that exogenous TNF-α can mimic pre-conditioning at doses of 0.5 ng/mL and 0.1 µg/kg in a cell culture and animal model respectively. Many attempts have been made to try to "neutralize" TNF-α using anti-TNF therapy in patients with heart failure, however, results of such trials actually showed that heart failure worsened and caused a time-and dose-dependent increase in hospitalization and death (Mann, 2002).

Findings by Lou *et al*., (2004) showed that TNF-α mRNA and protein were not up-regulated in a rat model of sub-chronic DOX-induced heart failure and this is consistent with studies who have reported a time- and dose-dependent decrease in TNF-α expression after exposure to DOX (Safrit and Bonavida, 1992; Xu *et al*., 2008). During DOX treatment, cell death is observed earlier than the development of heart failure. Likewise, TNF-α is not detected in the early time points and it is only during the late stage that TNF-α declines below control samples. This suggests that TNF-α is not involved in DOX-induced heart failure and that other causative factors are at play (Lou *et al*., 2004).

Although many studies have identified TNF-α as a harmful cytokine, many have reported improved left ventricular performance (Murray and Freeman, 1996), hypertrophy (Dibbs *et al*., 2003) and adaptation to stress (Haudek *et al*., 2001) following TNF-α administration. It has also been reported that endogenous TNF-α may exert a protective effect during DOX-induced cardiotoxicity by up-regulating mitochondrial SOD (MnSOD) (Watanabe *et al*., 1996) and the anti-apoptotic members of the Bcl-2 family (Xu *et al*., 2008). TNF-α exerts its anti-apoptotic effects through NF-κB signaling, which may explain how TNF-α can play a protective role

during DOX-induced cardiotoxicity and heart failure (Xu *et al*., 2008). NF-κB is a transcription regulator that is localized in the cytoplasm and under the inhibitory control of IκB (Ozes *et al*., 1999). However, TNF-α induces the formation of a signaling complex containing TNF-receptor associated factor 2 (TRAF-2), resulting in IκB phosphorylation and degradation by the ubiquitin/proteasome system (Ozes *et al*., 1999). This allows NF-κB to translocate to the nucleus where it activates the transcription of several target genes (Chiosi *et al*., 2007). Since TNF-α has been reported to induce anti-apoptotic effects through NFκB activation, decreased expression of TNF-α during the development of heart failure may modulate disease progression (Lou *et al*., 2004). Binding of TNF-α to TNFR1 also induces phosphorylation of the p85 subunit of PI3K and Akt phosphorylation is increased in a time-dependent manner (Ozes *et al*., 1999). This mechanism may also possibly explain how TNF-α exerts its beneficial effects.

**Table 2:** Comparison of the roles and responses of TNF-α in *in vivo* and *in vitro* models

| Author | Model | [DOX] | [TNF-α] | Incubation | Result |
|---|---|---|---|---|---|
| Krown *et al*., (1996) | Neonatal rat cardiomyocytes | | 4 nM | 18 hours | Apoptosis |
| Chiosi *et al*., (2007) | H9c2 embryonic rat heart cells | 1 µM | 10 ng/mL | 24 hours | ↑ apoptosis |
| | | | 10 ng/mL | 24 hours | No apoptosis |
| Tolosa *et al*., (2005) | C2C12 myotubes | | 1- 40 ng/mL | 48 hours | ↑ apoptosis |
| Mohamed *et al*., (2004) | Adult male albino rats | 12 mg/kg/week/6 weeks | | | ↑ TNF-α in plasma |
| Xu *et al*., (2008) | Wistar rat cardiomyocytes | 0.1 – 1 µM for 1, 4, 8 and 16 hours | | | ↓ TNF-α in culture medium |
| Mukherjee *et al*., (2003) | Male and female Wistar rats | 30 mg/kg (single dose) | | | ↑ TNF-α in myocardium and blood |
| Lou *et al*., (2004) | Male Sprague-Dawley rats | 2.5 mg/kg x 6 over 2 weeks[4] | | | ↓ TNF-α mRNA and protein[5] |
| Watanabe *et al*., (1996) | Pancreatic carcinoma cell lines | 0.002 – 200 uM | 0.02 – 2000U/mL | 72 hours | TNF-α ↑ MnSOD[6] |

[4] Acute group sacrificed at the end of treatment, sub-chronic group sacrificed in week 6.
[5] Myocardial mRNA and protein in the sub-chronic group
[6] Endogenous TNF-α provides protection against DOX by inducing manganese SOD

When evaluating contradictory studies it is important to consider all the factors that may influence the results. The above mentioned studies have used both animal (Mohamed *et al*., 2004) and cell culture models (Krown *et al*., 1996). Furthermore, several different cell types have been studied (Chiosi *et al*., 2007; Tolosa *et al*., 2005; Xu *et al*., 2008). Studies have evaluated acute (Xu *et al*., 2008) and chronic models (Lou *et al*., 2004), as well as clinically relevant and irrelevant doses of DOX (Watanabe *et al*., 1996). Clearly, the different responses induced by TNF-α exerts are undoubtedly context-dependent.

### 1.9.2 TNF-alpha and its receptors

Important and helpful findings are those of the TNF-α receptors, which have highlighted that receptor expression plays a vital role in modulating the cardiotoxicity of DOX and that the bi-directional role of TNF-α may depend on which of its two receptors it binds to (Monden *et al*., 2007; Schulz and Heusch, 2009). Since TNFR1 is the predominant receptor expressed within the heart (Krown *et al*., 1996), it is possible that TNF-α mediates its negative effects in cardiomyocytes via TNFR1 and not TNFR2 (Schulz and Heusch, 2009; Torre-Amione *et al*., 1996). This fact is supported by Chiosi *et al.*, (2007) who observed a significant increase and decrease in TNFR1 and TNFR2 respectively, in H9c2 cells after 1 µM DOX treatment.

A study by Hamid *et al*., (2009). further outlined the ambivalent role that TNF-α plays by reporting that knockout of TNFR1 improved left ventricular ejection fraction, cardiomyocyte hypertrophy, apoptosis, inflammation and survival, whereas knockout of TNFR2 increased cardiomyocyte hypertrophy and apoptosis, in a model of MI. A genetic deficiency of TNFR1 was found to protect the diaphragm against DOX-induced muscle weakness, confirming a negative role for TNFR1 signaling (Gilliam *et al*., 2011). Hence, TNF-α is likely to worsen cardiac function via TNFR1 and improve it via TNFR2 (Monden *et al*., 2007).

Based on the above studies, it is clear that TNF-α can exert both beneficial and detrimental effects depending on its mode of secretion, concentration, receptor, duration of exposure, cell type, species and experimental model (Krown *et al*., 1996; Lou *et al*., 2004; Xu *et al*., 2008). Nevertheless, one can conclude that the TNF-α/TNF receptor axis is involved in DOX-induced cardiotoxicity and apoptosis of cardiomyocytes, and these events are modulated by receptor expression, however, its overall affect, whether pro- or anti-apoptotic, requires further research

in this context. Even though myocardial infarction and DOX-induced cardiotoxicity are two distinct, unrelated heart conditions, it is possible that TNF-α exerts similar effects in each scenario. Such studies can therefore be used to speculate the role that TNF-α may play in the context of DOX-induced cardiotoxicity. How and whether TNF-α contributes to cardiac injury during chronic DOX-induced cardiotoxicity remains to be elucidated.

### 1.9.3 Jak2 and STAT3

Although TNF-α has been reported to be a contributor to reperfusion injury, this cytokine is involved in the activation of a novel protective pathway termed the SAFE pathway (Figure 1.6) (Lecour, 2009b). This pathway includes the activation of Janus kinase (JAK) and signal transducer and activator of transcription 3 (STAT-3), which convey stress signals from various cytokines on the plasma membrane to the nucleus, where the transcription of several proteins is altered (Hausenloy, 2009). In the heart, JAK and STAT have been implicated in hypertrophy, apoptosis, inflammation (Kunisada *et al*., 2000) proliferation and defense (Kisseleva *et al*., 2002). JAKs belong to a family of tyrosine kinases that play an important role in transducing signals from the cell surface to the nucleus (Imada and Leonard, 2000) and have been implicated in cell proliferation, differentiation and apoptosis (Rawlings *et al*., 2004). JAKs are constitutively associated with cytokine receptors, which, once activated by a ligand (e.g. TNF- α), activate JAK. This leads to tyrosine phosphorylation and homo-dimerization of the receptor, creating 'docking sites' for STATs via their Src-homology-2 (SH2) domains (Boengler *et al*., 2008). Subsequently, the activated JAK then phosphorylates STAT-3 at a tyrosine residue approximately 700 residues from the N-terminus ($Tyr^{705}$) (Kisseleva *et al*., 2002). STAT-3 then forms a homodimer and translocates to the nucleus where it up-regulates the transcription of target genes (Imada and Leonard, 2000). It is not yet clear whether phosphorylation on serine 727 ($Ser^{727}$) is of functional importance to all STATs, but it is believed that Erk1/2 is responsible for this phosphorylation event (David *et al*., 1995). Phosphorylation at this residue significantly enhances the transcriptional activity of STAT3 (Boengler *et al*., 2008).

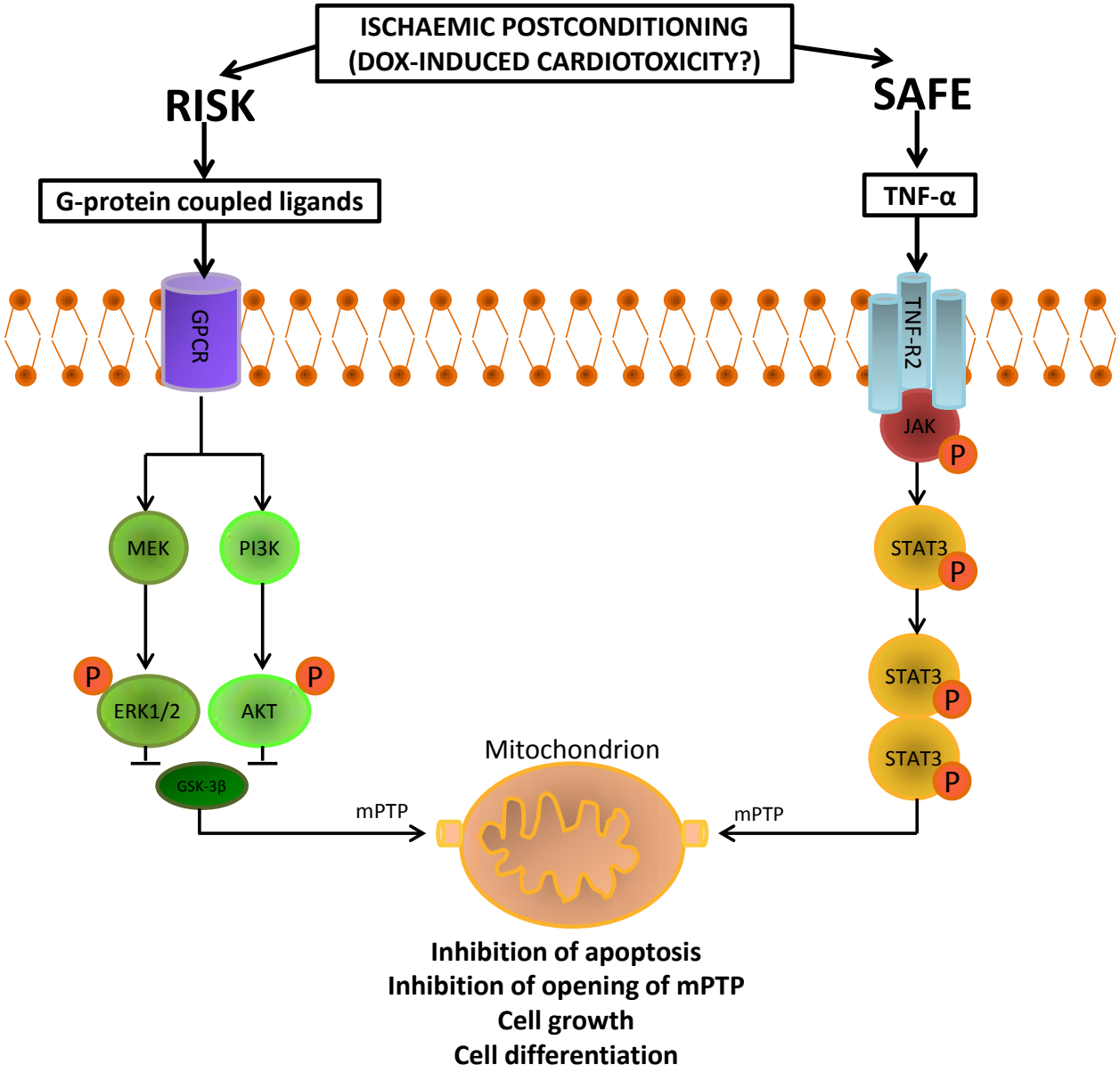


**Figure 1.6: Schematic representation of the RISK and SAFE pathways.** Binding of G-protein coupled ligands to G-protein coupled receptors activates MEK and PI3K which subsequently activate Erk1/2 (extracellular signal-related kinases) and Akt. Binding of TNF-α to TNF receptors activates JAK (janus kinase), which then activates STAT-3 (signal transducer and activator of transcription). Both pathways are likely to converge at the mitochondria where they enhance cardioprotection against ischemia reperfusion injury. Adapted from Lacerda *et al*., (2009)

STAT3 belongs to the signal transducer and activator of transcription family and resides in the cytoplasm as an inactive form (Rébé *et al*., 2013). Once activated, STAT3 translocates to the nucleus within 15 minutes where it induces the transcription of several target genes (Darnell,

1997). In the heart, STAT proteins regulate the expression of the genes involved in inflammation, apoptosis, angiogenesis and cell signaling (Hilfiker-Kleiner *et al*., 2004), as well as growth, differentiation (Nakajima *et al*., 1996), cell death and cell survival (Fukada *et al*., 1996). STAT3 has been observed in the heart during MI and ischemic preconditioning and its activation during ischemia-reperfusion injury suggests that it provides protection against stress (Negoro *et al*., 2001). Many of the cytoprotective actions of the SAFE pathway have been attributed to the activation of STAT3 specifically, however, since STAT3 is involved in the transcriptional up-regulation of such a vast array of genes, it is not quite clear which of the responses are required by the heart. Activation of the SAFE pathway increases the transcription of the anti-apoptotic gene Bcl-2 and reduces transcription of the pro-apoptotic genes Bax and Bad (Bolli *et al*., 2001; Hattori *et al*., 2001). In addition, cytokine signaling through the SAFE pathway has been shown to increase cell survival via PI3K/Akt (Tolosa *et al*., 2005).

Kunisada *et al*., (2000) investigated the effects of STAT-3 over-expression in the context of DOX-induced cardiotoxicity. Three-month-old mice were given an intra-peritoneal injection of DOX as a single dose of 15 mg/kg. Subsequently, only 25% of the wild-type mice survived, compared to 80% of the mice over-expressing STAT-3. The dead mice were found to have significant pleural effusion and ascites, confirming DOX-induced heart failure. Caspase activation as well as apoptotic DNA fragmentation was increased in anti-STAT3 siRNA transfected cells (Frias *et al*., 2008), emphasizing the protective role of STAT3 against DOX-induced apoptosis. To the best of our knowledge, these are the only studies of DOX-induced cardiotoxicity that have identified markers of the SAFE pathway.

Although the SAFE pathway can function independently of the RISK pathway, studies aimed at delineating the role of potential crosstalk between the two pathways have revealed a complex interaction (Lacerda *et al*., 2009). If either the RISK or SAFE pathways are inhibited, the protective effects of these pathways are completely ablated (Lecour, 2009a; Suleman *et al*., 2008). This suggests that dual functioning of both the RISK and SAFE pathways may be required for cardioprotection (Hausenloy, 2009). Evidence for cross-talk is found in STAT-3 inhibition studies, where a parallel reduction in the phosphorylation of Akt was observed. Similarly, in the presence of Wortmannin, a PI3K/Akt pathway inhibitor, phosphorylation and hence activation of STAT-3 was inhibited (Suleman *et al*., 2008). Furthermore, the p85

regulatory subunit of PI3K promotes the phosphorylation of STAT-3 (Pfeffer *et al*., 1997) and JAK can phosphorylate Akt after recruiting to the p85 subunit of PI3K to the docking sites on the receptor (Rawlings *et al*., 2004). As mentioned before, serine phosphorylation of STAT3 is thought to involve members of the MAPK family (Aznar *et al*., 2001), therefore the administration of an Erk1/2 inhibitor strongly reduces the anti-apoptotic effect offered by prostaglandin $E_2$ ($PGE_2$)-induced STAT-3 activation during DOX treatment (Frias *et al*., 2008) and thus further highlights the possible cross-talk between the two pathways. Since DOX-induced cardiotoxicity, like reperfusion injury, is also characterized by apoptosis and oxidative stress, it is possible that the SAFE pathway may provide protection in this context (Frias *et al*., 2010; Mitra *et al*., 2007).

## 1.10 Where to from here?

As evident from the literature, unimaginable cross-talk exists within the human body in an attempt to maintain homeostasis. While a fair amount is known about DOX-induced cardiotoxicity, little is known about the involvement of the RISK and SAFE pathways in this context. Although various studies have reported up-regulation of Akt and Erk1/2, many of these studies have been performed at supraclinical concentrations of DOX and are unlikely to be a true reflection. In an appropriate model of chronic DOX-induced cardiotoxicity using clinically relevant concentrations of the drug, the true role of Akt and Erk1/2 can be elucidated. As pro-survival kinases, it is speculated that Akt and Erk1/2 will increase in a time- and dose-dependent manner during treatment with DOX, in order to confer protection. Based on the literature, TNF-α is likely to exert beneficial effects through TNFR2 in this context, however, this will depend on how much TNF-α is present in this model of chronic cardiotoxicity. Since DOX-induced cardiotoxicity and ischemia-reperfusion injury share common characteristics, namely ROS production, cardiomyocyte death, and the progression to heart failure, it is possible that the protective pathways activated during ischemia reperfusion may also be activated following exposure to DOX. TNF-α is likely to be present in this model but the effects it exerts will likely be dependent on which of its two receptors it binds to. Seeing that exogenous TNF-α can mimic ischemic pre-conditioning during reperfusion in a time and dose dependent manner, it is possible that TNF-α may confer protection during DOX-induced cardiotoxicity too and subsequently activate the SAFE pathway. It is not known whether TNF-α may in fact also trigger the RISK

pathway, but there is evidence that this pathway is activated via cross-talk with the SAFE pathway. It is known that components of the RISK pathway are present during DOX-induced cardiotoxicity, but whether they are up- or –down-regulated depends on the model in question. Most studies have used concentrations of DOX that are unattainable in a clinical setting and therefore generate inaccurate and intensified results. Furthermore, very few studies have focused on chronic-cardiotoxicity, which is the most debilitating, life-threatening form. Since cardiotoxicity develops as a result of chronic and cumulative exposure to DOX, we have employed an *in vitro* model that simulates this scenario. By treating two different cell lines daily for 5 days, our results will provide insight into the dose-dependent, damaging effects of DOX. To further add to the novelty of our model, we have employed concentrations that are well within the clinical range in order to generate more realistic results. It is important to note that when referring to our *in vitro* study, the term 'cytotoxicity' is used, whereas when referring to the human DOX-induced cardiovascular condition, the term 'cardiotoxicity' is used.

DOX has the potential to improve cancer survival and quality of life in our country's cancer patients, yet currently causes severe side effects such as cardiotoxicity, that pose a threat to their survival. It is therefore the intention of this study to identify the roles of two potentially protective pathways (the SAFE and RISK) as an alternative mechanism to reducing DOX-induced cardiotoxicity and what role they play in this context. In addition, it is of interest to determine what role TNF-α plays and whether it triggers the aforementioned pathways in this scenario. The aim of identifying pathways that could provide protection during cardiotoxicity is an important one, as a patient cured of cancer today does not want to be a patient of heart failure a few years down the line. With this in mind it is therefore vital to understand the cellular and molecular dynamics of DOX-induced cardiotoxicity in the hope of identifying signaling mechanisms that will offer cardioprotection while still eradicating the tumor.

## 1.11 Research Problem

The SAFE pathway, activated via TNF-α, and the RISK pathway are stimulated as a possible protective mechanism during chronic DOX-induced cytotoxicity.

## 1.12 Research Aims

- To determine the activity of the SAFE pathway by measuring TNF-α production and the protein expression of Jak2 and STAT3 in an *in vitro* model of chronic DOX-induced cytotoxicity
- To assess the activity of the RISK pathway (Erk1/2/Akt) in this model

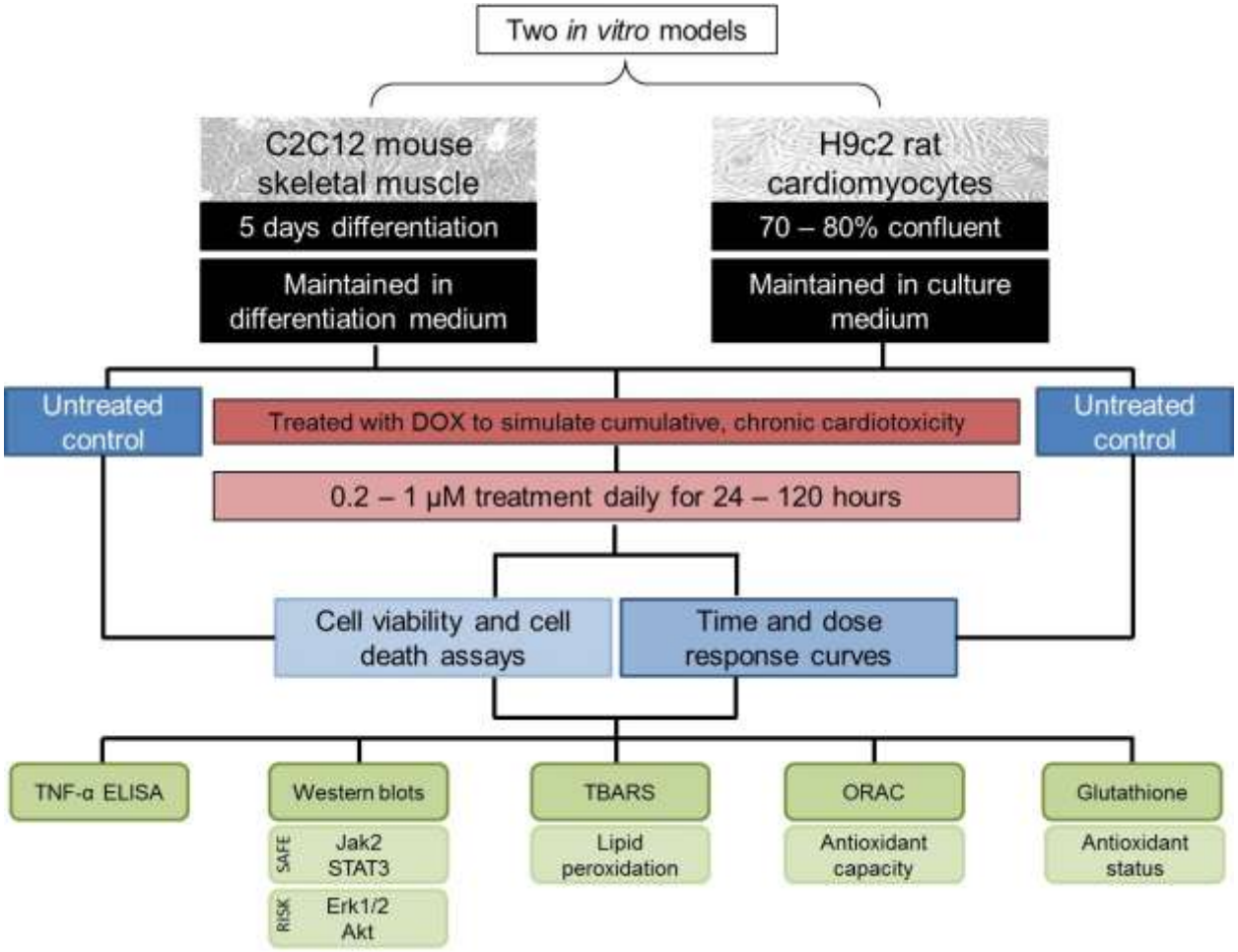


**Figure 1.7: A schematic diagram summarizing the approach used to achieve the research aims**

# CHAPTER 2

## 2.1 Materials and Methods

### 2.1.1 Cell culture model

H9c2 cells, derived from embryonic rat cardiomyocytes, were purchased from American Type Culture Collection (ATCC, Manassas, Virginia, USA; CRL-1446) The cells were grown and maintained in Dulbecco's modified Eagle's medium (DMEM) (Gibco, 41965-039), supplemented with 10% fetal bovine serum (FBS) (Invitrogen Gibco, 10270-106) and 1% Antibiotic-Antimycotic (AA) (Gibco, 15240-062), hereafter collectively referred to as growth medium, in a humidified atmosphere of 5% $CO_2$ at 37 °C. Cells were routinely sub-cultured by trypsinsation (0.25% Trypsin-EDTA, Gibco, 25200-012), upon reaching 70 - 80% confluency (Figure 2.1A), where after they were seeded at appropriate densities into culture plates (refer to appendix B, protocol 1)

Mouse skeletal muscle cells (C2C12, ATCC, Manassas, Virginia, USA; CRL-1772,) were grown and maintained under the same conditions. Subsequent to reaching ± 80% confluency (Figure 2.1B), C2C12 myotube differentiation was induced by replacing growth medium with differentiation medium: DMEM supplemented with 2% horse serum (Biochrom, S9133). Cells were maintained in differentiation medium for the duration of the experiment. Differentiation medium was refreshed every 48 hours, whilst myotube formation was examined using a light microscope (Figure 2.1C).

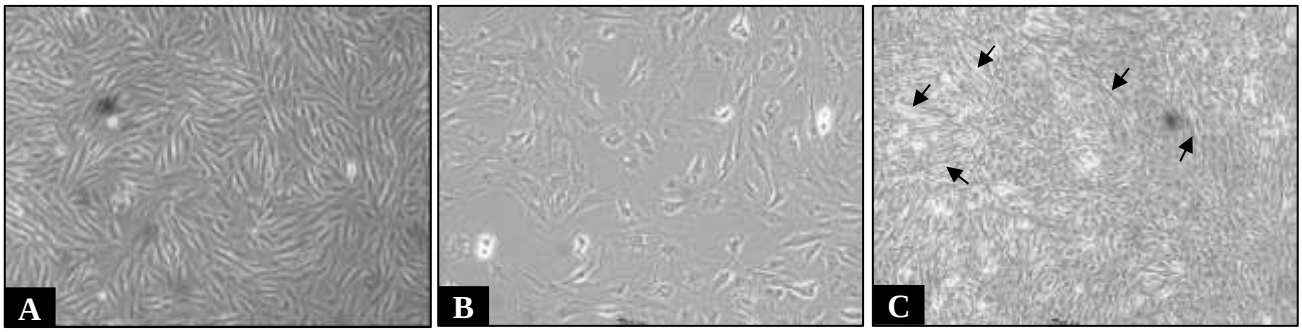


**Figure 2.1 A, B and C: Images of H9c2 and C2C12 cells. A:** H9c2 cells upon reaching 80% confluency (10x). **B:** C2C12 cells shown at low density in the myoblast stage (20x) and **C:** C2C12 cells at high

density as differentiated myotubes after 5 days of differentiation (4x).Black arrows indicate myotubes. Scale bar: 1000 µm

### 2.1.2 Treatment of Cells with Doxorubicin

3 mM DOX stock (Sigma-Aldrich, D1515) was prepared in sterile DMEM and stored at -20 °C, protected from light, until needed. Treatments were prepared on the day of experimentation. Fully differentiated C2C12 cells and 80% confluent H9c2 cells were treated daily with increasing concentrations of DOX (0.2 – 1 µM) for a total period of 120 hours (24 – 120 hours), simulating cumulative, chronic DOX-induced cardiotoxicity. For example, treatment with 0.2 µM every day for five days (120 hours) results in a cumulative dose of 1 µM, whereas treatment with 0.2 µM for 48 hours results in a cumulative dose of 0.4 µM.

### 2.1.3 Assessment of Cell Viability (MTT Assay)

Cell viability of H9c2 and differentiated C2C12 cells was determined using the 3-[4, 5-dimethylthiazol-2-yl]-2, 5-diphenyl tetrazolium bromide (MTT) assay as previously described (Mosmann, 1983). This assay makes use of the principle whereby viable cells reduce yellow MTT into purple formazan crystals, thus giving an indication of cell death. MTT (Sigma-Aldrich, M2128) was prepared as a 0.01 g/mL solution in sterile phosphate buffered saline (PBS) at room temperature. The MTT solution was further sterilised by filtration, where after 500 µL of the 0.01 g/mL MTT stock solution was added to each well. After 2 hours incubation at 37 °C, the supernatant was carefully discarded and 500uL of Isopropanol (1%)/Triton (0.1%) solution was added to each well. Following a short agitation period, absorbance was determined at 540 nm using the EL800 Universal Microplate reader (Bio-Tek Instruments Inc., Vermont, USA). Cell viability was expressed as the percentage of treated cells relative to untreated (control) cells.

### 2.1.4 Determination of Caspase Activity (Caspase-Glo®3/7 Assay)

The Caspase-Glo® 3/7 Assay (Promega, G8091) is a standardized, luminescent assay that measures the activity of caspase-3 and -7. Caspase-3 and -7 are members of the cysteine aspartic acid-specific protease family and play key roles as effector caspases during apoptosis. The assay provides a luminogenic caspase-3/7 substrate (containing the tetrapeptide sequence DEVD) that is cleaved by caspases, resulting in a luminescent signal produced by luciferase (Figure 2.2). The

level of luminescence is directly proportional to the amount of caspase cleavage, therefore giving an indication of the level of apoptotic cell death taking place.

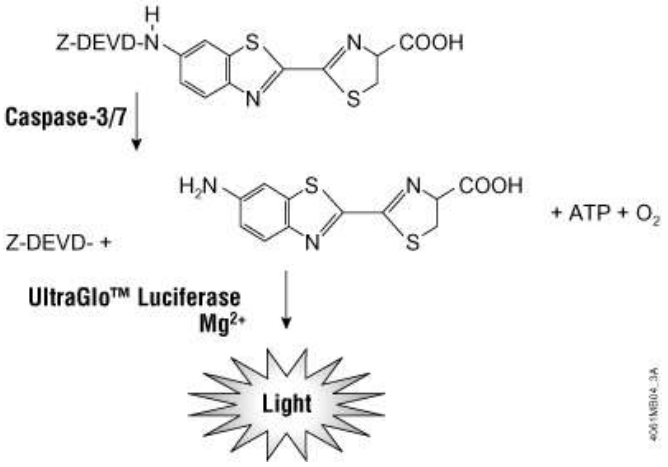


**Figure 2.2: Caspase-Glo reaction.** Caspase-3/7 cleaves the luminogenic substrate (DEVD sequence), resulting in light production. Promega Caspase-Glo ®3/7 Assay protocol.

Each assay consisted of a blank reaction (Caspase-Glo®3/7 reagent, culture medium and no cells), a negative control (Caspase-Glo®3/7 reagent and cells in culture medium) and DOX-treated samples. Following treatment with DOX, 100 µL Caspase-Glo®3/7 reagent was added to each well containing 100 µL culture medium and incubated for 1 hour at room temperature with gentle mixing. Luminescence was then measured using the GloMax® 96 Microplate Luminometer (Promega, Wisconsin, USA).

### 2.1.5 Cytotoxicity Assay (Lactate Dehydrogenase Assay)

The CytoTox 96® Non-Radioactive Cytotoxicity Assay (Promega, G1780) is a colorimetric assay that quantitatively measures lactate dehydrogenase (LDH), a soluble, cytosolic enzyme that is released following damage to the plasma membrane. LDH catalyzes the oxidation of lactate to pyruvate, resulting in the production of NADH. A tetrazolium salt (INT) is then converted to red formazan, using the previously formed NADH. LDH released into cell culture medium is measured by this enzymatic assay. The amount of color formed is directly proportional to the number of lysed cells, therefore giving an indication of necrotic cell death. Following treatment, 10 µL lysis solution was added to the wells of a 96-well plate containing 100 µL culture medium and incubated for 45 minutes at 37 °C. After substrate mix was added to each well, the plate was

covered with foil and incubated for a further 30 minutes at room temperature. Following the incubation period, stop solution was added to each well and absorbance was read immediately at 490 nm using the EL800 Universal Microplate reader (Bio-Tek Instruments Inc., Vermont, USA).

### 2.1.6 Quantification of TNF-α in cell culture medium (ELISA)

TNF-α is a pleiotropic cytokine that is involved in several pathological conditions such as asthma, arthritis, obesity, diabetes and cancer. Quantikine® rat and mouse ELISAs (R&D Systems, RTA00 and MTA00B) were used to measure the levels of TNF-α in cell culture medium. The immunoassay employs the sandwich, enzyme-linked immunosorbent assay in which a monoclonal TNF-α antibody has been pre-coated into the wells of a microplate. TNF-α present in samples, standards and controls is bound by the antibody. After the addition of a TNF-α polyclonal antibody and a substrate colour solution, the reaction yields a blue product which turns yellow upon addition of the stop solution. The intensity of the yellow colour is directly proportional to the amount of TNF-α which was bound in the first step. The plate is read at 450 nm and the values are read off a standard curve. Prior to the assay, culture medium was collected after each day of treatment with DOX, for a total of five days, and placed into pre-chilled falcon tubes. The tubes were immediately placed into a -20 °C freezer. On the last day of collection the assay was performed. Samples were thawed immediately prior to starting the assay. The ELISA was carried out three times in triplicate according to the manufacturer's instructions. (Refer to Appendix B, Protocol 8).

### 2.1.7 Determination of Anti-oxidant Capacity (ORAC assay)

Oxidative stress is a physiological condition that results due to an imbalance between ROS and antioxidants. Under normal conditions, ROS production is compensated for by the activity of antioxidant enzymes; however, excessive ROS production leads to DNA, protein and membrane damage. All of this ROS-induced injury has been implicated in the development of several disease states such as cancer, CVD and neurodegenerative disease. In order to evaluate the capacity of cellular antioxidant systems to overcome the deleterious effects of DOX-induced oxidative stress in H9c2 and C2C12 cells, the Oxygen Radical Absorbance Capacity (ORAC) assay was used, as previously described (Ou *et al*., 2001). The assay is based on the oxidation of

the fluorophore 'fluorescein' by the peroxyl radical 2,2'-azobis (2-methylpropionamidine) dihydrochloride (AAPH). Antioxidants in the assay block the oxidation of the fluorophore until the antioxidant activity in the sample is depleted. The samples' antioxidant capacity correlates with the fluorescence decay curve, represented as the area under the curve (AUC), which is compared to the standard curve of the vitamin E analog 'Trolox™' (Sigma, 238831) and expressed as µmol Trolox standard equivalents per gram. The Fluoroskan Ascent™ microplate fluorometer (Thermo Fisher Scientific, Massachusetts, U.S.A.), equipped with an incubator, was set at 37 ◦C. A fluorescein stock solution (Sigma, F6377) was prepared in phosphate buffer and further diluted for use in the assay. AAPH (Sigma, 440914) (25 mg/mL in phosphate buffer) and fluorescein were added to each well with a multichannel pipette. The fluorescence of each well, containing 12 µL sample, was read every 5 minutes for 2 hours. Fluorescence filters with an excitation wavelength of 485 nm and emission wavelength of 538 nm were used. Final ORAC values were calculated using the regression equation $y = ax^2 + bx + c$ between Trolox concentration (µM) and the area under the curve. (Refer to Appendix B, protocol 9).

### 2.1.8 Measurement of Lipid Peroxidation (TBARS assay)

It is well known that lipid peroxidation causes cell damage in both plants and animals. Lipid peroxides can be used as indicators of oxidative stress in cells as they decompose to form stable complexes such as MDA. Measuring the natural bi-products of lipid peroxidation, like MDA, is a commonly used assay to assess oxidative damage and therefore the levels of oxidative stress. Thiobarbituric acid reactive substances (TBARS) is a widely used assay for assessing lipid peroxidation since MDA forms a 1:2 adduct with TBA which can be measured colorimetrically. Cell samples were resuspended in butylated hydroxytoluene (BHT) on ice in order to prevent oxidation during processing, sonication and storage. Samples were centrifuged at 2000 rpm, 4 °C, for 15 minutes. A serial dilution of MDA (Merck, 805797) was prepared. Unknown MDA-containing samples as well as known standards were incubated with TBA reagent (Sigma, T5500) at 90 °C for 45 minutes. After cooling in an ice bath, butanol and saturated salt were added to each sample to separate the phases. The top phase of samples and standards were transferred to a 96-well plate and the absorbance was measured at 532 nm in the Multiskan® Spectrum microplate spectrophotometer (Thermo Fisher Scientific, Massachusetts, USA). (Refer to Appendix B, protocol 10)

### 2.1.9 Assessment of Antioxidant Status (Glutathione Assay)

The ratio of GSH and GSSG was determined according to the method previously described by Asensi *et al*., (1999). In a clear, 96-well plate, 1U glutathione reductase (Sigma, G3664), 50 µL 0.3 mM DTNB (Sigma, D21820) and 50 µl sample for GSH (Sigma, G4251) or 50 µl sample treated with M2VP (Sigma, 69701) for GSSG were incubated at 25 °C for 5 min. The reaction was then initiated with 50 µL 1mM NADPH (Sigma, N6785) and measured at 412 nm for 5 minutes at 30 second intervals in a Multiskan® Spectrum microplate spectrophotometer (Thermo Fisher Scientific, Massachusetts, USA). The concentration of total glutathione, GSH and GSSG were determined using GSH as standard. (Refer to Appendix B, protocol 11).

### 2.1.10 Western Blot Analysis

#### 2.1.10.1 Preparation of cell lysates

For protein isolation, cells were incubated in 50 µL modified radio-immunoprecipitation (RIPA) buffer (pH 7.4) containing Tris-HCL 2.5 mM, EDTA 1 mM, NaF 50 mM, dithiothreitol 1 mM, phenylmethylsulfonyl fluoride (PMSF) 0.1 mM, benzamidine 1 mM, 4 mg/ml SBTI, 10 mg/ml leupeptin, 1% NP40, 0.1% SDS and 0.5% Na deoxycholate. Cells were scraped using a sterile cell scraper, and contents were placed into chilled eppendorf tubes on ice. Cell lysates were sonicated for 15 seconds with an Ultrasonic Liquid Processor (Misonix), in order to rupture cell membranes. Lysates were then centrifuged at 8000 rpm (5900 x g) for 10 minutes, where after protein concentration was determined using the Bradford method, as previously described (Bradford, 1976), with bovine serum albumin (BSA) used as a standard. Protein samples were prepared in Laemmli's loading buffer and stored at -80 °C until needed.

#### 2.1.10.2 Sodium dodecyl sulfate-polyacrylamide gel electrophoresis

Samples were thawed and then boiled at 95 ˚C for 5 minutes. 50 µg protein of each sample was separated by 12% SDS-PAGE for 10 minutes, at 100 V, 400 mA (constant), followed by 200 V for 50 minutes. Proteins were transferred onto polyvinylidene fluoride (PVDF) membranes (Trans-Blot® Turbo™ Mini PVDF Transfer Packs, Bio-Rad, 170-4156) using the TransBlot® Turbo™ Transfer System (Bio-Rad) for 12 minutes at 15 V. PDVF membranes were then blocked for 2 hours in 100 mL 5% fat-free milk powder dissolved in Tris Buffered Saline-Tween

Solution (TBS-T) at room temperature. After blocking, membranes were rinsed 3 times for 5 minutes with TBS-T and incubated overnight at 4 ˚C with the respective primary antibodies (table 3) diluted 1: 1000 in TBS-T. Subsequent to primary antibody incubation, membranes were again washed 3 times with TBS-T and incubated with HRP-linked anti-rabbit/anti-mouse secondary antibody for 1 hour at room temperature. Membranes were washed with TBS-T (3 x 5 minutes) and incubated with Pierce ECL western blotting substrate (Thermo Scientific, #32106). Bands were detected using the ChemiDoc™ XRS+ System with the Image Lab™ Software (Bio-Rad). The bands generated were expressed using a volume analysis tool and represented as the fold change relative to the control sample (untreated). GAPDH was used as a loading control in the H9c2 cardiomyocytes, however, a ponceau stain was used as a loading control in the differentiated C2C12 myotubes since GAPDH exhibits poor stability in the differentiation process and is therefore an unreliable reference gene (Hildyard and Wells, 2014). Partial, representative ponceau images will be displayed with the accompanying blots (refer to the appendix for the full ponceau images and to Appendix B, protocols 12 - 14 for the complete western blotting protocol).

**Table 3:** Primary antibodies used in Western Blot analysis, as well as their respective secondary antibodies and appropriate dilutions.

| PRIMARY ANTIBODY | SECONDARY ANTIBODY | 2° DILUTION |
|---|---|---|
| P-Jak2 | Anti-rabbit | 1: 2500 |
| T-Jak2 | Anti-rabbit | 1.5: 5000 |
| P-STAT3 Ser 727 | Anti-rabbit | 1: 10000 |
| P-STAT3 Tyr 705 | Anti-rabbit | 1: 10000 |
| T-STAT3 | Anti-mouse | 1.5: 5000 |
| TNFR2 | Anti-rabbit | 1: 10000 |
| P-Akt | Anti-rabbit | 1: 2500 |
| T-Akt | Anti-rabbit | 1: 10000 |
| TNFR1 | Anti-mouse | 1: 10000 |
| P-Erk | Anti-rabbit | 1: 5000 |
| T-Erk | Anti-rabbit | 1: 10000 |

| | | |
|---|---|---|
| TNF-α | Anti-rabbit | 1: 2500 |
| Cleaved caspase-3 | Anti-rabbit | 1: 10000 |
| GAPDH | Anti-rabbit | 1: 10000 |

### 2.1.11 Statistical Analysis

GraphPad Prism version 5.0.3 (GraphPad Inc., San Diego, CA) was used for visual representation and statistical analysis of data. Comparisons between the different groups were performed by one-way analysis of variance (ANOVA) followed by Dunnett's multiple comparisons test as post-test. *p*-values are represented as follows: * $p < 0.05$; ** $p < 0.01$; *** $p < 0.001$ versus the control. When comparisons are made to groups other than the control, the following symbols are used: ● $p< 0.05$, ●● $p< 0.01$, ●●● $p<0.001$. Unless otherwise indicated, all experiments were conducted in at least duplicate and three independent experiments were carried out for each technique. All data are presented as mean ± SEM.

# CHAPTER 3

## Results Part I

### Pilot Study

A pilot study was initially conducted in which H9c2 cells and differentiated C2C12 myotubes were treated with increasing concentrations of DOX for a total period of five days, in order to simulate cumulative, chronic DOX-induced cardiotoxicity. Our preliminary work was to establish the most appropriate treatment concentrations whilst still keeping within clinically relevant levels. The effects of DOX on the viability of these cell types was determined using the MTT assay, whereas the extent of apoptosis and necrosis was investigated using the Caspase Glo and LDH assays, respectively. H9c2 cells were employed in this study because they are an animal-free alternative, easy to maintain and extensively used in various other laboratories. However, it has not yet been established whether H9c2 cells accurately mimic the responses of primary cardiac myocytes. To address this limitation, this study compared the responses of H9c2 cells with differentiated C2C12 myotubes. These cells share similar characteristics with primary cardiac myocytes in that they have the ability to form myotubes which have been demonstrated to undergo pre-conditioning in a similar manner to that of the whole heart (Lecour *et al*., 2005).

### 3.1 Results

#### 3.1.1 DOX Concentrations

In this study, the concentrations of DOX that were employed were based on a review by Minotti *et al*., (2004a). Many *in vitro* studies that have reported on the mode of action of anthracyclines have been performed at concentrations that were too high when compared to the peak (5 μM) or steady state (25 – 250 nM) concentrations observed clinically in patients. Since plasma concentrations generally fall between 1 – 2 μM, it was suggested that studies investigating the detrimental effects of anthracyclines (particularly DOX), should not exceed this range. Based on this information, this study performed a dose- and time-response curve using increasing concentrations of DOX (0.2 – 1 μM). Since chronic cardiotoxicity is believed to develop in direct proportion to the total cumulative dose of DOX (Montaigne *et al*., 2012), this study administered

these concentrations on a daily basis for a total of 120 hours to simulate this condition. Therefore for example, treatment of cells for 120 hours with 1 µM will result in a cumulative dose of 5 µM, whereas treatment of cells with 0.2 µM for 72 hours will result in a cumulative dose of 0.6 µM. Seeing that DOX is known to concentrate within cardiomyocytes, the intracellular concentrations of DOX are believed to be greater than the extracellular concentrations (Takemura and Fujiwara, 2007). However, despite this it is believed that the intracellular concentration of DOX will not exceed the cumulative concentrations of this study due to its relatively short half-life of approximately 25 hours (Mross *et al*., 1988). Acute cardiotoxicity does not present as a major clinical problem, however, chronic cardiotoxicity poses a serious threat to the survival of cancer patients since it is associated with a much larger risk of morbidity and mortality (Swain *et al*., 2003). For this reason, a treatment period of 24 – 120 hours was chosen to highlight the differences between the acute and chronic effects. For this study, 24 and 48 hours were classified as acute, 72 hours was classified as sub-chronic and 96 and 120 hours were classified as chronic.

### 3.1.2. DOX reduces cell viability in a time- and dose-dependent manner

The MTT assay is based on the principle whereby metabolically viable cells reduce yellow MTT into purple formazan crystals. The absorbance of each sample is directly proportional to the reductive capacity of mitochondria in viable cells and therefore gives an indication of cell viability. The capacity of H9c2 cells to reduce MTT (Figure 3.1) became significantly reduced by as early as 24 hours [76.49 ± 3.48% ($p = 0.0004$)] following treatment with 1 µM when compared to its respective control (100 ± 4.47%). As the concentration increased cell viability declined, reaching its lowest after 96 hours across all concentrations tested. An interesting phenomenon, however, occurred after 120 hours: cell viability was substantially improved compared to 96 hours, although remaining below control values.

In differentiated C2C12 myotubes, DOX induced a time- and dose-dependent reduction in cell viability (Figure 3.2). Although no significant change was observed after the first 24 hours across all concentrations, cell viability gradually declined as the concentration increased. What was interesting to note was that a single DOX treatment of 1 µM over 24 hours resulted in no change in viability, whereas a cumulative dose of 1 µM DOX over 120 hours (0.2 µM x 5) significantly reduced cell viability [78.42 ± 2.10% ($p < 0.0001$)] compared to the control (100 ± 7.73%). This

observation was also noted in the H9c2 cardiomyocytes, where cumulative treatment with DOX reduced cell viability more than treatment with a single dose.

These observations thus demonstrate the detrimental effects of cumulative concentrations of DOX and how chronic cardiotoxicity poses a more serious threat to the survival of cancer patients than acute cardiotoxicity.

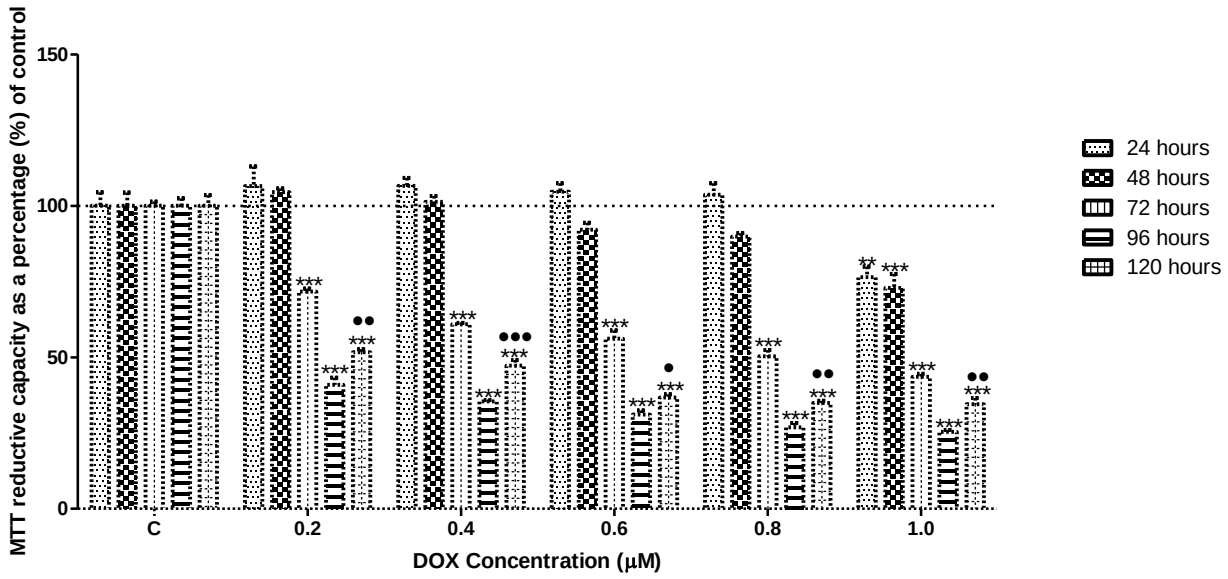


**Figure 3.1: The effect of DOX on the MTT reductive capacity of H9c2 cells**. Cell viability was quantified using the MTT assay as described in the methods section. All values are expressed as a percentage of the control (100%) and presented as mean ± SEM, n = 4. *p< 0.05, **p< 0.01, ***p< 0.001 vs control. ●p< 0.05, ●●p< 0.01, ●●●p< 0.001 (96 vs 120 hours).

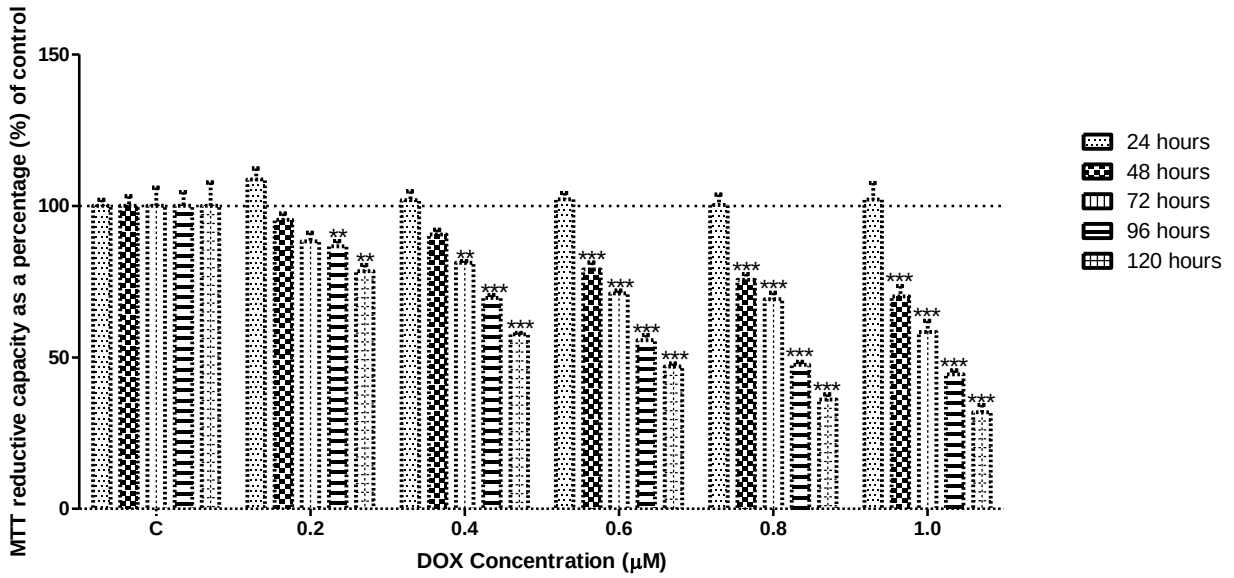


**Figure 3.2: The effect of DOX on the MTT reductive capacity in C2C12 myotubes**. Cell viability was quantified using the MTT assay as described in the methods section. All values are expressed as a percentage of the control (100%) and presented as mean ± SEM, n = 3. *p< 0.05, **p< 0.01, ***p< 0.001 vs control.

### 3.1.3 The DOX-induced decrease in cell viability can be attributed to apoptotic cell death

To determine the relative contribution of apoptotic cell death after DOX treatment, the Caspase-Glo®3/7 assay was employed. Based on the results obtained, caspase-3 and -7 activities were significantly up-regulated in the H9c2 cells by as early as 24 hours and remained elevated even after 96 hours relative to the control (Figure 3.3). By 120 hours however, caspase activity was substantially reduced although remaining above control values. This reduction in caspase activity may have accounted for the improved cell viability observed at this point.

The results for caspase activity in the differentiated myotubes were rather surprising (Figure 3.4). Where caspase activity was expected to be significantly elevated, no major changes were observed. In fact, caspase activity was substantially reduced by 120 hours after treatment with 0.6, 0.8 and 1 µM DOX. This observation was rather strange considering the time- and dose-dependent decline in cell viability. It is therefore possible that at the time of assessment, apoptotic damage may have already taken place and thus the activity of the caspases had declined.

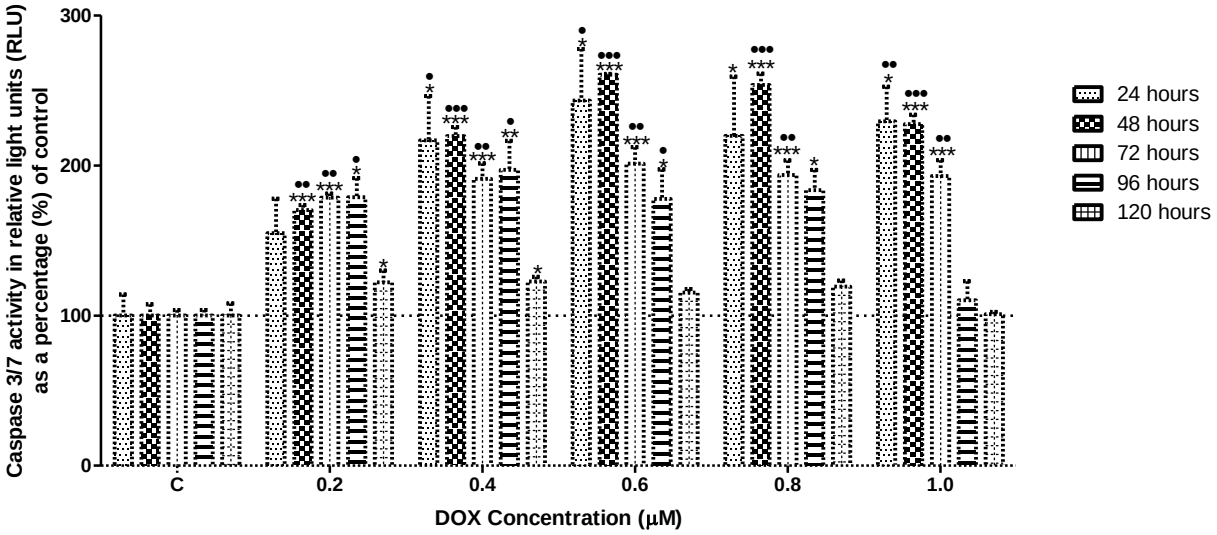


**Figure 3.3: Caspase-3 and -7 activities in H9c2 cells after DOX treatment.** The luminescent signal produced in this assay is directly proportional to caspase 3/7 activity. All values are expressed as a percentage of the control (100%) and presented as mean ± SEM, n = 4. *p< 0.05, **p< 0.01, ***p< 0.001 vs control. ●p< 0.05, ●●p< 0.01, ●●●p< 0.001 vs 120 hours.

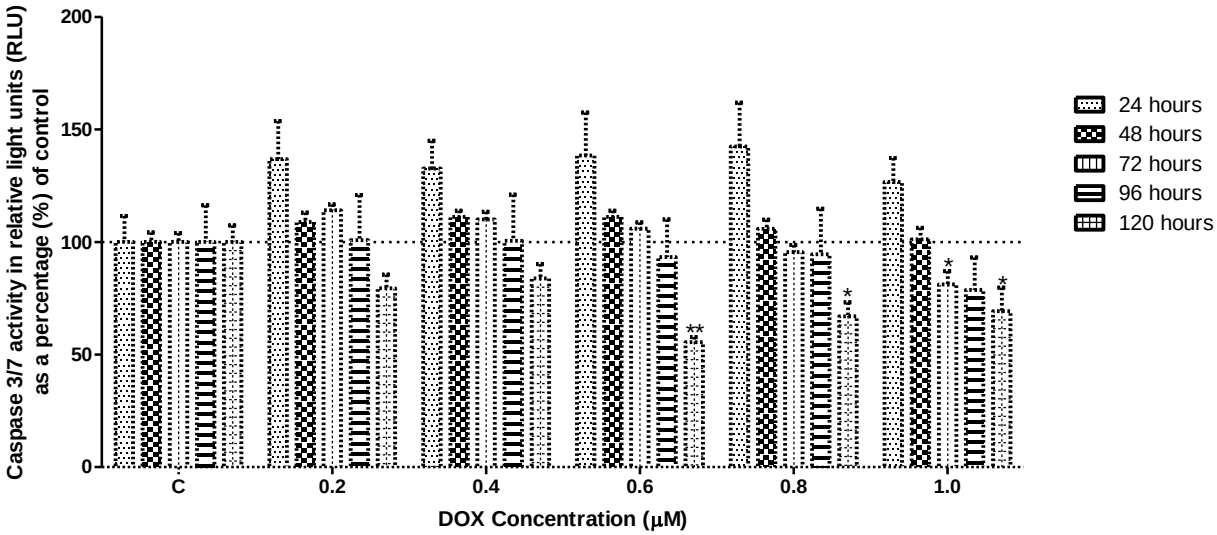


**Figure 3.4: Caspase-3 and -7 activities in differentiated C2C12 cells after DOX treatment.** The luminescent signal produced in this assay is directly proportional to caspase3/7 activity. All values are expressed as a percentage of the control (100%) and presented as mean ± SEM, n = 3, *p< 0.05, **p< 0.01, ***p< 0.001. RLU = relative light units.

### 3.1.4 Necrosis was observed in the chronic setting in C2C12 myotubes but not in H9c2 cardiomyocytes

In order to investigate whether necrotic cell death plays a role in DOX-induced cytotoxicity, the LDH assay was employed. The release of LDH from cells as a result of membrane damage is often used as an indicator for necrotic cell death (Horenstein *et al.*, 2000). As indicated in Figure 3.5, necrotic cell death did not play a major role in this model of cardiotoxicity as much of the LDH detected remained below baseline values for the entire treatment duration.

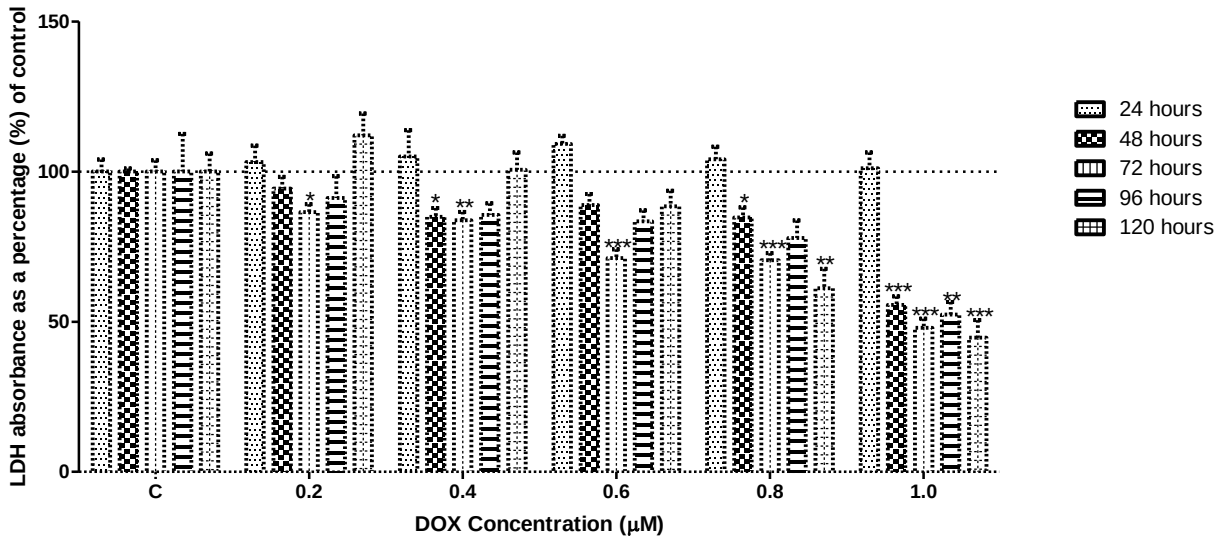


**Figure 3.5: Lactate dehydrogenase assay of H9c2 cells after treatment with DOX.** The LDH assay was employed as an indicator of necrosis since LDH is released in response to cell membrane damage. All values are expressed as a percentage of the control (100%) and presented as mean ± SEM, n = 4, *p< 0.05, **p< 0.01, ***p< 0.001. AU = arbitrary units.

A similar effect was observed in the differentiated C2C12 myotubes (Figure 3.6), however, the levels of LDH were substantially higher than the respective controls after treatment with 0.2 – 0.8 µM for 120 hours. Treatment with a single (24 hours) dose of 1 µM DOX resulted in no significant change in LDH release, yet a cumulative dose of 1 µM DOX over 120 hours (0.2 µM x 5) significantly increased LDH levels [118.8 ± 0.67% (p = 0.0017)] when compared to the control (100 ± 4.08%). Other than indicating the sensitivity of these cells to cumulative doses of DOX, this observation also emphasizes the detrimental effects of chronic DOX treatment as opposed to acute treatment.

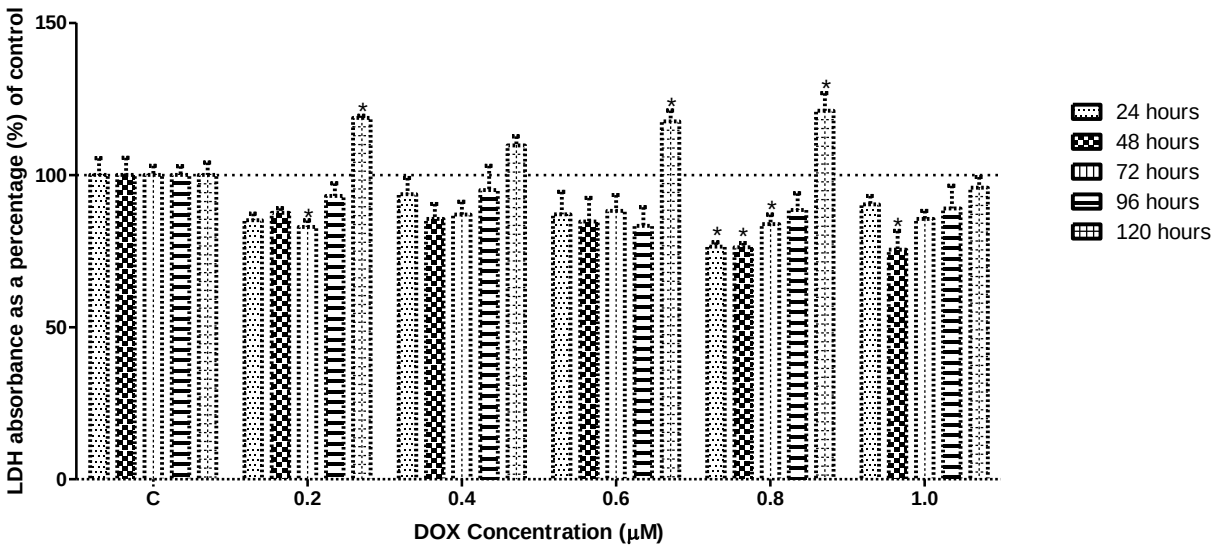


**Figure 3.6: LDH assay of C2C12 myotubes after treatment with DOX.** The LDH assay was employed as an indicator of necrosis since LDH is released in response to cell membrane damage. All values are expressed as a percentage of the control (100%) and presented as mean ± SEM, n = 4, *p< 0.05, **p< 0.01, ***p< 0.001. AU = arbitrary units.

Based on the above results, all subsequent experiments in this study were conducted using the 0.2 and 1 µM concentrations of DOX. The 0.2 µM dose was chosen since it is still clinically relevant after 120 hours. For example, treatment with 0.2 µM every day for 120 hours results in a cumulative dose of 1 µM, which is still within the clinically relevant range as suggested by Minotti *et al*., (2004a). Although the 1 µM dose no longer falls within the clinically relevant range after 120 hours (5 µM), this concentration was chosen to indicate the adverse effects of DOX when the recommended clinical doses are exceeded.

# CHAPTER 4

## Results Part II

### 4.1 Caspase cleavage is evident in the differentiated C2C12 myotubes

Since caspase activity did not change significantly in the Caspase-Glo®3/7 assay when compared to the control, the protein expression of cleaved caspase-3 was determined in the differentiated C2C12 myotubes. As observed in Figure 4.1, the treatment of differentiated C2C12 myotubes with the low concentration of DOX (0.2 µM) did not significantly change the expression of cleaved caspase-3 compared to the control. However, when the concentration was higher (1 µM), cleaved caspase-3 expression was up-regulated acutely (24 and 48 hours), significantly more than the control. Over time the expression of this protein declined, reaching a minimum after 120 hours [0.44 ± 0.19 AU (p = 0.0305)].

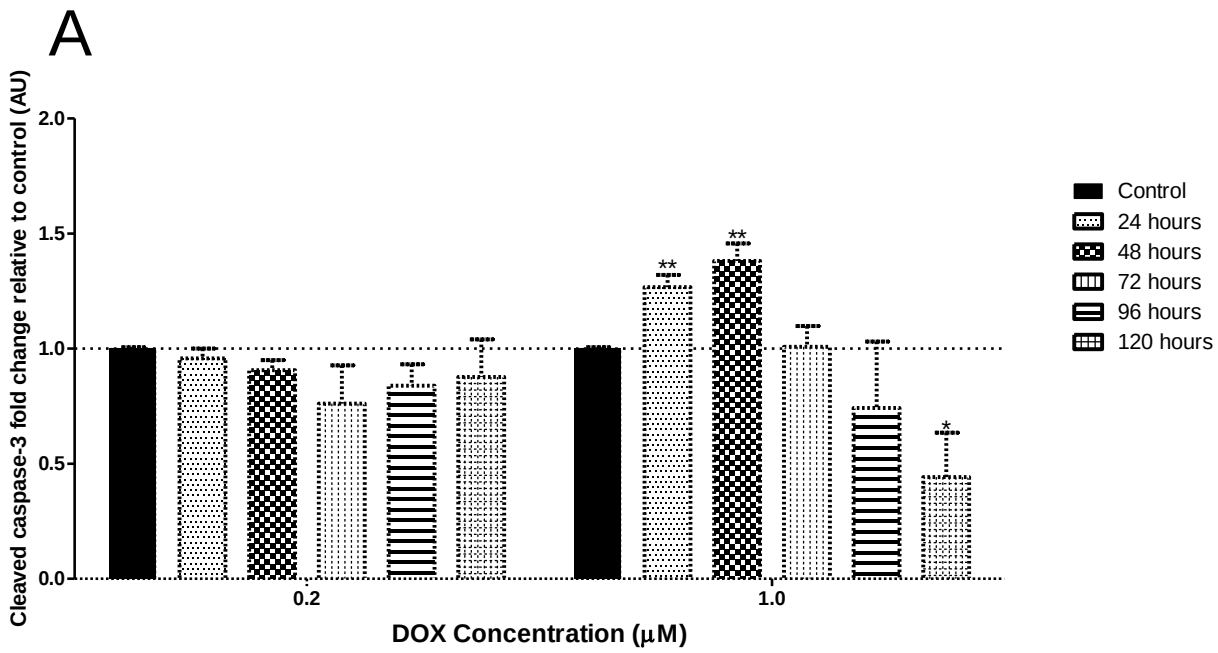

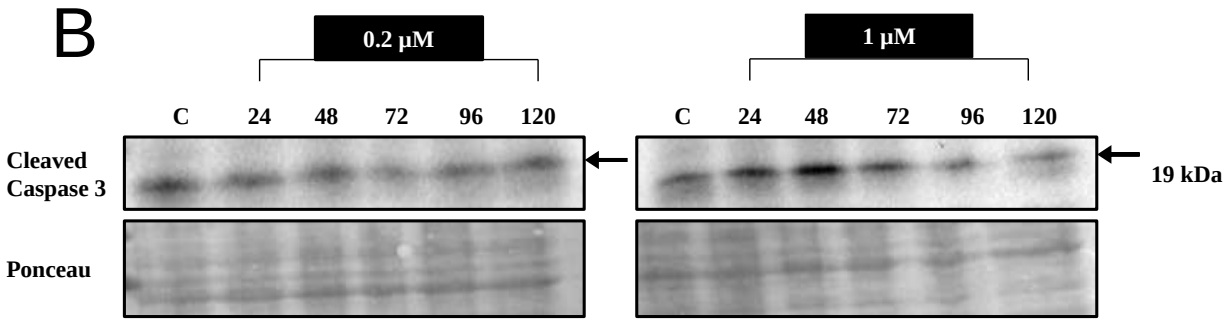


**Figure 4.1: Caspase-3 cleavage in C2C12 myotubes after treatment with DOX.** The lane profile analysis (**A**) and western blots (**B**) are represented. The fold change relative to the control was calculated. All values are presented as mean ± SEM, arbitrary units (AU), n = 3, *p< 0.05, **p< 0.01, ***p< 0.001. Ponceau was used as a loading control.

## 4.2 Chronic DOX treatment stimulates TNF-α production

TNF exerts both physiological and pathological effects including tumor cell necrosis and apoptosis, immunity and cell survival (Chu, 2013; Locksley *et al*., 2001). One of the aims of this study was to investigate whether DOX induces an inflammatory response, mediated by TNF-α. TNF-α is notorious for being the central mediator of inflammation, however, its role in this context is relatively unknown. Therefore, to establish the levels of TNF-α produced after DOX treatment, Quantikine® ELISA kits were employed.

In response to a low concentration of DOX (0.2 µM), TNF-α production in the H9c2 cardiomyocytes (Figure 4.2) was significantly up-regulated after 120 hours [3.82 ± 0.07 pg/mL ($p = 0.0304$)] when compared to the control (3.63 ± 0.01 pg/mL). In response to a higher concentration of DOX, a larger and biphasic pattern of TNF-α release was observed. TNF-α was first significantly elevated after 24 hours [4.24 ± 0.004 pg/mL ($p < 0.0001$)] with a return to insignificant levels thereafter, when compared to the control. The second peak in TNF-α was observed after 96 hours [4.04 ± 0.03 pg/mL ($p< 0.0001$)], which remained elevated even after 120 hours of treatment [4.22 ± 0.15 pg/mL ($p = 0.006$)] compared to the control.

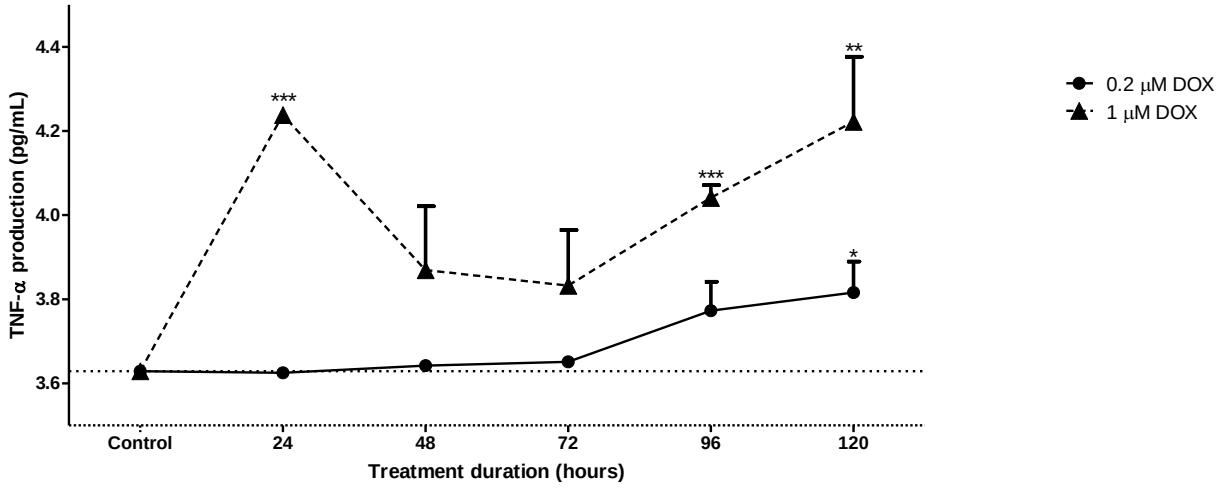


**Figure 4.2: Determination of TNF-α production by H9c2 cells after treatment with DOX.** TNF-α in the cell culture medium was quantified using an ELISA kit. All values are presented as mean ± SEM, n = 3, *p< 0.05, **p< 0.01, ***p< 0.001.

In the differentiated C2C12 myotubes (Figure 4.3), TNF-α production was dependent on both a high concentration of DOX and a longer treatment period. TNF-α was significantly up-regulated after 120 hours of treatment with 0.2 μM DOX [9.33 ± 0.31 pg/mL (p = 0.0004)] compared to the control (7.97 ± 0.16 pg/mL). However, when treatment concentrations of DOX were high (≥ 1 μM), TNF-α was constantly produced at significantly high levels.

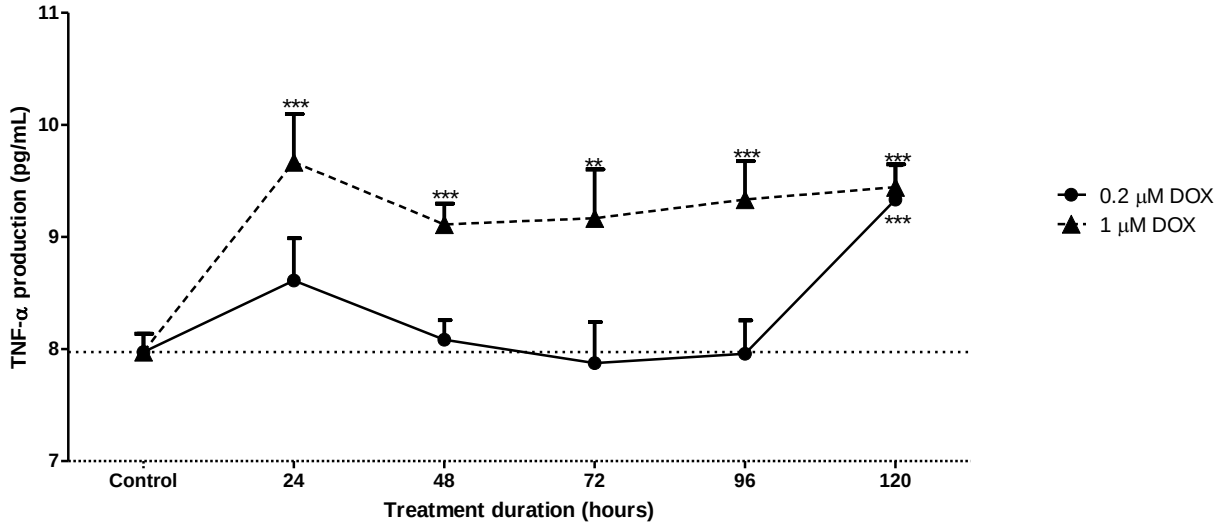


**Figure 4.3: Quantification of TNF-α production by C2C12 myotubes after DOX treatment.** TNF-α in cell culture medium was quantified using an ELISA kit. All values are presented as mean ± SEM, n = 3, *p< 0.05, **p< 0.01, ***p< 0.001.

### 4.2.1 TNF-α is expressed in a time- and dose-dependent manner

TNF-α is a pleiotropic cytokine that is produced as a 26 kDa plasma membrane-associated protein, which can be cleaved into a 17 kDa soluble subunit. In addition to the ELISA, this study wanted to determine the protein expression of this protein. As indicated in Figure 4.4, TNF-α protein expression was significantly up-regulated in a time- and dose-dependent manner in the H9c2 cells. What was interesting to note was the relatively lower levels of TNF-α expression when treatment concentrations were high, compared to when they were lower. In addition, significantly more TNF-α was produced after treatment with 0.2 µM for 120 hours (resulting in a cumulative dose of 1 µM) compared to a single treatment of 1 µM for 24 hours.

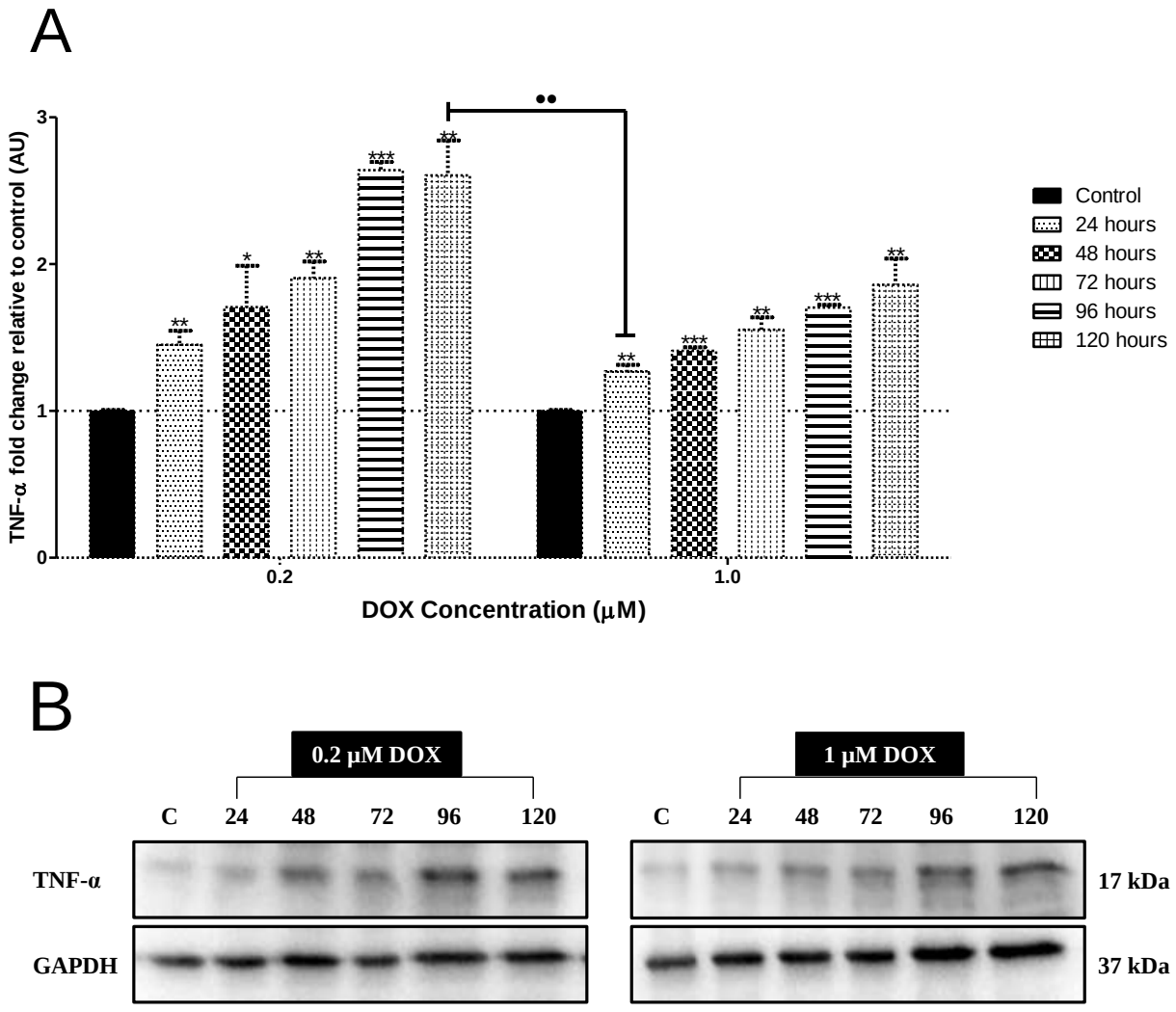


**Figure 4.4: Evaluation of TNF-α protein expression in H9c2 cardiomyocytes.** The lane profile analysis (**A**) and western blots (**B**) are represented. The fold change relative to the control was

calculated. All values are presented as mean ± SEM, arbitrary units (AU), n = 3, *p< 0.05, **p< 0.01, ***p< 0.001 vs control. ●●p < 0.01 120h (0.2 µM) vs 24h (1 µM). GAPDH was used to correct for any loading discrepancies.

The response in the differentiated C2C12 myotubes was different (Figure 4.5), as TNF-α expression was delayed and peaked only after 48 hours when compared to the control. This increased expression remained significantly elevated through-out the treatment period at both concentrations of DOX. However, by 120 hours, after treatment with 1 µM DOX, TNF-α expression had returned to baseline. Significantly more TNF-α was again observed after cumulative treatment with 0.2 µM for 120 hours (1 µM) than after a single treatment of 1 µM for 24 hours. Furthermore, while the 17 kDa fragment of TNF-α was detected in the H9c2 cardiomyocytes, the 25 kDa fragment was detected in C2C12 myotubes.

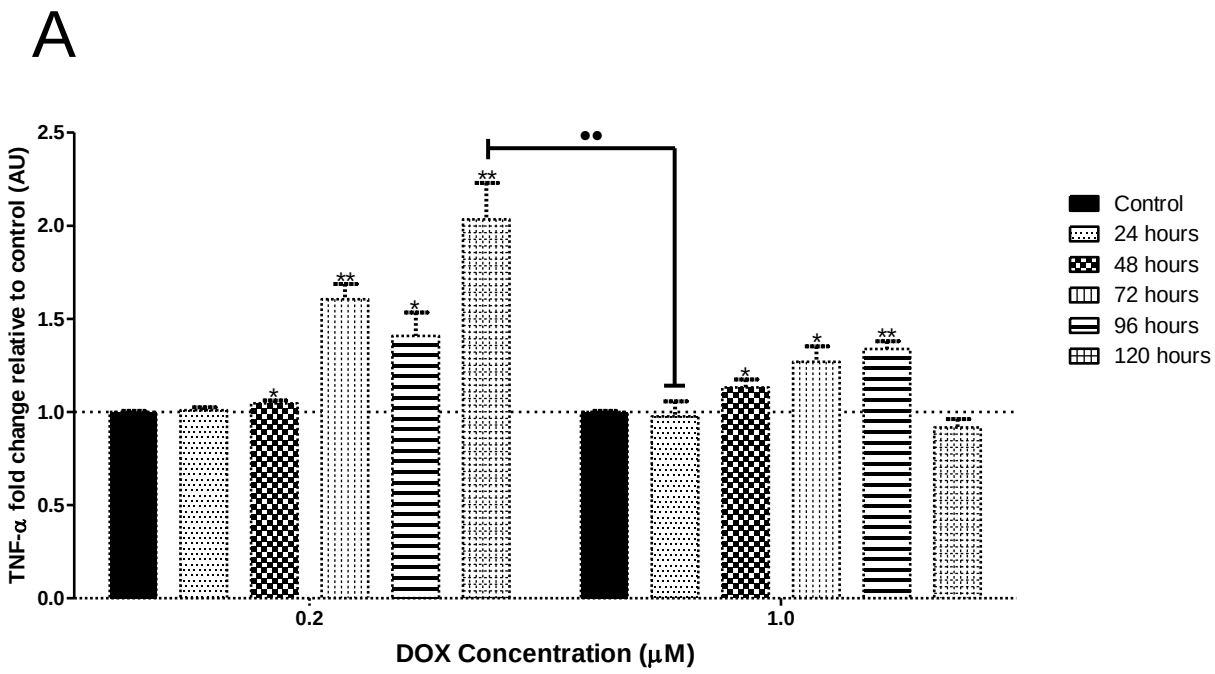

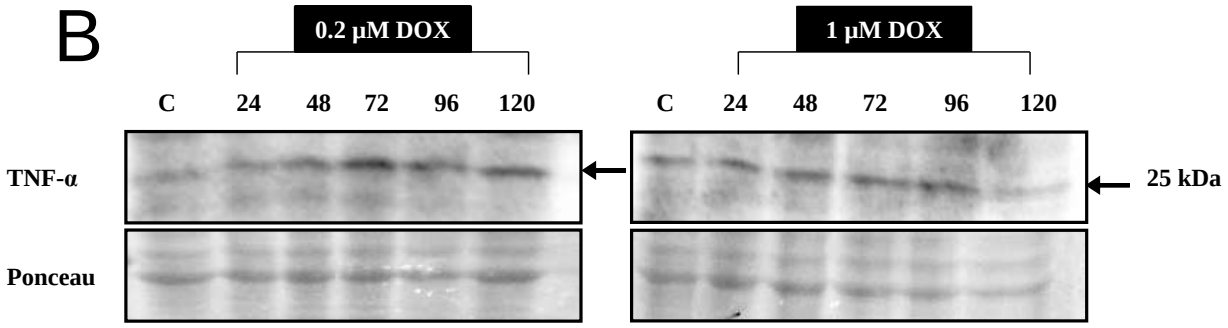


**Figure 4.5: Analysis of TNF-α protein expression in differentiated C2C12 myotubes.** The lane profile analysis (**A**) and western blots (**B**) are represented. The fold change relative to the control was calculated. All values are presented as mean ± SEM, arbitrary units (AU), n = 3, *p< 0.05, **p< 0.01, ***p< 0.001 vs control. ●●p < 0.01: 120h (0.2 µM) vs 24h (1 µM). Ponceau was used as a loading control.

### 4.2.2 TNF-α functions via two receptors

TNF-α functions through two distinct receptors, TNFR1 and TNFR2, found on the surface of almost every nucleated cell type (Vandenabeele *et al.*, 1995). While the affinity of TNF-α for TNFR2 is almost 5 times that for TNFR1, it is TNFR1 that performs the majority of biological activities (Tartaglia and Goeddel, 1992) Although TNF-α can exert both beneficial and detrimental effects depending on which receptor it activates, the overall effects of TNF-α appear to be dependent on the concentration of the cytokine (Tracey *et al*., 1989).

On the one hand our results illustrate that TNF-α receptor expression was heavily influenced by the dose and duration of treatment in the H9c2 cardiomyocytes (Figure 4.6). Significant TNFR1 expression was evident by 48 hours and gradually increased as the concentration increased. These results mimicked those observed for TNF-α expression (Figure 4.4) in the H9c2 cells. A significant increase in TNFR1 expression was also observed after chronic treatment with 0.2 µM (giving a cumulative dose of 1 µM) compared to acute treatment with 1 µM, suggesting that in chronic cytotoxicity TNF-α exerts detrimental effects through TNFR1 signaling.

In the differentiated C2C12 myotubes, TNFR1 was significantly down-regulated by 120 hours irrespective of the treatment concentration (Figure 4.7). Although a significant increase was observed after 72 hours of treatment with 0.2 µM DOX [1.61 ± 0.11 AU (p = 0.0046)], this effect was transient and was thus not maintained.

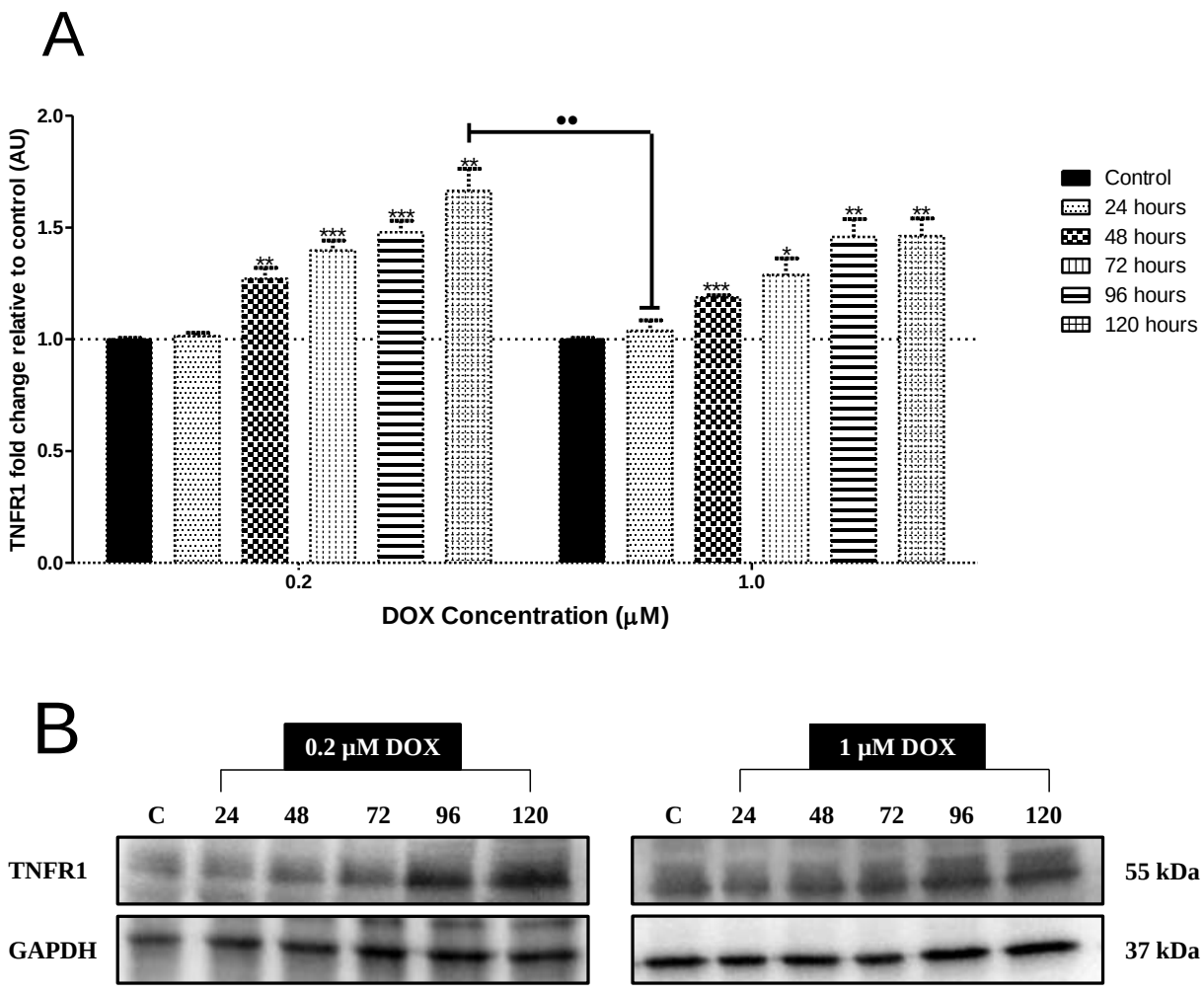


**Figure 4.6: Evaluation of TNFR1 expression in H9c2 cardiomyocytes treated with DOX.** The lane profile analysis (**A**) and western blots (**B**) are represented. The fold change relative to the control was calculated. All values are presented as mean ± SEM, arbitrary units (AU), n = 3, *p< 0.05, **p< 0.01, ***p< 0.001 vs control. ●● p< 0.01 120h (0.2 µM) vs 24h (1 µM). TNFR1, tumor necrosis factor receptor 1. GAPDH was used as a correction for any loading discrepancies.

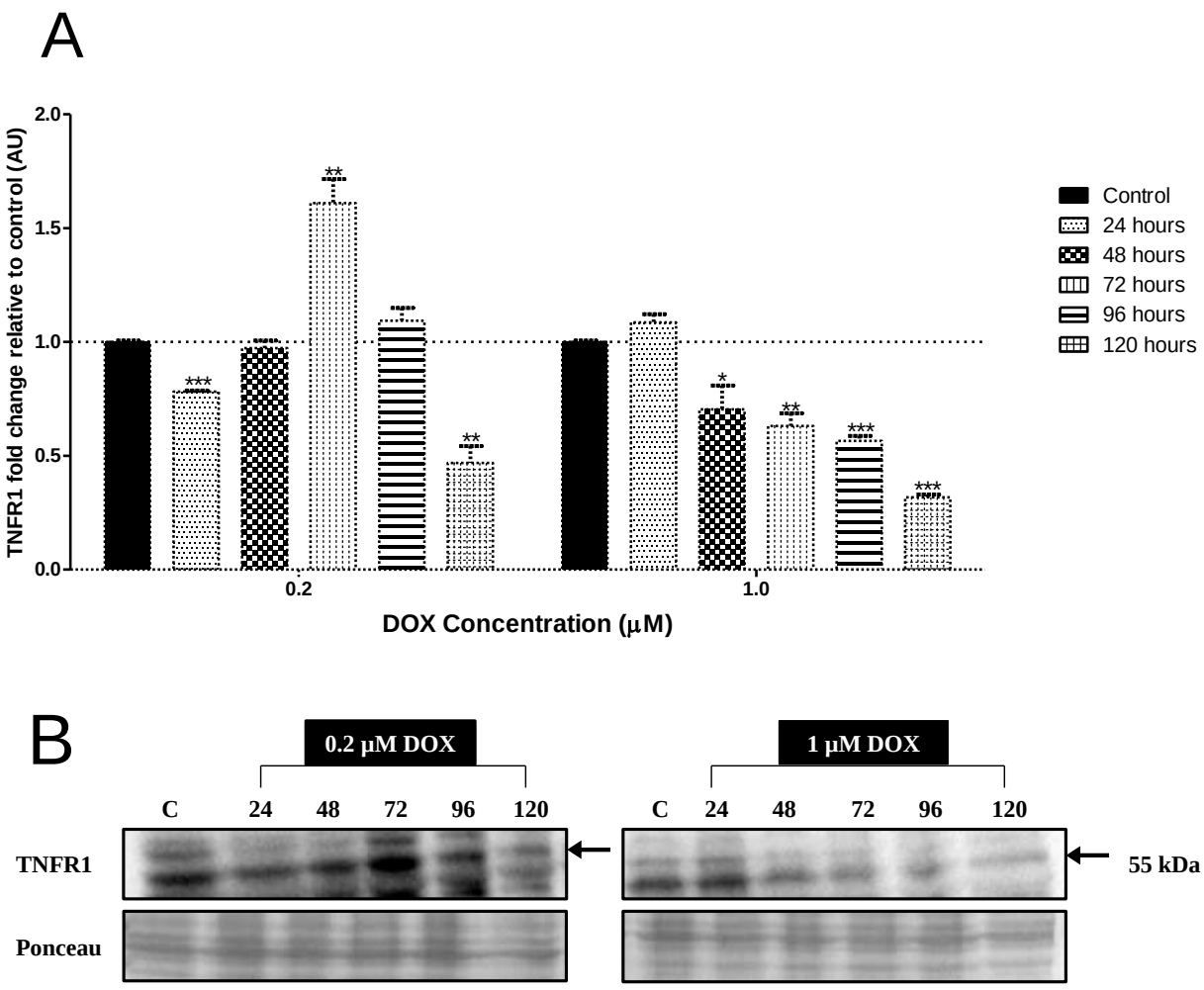


**Figure 4.7: Analysis of TNFR1 protein expression in differentiated C2C12 myotubes.** The lane profile analysis (**A**) and western blots (**B**) are represented. The fold change relative to the control was calculated. All values are presented as mean ± SEM, arbitrary units (AU), n = 3, *p< 0.05, **p< 0.01, ***p< 0.001. A Ponceau stain was used as a loading control.

On the other hand, TNFR2 expression in the H9c2 cardiomyocytes remained below baseline for the first 48 hours at both concentrations of DOX (Figure 4.8). However, a unique observation was noted after 48 hours; TNFR2 expression was severely down-regulated at both the low and high concentration [0.04 ± 0.01 AU and 0.05 ± 0.01 AU ($p < 0.0001$) respectively]. As treatment continued, TNFR2 became significantly expressed, reaching a maximum after 96 hours of treatment with 0.2 µM [2.17 ± 0.26 AU ($p = 0.0007$)] and 1 µM [1.78 ± 0.17 AU ($p = 0.0006$)]. A significant difference was again observed between chronic treatment with a low dose and acute treatment with a high dose. This suggests that during chronic treatment with DOX, TNFR2

signaling is also up-regulated in an attempt to oppose the detrimental effects associated with TNFR1.

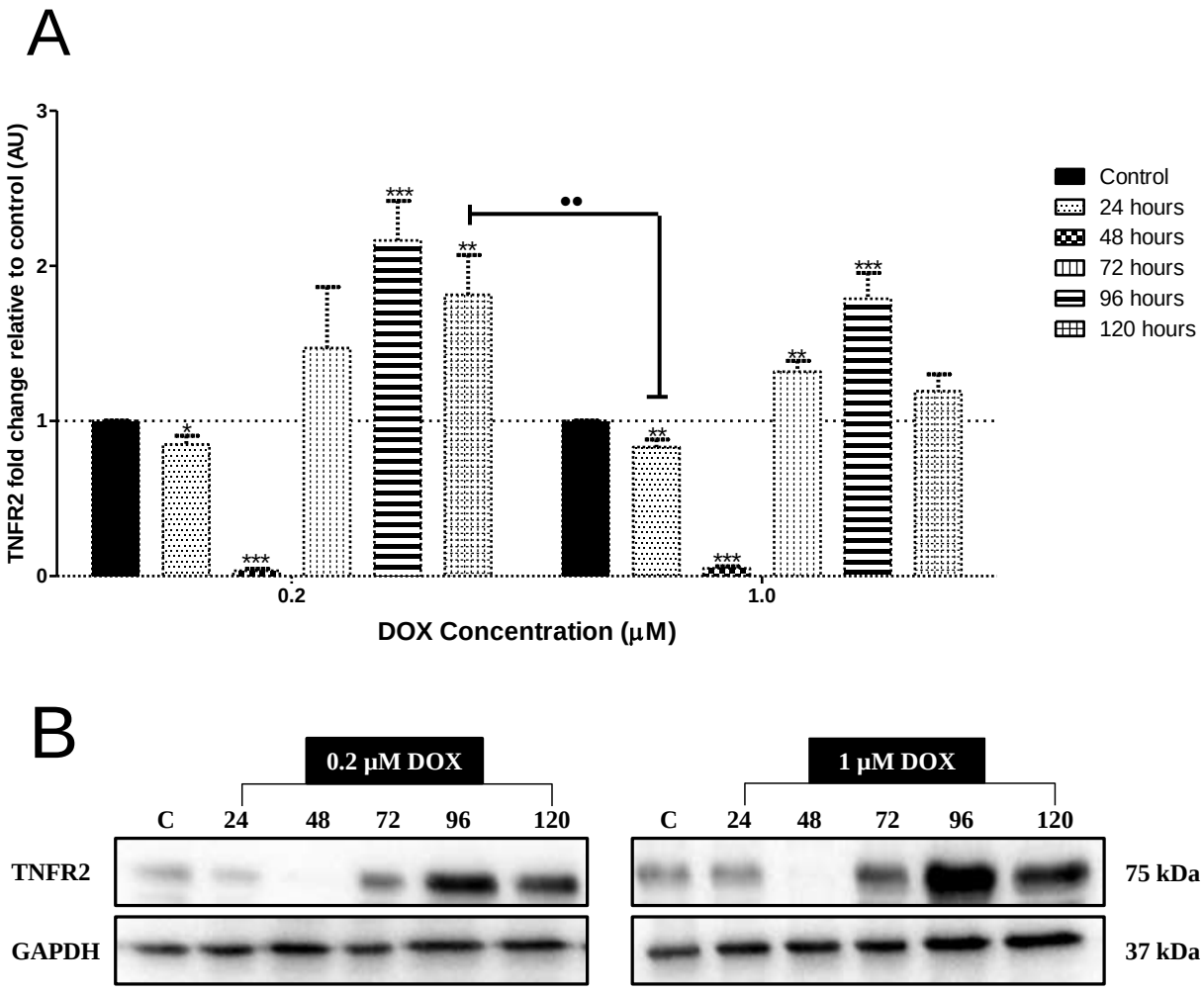


**Figure 4.8: Evaluation of TNFR2 expression in H9c2 cardiomyocytes treated with DOX.** The lane profile analysis (**A**) and western blots (**B**) are represented. The fold change relative to the control was calculated. All values are presented as mean ± SEM, arbitrary units (AU), n = 3, *p< 0.05, **p< 0.01, ***p< 0.001 vs control. ●●p< 0.01 120h (0.2 µM) vs 24h (1 µM). TNFR2, tumor necrosis factor receptor 2. GAPDH was used to correct any loading discrepancies.

TNFR2 was barely detectable in the differentiated C2C12 myotubes (Figure 4.9), with receptor expression being down-regulated for the majority of the treatment period. It was interesting to note that both receptors in this cell line were below control levels for the majority of the treatment duration. This may suggest either receptor saturation or receptor shedding (Zhang *et*

*al*., 2001) as a result of the elevated TNF-α levels detected, as well as highlighting TNF-α's ability to function independently of its receptors.

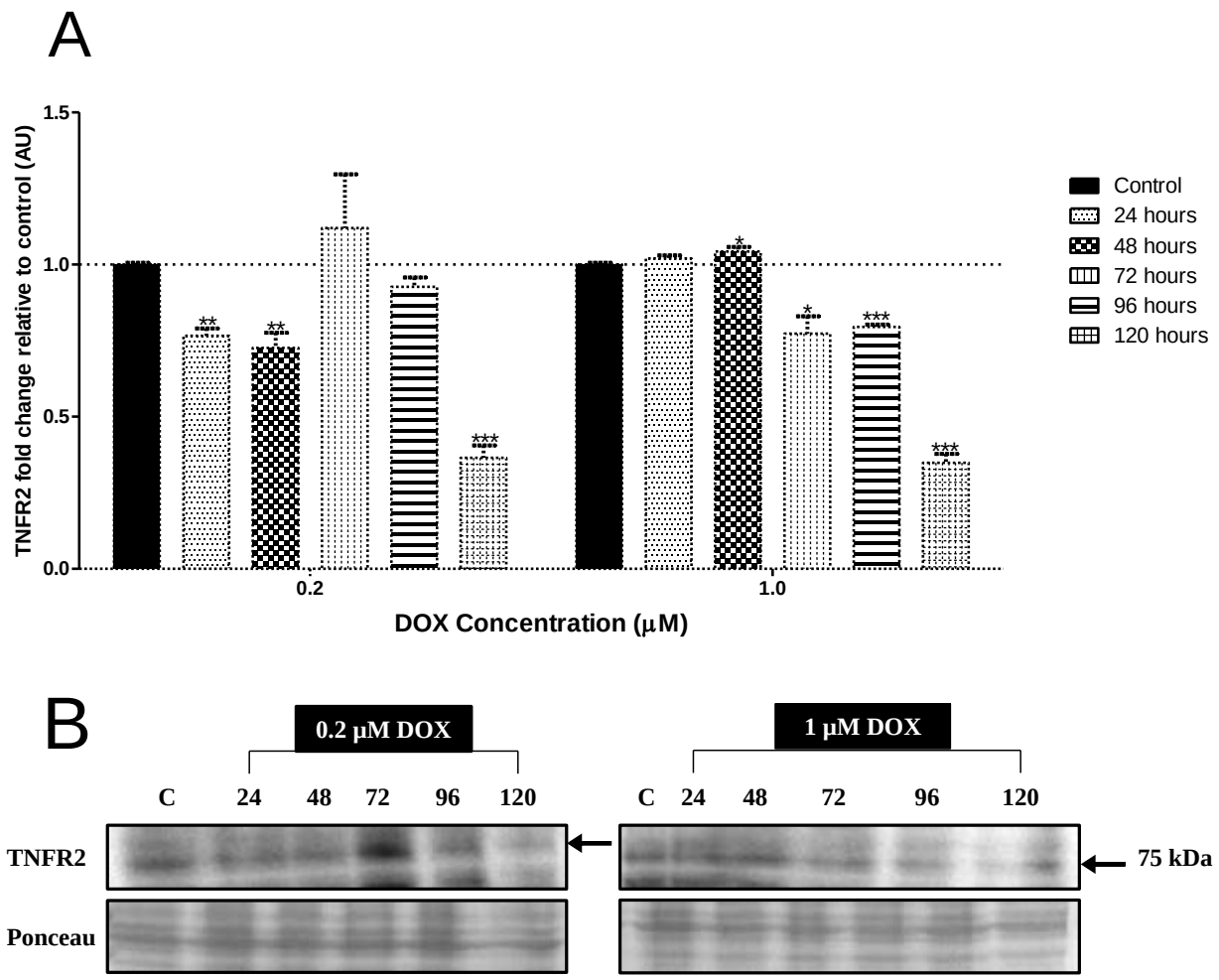


**Figure 4.9: Analysis of TNFR2 protein expression in differentiated C2C12 myotubes.** The lane profile analysis (**A**) and western blots (**B**) are represented. The fold change relative to the control was calculated. All values are presented as mean ± SEM, arbitrary units (AU), n = 3, *p< 0.05, **p< 0.01, ***p< 0.001. TNFR2, tumor necrosis factor receptor 2. A Ponceau stain was used to correct for loading discrepancies.

### 4.3 DOX treatment is (un)SAFE for the heart

The JAK-STAT pathway has been evolutionarily conserved from slime molds to humans and facilitates intercellular communication (Aaronson and Horvath, 2002). Once activated by cytokines such as TNF-α, the JAK-STAT pathway modulates proliferation, differentiation, cell

migration and apoptosis, ultimately providing a mechanism to transduce extracellular signals into transcriptional responses (Rawlings *et al*., 2004). Since TNF-α was detected in this model of cytotoxicity, this study investigated whether the SAFE pathway was also activated in the context of cytotoxicity.

In H9c2 cardiomyocytes, p-Jak2 expression was increased significantly in a time- and dose-dependent manner after treatment with the low dose of DOX (Figure 4.10A and B). This effect was however lost after treatment with the high concentration (1 µM) of DOX. Treatment with the low dose of DOX not only affected Jak2 phosphorylation but also had a positive impact on total Jak-2 protein expression (Figure 4.10C). A 2.5 – to 3-fold increase in total Jak2 protein expression was observed compared to the control, suggesting that treatment with low doses of DOX up-regulates the protein synthesis of Jak2. No changes in total protein expression were observed following treatment with the high concentration of DOX when compared to the control. Figure 4.10D represents the phosphorylated protein to total protein ratio. From this graph it is clear that Jak-2 was activated in the chronic setting but not in the acute setting following treatment with the low dose of DOX, however, treatment with the high concentration (1 µM) did not induce Jak-2 phosphorylation. A similar pattern was also observed in TNFR2 expression, suggesting that TNF-α-TNFR2-Jak2 signaling may have contributed to the increase in cell viability and the decrease in apoptotic cell death that was observed at this point in the H9c2 cardiomyocytes.

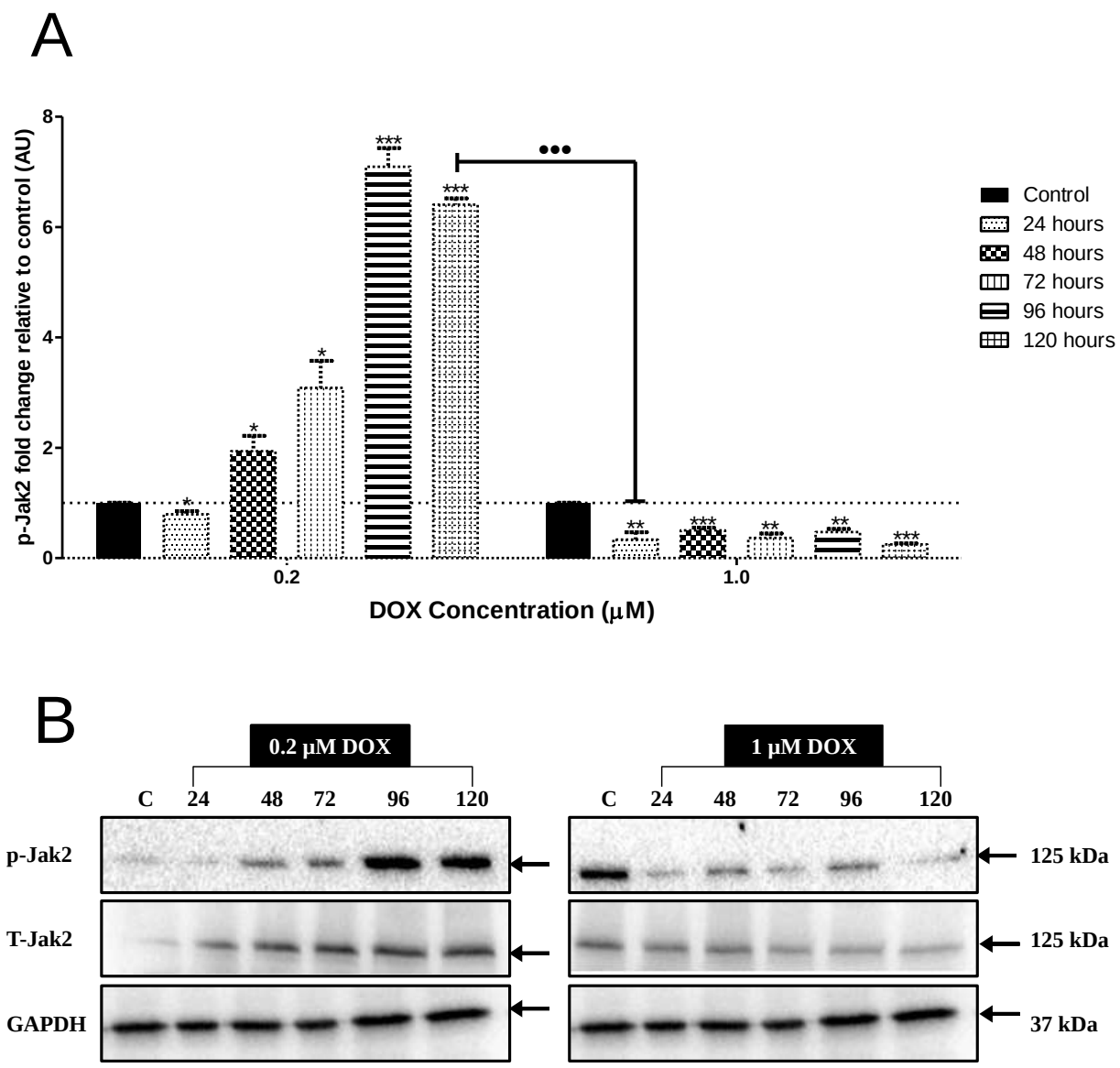


**Figure 4.10A and B: Protein expression of p-Jak2 and T-Jak2 in H9c2 cells.** The lane profile analysis of p-Jak-2 (**A**) and western blots of p-Jak2 and T-Jak-2 (**B**) are represented. The fold change relative to the control was calculated. All values are presented as mean ± SEM, arbitrary units (AU), n = 3, *p< 0.05, **p< 0.01, ***p< 0.001. p-Jak2, phospho-Jak2, T-Jak2, total-Jak2. GAPDH was used to correct for any loading discrepancies.

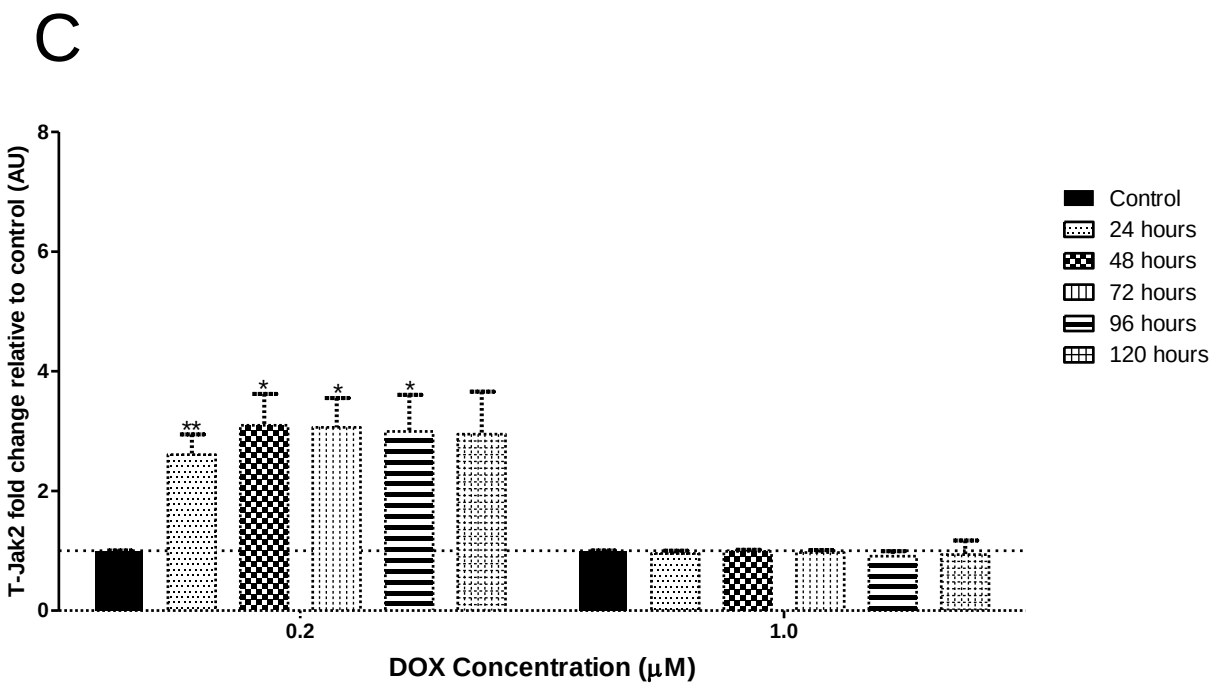


**Figure 4.10C: Protein expression of T-Jak2 in H9c2 cells.** The lane profile analysis of T-Jak-2 is represented. The fold change relative to the control was calculated. All values are presented as mean ± SEM, arbitrary units (AU), n = 3, *p< 0.05, **p< 0.01, ***p< 0.001. GAPDH was used to correct for any loading discrepancies.

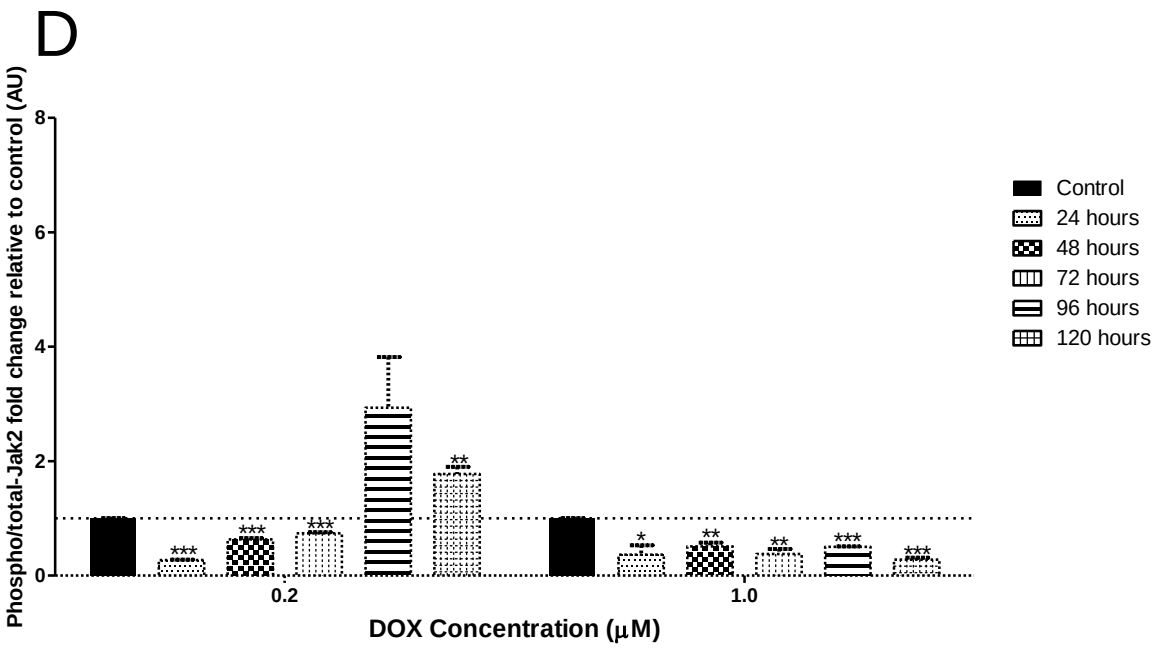


**Figure 4.10D: Protein expression of Jak2 in H9c2 cells.** The lane profile analysis of phosphorylated protein to total protein ratio of Jak2 is represented. The fold change relative to the control was calculated.

All values are presented as mean ± SEM, arbitrary units (AU), n = 3, *p< 0.05, **p< 0.01, ***p< 0.001. GAPDH was used to correct for any loading discrepancies.

Treatment with DOX significantly down-regulated the protein expression of p-Jak2 compared to the controls in the differentiated C2C12 myotubes (Figure 4.11A and B) and this effect was noted in every treatment group. No significant differences were observed in the protein expression of total Jak2. Analysis of total Jak2 can be found in appendix A, page 129.

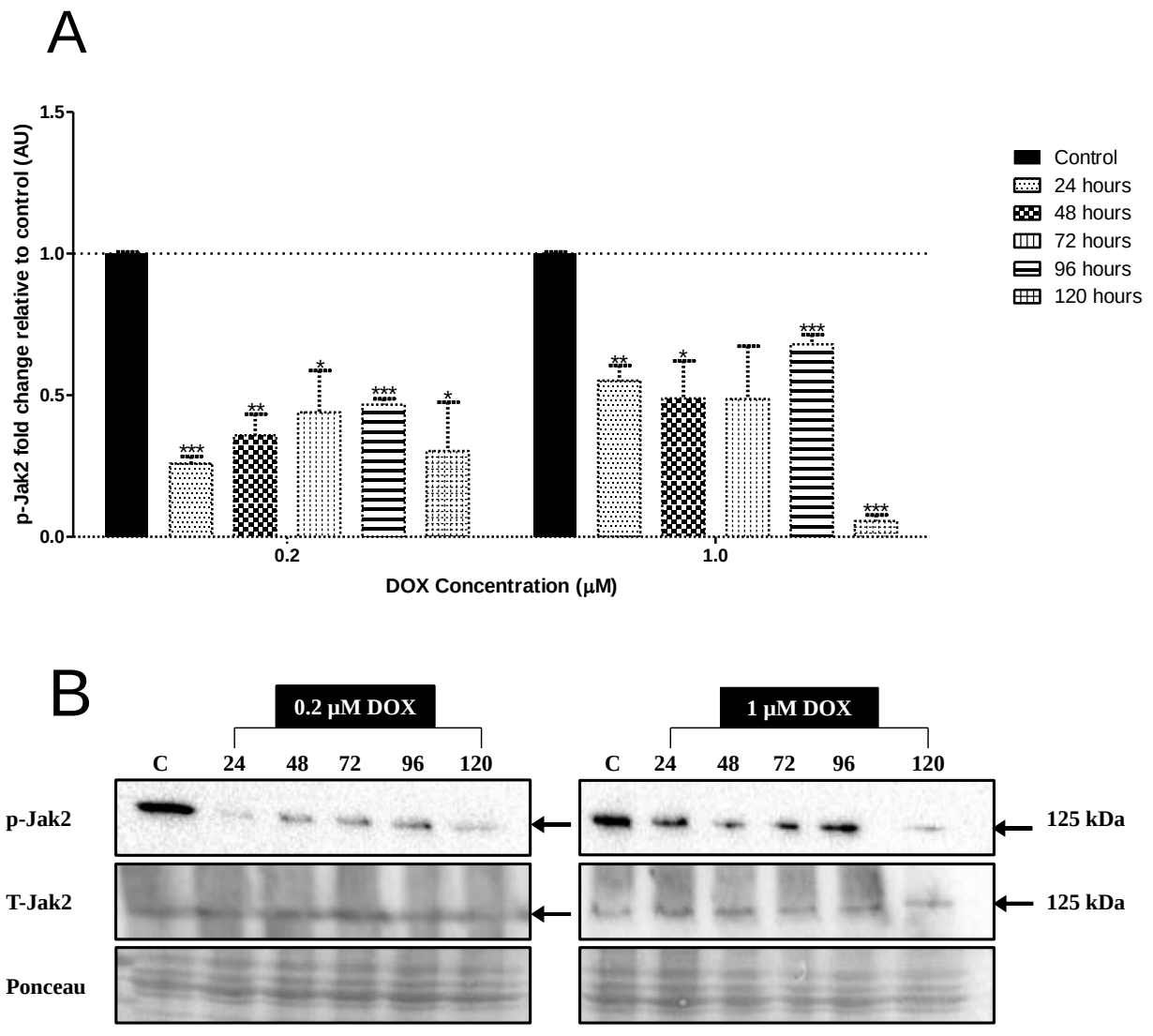


**Figure 4.11A and B: Protein expression of p-Jak2 and T-Jak2 in differentiated C2C12 myotubes.** The lane profile analysis (**A**) and western blots (**B**) of Jak2 are represented. The fold change relative to the control was calculated. All values are presented as mean ± SEM, arbitrary units (AU), n = 3, *p< 0.05, **p< 0.01, ***p< 0.001. Ponceau was used to correct for loading discrepancies.

STATs reside as inactive transcription factors in the cytoplasm, until they are activated by several growth factors and cytokines such as TNF-α (Levy and Darnell, 2002). STATs are phosphorylated at a single tyrosine residue which is essential for activation (Levy and Darnell, 2002). Phosphorylation at this site allows STAT to homodimerize and translocate to the nucleus where it stimulates transcription (Paulson, 1999). In addition, ligand-dependent phosphorylation at serine 727 is thought to enhance transcriptional activation of STAT3 (Levy and Darnell, 2002).

As indicated in the figures below, STAT3 phosphorylation was significantly up-regulated in the H9c2 cardiomyocytes at both tyrosine 705 (Figure 4.12A and B) and serine 727 (Figure 4.12C and D) when compared to the control. This effect was however only noted with low concentrations of DOX. High concentrations of DOX significantly reduced the phosphorylation of both STATs, possibly as a result of the decreased phosphorylation of Jak2 (Figure 4.10). When two bands were present in p-STAT3 expression, the lane profile analysis was calculated as a sum of the 79 kDa and 86 kDa fragments. Total protein expression remained unchanged throughout the treatment regime. Analysis of total STAT3 expression can be found in appendix A, page 129.

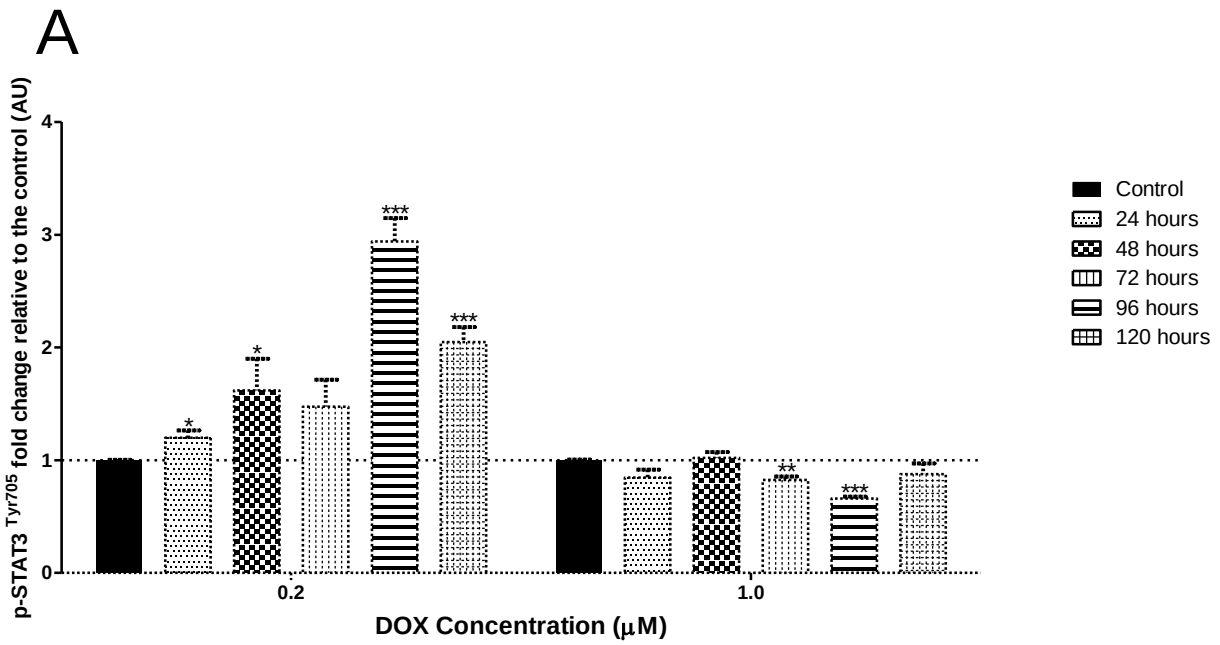

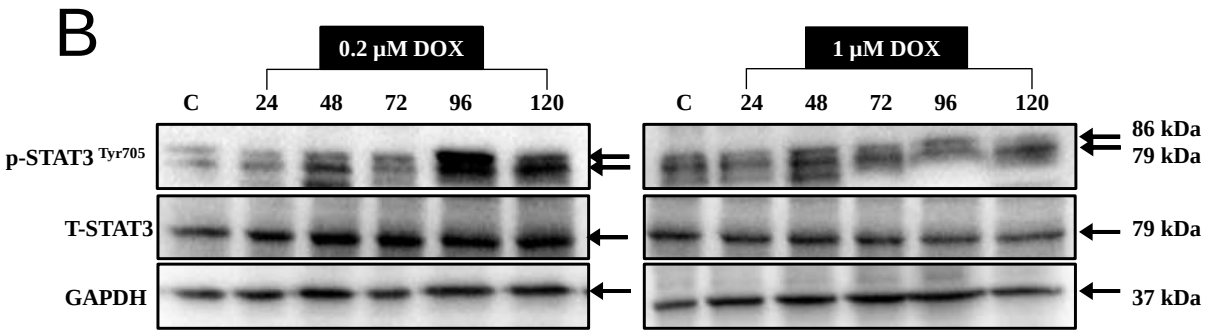


**Figure 4.12A and B: Protein expression of p-STAT3 $^{Tyr705}$ and T-STAT3 in H9c2 cells.** The lane profile analysis (**A**) and western blots (**B**) are represented. The fold change relative to the control was calculated. All values are presented as mean ± SEM, arbitrary units (AU), n = 3, *p< 0.05, **p< 0.01, ***p< 0.001. GAPDH was used as a loading control to correct for any discrepancies.

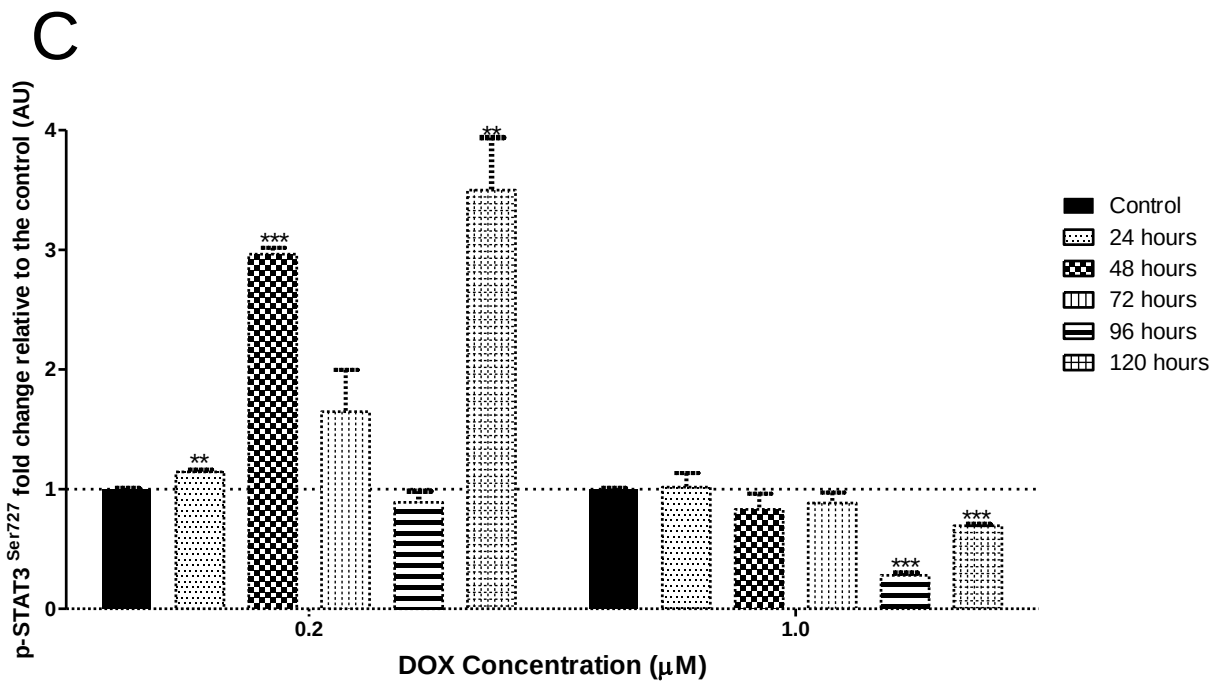

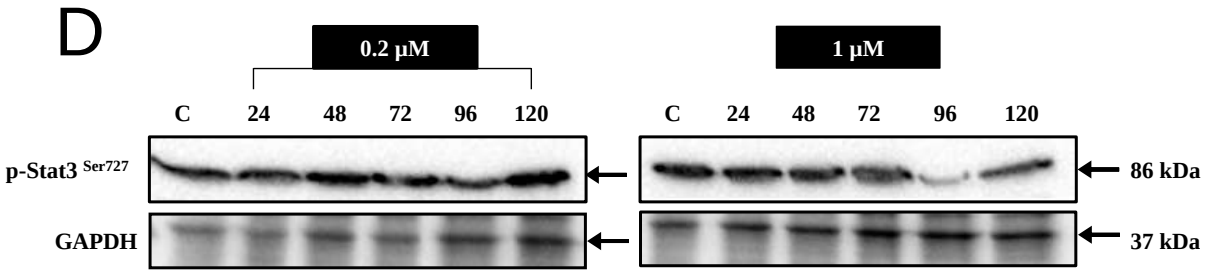


**Figure 4.12C and D: Protein expression of p-STAT3 $^{Ser727}$ in H9c2 cells.** The lane profile analysis (**C**) and western blots (**D**) are represented. The fold change relative to the control was calculated. All values are presented as mean ± SEM, arbitrary units (AU), n = 3, *p< 0.05, **p< 0.01, ***p< 0.001. GAPDH was used as a loading control to correct for any discrepancies.

In the differentiated C2C12 myotubes treatment with 0.2 µM DOX resulted in relatively no change in STAT3 $^{Tyr705}$ phosphorylation (Figure 4.13A and B). When the concentration of DOX was higher (1 µM), p-STAT3 $^{Tyr705}$ expression increased as the concentration increased, reaching maximum after 96 hours of treatment [2.22 ± 0.13 AU (p = 0.0007)]. p-STAT3 $^{Ser727}$ was acutely activated following treatment with the low dose of DOX (Figure 4.13C and D), but activation of this residue declined significantly by 120 hours [0.56 ± 0.03 AU (p = 0.0002)]. Phosphorylation on serine727 decreased in a time- and dose-dependent manner after treatment with the high dose of DOX, when compared to the control. When two bands were present in p-STAT3 expression, the lane profile analysis was calculated as a sum of the 79 kDa and 86 kDa fragments. Total protein expression remained unchanged throughout the treatment regime. Analysis of total STAT3 expression can be found in appendix A, page 130.

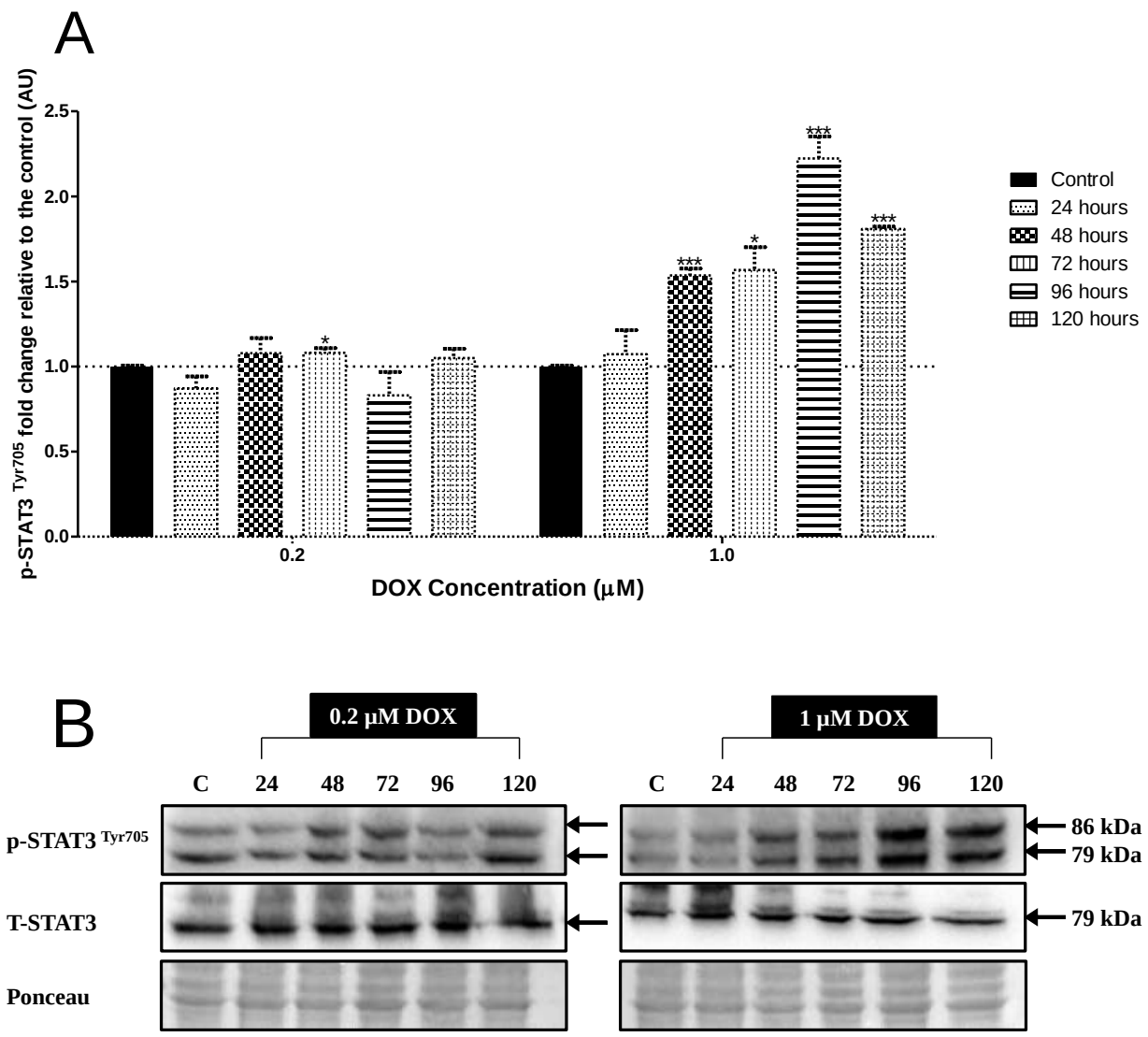


**Figure 4.13A and B: Protein expression of p-STAT3 $^{Tyr705}$ and T-STAT3 in C2C12 myotubes.** The lane profile analysis (**A**) and western blots (**B**) are represented. The fold change relative to the control was calculated. All values are presented as mean ± SEM, arbitrary units (AU), n = 3, *p< 0.05, **p< 0.01, ***p< 0.001. Ponceau was used as a loading control to correct for any discrepancies.

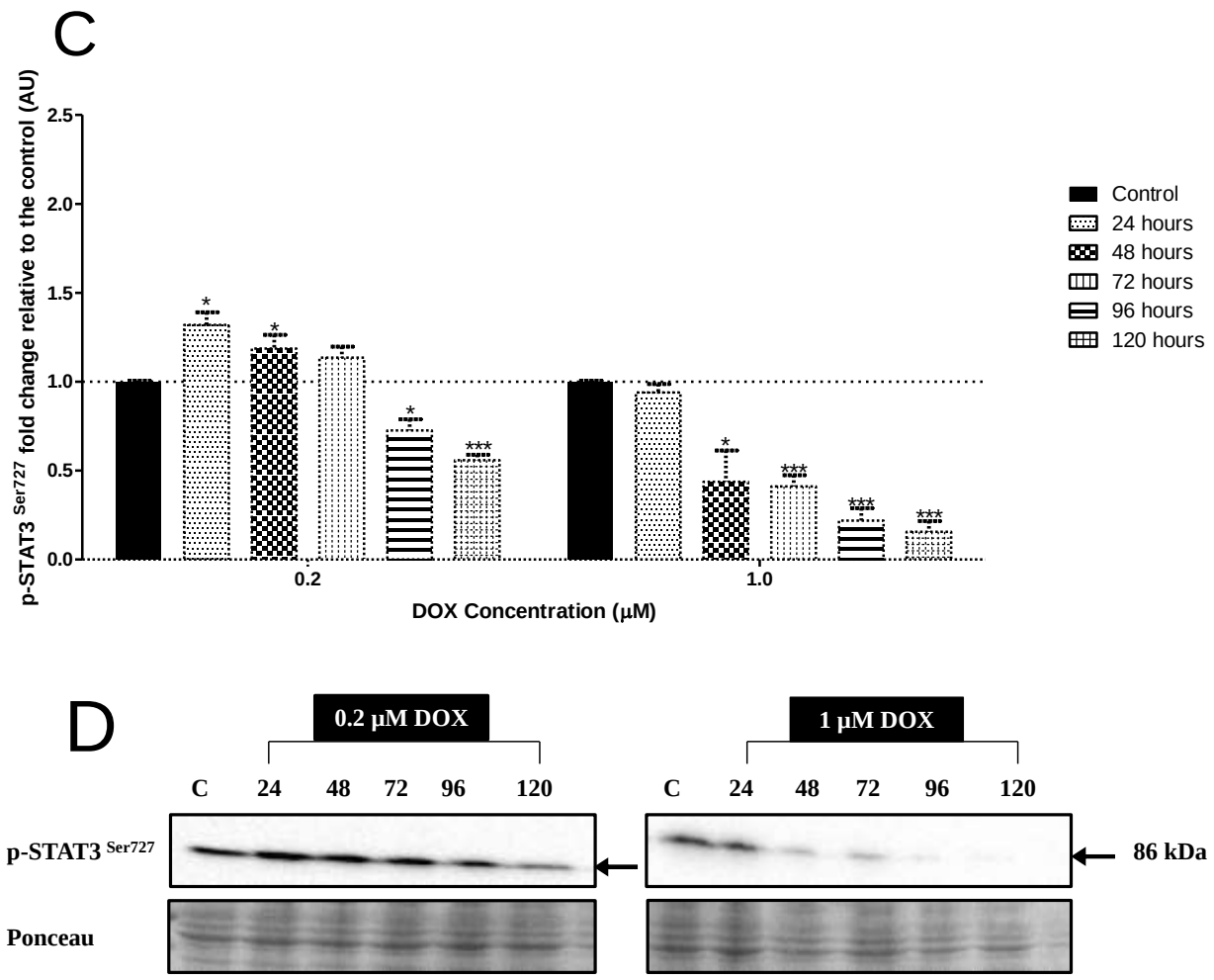


**Figure 4.13C and D: Protein expression of p-STAT3 $^{Ser727}$ in C2C12 myotubes.** The lane profile analysis (**C**) and western blots (**D**) are represented. The fold change relative to the control was calculated. All values are presented as mean ± SEM, arbitrary units (AU), n = 3, *p< 0.05, **p< 0.01, ***p< 0.001. Ponceau was used as a loading control to correct for any discrepancies.

Based on these results it is clear that activation of the SAFE pathway is the presence of DOX is quite distinct between the two cell lines. While the SAFE pathway in the H9c2 cardiomyocytes was activated after chronic exposure to low doses of DOX, activation of this pathway in the presence of high concentrations of DOX was not evident. In the differentiated C2C12 myotubes, STAT3 activation occurred independently of Jak2 phosphorylation. Furthermore, phosphorylation of the tyrosine residue required chronic, high levels of DOX treatment whereas phosphorylation of the serine residue required acute low levels of DOX.

### 4.4 The 'RISK' associated with DOX-induced cytotoxicity

Ischemic pre- and post-conditioning have been shown to activate the pro-survival kinases of the RISK pathway, Erk1/2 and Akt (Hausenloy and Yellon, 2004). Like the SAFE pathway, activation of the RISK pathway reduces the amount of reperfusion-injury related myocardial damage. Both of the above mentioned kinases are members of pro-survival pathways and it is believed that activation of these pathways confers protection through phosphorylation and inhibition of several pro-apoptotic proteins (Hausenloy and Yellon, 2004). Since oxidative stress and apoptosis mediate the damage induced by reperfusion injury, we proposed that the RISK pathway might also be activated in response to DOX treatment, seeing that apoptosis and oxidative stress are the two main role players in this scenario.

In the H9c2 cardiomyocytes, protein expression of p-Akt was significantly greater than that of the control during the first three days of treatment with 0.2 µM DOX (Figure 4.14A and B). Thereafter phosphorylation declined significantly by 120 hours when compared to the control. Treatment with 1 µM DOX did not affect Akt phosphorylation after the first 24 hours, however, expression was significantly down-regulated as the concentration of DOX increased, reaching a minimum after 120 hours [0.24 ± 0.09 AU ($p = 0.0002$)]). Total Akt expression remained unchanged throughout the treatment period. Analysis of total Akt can be found in appendix A, page 130.

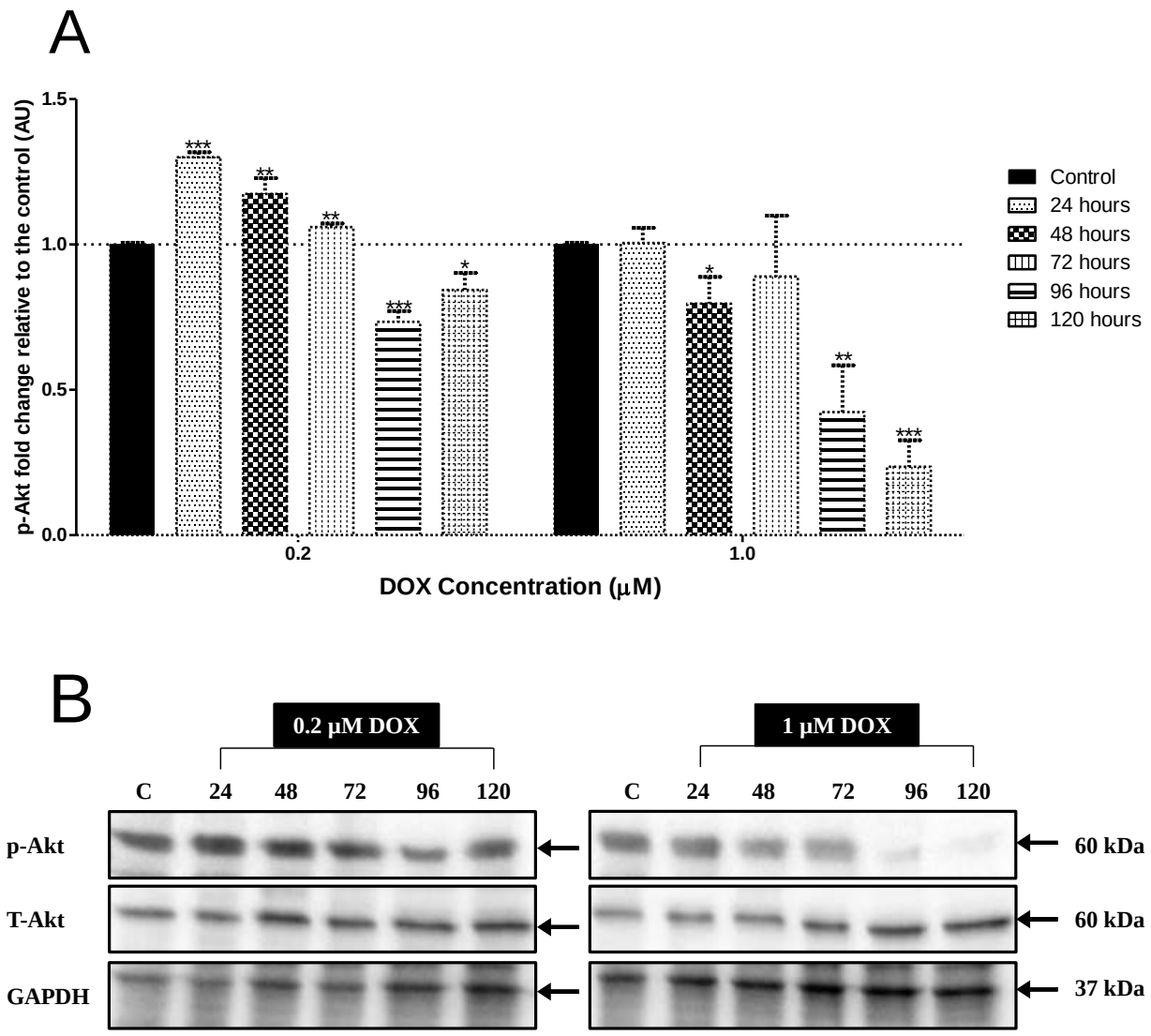


**Figure 4.14A and B: Protein expression of p-Akt and T-Akt in H9c2 cells after DOX treatment.** The lane profile analysis (**A**) and western blots (**B**) are represented. The fold change relative to the control was calculated. All values are presented as mean ± SEM, arbitrary units (AU), n = 3, *p< 0.05, **p< 0.01, ***p< 0.001. p-Akt, phospho-Akt. T-Akt, total-Akt. GAPDH was used to correct for loading discrepancies.

In the differentiated C2C12 myotubes, phosphorylation of Akt was significantly increased during the first 72 hours of treatment with the low dose of DOX, however, this effect had returned to control levels by 120 hours (Figure 4.15A and B). While acute treatment with the high dose of DOX did not cause any changes in Akt phosphorylation during the first 24 hours, Akt phosphorylation increased significantly as treatment continued, reaching a maximum after 96 hours [1.73 ± 0.12 AU (p = 0.0035)]. Again, p-Akt expression returned to baseline by 120 hours

after treatment with this dose. Total Akt protein levels were also affected by treatment with DOX as noted by the significant decrease in expression after treatment with the low dose of DOX and an increasing trend in total Akt expression at the high dose of DOX (Figure 4.15C). Analysis of the phosphorylated Akt to total Akt ratio (Figure 4.15D) revealed an increase after treatment with the low dose of DOX, suggesting that although the total protein was down-regulated, the majority of this protein was phosphorylated. However, treatment with the high concentration of DOX did not induce significant changes, therefore suggesting that DOX prevented Akt phosphorylation of the newly synthesized protein.

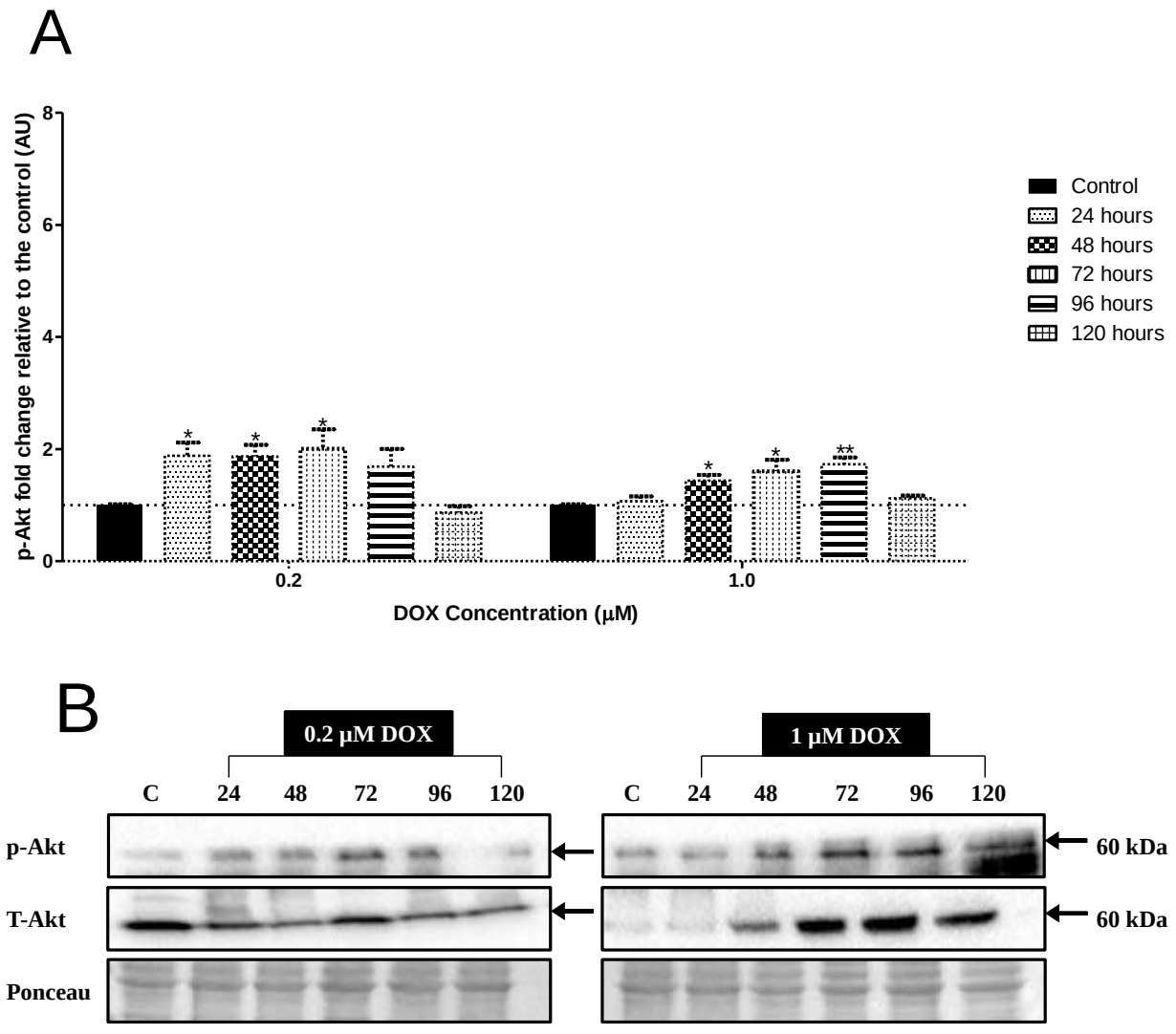


**Figure 4.15A and B: Analysis of p-Akt and T-Akt in C2C12 myotubes.** The lane profile analysis (**A**) and western blots (**B**) are represented. The fold change relative to the control was calculated. All values

are presented as mean ± SEM, arbitrary units (AU), n = 3, *p< 0.05, **p< 0.01, ***p< 0.001. Ponceau was used as a loading control to correct for any discrepancies.

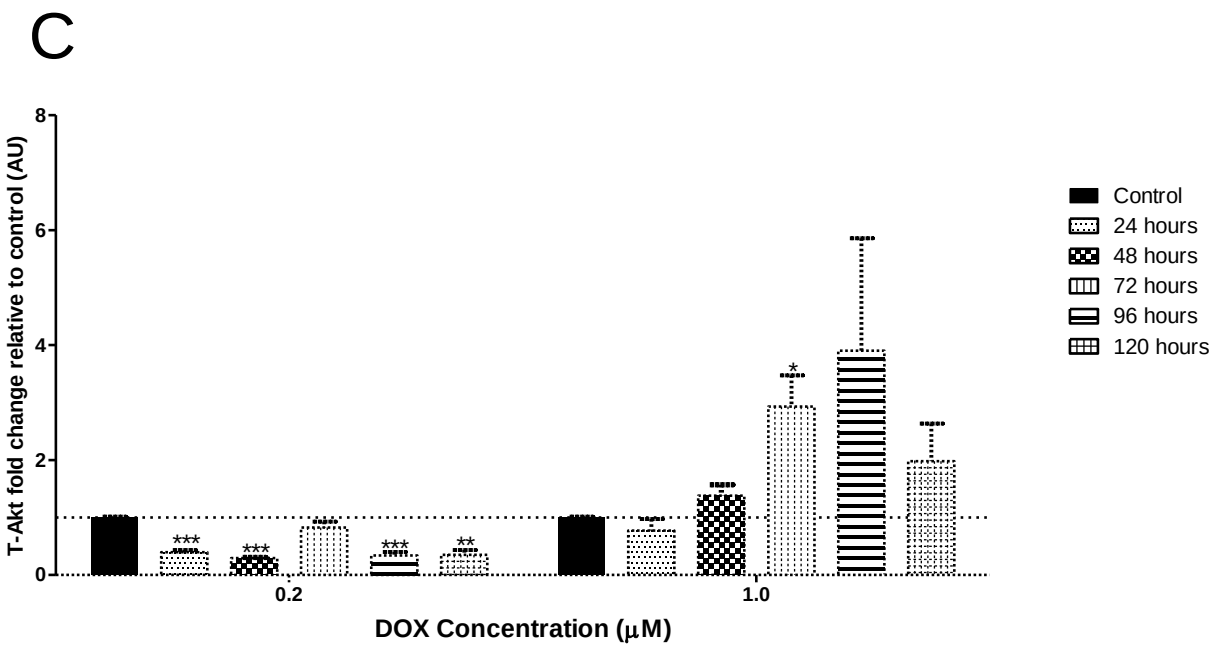


**Figure 4.15C: Analysis of T-Akt in C2C12 myotubes.** The lane profile analysis (**C**) is represented. The fold change relative to the control was calculated. All values are presented as mean ± SEM, arbitrary units (AU), n = 3, *p< 0.05, **p< 0.01, ***p< 0.001. Ponceau was used as a loading control to correct for any discrepancies.

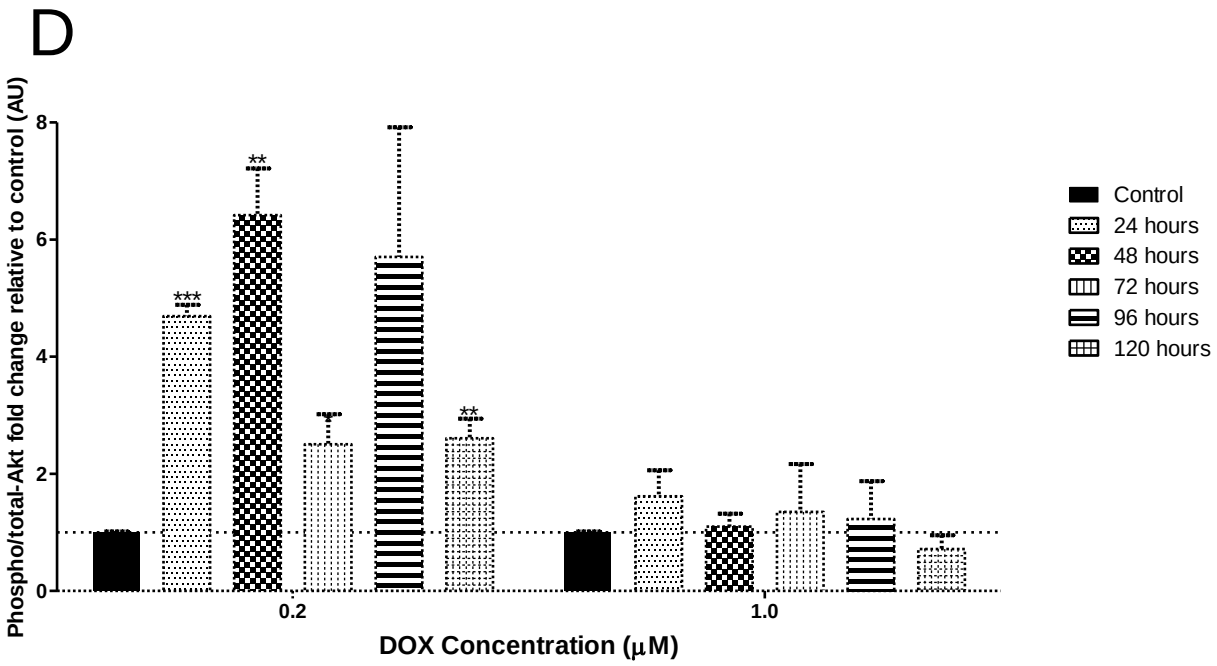


**Figure 4.15D: Analysis of the ratio of phospho/total-Akt in C2C12 myotubes.** The lane profile analysis is represented. The fold change relative to the control was calculated. All values are presented as mean ± SEM, arbitrary units (AU), n = 3, *p< 0.05, **p< 0.01, ***p< 0.001. Ponceau was used as a loading control to correct for any discrepancies.

In the H9c2 cardiomyocytes, Erk1/2 phosphorylation remained unchanged during the first 48 hours of treatment with 0.2 µM DOX (Figure 4.16A and B). However, as the treatment continued, Erk1/2 phosphorylation significantly declined. This observation was also noted when a high concentration (1 µM) of DOX was used. In all instances, only the 42 kDa band was detected. Since the expression of both the 42 kDa and the 44 kDa fragments varies between cell and tissue types, the possibility exists that only one of the two bands is expressed in response to DOX treatment, which is consistent with Zhu *et al*., (1999). Total Erk1/2 expression remained unchanged throughout the treatment regime. Analysis of total Erk1/2 can be found in appendix A, page 131.

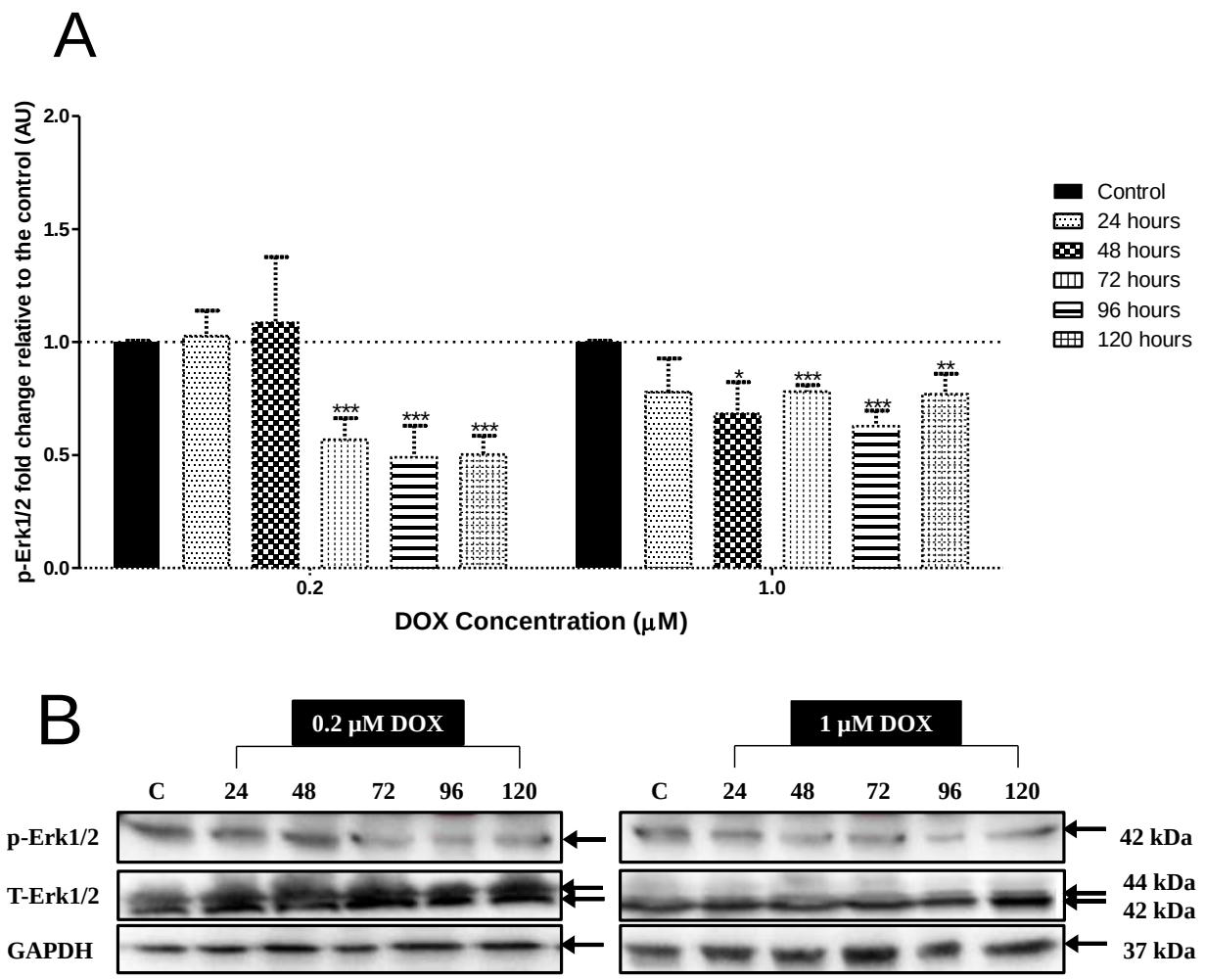


**Figure 4.16A and B: Protein expression of p-Erk1/2 and T-Erk1/2 in H9c2 cells after DOX treatment.** The lane profile analysis (**A**) and western blots (**B**) are represented. The fold change relative to the control was calculated. All values are presented as mean ± SEM, arbitrary units (AU), n = 3, *p< 0.05, **p< 0.01, ***p< 0.001. p-Erk1/2, phospho-Erk1/2. T-Erk1/2, total Erk1/2. GAPDH was used to correct for any loading discrepancies.

In the differentiated C2C12 myotubes, Erk1/2 phosphorylation was down-regulated for the majority of the treatment regime (Figure 4.17A and B). A significant increase in phosphorylation was only observed after 96 hours of treatment with the low dose [1.28 ± 0.07 AU (p = 0.0117)] when compared to the control. Treatment with the high dose of DOX caused an increase in p-Erk1/2 expression after 24 hours, though this was not significant. Further treatment with the low concentration of DOX significantly down-regulated p-Erk1/2 expression. The expression of total

Erk1/2 remained unchanged throughout the treatment protocol. Analysis of total Erk1/2 can be found in appendix A, page 131.

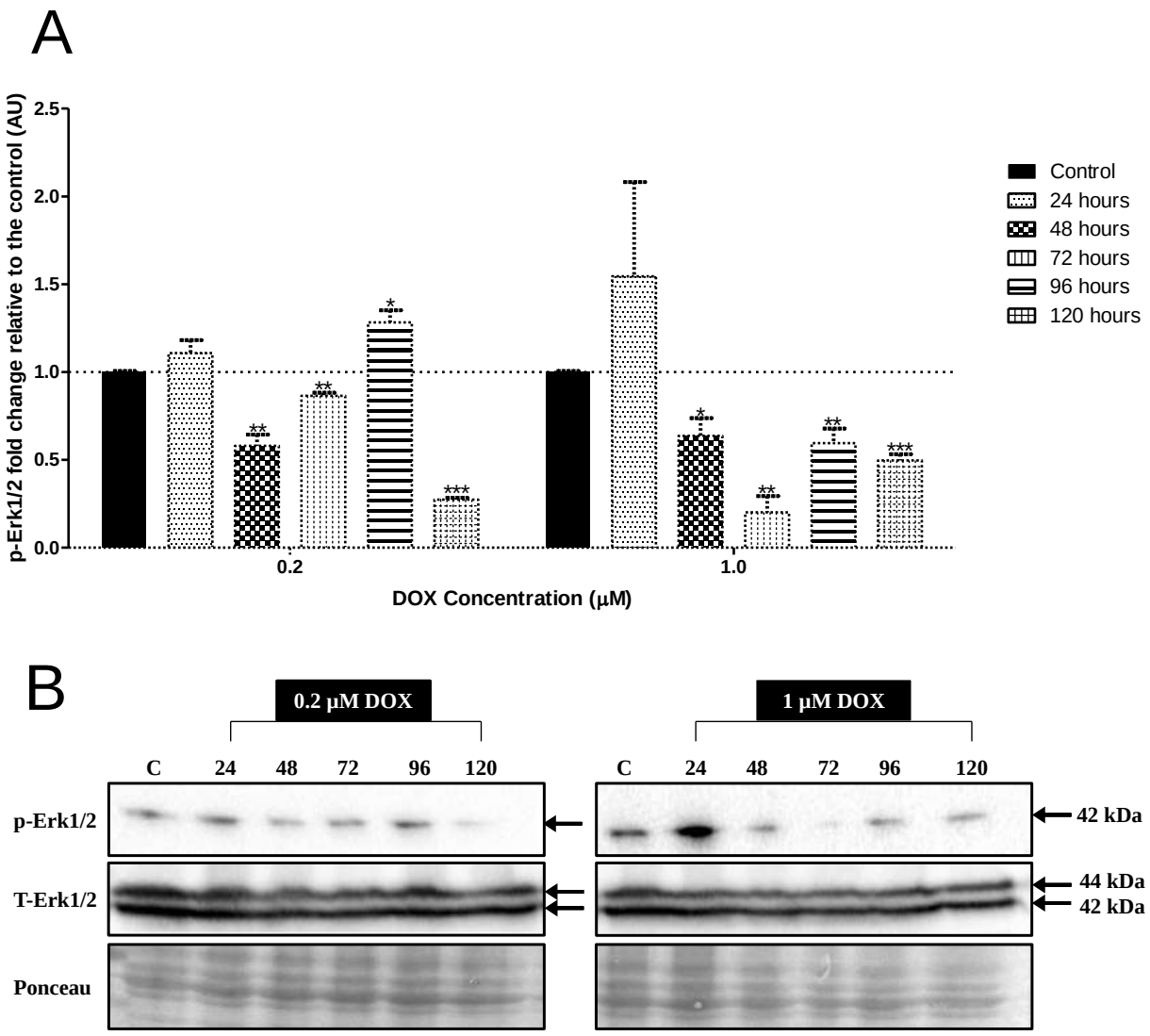


**Figure 4.17A and B: Analysis of p-Erk1/2 and T-Erk1/2 expression in differentiated C2C12 myotubes.** The lane profile analysis (**A**) and western blots (**B**) are represented. The fold change relative to the control was calculated. All values are presented as mean ± SEM, arbitrary units (AU), n = 3, *p< 0.05, **p< 0.01, ***p< 0.001. A Ponceau stain was used to correct for any loading discrepancies.

Based on the above results, it is clear that the RISK pathway is more sensitive to DOX treatment than the SAFE pathway, since it is easily inactivated. This is particularly evident after chronic treatment with the low dose or when the dose of DOX exceeds 1 µM. The inhibition of both pro-survival kinases by DOX may therefore contribute to its cardiotoxic effects.

## 4.5 DOX-induced cytotoxicity is associated with oxidative stress and an antioxidant deficit

### 4.5.1 Treatment with DOX is accompanied by an increase in oxidative stress

It is well known that treatment with DOX results in the production of ROS including peroxyl radicals and hydrogen peroxide. These then mediate the conversion of unsaturated membrane fatty acids into lipid peroxides, which quickly decompose into products such as MDA (Zimmermann *et al*., 1973). Therefore, in order to determine the extent of ROS-induced damage throughout the course of the treatment period, MDA, as measured by the TBARS assay, was assessed.

In H9c2 cardiomyocytes, lipid peroxidation was detected later after treatment with the low dose of DOX and earlier after treatment with the high dose of DOX (Figure 4.18). Treatment with 0.2 µM DOX caused a significant increase in lipid peroxidation after 96 hours [0.38 ± µM ($p = 0.0201$)] and 120 hours [0.31 ± 0.0 µM ($p = 0.0002$)]. Treatment with 1 µM DOX also induced oxidative stress, however, at this concentration a significant level of lipid peroxidation was evident by as early as 72 hours [0.39 ± 0.02 µM ($p = 0.0025$)] and was maintained until after 96 hours [0.30 ± 0.04 µM ($p = 0.0055$)], when compared to the control (0.13 ± 0.03 µM). Although lipid peroxidation had declined by 120 hours, the level was still above that of the control. This decline may be explained by low cell numbers as suggested by the significant decrease in cell viability. A significant increase in lipid peroxidation was also observed between chronic treatment with 0.2 µM (giving a cumulative dose of 1 µM) and acute treatment with 1 µM, emphasizing how chronic cardiotoxicity is more detrimental than acute cardiotoxicity.

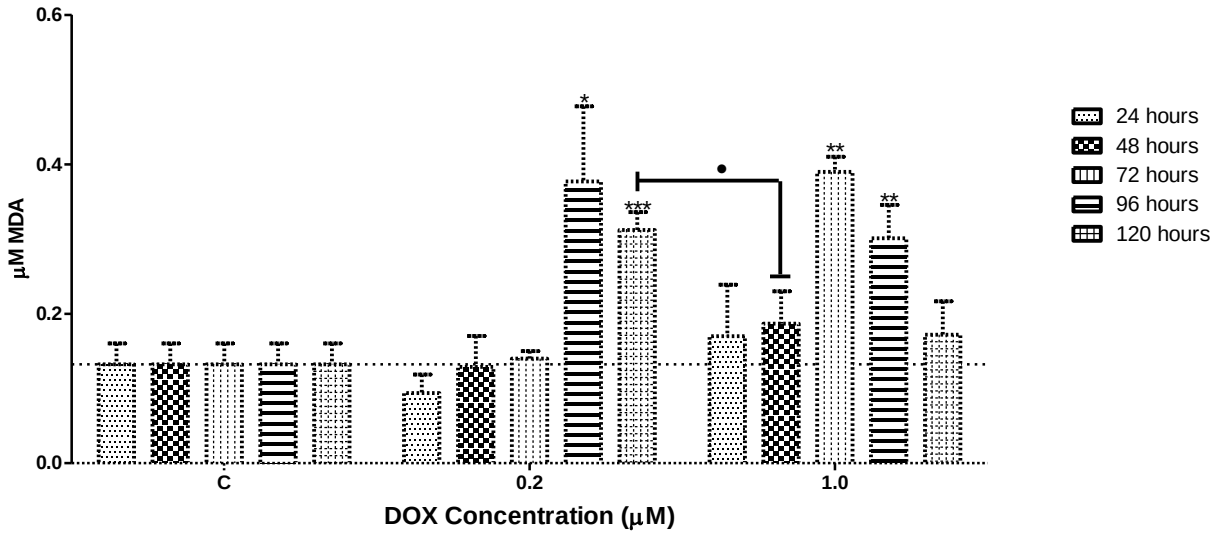


**Figure 4.18: TBARS assay as an indicator of lipid peroxidation in H9c2 cells.** H9c2 cells were treated with two concentrations of DOX for a total of 120 hours. The presence of MDA in this assay is a sign of membrane damage. All values are presented as mean ± SEM, n = 3, *p< 0.05, **p< 0.01, ***p< 0.001 vs control. ●p < 0.05 120h (0.2 µM) vs 24h (1 µM).

In differentiated C2C12 cells, significant amounts of lipid peroxidation were observed at both low and high doses of DOX, across all time points (Figure 4.19). This response showed that differentiated C2C12 cells were more sensitive to DOX-induced oxidative stress and experienced more membrane damage during treatment than the H9c2 cardiomyocytes. Similarly to the H9c2 cardiomyocytes, the level of lipid peroxidation in the C2C12 myotubes had declined to control levels by 120 hours after treatment with the high concentration. This may also be due to low cell numbers as suggested by the significant reduction in the MTT reductive capacity of these cells.

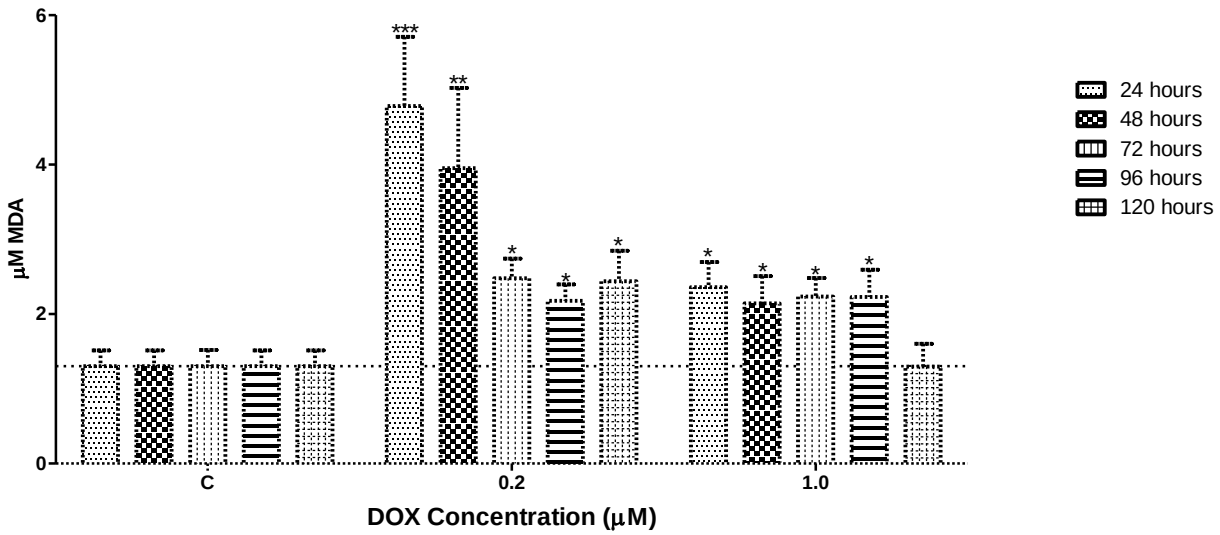


**Figure 4.19: TBARS assay as an indicator of lipid peroxidation in differentiated C2C12 myotubes.** Differentiated C2C12 cells were treated with two concentrations of DOX for a total of 120 hours. High levels of MDA produced in this assay indicate significant membrane damage. All values are presented as mean ± SEM, n = 3, *p< 0.05, **p< 0.01, ***p< 0.001.

### 4.5.2 DOX treatment affects the antioxidant capacity in both cell lines

Antioxidants are associated with a reduced incidence of cancer and heart disease (Rautenbach *et al*., 2010), however, treatment with many drugs including DOX can reduce these endogenous defense systems (Olson and Mushlin, 1990). Using the ORAC method for determining anti-oxidant capacity, no change in antioxidant capacity was detected at the acute (24 and 48 hours) and sub-chronic (72 hours) time points in H9c2 cardiomyocytes (Figure 4.20). This was followed by a significant increase in antioxidant capacity after treatment with 0.2 µM DOX for 96 and 120 hours [557.7 ± 2.91 µmol TE/L (p = 0.0053) and 553.2 ± 1.55 µmol TE/L (p = 0.0192)], respectively and after 1 µM for 96 hours [543.7 ± 2.98 µmol TE/L (p = 0.0053)]. This increase in anti-oxidant capacity occurred at the same time as the increase in lipid peroxidation.

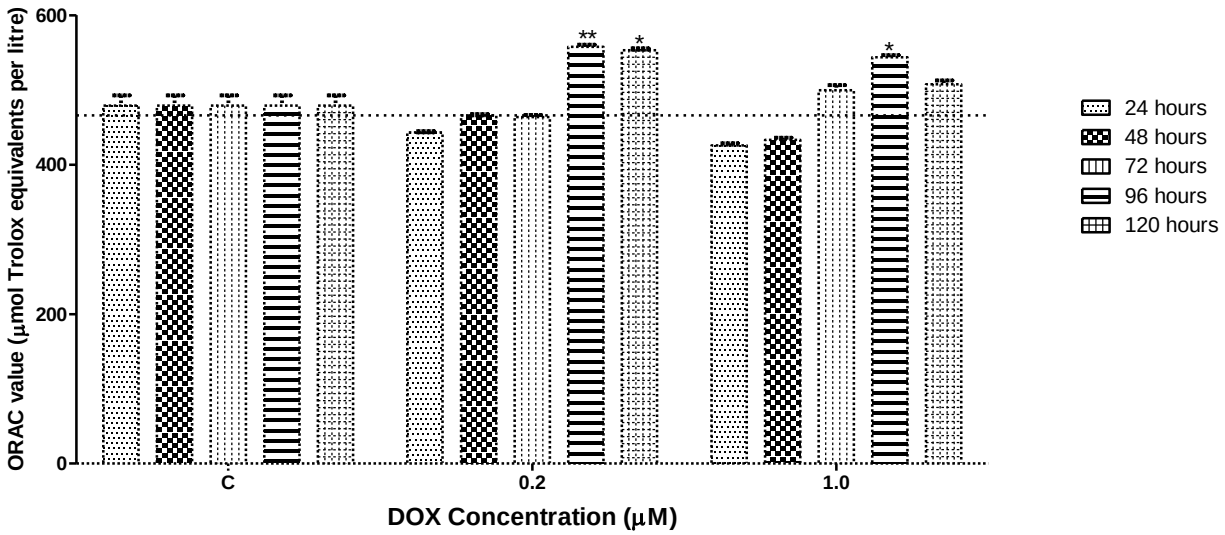


**Figure 4.20: Determination of antioxidant capacity of H9c2 cells after treatment with DOX.** Antioxidant capacity was assessed using the ORAC assay, whereby the antioxidants in a sample scavenge a free radical until the reaction is complete. All values are presented as mean ± SEM, n = 3, *p< 0.05, **p< 0.01, ***p< 0.001.

The opposite effect was observed in the differentiated C2C12 myotubes (Figure 4.21). Initially, treatment with 0.2 µM DOX caused a significant increase in antioxidant capacity after 24 and 48 hours [378.2 ± 6.23 µmol TE/L (p = 0.0032) and 382.4 ± 8.32 µmol TE/L (p = 0.0022)], respectively. Longer exposure at the same concentration then caused a significant reduction in antioxidant capacity, as did treatment with the high dose (1µM) at all 5 time points

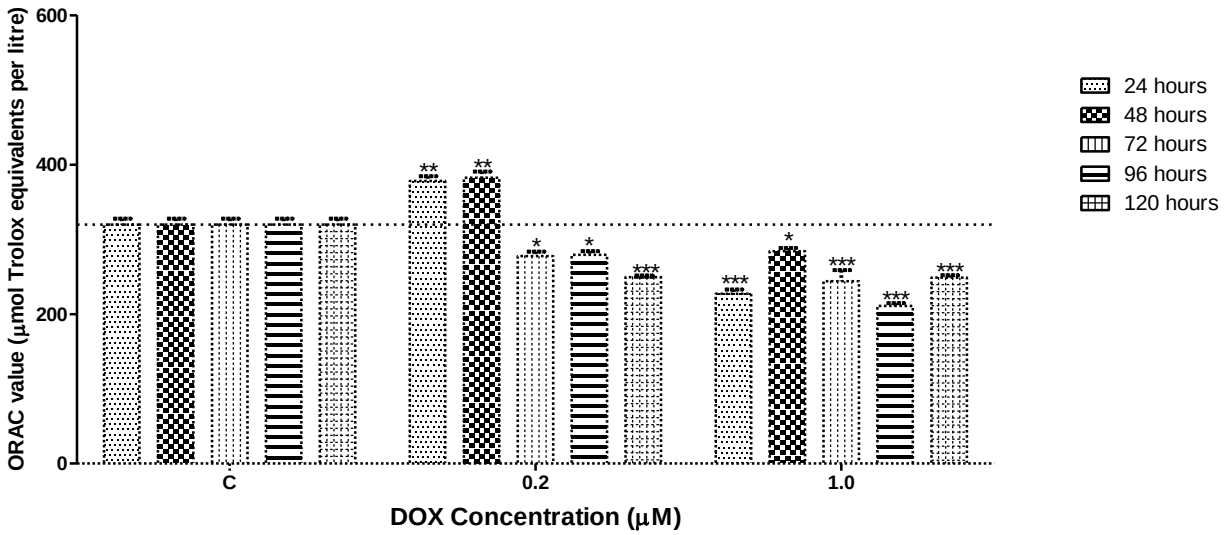


**Figure 4.21: Antioxidant capacity of differentiated C2C12 myotubes after treatment with DOX.** Antioxidant capacity was assessed using the ORAC assay, whereby the antioxidants in a sample scavenge a free radical until the reaction is complete. All values are presented as mean ± SEM, n = 3, *p< 0.05, **p< 0.01, ***p< 0.001.

### 4.5.3 DOX treatment decreases the ratio of GSH: GSSG

GSH is one of the most important antioxidants in a cell since it eliminates and detoxifies peroxides and maintains α-tocopherol and ascorbate in their reduced forms (Jones, 2002; Valko *et al*., 2007). In doing so, GSH is converted to its disulphide form, GSSG, which accumulates within a cell. Thus, the ratio between GSH and GSSG is a widely used indicator for reflecting the level of oxidative stress in a cell (Jones, 2002).

In H9c2 cells, the ratio of GSH to GSSG was significantly reduced throughout the treatment duration, indicative of high levels of oxidative stress in these cells (Figure 4.22). Chronic treatment with 0.2 µM DOX increased this ratio, though not significantly, coinciding with the increased ORAC value at this point. In differentiated C2C12 cells, significant amounts of GSSG were detected in the cells and therefore resulted in a significantly reduced ratio of GSH: GSSG at every time point treated with 0.2 µM DOX (Figure 4.23). This ratio remained significantly reduced after acute treatment with 1 µM, however, a significant increase in the ratio of GSH: GSSG was observed at 72 hours (21.64 ± 4.04%), followed by a return to baseline.

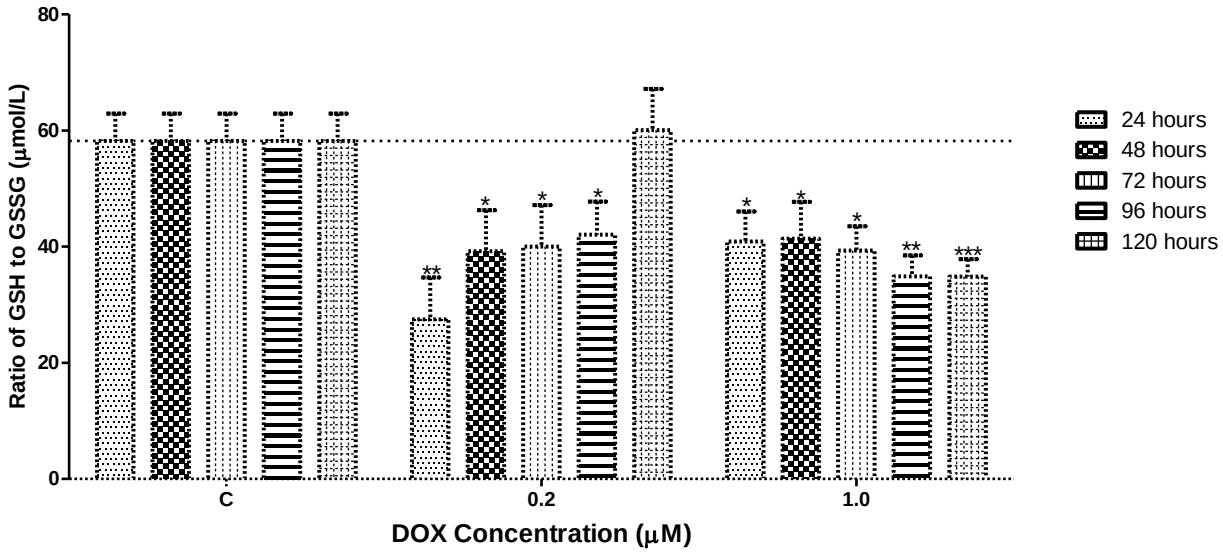


**Figure 4.22: Determination of glutathione content in response to DOX treatment in H9c2 cells.** GSH is an important antioxidant in eukaryotic cells and its ratio to GSSG gives an indication of oxidative stress. GSH content is presented as the ratio of reduced to oxidized glutathione. All values are presented as mean ± SEM, n = 3, *p< 0.05, **p< 0.01, ***p< 0.001.

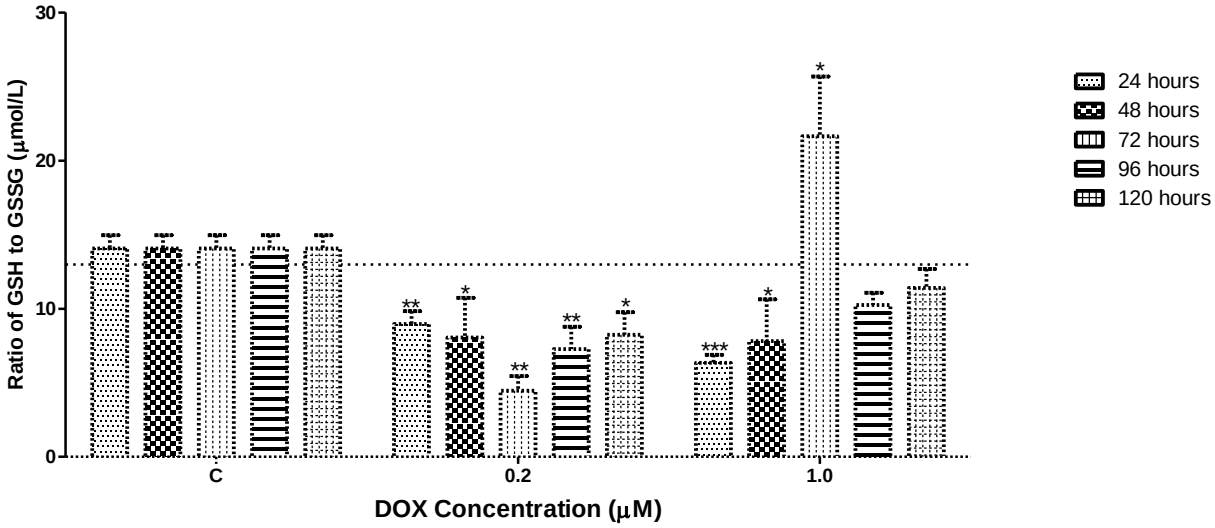


**Figure 4.23: Determination of glutathione content after DOX treatment in C2C12 myotubes.** GSH is an important antioxidant in eukaryotic cells and its ratio to GSSG gives an indication of oxidative stress. GSH content is presented as the ratio of reduced to oxidized glutathione. All values are presented as mean ± SEM, n = 3, *p< 0.05, **p< 0.01, ***p< 0.001.

Based on these results it is clear that treatment with DOX caused significant oxidative stress, but more specifically damage to the cell membrane. This may be due to the reduced ratio of GSH to GSSG, which indicates an increase in the oxidized version of glutathione in the cell. A further explanation for the reduced amount of GSH is that DOX has been shown to inhibit the action of GSH-Px1 (Doroshow *et al*., 1980). The reduced ratio of GSH to GSSG may also account for the limited antioxidant capacity in both cell lines.

**Table 4:** Summary of results in H9c2 cardiomyocytes and differentiated C2C12 myotubes

| | **H9c2 cardiomyocytes** | | **Differentiated C2C12 myotubes** | |
|---|---|---|---|---|
| **DOX** | **0.2 – 1 µM** | | **0.2 – 1 µM** | |
| **Cell viability** | Time-/dose-dependent ↓ | | Time-/ dose-dependent ↓ | |
| **Apoptosis** | ↑ 24 – 96 hr, ↓ at 120 hr | | Apoptosis evident in western blots at 1 µM | |
| **Necrosis** | No major necrotic cell death | | Necrosis evident after 120 hr | |
| | | | | |
| **DOX** | **0.2 µM** | **1 µM** | **0.2 µM** | **1 µM** |
| **ELISA** | ↑ at 120 hr | ↑ 24/96/120 hr | ↑ at 120 hr | ↑ |
| **TNFR1** | ↑ | ↑ | ↓ after 120 hr | ↓ |
| **TNFR2** | ↑ chronically | ↑ chronically | ─ | ─ |
| **SAFE** | ↑ | ─ | ─ Jak2<br>─ STAT3 $^{Tyr705}$<br>↑ STAT3 $^{Ser727}$ | ─ Jak2<br>↑STAT3 $^{Tyr705}$<br>─ STAT3 $^{Ser727}$ |
| **RISK** | ↑ Akt until 72 hr<br>─ Erk1/2 | ─ Akt<br>─ Erk1/2 | ↑ Akt until 120 hr<br>─ Erk1/2 | ↑ Akt until 120 hr<br>─ Erk1/2 |
| **TBARS** | ↑ chronically | ↑ chronically | ↑ | ↑ |
| **ORAC** | ↑ chronically | ↑ chronically | ↑ acutely | ↓ |
| **GSH: GSSG** | ↓ | ↓ | ↓ | ↓ |

Key: ↓ decrease; ↑ increase; ─ no significant change in expression; hr - hours

# CHAPTER 5

## Discussion

### Introduction

DOX remains one of the most widely used and effective anthracyclines despite causing severe cardiotoxicity. Approximately 2000 analogues of DOX have been produced in an attempt to reduce the side effects associated with these drugs whilst still effectively preventing tumor cell growth. Unfortunately, none have proved to be superior to DOX with regards to cytotoxicity and cardiac tolerability (Weiss, 1992). It is therefore imperative to try to fully understand the mechanisms by which cardiotoxicity occurs and to identify better strategies for reducing the DOX-induced side effects. In order to do this, it is often useful to turn to seemingly unrelated models to formulate a platform from where to start so we therefore used myocardial infarction as an example. Restoring oxygenated blood to the heart after a myocardial infarction results in a phenomenon known as lethal reperfusion injury (Braunwald and Kloner, 1985), The activation of intrinsic survival pathways such as the RISK and SAFE pathways during pre- and post-conditioning were shown to protect the heart from this lethal reperfusion injury (Hausenloy, 2009; Zhao *et al.*, 2003).

TNF-α has previously been shown to contribute to various pathophysiological conditions, however recent studies have shown that it may contribute to the heart's adaptive response to stress (Mann, 2003). Seeing that TNF-α is a primitive cytokine that has been conserved throughout evolution for nearly 600 000 million years and is observed in nearly all forms of cardiac injury, it is possible that it confers some or other survival benefit (Mann, 2003) which is likely dependent on its concentration. In fact, it has previously been shown that pharmacological pre-conditioning with TNF-α protects the heart against ischemia reperfusion injury and its knock out abrogates this protection (Lacerda *et al.*, 2009). One of the mechanisms by which TNF-α confers protection is through activation of the SAFE (JAK2/STAT3) pathway (Lecour, 2009a), which, once activated, is implicated in cell survival. Since DOX-induced cardiotoxicity and ischemia-reperfusion injury are often characterized by elevated oxidative stress and apoptosis, this study was thus designed to: (i) determine whether TNF-α is produced in response to DOX,

(ii) investigate whether or not the RISK and SAFE pathways also play a role in this context and (iii) provide in-depth insight into the signaling pathways that may contribute to DOX-induced cardiotoxicity.

**DOX-induced cytotoxicity is associated with a reduction in cell viability and an increase in cell death**

Cardiotoxicity is believed to arise after recurrent damage to cardiomyocytes in direct proportion to the cumulative dose of DOX (Allen, 1992). Our cell viability results support this observation since the greatest proportion of cell death took place at the most cumulative doses of DOX in both cell lines (Figures 3.1 and 3.2). Our findings are in agreement with work by Liu *et al*., (2008) who also reported a time-dependent decrease in cardiomyocyte viability after treatment with 1 µM DOX for 1 – 48 hours. Similarly, Das *et al*., (2011) reported a dose-dependent decrease in cell viability after treatment with 0.1 – 2 µM DOX. While these studies have reported similar findings, no other *in vitro* study has been performed that is as chronic as our own. Furthermore, the above mentioned studies only administered a single treatment of DOX which was followed by various incubation times, as opposed to our own study in which cells were treated daily.

Several theories have been proposed regarding the mechanisms of DOX-induced cardiotoxicity including calcium overload (Wang and Korth, 1995), the release of cardiotoxic cytokines (Li *et al*., 2006) and lipid peroxidation (Siveski-Iliskovic *et al*., 1994). These mechanisms contribute to cardiomyocyte death and over the last several decades, most *in vitro* and *in vivo* studies have pointed towards apoptosis (Arola *et al*., 2000; Gamen *et al*., 2000; Ueno *et al*., 2006) and necrosis (Sugimoto *et al*., 2002; Zhang *et al*., 2009). DOX-induced apoptosis has been extensively studied in both acute and chronic models of cardiotoxicity, results of which have shown that multiple signaling pathways are involved (Kawamura *et al*., 2004; Kim *et al*., 2006; Liu *et al*., 2008). It is again important to note that such studies have used of a wide variety of treatments (multiple versus single doses), different cumulative doses, species and cell types. In addition, many of these studies have been performed at concentrations of DOX that are not clinically relevant. Furthermore, since chronic cardiotoxicity poses a serious threat to the survival of cancer patients, it is important that studies employ chronic models of cardiotoxicity, as opposed to acute cardiotoxicity, which does not present as a major clinical problem.

In the H9c2 cardiomyocytes (Figure 3.3), a potent increase in apoptosis was observed during the first 96 hours of treatment, however, apoptosis declined after 120 hours and returned to control levels. This observation correlated with an improvement in cell viability at this time point, suggesting that the slight increase in cell viability was due to a reduction in apoptotic cell death. However, apoptotic cell death remained significantly below control levels which may have been as a result of the substantial damage induced by DOX and therefore low cell numbers by this time. In support of our observations, Arola *et al*., (2000) reported significant apoptosis between 24 and 72 hours after a single DOX injection (2.5 mg/kg) in rats. However, by day 7, apoptotic activity had declined to baseline levels. This study has therefore also demonstrated that low cell numbers and extensive damage induced by DOX at this time are possible explanations for the decline in apoptosis. In addition, since apoptosis is an energy-dependent process, it is highly possible that by 120 hours after treatment, cellular ATP was depleted and a switch to an energy-independent form of cell death had taken place.

In contrast to the results obtained for the H9c2 cardiomyocytes, apoptosis was not observed in differentiated C2C12 myotubes (Figure 3.4), as suggested by the lack of caspase-3 and -7 activities in the Caspase Glo assay. This was a surprising finding, since cell viability was significantly decreased in the myotubes despite no evidence of apoptosis. A possible explanation for this is that because the C2C12 cells were differentiated into myotubes in 96-well plates for this assay, limited space caused some of the cells to lift which would have subsequently lead to a smaller cell number in those wells. In addition, since the assay was performed at the end of the 120 hour treatment period, caspase-3 and -7 activities may have already declined by the time the assay was performed. These results therefore prompted us to assess the protein expression of cleaved caspase-3 using western blotting. Protein expression of cleaved caspase-3 was increased after acute treatment with high concentrations of DOX (Figure 4.1), but not at low concentrations of DOX. This increase was followed by a significant decline in cleaved caspase-3 expression by 120 hours, suggesting a switch to a different form of cell death in the chronic setting as no improvement in cell viability was observed. Interestingly, Hayward *et al*., (2013) reported significantly more DOX accumulation in cardiac muscle compared to smooth and skeletal muscle and thus possibly explains why substantially more apoptotic activity was observed in the cardiomyocytes compared to the myotubes.

Since apoptosis was not observed in the chronic setting of both cell lines, we hypothesized that necrotic cell death may have been active at this point. Necrotic cell death is an irreversible form of cell death that has been implicated in the context of cardiotoxicity. During necrosis, intracellular proteins such as LDH are released from compromised cell membranes and the detection of these proteins can be used as an indicator of cellular injury and consequently necrotic cell death (Horenstein *et al*., 2000). This study illustrated that necrotic cell death did not contribute to the decline in cell viability in H9c2 cardiomyocytes as evident by the significantly low levels of LDH (Figure 3.5). It is therefore possible that other forms of cell death such as autophagy (Dirks-Naylor, 2013), senescence (Zhang *et al*., 2009) and mitotic catastrophe (Eom *et al*., 2005) contributed to the reduction in cell viability in the chronic setting in H9c2 cardiomyocytes. In contrast, our results indicated that necrosis may have contributed to the reduction in cell viability in the chronic setting in C2C12 myotubes, since an increase in LDH was observed after 120 hours of treatment with most of the concentrations of DOX that were tested (Figure 3.6). This is in accordance with Franco (2006) who reported that necrotic cell death was more prevalent than apoptotic cell death following longer exposure and higher concentrations of DOX, however, this observation was reported in H9c2 cardiomyocytes. Nevertheless, since DOX induces mitochondrial damage and renders the electron transport chain dysfunctional, depletion of ATP will result in necrotic cell death as opposed to ATP-dependent apoptosis (Zhou *et al*., 2001).

**TNF-α is produced during chronic DOX-induced cytotoxicity**

TNF-α has been implicated in several pathological conditions such as inflammation, infection and malignancies (Bradley, 2008) and release of this cardiotoxic cytokine might be implicated in the pathogenesis of DOX-induced cardiotoxicity (Mohamed *et al*., 2004). However, research has also shown that that endogenous TNF-α exerts a protective effect against DOX-induced cytotoxicity (Watanabe *et al*., 1996). Low level TNF-α exposure for a short period of time may provide the heart with an adaptive response to stress, but high levels of TNF-α for extended periods of time can induce apoptosis and inflammation (Lien *et al*., 2006; Sack *et al*., 2000). These paradoxical reports clearly demonstrate that this pleiotropic cytokine exerts both beneficial and detrimental effects that are concentration and time dependent.

In our models of chronic cytotoxicity, we expected H9c2 cardiomyocytes and differentiated C2C12 myotubes to produce TNF-α in response to DOX treatment. TNF-α was produced by both cell types (Figure 4.2 and Figure 4.3) and its production appeared to coincide with chronic, high doses of DOX. In the H9c2 cardiomyocytes, TNF-α production was significantly increased after 120 hours of treatment with the low dose of DOX. However, treatment with the high dose of DOX elicited a biphasic response, peaking after 24 hours and again after 96 and 120 hours. Yokoyama *et al*., (1997) reported a similar biphasic response in TNF-α in a mouse model of renal disease and suggested that the second increase in TNF-α was in proportion to the severity of renal tissue injury. This may provide an explanation for our findings, since the greatest reduction in cell viability was observed at the same time as the second increase in TNF-α. Likewise, Reil *et al*., (2007) demonstrated the biphasic pattern of TNF-α release in a murine model of reperfusion and suggested that the initial release of TNF-α protected the heart during early reperfusion but the larger subsequent release of TNF-α was thought to account for its detrimental effects. This may explain the pattern observed in our own results since the initial increase may have provided slight protection from the toxic effects of DOX by activating the SAFE pathway, whereas the second increase may have contributed to the DOX-induced decrease in cell viability.

Compared to the inflammatory response observed in the H9c2 cardiomyocytes, the response to DOX in the C2C12 myotubes was much greater, as evident by the significant increase in TNF-α when the high dose of DOX (1 µM) was used, but also after 120 hours of treatment with the low dose (0.2 µM). This suggests that the C2C12 myotubes are more sensitive to DOX and thus elicit a greater inflammatory response. However, Cacciapaglia *et al*., (2014) demonstrated that 0.01 ng/mL TNF-α could pre-condition cardiomyocytes to high levels of TNF-α, thereby conferring a protective effect. Since 0.01 ng/mL (10 pg/mL) was the concentration of TNF-α produced by the differentiated C2C12 myotubes in our study, we can speculate that this pre-conditioned and hence protected these cells, against increasing levels of TNF-α, until this protective mechanism was overcome. It is possible that treatment with DOX initiates cell death, causing the cells to produce TNF-α as a protective mechanism. TNF-α then stimulates a host of beneficial signaling pathways, however, when the DOX-induced damage becomes too severe, these adaptive mechanisms are overcome. Furthermore, it is highly plausible that TNF-α, beyond a certain threshold, contributes to the detrimental effects of DOX.

Since the ELISA was employed to measure 'released' TNF-α, western blot analysis was employed to determine the protein expression of the total TNF-α produced. In both cell lines (Figure 4.4 and Figure 4.5), the protein expression of TNF-α was increased significantly at both concentrations of DOX in a time- and dose-dependent manner. A significant difference between acute and chronic treatment with DOX was also observed, since chronic treatment with 0.2 µM (giving a cumulative dose of 1 µM) resulted in significantly more TNF-α production than acute treatment with 1 µM. This observation emphasizes the significance of the time factor in the development of DOX-induced cardiotoxicity and why it is chronic cardiotoxicity that bares the greatest risk.

In cells, TNF-α is synthesized as a 26 kDa membrane-bound protein from which a 17 kDa soluble form is cleaved (Chu, 2013; Hehlgans and Pfeffer, 2005). Both membrane-associated and soluble TNF-α exist as biologically active trimeric proteins (Cabal-Hierro and Lazo, 2012), though each may exert distinct biological functions (Bradley, 2008). The majority of TNF-α's activities have been attributed to the soluble form, since it is involved in acute and chronic inflammation (Richter *et al*., 2012) and therefore associated with negative effects. In contrast , the membrane-bound form exerts distinct beneficial functions such as controlling infection (Garcia *et al*., 2011) and offering protection against inflammation and auto-immunity (Richter *et al*., 2012). Interestingly, TNF-α in DOX-treated H9c2 cardiomyocytes revealed that only the soluble form of TNF-α (17 kDa) was expressed, whereas in C2C12 myotubes it was the membrane-bound form (26 kDa) that was expressed. From this evidence it is possible that TNF-α signaling may be adding to the negative effects induced by DOX in the H9c2 cardiomyocytes but may be providing some form of protection in the C2C12 myotubes, albeit non-effective in the presence of DOX.

Based on the results of the ELISA and the western blots, it is clear that a few discrepancies exist between the results of the two techniques. In the H9c2 cardiomyocytes, TNF-α protein expression was evident from as early as 24 hours post treatment at both doses and continued to increase throughout the treatment period, however, the ELISA showed that TNF-α was only first produced after 120 hours at the low dose. Furthermore, while the H9c2 ELISA elicited a biphasic response at the high dose of DOX, the results of the western blot indicate a time- and dose-dependent response. In the C2C12 ELISA, significance was only obtained after 120 hours with

the low dose of DOX whereas the high dose gave significance at all time points. In contrast, protein expression increased with time at both of the doses in the C2C12 myotubes. The western blots of both cell lines therefore give an indication of a greater TNF-α response compared to the ELISA, but there are several explanations for this: **i)** the ELISA was employed to determine the amount of TNF-α produced by the cells in response to DOX, however, it is likely that even though TNF-α was produced, it was not excreted into the culture medium. The ELISA will then only measure what is released into the culture medium if the cell membrane is compromised. Western blots make use of whole cell lysates, measuring the total protein content. They therefore give a more pronounced response, **ii)** upon production, TNF-α will be bound by its receptors, therefore the ELISA will not measure TNF-α that is membrane-bound even though it was produced and **iii)** ELISAs work on perfectly folded, native proteins while westerns work on denatured proteins, therefore if the TNF-α had even slightly denatured during the 120 hours of processing, the ELISA would not detect that protein and the results would be underestimated. Since TNF-α has a half-life of only 6 – 18 minutes, this is not impossible (Beutler *et al*., 1985; Oliver *et al*., 1993). Although the results of the ELISA and the western can't be directly compared, they each give an indication of the inflammatory response to DOX, however one is on a cellular level and the other is on a protein level. The ELISA provides a more quantitative measurement of TNF-α, while the western provides a qualitative image.

Depending on the cell type and the context in which the TNF-α receptors are activated, TNFR1 and TNFR2 can trigger both cell death or survival pathways (Cabal-Hierro and Lazo, 2012). DOX may therefore induce cardiotoxicity by affecting TNF-α signaling pathways mediated by the TNF-α receptors. In H9c2 cardiomyocytes, the protein expression of TNFR1 (Figure 4.6) increased in a time- and dose-dependent manner. This supports the argument that TNF-α signaling through TNFR1 is detrimental since this time- and dose-dependent increase in receptor expression may be associated with the decrease in cell viability and increase in apoptosis observed in this cell line. This observation is in agreement with Chiosi *et al*., (2007) who reported a significant increase in TNFR1 expression in H9c2 cardiomyocytes after acute treatment with 1 µM DOX. A similar effect was observed in TNFR2 protein expression (Figure 4.8), however, a decline in protein expression was observed after 120 hours. Expression of TNFR1 remained elevated at this point, suggesting that in the most chronic conditions of DOX treatment, TNFR1 still exerts its effects. Again, the differences between acute and chronic DOX

treatment were evident, since TNFR2 was significantly expressed after 120 hours of treatment with 0.2 µM (cumulative dose of 1 µM) but significantly down-regulated after 24 hours with 1 µM. This suggests that chronic treatment with a low concentration of DOX causes the cells to up-regulate signaling through TNFR2 in an attempt to overcome the toxic effects of DOX. However, TNFR1 expression remained significantly elevated at both low and high concentrations of DOX, suggesting that DOX-induced damage may occur via TNFR1 regardless of the concentration or duration of exposure to DOX.

In differentiated C2C12 myotubes, TNFR1 protein expression (Figure 4.7) was down-regulated during most of the treatment regime. This observation supports the presence of membrane-bound TNF-α, since a lack of TNFR1 may confer protection in these cells, which would be mediated by the membrane TNF-α. However, protein expression of TNFR2 was also down-regulation for the majority of the treatment period (Figure 4.9), suggesting that TNF-α may mediate its effects independently of its cell surface receptors (Dudich *et al*., 1999). Further support for our findings is provided by Lacerda *et al*., (2010) who showed that administration of TNF-α to cardiac mitochondria obtained from TNFR1 and TNFR2 knock out mice induced several beneficial effects on mitochondrial respiratory function. This is possible due to a mitochondrial binding protein that traffics TNF-α directly to the mitochondria, by-passing its cell surface receptors (Ledgerwood *et al*., 1998). Whether TNF-α provides an innate defense mechanism against DOX or whether it aids in the pathogenesis of cardiotoxicity remains to be elucidated. It is possible that TNF-α does exert a beneficial effect until its concentrations become too high or are sustained for too long, however, further research is needed to determine when the switch between good and bad occurs.

**DOX-induced cytotoxicity and the SAFE pathway**

During ischemia reperfusion the SAFE pathway (Jak2 and STAT3) is triggered via TNF-α as a protective mechanism against oxidative stress and apoptosis. Upon ligand binding, Jaks become phosphorylated and subsequently catalyze the phosphorylation of tyrosine residues on the receptor (Leonard, 2001). This promotes the binding and phosphorylation of STAT proteins, which translocate to the nucleus to induce the transcription of target genes (Leonard, 2001). The Jak-STAT pathway is therefore a rapid means by which to induce a signal from the membrane to the nucleus. Seeing that both Jak2 and STAT3 are found within the heart (Boengler *et al*., 2008)

and TNF-α was produced in this model, this study assessed whether the SAFE pathway is active under conditions of cytotoxicity induced by DOX.

Based on our observations, DOX did trigger the activation of the SAFE pathway, however, above a certain concentration of DOX, both Jak2 and STAT3 were significantly down-regulated. In H9c2 cardiomyocytes, protein expression of p-Jak2 (Figure 4.10) revealed a time- and dose-dependent increase after treatment with the low dose of DOX. Similarly, analysis of total Jak2 revealed a significant increase in total protein as early as 24 hours after treatment with this dose. This suggests that the low dose of DOX presented a toxic challenge to which the cells still had the ability to adapt to, causing them to increase the protein synthesis of Jak2. One would therefore expect the ratio of phosphorylated Jak2 to total Jak2 (phospho/total) to also increase over time, since a greater amount of phosphorylation can take place if there is a greater amount of Jak2. However, analysis of this ratio revealed significantly less Jak2 phosphorylation during the first 72 hours of treatment, where after an increase was observed in the chronic setting. These results indicate that the rate of degree of phosphorylation was not greater than the rate of degree of protein synthesis during the earlier time points. Although DOX caused the cells to increase protein synthesis of Jak2, this additional protein was not phosphorylated. At the high dose of DOX, protein expression of p-Jak2 was significantly down-regulated, while the total protein remained unchanged. It seems as if chronic administration of a low dose of DOX induces Jak2 activation, however doses exceeding 1 µM completely stunt this activation. Although this observation suggests that the high dose of DOX was too noxious for the cells to adapt, DOX may also actively suppress the activation of Jak2 at this concentration. Furthermore, chronic treatment with 0.2 µM (cumulative dose of 1 µM) stimulated Jak2 phosphorylation, whereas acute treatment with 1 µM down-regulated p-Jak2 expression, highlighting the differences between acute and chronic treatment with DOX.

A similar effect on tyrosine phosphorylation of STAT3 was observed. In a time- and dose-dependent manner, protein expression of p-STAT3 $^{Tyr705}$ (Figure 4.12A) was significantly increased in H9c2 cardiomyocytes treated with 0.2 µM DOX, despite a reduction in p-Jak2 expression. This may suggest that STAT3 phosphorylation in this context can occur independently of Jak2 activation. In addition, cross-talk between the RISK and SAFE pathways has been suggested (Somers *et al*., 2012) and therefore could have accounted for the activation of

STAT3, irrespective of Jak2 inactivity. Phosphorylation of STAT3 on serine 727 is not required for STAT3 activation but it does enhance transcriptional activity (Kisseleva *et al*., 2002). We observed elevated protein expression of p-STAT3 $^{Ser727}$ (Figure 4.12C) in the H9c2 cardiomyocytes following treatment with the low dose of DOX, but once again, doses exceeding 1 µM significantly down-regulated the protein expression of both p- STAT3 $^{Tyr705}$ and p-STAT3 $^{Ser727}$. These findings are in agreement with those obtained by Mitra *et al*., (2007) who reported a decrease in both Jak2 and STAT3 phosphorylation in a rat model of DOX-induced cardiotoxicity. More specifically, Jak2 phosphorylation was significantly decreased as early as two days post-injection, whereas STAT-3 only declined by day 8. Based on these observations, high concentrations of DOX (> 1 µM), regardless of exposure time, significantly down-regulate the SAFE pathway and may thus be a mechanism by which cardiotoxicity develops. Since the SAFE pathway has been shown to promote cell survival, down-regulation of this pathway will likely promote cell death. The manner by which this occurs is based on the function of STAT3. STAT3 mediates cell survival by promoting the transcription of the anti-apoptotic gene Bcl-2 and down-regulation of the pro-apoptotic gene Bax (Hattori *et al*., 2001). Furthermore, the function of STAT3 is determined by the intensity and duration of STAT activity, as well as the amount of STAT proteins ready to be activated (Kunisada *et al*., 2000). It is then likely that DOX reduces the transcription of STAT3 mRNA which subsequently reduces the amount of STAT3 protein in a cell. However, in our study, total STAT3 protein expression was not statistically different from the control, suggesting that DOX does not affect the STAT3 mRNA in this model but rather prevents its phosphorylation or degradation. This appears to be concentration dependent, since phosphorylation of STAT3 became significantly reduced as the concentration of DOX increased.

p-Jak2 protein expression in the differentiated C2C12 myotubes was severely down-regulated irrespective of the dose, cumulative concentration and duration of treatment (Figure 4.11) and thus implies a potent inhibitory effect by DOX on Jak2 activation. Despite the absence of Jak2 activation, STAT3 was again still phosphorylated, emphasizing a Jak2-independent pathway to STAT3 activation. In contrast to what was observed in H9c2 cardiomyocytes, the expression of p-STAT3 $^{Tyr705}$ in the C2C12 myotubes was not pronounced at the low concentration of DOX but rather significantly elevated at the high concentration (Figure 4.13A). The expression of p-STAT3 $^{Ser727}$, however, was up-regulated following treatment with low concentrations of DOX

but down-regulated when the concentrations increased (Figure 4.13C). These results suggest that in this cell line the activation of STAT3, either on the tyrosine or serine residue, is dependent on the concentration of DOX or that phosphorylation of these residues functions in a compensatory manner so that when one residue is inactive, the other can dominate.

Interestingly, the expression and phosphorylation of STAT3 was found to be significantly down-regulated in the myocardium of patients with dilated cardiomyopathy (Podewski, 2003) and may therefore contribute to the development of heart failure in these patients (Hilfiker-Kleiner *et al*., 2004). Since the end result of DOX-induced cardiotoxicity is also heart failure, down-regulation of the SAFE pathway by DOX, as observed in our study, may contribute to the mechanisms by which DOX mediates its cardiotoxic effects. In an *in vivo* study by Jacoby *et al*., (2003), a cardiac-specific STAT3 knock out model was employed to determine the susceptibility of mice to DOX-induced heart failure, however, heart failure was evident even before DOX treatment. Treatment with DOX caused a greater decline in cardiac function compared to the wild type mice, and this observation was associated with a higher level of apoptosis. This study provides insight into the beneficial roles of both Jak2 and STAT3, however, very little is known about this pathway in the context of DOX-induced cardiotoxicity. We can speculate that DOX-induced down-regulation of the SAFE pathway contributes to cardiomyocyte apoptosis and makes cardiomyocytes more susceptible to DOX-induced injury. Therefore, stimulating this pathway may potentially promote cell survival during cytotoxicity. Our own work as well as that of others highlights the importance and benefit of a functional SAFE pathway during DOX treatment and demonstrates that stimulation of this pathway is an avenue worth exploring.

**Weighing out the RISKs: DOX and the Erk1/2 and Akt kinases**

The RISK pathway involves the activation of the pro-survival kinases Erk1/2 and Akt, both of which are involved in promoting cell survival by inducing anti-apoptotic pathways (Cross *et al.*, 2000). It is therefore not surprising that a number of studies have examined the protein expression of Erk1/2 and Akt as pro-survival kinases during treatment with DOX, however their roles in a chronic model of cardiotoxicity have not been determined.

In our models of DOX-induced cytotoxicity, the Erk1/2 leg of the RISK pathway was not activated in response to DOX treatment (Figure 4.16 and Figure 4.17) since a down-regulation in

Erk1/2 phosphorylation, and thus activation, was observed in both cell lines, irrespective of dose and exposure time. This finding suggests that DOX-induced Erk1/2 inactivation occurs irrespective of cell type. This finding is in agreement with Lou *et al*., (2005) and Li *et al*., (2006) who reported that Erk1/2 phosphorylation was significantly inhibited in rat and mice models of DOX-induced cardiomyopathy, respectively. Since Erk1/2 inhibition enhanced Daunomycin-induced apoptosis of cardiomyocytes (Zhu *et al*., 1999), it is possible that the inhibition of Erk1/2 phosphorylation by DOX, as observed in our own study, may also account for the observed cardiomyocyte death. Activation of the Erk1/2 survival pathway protects cell from apoptosis and may therefore be a possible target for DOX during cardiotoxicity. This may also occur indirectly through DOX-induced apoptosis, since activated caspase-3 can cleave and inactive Raf-1, an upstream activator of Erk1/2 (Widmann, 1998). Hence, an increase in DOX-induced caspase-3 activation may indirectly inhibit the pro-survival function of Erk1/2 by preventing its activation.

Although Erk1/2 was not activated in response to DOX treatment, Akt phosphorylation was evident and possibly implies that this survival kinase compensated for the lack of Erk1/2 phosphorylation. In the H9c2 cardiomyocytes, significant Akt phosphorylation (Figure 4.14) occurred during acute (24 and 48 hours) and sub-chronic (72 hours) exposure to the low concentration of DOX (0.2 µM). As the exposure to DOX became longer and the concentration became higher, Akt phosphorylation was significantly down-regulated. These findings are consistent with those of Das *et al*., (2011) who reported significantly down-regulated Akt phosphorylation in cardiomyocytes exposed to 1 µM DOX for 24 hours. Similarly, we observed that Akt activation was significantly up-regulated following treatment with low concentrations of DOX in the C2C12 myotubes (Figure 4.15), but remained unchanged compared to the control at the higher concentrations of DOX. These observations were based on the ratio of phosphorylated Akt to total Akt, since DOX treatment also caused significant changes in total protein expression. In the presence of low concentrations of DOX, total Akt expression was significantly reduced, whereas in the presence of high concentrations of DOX, total Akt expression was elevated. These findings suggest that the initial exposure to DOX induced a potent increase in Akt phosphorylation in an attempt to overcome the toxic effects of DOX. However, when the concentrations of DOX became too high, phosphorylation did not occur despite an increase in total protein levels. These observations can be explained by the fact that the inactivation/de-

phosphorylation of Akt is regulated by Serine/Threonine protein phosphatases, PP1 and PP2 (Andreozzi *et al*., 2011) and Fan *et al*., (2008) have reported that DOX significantly up-regulates protein phosphatase PP1. As a result, after chronic exposure to high concentrations of DOX, cells are unable to maintain the phosphorylated state of Akt due to an increase in DOX-induced PP1 expression, thus rendering Akt inactive (Andreozzi *et al*., 2011). Phosphorylated Akt is usually responsible for phosphorylating and inhibiting Bad (Downward, 2004) and in this manner prevents caspase-3 activation (Li *et al*., 2013). Therefore, DOX-induced inhibition of Akt phosphorylation likely contributed to the increased apoptosis by preventing Akt activation/phosphorylation. DOX thus mediates cardiotoxicity by preserving the pro-apoptotic function of Bad and induces cardiomyocyte apoptosis by increasing caspase activity. An interesting finding was reported by Hausenloy *et al*., (2004), who suggested that cross-talk exists between the two legs of the RISK (Erk1/2 and Akt) pathway. It was shown that when Erk1/2 activity was inhibited, Akt phosphorylation was increased, and vice versa. This study therefore concluded that although Akt was found to be the dominant kinase in promoting cell survival, activation of both kinases is required to provide protection during ischemic post conditioning. This too is consistent with our results, since the lack of Erk1/2 activation was accompanied by an increase in p-Akt expression at the low concentration of DOX. However, activation of Akt, without the activation of Erk1/2, was not sufficient to protect the cells from the toxic effects of DOX.

Our study therefore demonstrates that treatment with DOX significantly affects cell survival at least in part by down-regulating the pro-survival kinases of the RISK pathway during chronic cytotoxicity. While our own findings demonstrated a reduction in both Erk1/2 and Akt activation, Gharanei *et al*., (2013) reported a significant increase in both kinases after treatment with 1 µM DOX for 120 minutes in an isolated heart model. Considering the short treatment duration, it is possible that Erk1/2 and Akt are increased as an early protective mechanism to counteract the damaging effects of DOX. Although relatively few changes were observed in the acute setting of our models, distinct changes were observed chronically, emphasizing the severity of chronic cardiotoxicity in contrast to acute cardiotoxicity. This study has thus demonstrated that Erk1/2 and Akt may be increased as an early survival strategy against DOX, but chronic exposure to increasing concentrations of DOX inhibits these pathways. When the toxic effects of

DOX become severe, neither Erk1/2 nor Akt can rescue the dying cells, as evident by the dose-dependent decrease in cell viability.

**Oxidative stress, anti-oxidant capacity and anti-oxidant status**

Despite the years of research, the mechanisms by which DOX induces cardiotoxicity are still not well defined, however, undoubtable evidence points towards oxidative stress (Choi *et al*., 2007; Das *et al*., 2011; Fan *et al*., 2008; Šimùnek *et al*., 2009). The chemical structure of DOX lends itself to the production of free radicals in a process known as redox cycling (Keizer *et al*., 1990). Superoxide radicals produced in this process can damage cell components wherever they are formed (Benchekroun *et al*., 1993), including the heart. This is of particular importance seeing that the heart has a high level of oxidative metabolism, but limited antioxidant defenses compared to other organs (Choi *et al*., 2007; Doroshow *et al*., 1980). It has been previously shown that superoxide radicals can decompose to form hydroxyl radicals, peroxyl radicals and hydrogen peroxides (Olson *et al*., 1981). These in turn are able to convert membrane unsaturated fatty acids into lipid peroxides.

Lipid peroxides decompose into products such as MDA, which can therefore be used as an indicator of the level of lipid peroxidation taking place (Rautenbach *et al*., 2010). The heart is so susceptible to DOX-induced damage because several enzymatic reactions necessary for regulating redox state are inhibited. GSH-Px1 is an important enzyme for protecting cells against oxidative damage because it assists in the detoxification process. Studies have shown that when GSH is depleted, cells are more susceptible to oxidative-stress induced damage. Enhanced lipid peroxidation occurs in the heart if the activity of GSH-Px1 is reduced (Simmons and Jamall, 1989; Siveski-Iliskovic *et al*., 1994). GSH is one of the most important components of a cells antioxidant defense (Jones, 2002; Monostori *et al*., 2009) and is directly involved in the scavenging of ROS and maintenance of thiol proteins in their reduced state (Hampton and Orrenius, 1998). It is often used as an indicator of oxidative stress since the amount of GSH will decrease as it scavenges ROS, resulting in an increase in GSSG. GSH is oxidized to GSSG during the detoxification of ROS in the presence of GSH-Px1 and regenerated back to GSH by glutathione reductase (Monostori *et al*., 2009). Since it is well established that ROS plays a causative role in numerous human pathologies, the idea that antioxidants could control the state of oxidative stress in various organisms is credible line of defense. Since so many antioxidants

exist and it is difficult to measure each one of its own, a useful technique called ORAC was developed. This method measures the oxygen-radical absorbing capacity of a sample and compares it to a known standard (Cao *et al*., 1993).

In the H9c2 cardiomyocytes, lipid peroxidation was not observed during the first 72 hours of treatment with the low concentration (0.2 µM) of DOX (Figure 4.18), however, a significant increase in MDA was evident after chronic treatment. A significant increase in lipid peroxidation was also observed after 72 and 96 hours of treatment with the high dose (1 µM) of DOX. Chronic treatment with 0.2 µM also resulted in significantly more lipid peroxidation compared to acute treatment with 1 µM, emphasizing how chronic cardiotoxicity is associated with more detrimental effects than acute cardiotoxicity. The increase in lipid peroxidation in this study was accompanied by a parallel increase in the ORAC value (Figure 4.20) at these times, suggesting that H9c2 cardiomyocytes increased their antioxidant capacity in response to high doses of DOX. However, treatment with DOX also significantly reduced the ratio of GSH to GSSG (Figure 4.22), indicating the limited antioxidant defense of these cells against the increasing oxidative stress as indicated through lipid peroxidation. In a chronic rat model of DOX-induced cardiotoxicity, Zanwar *et al.*, (2013) also reported a significant reduction in cardiac GSH content following DOX treatment. Together, the combination of severe oxidative stress and poor antioxidant defense most likely contributed to the reduction in cell viability and significant levels of apoptosis in the cardiomyocytes.

As observed in the differentiated C2C12 myotubes, MDA increased almost 4-fold throughout the entire treatment period when compared to the control (Figure 4.19), suggesting that a larger degree of membrane damage occurred in these cells. The highest level of lipid peroxidation occurred during the first 48 hours of treatment with the low dose of DOX and this correlated with a significant increase in antioxidant capacity (Figure 4.21) at this time. This suggests that the myotubes initially increased their antioxidant defense systems to prevent the oxidation of cellular components, however, beyond 48 hours of treatment, as the dose of DOX accumulated, the antioxidant capacity was significantly reduced, leading to severe lipid peroxidation. Work by Jiang *et al*., (2008) supports these observations, since they observed a significantly reduced anti-oxidant capacity in DOX-treated mouse hearts, together with a significant increase in MDA. Similarly, Alkreathy *et al*., (2010) observed a 12-fold increase in plasma MDA of rats treated

with a single dose (25 mg/kg) DOX. It has also been well documented that oxidative stress activates MAPKs such as Erk1/2 and Akt (Lou *et al*., 2005). This observation is in agreement with our own findings, since the significant increase in oxidative stress caused a parallel increase in p-Akt expression, suggesting that oxidative stress within a cell activates this pro-survival kinase. In C2C12 myotubes, the ratio of GSH to GSSG was significantly reduced (Figure 4.23), therefore explaining the poor antioxidant capacity of these cells. However, loss of GSH can be influenced by differentiation and apoptosis (Jones, 2002) and thus in this context, both of these events would have contributed to the decreased ratio. Depletion of GSH following DOX treatment indicates a loss of antioxidant defense in these cells, and as a result, reduced cell viability occurred.

Our results, together with many others, highlight the contribution of oxidative stress to the development of DOX-induced cardiotoxicity. Furthermore, our findings emphasize how DOX weakens the ability of antioxidant defense systems to scavenge free radicals, thereby leading to cell death. A reduction in antioxidant defense, combined with ROS-induced lipid peroxidation and a decrease in GSH, are certain to ensure an apoptotic fate in both cell types. Our results also highlight the different responses of these two cell lines to DOX, since C2C12 myotubes increased their antioxidant capacity immediately after DOX exposure, whereas H9c2 cardiomyocytes only increased their antioxidant capacity when lipid peroxidation became severe. However, the reduced ratio of GSH in both cell lines suggests that some of the toxic effects of DOX will occur regardless of the cell type. However, whether the depletion of antioxidant defense systems is a cause or consequence of DOX-induced cardiotoxicity remains to be elucidated. Our results have clearly indicated a correlation between lipid peroxidation, a reduction in antioxidant capacity and a significant increase in apoptosis. DOX-induced cytotoxicity is associated with ROS-induced membrane damage, an antioxidant deficit and a compromised antioxidant capacity. The combination of these mechanisms further explains how DOX may induce cardiomyocyte death in human patients and thus contribute to the development of heart failure.

# CHAPTER 6

## Conclusion

DOX is an anthracycline that has been shown to exhibit a greater therapeutic index than any other before it. Since its discovery in the 1960s, DOX has drastically improved the outcome of patients, both adults and children, suffering from several different malignancies. The efficacy of DOX is however limited by the development of severe dose-dependent cardiotoxicity which often presents itself years after treatment has ended. As a result, it is chronic cardiotoxicity that poses the most serious risk to cancer survivors. While the mechanisms by which DOX mediates cardiotoxicity are still under debate, apoptosis and oxidative stress are two that are generally agreed upon. An increase in ROS causes damage to DNA, cell membranes and mitochondria, all of which will culminate in apoptotic cell death. Similarly, during reperfusion, restoring blood flow to an ischemic heart also induces oxidative stress and cell death by apoptosis, which together, cause significant myocardial injury. Fortunately, pre- and post-conditioning have been shown to reduce reperfusion-related injury by activating the SAFE and RISK pathways. In addition, low levels of TNF-α produced by the heart during early reperfusion are thought to be responsible for the activation of the SAFE pathway. Based on the above similarities between DOX-induced cardiotoxicity and ischemia reperfusion injury, we hypothesized that the SAFE and RISK pathways would be stimulated as a protective mechanism during chronic DOX-induced cytotoxicity, via TNF-α.

We have confirmed the presence of a time- and dose-dependent relationship between the concentration of DOX and a decrease in cell viability in two different cell lines. Treatment with DOX was accompanied by an increase in both TNF-α and ROS production, both of which may have contributed to cell death. Binding of TNF-α to the death domain of TNFR1 would activate the extrinsic apoptotic pathway, while increased ROS would result in cytochrome c release from the mitochondria and subsequently activate the intrinsic apoptotic pathway. Both pathways converge on caspase-3 which, as also observed in this study, is cleaved in response to DNA damaging stimuli. The existence of DOX-induced apoptotic cell death was confirmed in both

differentiated C2C12 myotubes and H9c2 cardiomyocytes, while necrosis was only found to play a role in cell death in the chronic setting in the C2C12 myotubes.

A unifying summary of our findings is depicted in Figure 6.1 This study showed that treatment with DOX stimulates the production of TNF-α. While mild levels of TNF-α may initially be produced as a protective mechanism against DOX by activating the SAFE pathway, high levels most likely contribute to DOX-induced cell death. Further research is required to determine whether TNF-α is in fact beneficial in this context or whether it adds to the cardiotoxic effect of DOX. Furthermore, the exact concentration at which this effect occurs remains to be elucidated. Our study demonstrated that both TNF receptors were up-regulated in a time- and dose-dependent manner in the H9c2 cardiomyocytes, however, their contribution to an adaptive or a negative response remains undetermined. TNFR1 and TNFR2 were mostly down-regulated in the C2C12 myotubes, suggesting that TNF-α can function independently of its receptors in this cell line.

It is well documented that both DOX and TNF-α can increase ROS production and this observation may explain the significant lipid peroxidation and reduced ratio of GSH: GSSG that was observed in this study. Our study also demonstrated a reduced antioxidant capacity in both cell lines and these observations are in agreement with those in the clinical setting. While small amounts of ROS would have activated the RISK pathway, a level of ROS above a certain threshold would have triggered the opening of the mitochondrial permeability transition pore and sealed the apoptotic fate of both cell lines. Together, the increased oxidative stress and cell death observed in our study support the two most widely accepted mechanisms of DOX-induced cardiotoxicity.

The activation of the SAFE and RISK pathways were also observed in our study, however, this was only observed at low concentrations of DOX. The dose-dependent increase in TNF-α may have activated Jak2 at the low concentrations of DOX in the H9c2 cardiomyocytes. Consequently, activated Jak2 then phosphorylated STAT3, as evident in our study. At high concentrations of DOX, however, p-Jak2 and both p-STAT3 residues were significantly down-regulated. Although Erk1/2 was not activated in this cell line, p-Akt was activated after acute exposure to low concentrations of DOX. The RISK pathway, like the SAFE pathway, was then

down-regulated at high concentrations of DOX and thus identifies a potential mechanism by which DOX mediates cardiotoxicity. Phosphorylation of STAT3 on the tyrosine residue in the differentiated C2C12 myotubes was expressed at high concentrations of DOX, while phosphorylation on the serine residue was down-regulated at high concentrations but increased at low concentrations, suggesting that phosphorylation of these residues occurs in a compensatory manner. These observations occurred despite the absence of Jak2 phosphorylation suggesting that TNF-α can activate STAT3 independently of Jak2 and the TNF receptors. The Erk1/2 leg of the RISK pathway was again not activated during DOX treatment in this cell line, while p-Akt was only evident at low concentrations.

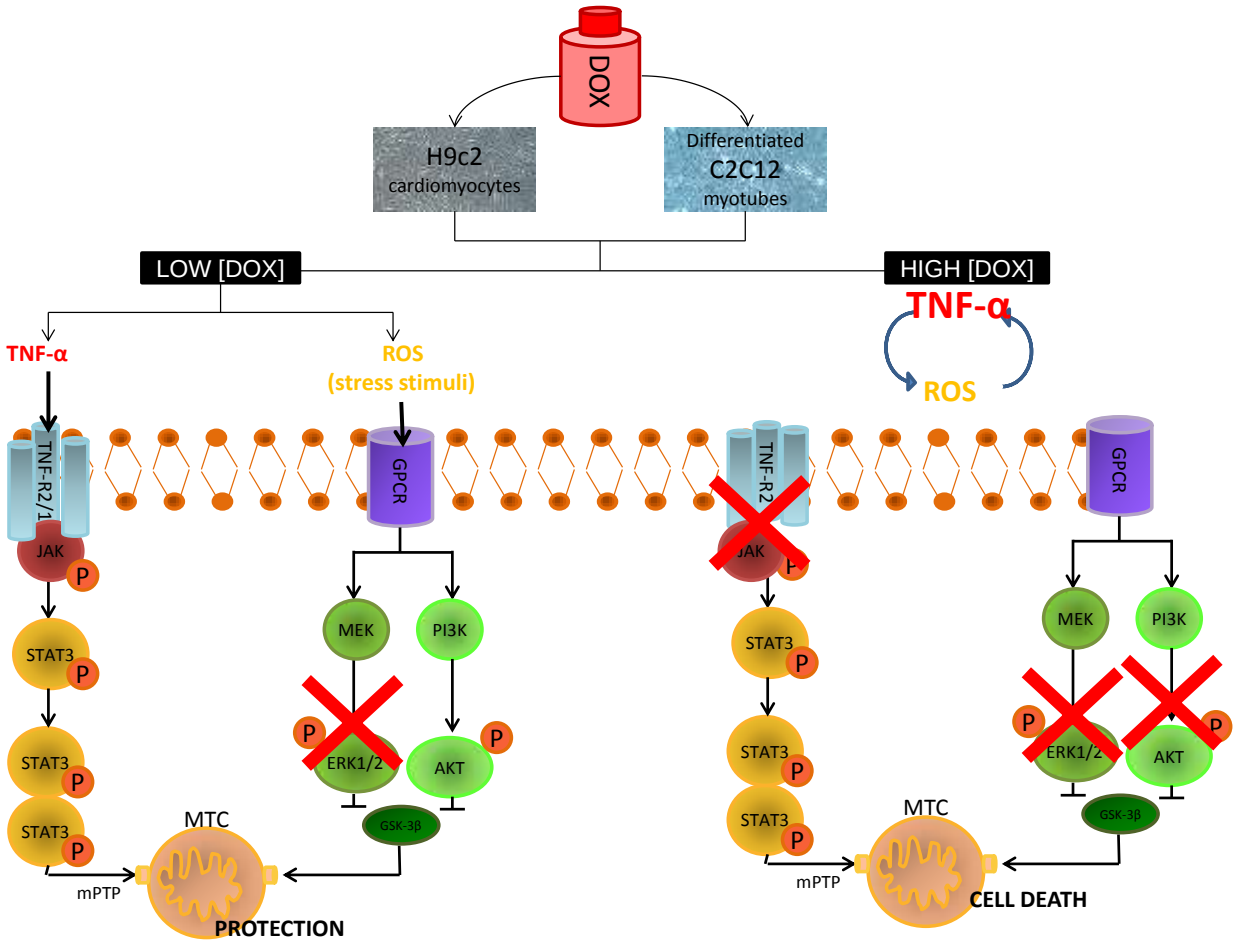


**Figure 6.1: DOX and the RISK and SAFE pathways.** This unifying diagram illustrates the activation of the SAFE and RISK pathways at low concentrations of DOX but down-regulation of these pathways after exposure to high concentrations of DOX. The low dose of DOX caused a mild increase in TNF-α which possibly provided protection by activating the SAFE pathway. High concentrations of DOX caused a larger increase in TNF-α, which, together with an increase in lipid peroxidation, may have then

contributed to the decrease in cell viability. High concentrations of DOX also prevent the activation of the SAFE and RISK pathways.

Although DOX-induced cardiotoxicity is believed to be mediated by large amounts of ROS, several studies making use of free radical scavengers have generated poor results. This suggests that the development of cardiotoxicity is mediated by alternative mechanisms. Therefore, since the SAFE and RISK pathways were shown to be down-regulated during cytotoxicity in this study, it is possible that inhibition of these pathways by DOX is another mechanism by which it mediates its cardiotoxic effects. Although the SAFE or RISK pathways were transiently activated, this activation did not provide sufficient protection due to the fact that activation of both pathways simultaneously, is required for full protection. Further studies are required to determine the exact roles of the SAFE and RISK pathways, as well as TNF-α, using their respective specific inhibitors. In this way, the intracellular signaling pathways associated with protection will be brought to light. Furthermore, inhibition of each pathway will provide insight into possible cross talk since these two cascades act in concert to promote maximal protection. Inhibiting the TNF-α/Jak2/ STAT-3 pathway affects the activation of the PI3K/Akt and vice versa. We believe that inhibition of these pathways by DOX may contribute to its cardiotoxic effects. Since our study is a simulation of cumulative, dose-dependent cardiotoxicity, we have provided a potential mechanism of action for DOX-induced cardiotoxicity, as well as a therapeutic target to explore by which to improve the viability of cardiomyocytes.

To the best of our knowledge, this study is the first to design an *in vitro* model of chronic DOX-induced cardiotoxicity. This study also employed two different cell lines in order to assess the appropriateness of each model. By treating cells daily, as opposed to once, with increasing concentrations of DOX for 120 hours, we have successfully designed a model that simulates the cardiotoxic effects of this anthracycline in the clinical setting. While the exact mechanisms of cardiotoxicity that occur in a clinical setting will always differ from *in vivo* or *in vitro* models, this study was able to document the significant apoptosis and oxidative stress that has been observed in human patients. The fact that this study made use of a range of clinically relevant concentrations of DOX and a chronic treatment, highlights the uniqueness and novelty of this model, since we have identified potential mechanisms that may occur in a clinical setting. One of the limitations of this study is the fact that two different methods for measuring apoptosis should

have been used, however, due to the fact that DOX is the same colour as a PI stain, this was not possible. Another limitation is the choice of cell type used in this study, as primary cardiac cells would have been a better representation of the cardiotoxic side effects of DOX in human hearts, however, due to the chronic nature of this study, we do not believe that primary cardiac cells would have survived the 120 hour treatment regime. In addition, it would not have been feasible (considering the principle of reduce, replace and refine) as too many animals would have been needed in order to obtain enough cells.

Our study has validated that TNF-α is produced in response to DOX, but it is still unknown whether TNF-α exerts beneficial or detrimental effects. Therefore, future studies should aim at delineating the role of TNF-α in the context of DOX-induced cardiotoxicity. This could be achieved using inhibitors of TNF-α, TNF-α knock out mice and treatment with different concentrations of TNF-α both in the presence and absence of DOX. Similarly, the protection offered by the SAFE and RISK pathways can be further explored by employing specific inhibitors of each pathway and assessing cell viability and cell death markers after treatment with DOX. An avenue that is definitely worth exploring would be to stimulate the SAFE and RISK pathways in order to determine whether additional protection is afforded. Once the roles of TNF-α, and the SAFE and RISK pathways have been validated, the study should be repeated in an animal model to determine whether their roles are also applicable *in vivo*. This will identify whether these pathways may provide protection during DOX-induced cardiotoxicity in a clinical setting.

# REFERENCES

Aaronson, D.S., Horvath, C.M., 2002. A road map for those who don't know JAK-STAT. *Science*. 296, 1653–1656.

Alkreathy, H., Damanhouri, Z.A., Ahmed, N., Slevin, M., Ali, S.S., Osman, A.M., 2010. Aged garlic extract protects against doxorubicin-induced cardiotoxicity in rats. *Food Chem. Toxicol*. 48, 951–956.

Allen, A., 1992. The cardiotoxicity of chemotherapeutic drugs. *Semin. Oncol*. 19, 529—542.

Andreozzi, F., Procopio, C., Greco, A., Mannino, G.C., Miele, C., Raciti, G. a, Iadicicco, C., Beguinot, F., Pontiroli, a E., Hribal, M.L., Folli, F., Sesti, G., 2011. Increased levels of the Akt-specific phosphatase PH domain leucine-rich repeat protein phosphatase (PHLPP)-1 in obese participants are associated with insulin resistance. *Diabetologia* 54, 1879–1887.

Arola, O.J., Saraste, A., Pulkki, K., Kallajoki, M., Parvinen, M., Voipio-Pulkki, L.M., 2000. Acute doxorubicin cardiotoxicity involves cardiomyocyte apoptosis. *Cancer Res*. 60, 1789–1792.

Asensi, M., Sastre, J., Pallardo, F. V, Lloret, A., Lehner, M., Garcia-de-la Asuncion, J., Viña, J., 1999. Ratio of reduced to oxidized glutathione as indicator of oxidative stress status and DNA damage, in: Oxidants and Antioxidants. *Academic Press*, pp. 267–276.

Aznar, S., Valerón, P.F., del Rincon, S. V, Pérez, L.F., Perona, R., Lacal, J.C., 2001. Simultaneous tyrosine and serine phosphorylation of STAT3 transcription factor is involved in Rho A GTPase oncogenic transformation. *Mol. Biol. Cell* 12, 3282–3294.

Bachur, N.R., Gee, M. V, Friedman, R.D., Friedman, R., 1982. Nuclear catalyzed antibiotic free radical formation. *Cancer Res*. 42, 1078–1081.

Bachur, N.R., Johnson, R., Yu, F., Hickey, R., Applegren, N., Malkas, L., 1993. Antihelicase action of DNA-binding anticancer agents: relationship to guanosine-cytidine intercalator binding. *Mol. Pharmacol*. 44, 1064–1069.

Barrett-Lee, P., Dixon, J., Farrell, C., Jones, A., Leonard, R., Murray, N., Palmieri, C., Plummer, C., Stanley, A., Verrill, M., 2009. Expert opinion on the use of anthracyclines in patients with advanced breast cancer at cardiac risk. *Ann. Oncol*. 20, 816–827.

Benchekroun, M.N., Sinha, B.K., Robert, J., 1993. Doxorubicin-induced oxygen free radical formation in sensitive and doxorubicin-resistant variants of rat glioblastoma cell lines. *FEBS Lett*. 322, 295–298.

Beutler, B.A., Milsark, I.W., Cerami, A., 1985. Cachectin/tumor necrosis factor: production, distribution, and metabolic fate in vivo. *J. Immunol*. 135, 3972–3977.

Boengler, K., Hilfiker-Kleiner, D., Drexler, H., Heusch, G., Schulz, R., 2008. The myocardial JAK/STAT pathway: from protection to failure. *Pharmacol. Ther*. 120, 172–185.

Bolli, R., Dawn, B., Xuan, Y.T., 2001. Emerging role of the JAK-STAT pathway as a mechanism of protection against ischemia/reperfusion injury. *J. Mol. Cell. Cardiol*. 33, 1893–1896.

Bradford, M.M., 1976. A rapid and sensitive method for the quantitation of microgram quantities of protein utilizing the principle of protein-dye binding. *Anal. Biochem*. 72, 248–254.

Bradley, J.R., 2008. TNF-mediated inflammatory disease. *J. Pathol*. 214, 149–160.

Brantley-Finley, C., Lyle, C.S., Du, L., Goodwin, M.E., Hall, T., Szwedo, D., Kaushal, G.P., Chambers, T.C., 2003. The JNK, ERK and p53 pathways play distinct roles in apoptosis mediated by the antitumor agents vinblastine, doxorubicin, and etoposide. *Biochem. Pharmacol*. 66, 459–469.

Braunwald, E., Kloner, R., 1985. Myocardial reperfusion: a double-edged sword? *J. Clin. Invest*. 76, 1713–1719.

Bristow, M., Thompson, P., Handolph, M., Mason, J., Billingham, M.E., Harrison, D., 1978. Early Anthracycline Cardiotoxicity. *Am. J. Med*. 65, 823–832.

Bryant, D., Becker, L., Richardson, J., Shelton, J., Franco, F., Peshock, R., Thompson, M., Giroir, B., 1998. Cardiac failure in transgenic mice with myocardial expression of tumor necrosis factor-α. *Circulation* 97, 1375–1381.

Bueno, O.F., Molkentin, J.D., 2002. Involvement of extracellular signal-regulated kinases 1/2 in cardiac hypertrophy and cell death. *Circ. Res*. 91, 776–781.

Burden, D., Osheroff, N., 1998. Mechanism of action of eukaryotic topoisomerase II and drugs targeted to the enzyme. *Biochim. Biophys. Acta* 1400, 139–154.

Busquets, S., Aranda, X., Ribas-Carbó, M., Azcon-Bieto, J., López-Soriano, F.J., Argilés, J.M., 2003. Tumour necrosis factor-alpha uncouples respiration in isolated rat mitochondria. *Cytokine* 22, 1–4.

Cabal-Hierro, L., Lazo, P.S., 2012. Signal transduction by tumor necrosis factor receptors. *Cell. Signal*. 24, 1297–1305.

Cacciapaglia, F., Salvatorelli, E., Minotti, G., Afeltra, A., Menna, P., 2014. Low level tumor necrosis factor-alpha protects cardiomyocytes against high level tumor necrosis factor-alpha: brief insight into a beneficial paradox. *Cardiovasc. Toxicol*.

Cao, G., Alessio, H., Cutler, R., 1993. Oxygen-Radical Absorbance Capacity Assay for Antioxidants. *Free Radic. Biol. Med*. 14, 303–311.

Cardinale, D., Sandri, M., Martinoni, A., Borghini, E., Civelli, M., Lamantia, G., Cinieri, S., Martinelli, G., Fiorentini, C., Cipolla, C., 2002. Myocardial injury revealed by plasma troponin I in breast cancer treated with high-dose chemotherapy. *Ann. Oncol*. 13, 710–715.

Chen, B., Peng, X., Pentassuglia, L., Lim, C.C., Sawyer, D.B., 2007. Molecular and cellular mechanisms of anthracycline cardiotoxicity. *Cardiovasc. Toxicol.* 7, 114–121.

Childs, A.C., Phaneuf, S.L., Dirks, A.J., Phillips, T., Leeuwenburgh, C., 2002. Doxorubicin treatment in vivo causes cytochrome C release and cardiomyocyte apoptosis, as well as increased mitochondrial efficiency, superoxide dismutase activity, and Bcl-2:Bax ratio. *Cancer Res*. 62, 4592–4598.

Chinnaiyan, A., O'Rourke, K., Tewari, M., Dixit, V., 1995. FADD , a novel death domain-containing protein interacts with the death domain of Fas and initiates apoptosis. *Cell* 81, 505–512.

Chiosi, E., Spina, A., Sorrentino, A., Romano, M., Sorvillo, L., Senatore, G., D'Auria, R., Abbruzzese, A., Caraglia, M., Naviglio, S., Illiano, G., 2007. Change in TNF-alpha receptor expression is a relevant event in doxorubicin-induced H9c2 cardiomyocyte cell death. *J. Interf. Cytokine Res*. 27, 589–597.

Choi, E.H., Chang, H.-J., Cho, J.Y., Chun, H.S., 2007. Cytoprotective effect of anthocyanins against doxorubicin-induced toxicity in H9c2 cardiomyocytes in relation to their antioxidant activities. *Food Chem. Toxicol*. 45, 1873–1881.

Chu, W.-M., 2013. Tumor necrosis factor. *Cancer Lett*. 328, 222–225.

Cortés-Funes, H., Coronado, C., 2007. Role of anthracyclines in the era of targeted therapy. *Cardiovasc. Toxicol.* 7, 56–60.

Cross, T.G., Scheel-Toellner, D., Henriquez, N. V, Deacon, E., Salmon, M., Lord, J.M., 2000. Serine/threonine protein kinases and apoptosis. *Exp. Cell Res*. 256, 34–41.

Cullinane, C., Cutts, S.M., Panousis, C., Phillips, D.R., 2000. Interstrand cross-linking by adriamycin in nuclear and mitochondrial DNA of MCF-7 cells. *Nucleic Acids Res*. 28, 1019–1025.

Cullinane, C., Phillips, D.R., 1990. Induction of stable transcriptional blockage sites by adriamycin: GpC specificity of apparent adriamycin-DNA adducts and dependence on iron(III) ions. *Biochemistry* 29, 5638–5646.

Cummings, J., Willmott, N., Hoey, B.M., Marley, E.S., SMyth, J.F., 1992. The consequences of doxorubicin quinone reduction in vivo in tumour tissue. *Biochem. Pharmacol*. 44, 2165–2174.

Curran, C.F., Narang, P.K., Reynolds, R.D., 1991. Toxicity profile of dexrazoxane (Zinecard, ICRF-187, ADR-529, NSC-169780), a modulator of doxorubicin cardiotoxicity. *Cancer Treat. Rev*. 18, 241–252.

Cutts, S.M., Nudelman, A., Rephaeli, A., Phillips, D.R., 2005. The power and potential of doxorubicin-DNA adducts. *IUBMB Life* 57, 73–81.

Cvetković, R.S., Scott, L.J., 2005. Dexrazoxane : a review of its use for cardioprotection during anthracycline chemotherapy. *Drugs* 65, 1005–1024.

Darnell, J.E., 1997. STATs and gene regulation. *Science* 277, 1630–1635.

Das, J., Ghosh, J., Manna, P., Sil, P.C., 2011. Taurine suppresses doxorubicin-triggered oxidative stress and cardiac apoptosis in rat via up-regulation of PI3-K/Akt and inhibition of p53, p38-JNK. *Biochem. Pharmacol*. 81, 891–909.

David, M., Petricoin, E., Benjamin, C., Pine, R., Weber, M.J., Larner, a C., 1995. Requirement for MAP kinase (ERK2) activity in interferon alpha- and interferon beta-stimulated gene expression through STAT proteins. *Science* 269, 1721–1723.

Deuchar, G.A., Opie, L.H., Lecour, S., 2007. TNFα is required to confer protection in an in vivo model of classical ischaemic preconditioning. *Life Sci*. 80, 1686–1691.

Di Marco, A., Gaetani, M., Scarpinato, B., 1969. Adriamycin (NSC-123, 127): A new antibiotic with antitumor activity. *Cancer Chemother. Reports* 53, 33–37.

Dibbs, Z.I., Diwan, A., Nemoto, S., DeFreitas, G., Abdellatif, M., Carabello, B.A., Spinale, F.G., Feuerstein, G., Sivasubramanian, N., Mann, D.L., 2003. Targeted overexpression of transmembrane tumor necrosis factor provokes a concentric cardiac hypertrophic phenotype. *Circulation* 108, 1002–1008.

Dirks-Naylor, A.J., 2013. The role of autophagy in doxorubicin-induced cardiotoxicity. *Life Sci*. 93, 913–916.

Doroshow, J.H., 1983. Effect of anthracycline antibiotics on oxygen radical formation in rat heart. *Cancer Res*. 43, 460–472.

Doroshow, J.H., Locker, G.Y., Baldinger, J., Myers, C.E., 1979. The effect of doxorubicin on hepatic and cardiac glutathione. *Res. Commun. Chem. Pathol. Pharmacol*. 26, 285—295.

Doroshow, J.H., Locker, G.Y., Myers, C.E., 1980. Enzymatic defenses of the mouse heart against reactive oxygen metabolites: alterations produced by doxorubicin. *J. Clin. Invest*. 65, 128–135.

Downward, J., 2004. PI 3-kinase, Akt and cell survival. *Semin. Cell Dev. Biol*. 15, 177–182.

Dudich, E., Semenkova, L., Dudich, I., Gorbatova, E., Tochtamisheva, N., Tatulov, E., Nikolaeva, M., Sukhikh, G., 1999. a-Fetoprotein causes apoptosis in tumor cells via a pathways independent of CD95, TNFR1 and TNFR2 through activation of caspase-3-like proteases. *Eur. J. Biochem*. 266, 750–761.

Eliot, H., Gianni, L., Myers, C., 1984. Oxidative destruction of DNA by the adriamycin-iron complex. *Biochemistry* 23, 928–936.

Eom, Y.-W., Kim, M.A., Park, S.S., Goo, M.J., Kwon, H.J., Sohn, S., Kim, W.-H., Yoon, G., Choi, K.S., 2005. Two distinct modes of cell death induced by doxorubicin: apoptosis and cell death through mitotic catastrophe accompanied by senescence-like phenotype. *Oncogene* 24, 4765–4777.

Ewer, M.S., Ewer, S.M., 2010. Cardiotoxicity of anticancer treatments: what the cardiologist needs to know. *Nat. Rev. Cardiol*. 7, 564–575.

Fan, G.-C., Zhou, X., Wang, X., Song, G., Qian, J., Nicolaou, P., Chen, G., Ren, X., Kranias, E.G., 2008. Heat shock protein 20 interacting with phosphorylated Akt reduces doxorubicin-triggered oxidative stress and cardiotoxicity. *Circ. Res*. 103, 1270–1279.

Fan, M., Chambers, T.C., 2001. Role of mitogen-activated protein kinases in the response of tumor cells to chemotherapy. *Drug Resist. Updat*. 5, 253–267.

Feinstein, E., Canaani, E., Weiner, L.M., 1993. Dependence of nucleic acid degradation on in situ free-radical production by adriamycin. *Biochemistry* 32, 13156–13161.

Ferlay, J., Shin, H.-R., Bray, F., Forman, D., Mathers, C., Parkin, D.M., 2010. Estimates of worldwide burden of cancer in 2008: GLOBOCAN 2008. *Int. J. cancer* 127, 2893–2917.

Ferrari, R., 1999. The role of TNF in cardiovascular disease. *Pharmacol. Res.* 40, 97–105.

Fornari, F.A., Randolph, J.K., Yalowich, J.C., Ritke, M.K., Gewirtz, D.A., 1994. Interference by doxorubicin with DNA unwinding in MCF-7 breast tumor cells. *Mol. Pharmacol.* 45, 649–656.

Franco, I.A.M., 2006. Mechanism of cell death in cardiac myocytes exposed to Doxorubicin. University of Florida.

Frias, M.A., Lang, U., Gerber-Wicht, C., James, R.W., 2010. Native and reconstituted HDL protect cardiomyocytes from doxorubicin-induced apoptosis. *Cardiovasc. Res.* 85, 118–126.

Frias, M.A., Somers, S., Gerber-Wicht, C., Opie, L.H., Lecour, S., Lang, U., 2008. The PGE2-Stat3 interaction in doxorubicin-induced myocardial apoptosis. *Cardiovasc. Res*. 80, 69–77.

Fukada, T., Hibi, M., Yamanaka, Y., Takahashi-Tezuka, M., Fujitani, Y., Yamaguchi, T., Nakajima, K., Hirano, T., 1996. Two signals are necessary for cell proliferation induced by a cytokine receptor gp130: involvement of STAT3 in anti-apoptosis. *Immunity* 5, 449–460.

Fukazawa, R., Miller, T.A., Kuramochi, Y., Frantz, S., Kim, Y.-D., Marchionni, M.A., Kelly, R.A., Sawyer, D.B., 2003. Neuregulin-1 protects ventricular myocytes from anthracycline-induced apoptosis via erbB4-dependent activation of PI3-kinase/Akt. *J. Mol. Cell. Cardio*l. 35, 1473–1479.

Gabrielson, K., Bedja, D., Pin, S., Tsao, A., Gama, L., Yuan, B., Muratore, N., 2007. Heat shock protein 90 and ErbB2 in the cardiac response to doxorubicin injury. *Cancer Res*. 67, 1436–1441.

Gamen, S., Anel, A., Pérez-Galán, P., Lasierra, P., Johnson, D., Piñeiro, A., Naval, J., 2000. Doxorubicin treatment activates a Z-VAD-sensitive caspase, which causes deltapsim loss, caspase-9 activity, and apoptosis in Jurkat cells. *Exp. Cell Res*. 258, 223–235.

Garcia, I., Olleros, M., Quesniaux, V., Jacobs, M., Allie, N., Nedospasov, S., Szymkowski, D., Ryffel, B., 2011. Roles of soluble and membrane TNF and related ligands in Mycobacterial infections: effects of selective and non-selective TNF inhibitors during infection, in: *Advances in TNF Family Research*. Chapter 20.

Gatta, G., Capocaccia, R., Coleman, M.P., Ries, L. a G., Berrino, F., 2002. Childhood cancer survival in Europe and the United States. *Cancer* 95, 1767–1772.

Gewirtz, D.A., 1999. A critical evaluation of the mechanisms of action proposed for the antitumor effects of the anthracycline antibiotics adriamycin and daunorubicin. *Biochem. Pharmacol*. 57, 727–741.

Gharanei, M., Hussain, A., Janneh, O., Maddock, H., 2013. Attenuation of Doxorubicin-Induced Cardiotoxicity by mdivi-1: A Mitochondrial Division/Mitophagy Inhibitor. *PLoS One* 8, e77713.

Gianni, L., Herman, E.H., Lipshultz, S.E., Minotti, G., Sarvazyan, N., Sawyer, D.B., 2008. Anthracycline cardiotoxicity: from bench to bedside. *J. Clin. Oncol.* 26, 3777–3784.

Gilliam, L.A., Moylan, J.S., Ferreira, L.F., Reid, M.B., 2011. TNF/TNFR1 signaling mediates doxorubicin-induced diaphragm weakness. *Am. J. Physiol. Cell. Mol. Physiol*. 300, L225–231.

Gilliam, L.A.A., Fisher-Wellman, K.H., Lin, C.-T., Maples, J.M., Cathey, B.L., Neufer, P.D., 2013. The anticancer agent doxorubicin disrupts mitochondrial energy metabolism and redox balance in skeletal muscle. *Free Radic. Biol. Med*. 65, 988–996.

Go, A.S., Mozaffarian, D., Roger, V.L., Benjamin, E.J., Berry, J.D., Borden, W.B., Bravata, D.M., Dai, S., Ford, E.S., Fox, C.S., Sheila Franco, Fullerton, H.J., Gillespie, C., Hailpern,

S.M., Heit, J.A., Howard, V.J., Huffman, M.D., Kissela, B.M., Kittner, S.J., Lackland, D.T., Lichtman, J.H., Lisabeth, L.D., Magid, D., Marcus, G.M., Marelli, A., Matchar, D.B., Darren K McGuire, Emily R Mohler, Moy, C.S., Mussolino, M.E., Nichol, G., Paynter, N.P., Schreiner, P.J., Sorlie, P.D., Stein, J., Turan, T.N., Virani, S.S., Wong, N.D., Woo, D., Turner, M.B., 2013. Heart disease and stroke statistics--2013 update: A report from the American Heart Association. *Circulation* 127, e6–e245.

Greene, R.F., Collins, J.M., Jenkins, J.F., Speyer, J.L., Myers, C.E., 1983. Plasma pharmacokinetics of Adriamycin and Adriamycinol : Implications for the design of in vitro experiments and treatment protocols. *Cancer Res*. 43, 3417–3421.

Gustafsson, Å.B., Gottlieb, R.A., 2003. Mechanisms of apoptosis in the heart. *J. Clin. Immunol*. 23, 447–459.

Hamid, T., Gu, Y., Ortines, R. V, Bhattacharya, C., Wang, G., Xuan, Y.-T., Prabhu, S.D., 2009. Divergent tumor necrosis factor receptor-related remodeling responses in heart failure: role of nuclear factor-kappaB and inflammatory activation. *Circulation* 119, 1386–1397.

Hampton, M.B., Orrenius, S., 1998. Redox regulation of apoptotic cell death. *BioFactors* 8, 1–5.

Haq, S., Choukroun, G., Lim, H., Tymitz, K.M., del Monte, F., Gwathmey, J., Grazette, L., Michael, A., Hajjar, R., Force, T., Molkentin, J.D., 2001. Differential activation of signal transduction pathways in human hearts with hypertrophy versus advanced heart failure. *Circulation* 103, 670–677.

Hasinoff, B.B., Schnabl, K.L., Marusak, R. a, Patel, D., Huebner, E., 2003. Dexrazoxane (ICRF-187) protects cardiac myocytes against doxorubicin by preventing damage to mitochondria. *Cardiovasc. Toxicol*. 3, 89–99.

Hattori, R., Maulik, N., Otani, H., Zhu, L., Cordis, G., Engelman, R.M., Siddiqui, M. a, Das, D.K., 2001. Role of STAT3 in ischemic preconditioning. *J. Mol. Cell. Cardiol*. 33, 1929–1936.

Haudek, S.B., Bryant, D.D., Giroir, B.P., 2001. Differential regulation of myocardial NFκB following acute or chronic TNF- α exposure. *J. Mol. Cell. Cardiol.* 33, 1263–1271.

Hausenloy, D.J., 2009. Signalling pathways in ischaemic postconditioning. *Thromb Haemost* 101, 626–634.

Hausenloy, D.J., Mocanu, M.M., Yellon, D.M., 2004. Cross-talk between the survival kinases during early reperfusion: its contribution to ischemic preconditioning. *Cardiovasc. Res.* 63, 305–312.

Hausenloy, D.J., Yellon, D.M., 2004. New directions for protecting the heart against ischaemia-reperfusion injury: targeting the Reperfusion Injury Salvage Kinase (RISK)-pathway. *Cardiovasc. Res*. 61, 448–460.

Hayward, R., Hydock, D., Gibson, N., Greufe, S., Bredahl, E., Parry, T., 2013. Tissue retention of doxorubicin and its effects on cardiac, smooth, and skeletal muscle function. *J. Physiol. Biochem*. 69, 177–187.

Hearse, D., Humphrey, S., Chain, E., 1973. Abrupt reoxygenation of the anoxic potassium-arrested perfused rat heart: a study of myocardial enzyme release. *J. Mol. Cell. Cardiol.* 5, 395–407.

Heba, G., Krzeminski, T., Porc, M., Grzyb, J., Al, E., 2001. The time course of tumor necrosis factor-(alpha), inducible nitric oxide synthase and vascular endothelial growth factor expression in an experimental model of chronic myocardial infarction in rats. *J. Vasc. Res*. 38, 288–300.

Hegewisch, S., Weh, H., Hossfeld, D., 1988. TNF-induced cardiomyopathy. *Lancet* 335, 294–295.

Hehlgans, T., Pfeffer, K., 2005. The intriguing biology of the tumour necrosis factor/tumour necrosis factor receptor superfamily: players, rules and the games. *Immunology* 115, 1–20.

Herman, E., Ardalan, B., Bier, C., Waravdekar, V., Krop, S., 1979. Reduction of daunorubicin lethality and myocardial cellular alterations by pretreatment with ICRF-187 in Syrian golden hamsters. *Cancer Treat. Rep*. 63, 89—92.

Hildyard, J.C.W., Wells, D.J., 2014. Identification and validation of quantitative PCR reference genes suitable for normalizing expression in normal and dystrophic cell culture models of myogenesis. *PLOS Curr. Muscular Dystrophy* March 6, 1–23.

Hilfiker-Kleiner, D., Hilfiker, A., Fuchs, M., Kaminski, K., Schaefer, A., Schieffer, B., Hillmer, A., Schmiedl, A., Ding, Z., Podewski, E., Podewski, E., Poli, V., Schneider, M.D., Schulz, R., Park, J.-K., Wollert, K.C., Drexler, H., 2004. Signal transducer and activator of transcription 3 is required for myocardial capillary growth, control of interstitial matrix deposition, and heart protection from ischemic injury. *Circ. Res.* 95, 187–195.

Hirata, H., Takahashi, A., Kobayashi, S., Yonehara, S., Sawai, H., Okazaki, T., Yamamoto, K., Sasada, M., 1998. Caspases are activated in a branched protease cascade and control distinct downstream processes in Fas-induced apoptosis. *J. Exp. Med*. 187, 587–600.

Horenstein, M.S., Vander Heide, R.S., L'Ecuyer, T.J., 2000. Molecular basis of anthracycline-induced cardiotoxicity and its prevention. *Mol. Genet. Metab*. 71, 436–444.

Ichihara, S., Yamada, Y., Kawai, Y., Osawa, T., Furuhashi, K., Duan, Z., Ichihara, G., 2007. Roles of oxidative stress and Akt signaling in doxorubicin cardiotoxicity. *Biochem. Biophys. Res. Commun*. 359, 27–33.

Imada, K., Leonard, W.J., 2000. The Jak-STAT pathway. *Mol. Immunol.* 37, 1–11.

Jacoby, J.J., Kalinowski, A., Liu, M., Zhang, S.S., Gao, Q., Chai, G., Ji, L., Iwamoto, Y., Li, E., Schneider, M., Russell, K.S., Jacoby, J.J., Kalinowskit, A., 2003. Cardiomyocyte-restricted knockout of STAT3 results in higher sensitivity to inflammation, cardiac fibrosis and heart failure with advanced age. *Proc. Natl. Acad. Sci*. 100, 12929–12934.

Jiang, B., Zhang, L., Li, M., Wu, W., Yang, M., Wang, J., Guo, D., 2008. Salvianolic acids prevent acute doxorubicin cardiotoxicity in mice through suppression of oxidative stress. *Food Chem. Toxicol*. 46, 1510–1515.

Jonassen, A.K., Sack, M.N., Mjøs, O.D., Yellon, D.M., 2001. Myocardial protection by insulin at reperfusion requires early administration and is mediated via Akt and p70s6 kinase cell-survival signaling. *Circ. Res.* 89, 1191–1198.

Jones, D.P., 2002. Redox potential of GSH/GSSG couple: assay and biological significance. *Methods Enzymol*. 348, 93–112.

Kalyanaraman, B., Joseph, J., Kalivendi, S., Wang, S., Konorev, E., Kotamraju, S., 2002. Doxorubicin-induced apoptosis: implications in cardiotoxicity. *Mol. Cell. Biochem*. 234, 119–124.

Kawamura, T., Hasegawa, K., Morimoto, T., Iwai-Kanai, E., Miyamoto, S., Kawase, Y., Ono, K., Wada, H., Akao, M., Kita, T., 2004. Expression of p300 protects cardiac myocytes from apoptosis in vivo. *Biochem. Biophys. Res. Commun*. 315, 733–738.

Keizer, H.G., Pinedo, H.M., Schuurhuis, G.J., Joenje, H., 1990. Doxorubicin (adriamycin): a critical review of free radical-dependent mechanisms of cytotoxicity. *Pharmacol. Ther*. 47, 219–231.

Kim, K.-H., Oudit, G., Backx, P., 2008. Erythropoietin protects against doxorubicin-induced cardiomyopathy via a phosphatidylinositol 3-kinase-dependent pathway. *J. Pharmacol. Exp. Ther*. 324, 160–169.

Kim, S.H., Kim, J.H., 1972. Lethal effect of adriamycin on the division cycle of HeLa cells. *Cancer Res*. 32, 323–325.

Kim, S.-Y., Kim, S.-J., Kim, B.-J., Rah, S.-Y., Chung, S.M., Im, M.-J., Kim, U.-H., 2006. Doxorubicin-induced reactive oxygen species generation and intracellular Ca2+ increase are reciprocally modulated in rat cardiomyocytes. *Exp. Mol. Med*. 38, 535–545.

Kisseleva, T., Bhattacharya, S., Braunstein, J., Schindler, C.W., 2002. Signaling through the JAK/STAT pathway, recent advances and future challenges. Gene 285, 1–24.

Krown, K.A., Page, M.T., Nguyen, C., Zechner, D., Gutierrez, V., Comstock, K.L., Glembotski, C.C., Quintana, P.J., Sabbadini, R.A., 1996. Tumor necrosis factor alpha-induced apoptosis in cardiac myocytes. Involvement of the sphingolipid signaling cascade in cardiac cell death. *J. Clin. Invest*. 98, 2854–2865.

Kumar, D., Kirshenbaum, L., Li, T., Danelisen, I., Singal, P.K., 2001. Apoptosis in Adriamycin cardiomyopathy and its modulation by Probucol. *Antioxidants Redox Signal*. 3, 135–145.

Kunisada, K., Negoro, S., Tone, E., Funamoto, M., Osugi, T., Yamada, S., Okabe, M., Kishimoto, T., Yamauchi-Takihara, K., 2000. Signal transducer and activator of transcription 3 in the heart transduces not only a hypertrophic signal but a protective signal against doxorubicin-induced cardiomyopathy. *Proc. Natl. Acad. Sci*. 97, 315–319.

L'Ecuyer, T., Horenstein, M.S., Thomas, R., Vander Heide, R., 2001. Anthracycline-induced cardiac injury using a cardiac cell line: potential for gene therapy studies. *Mol. Genet. Metab*. 74, 370–379.

Lacerda, L., McCarthy, J., Mungly, S.F.K., Lynn, E.G., Sack, M.N., Opie, L.H., Lecour, S., 2010. TNFα protects cardiac mitochondria independently of its cell surface receptors. *Basic Res. Cardiol.* 105, 751–762.

Lacerda, L., Somers, S., Opie, L.H., Lecour, S., 2009. Ischaemic postconditioning protects against reperfusion injury via the SAFE pathway. *Cardiovasc. Res*. 84, 201–208.

Lambertenghi-Deliliers, G., Zanon, P.L., Pozzoli, E.F., Bellini, O., 1976. Myocardial injury induced by a single dose of adriamycin: an electron microscopic study. *Tumori* 62, 517–528.

Lecour, S., 2009a. Activation of the protective Survivor Activating Factor Enhancement (SAFE) pathway against reperfusion injury: Does it go beyond the RISK pathway? *J. Mol. Cell. Cardiol*. 47, 32–40.

Lecour, S., 2009b. Multiple protective pathways against reperfusion injury: a SAFE path without Aktion? *J. Mol. Cell. Cardiol*. 46, 607–609.

Lecour, S., James, R.W., 2011. When are pro-inflammatory cytokines SAFE in heart failure? *Eur. Heart J*. 32, 680–685.

Lecour, S., Smith, R.M., Woodward, B., Opie, L.H., Rochette, L., Sack, M.N., 2002. Identification of a novel role for sphingolipid signaling in TNF alpha and ischemic preconditioning mediated cardioprotection. *J. Mol. Cell. Cardiol*. 34, 509–518.

Lecour, S., Suleman, N., Deuchar, G.A., Somers, S., Lacerda, L., Huisamen, B., Opie, L.H., 2005. Pharmacological preconditioning with tumor necrosis factor-a activates signal transducer and activator of transcription-3 at reperfusion without involving classic prosurvival kinases (Akt and Extracellular Signal – Regulated Kinase). *Circulation* 112, 3911–3918.

Ledgerwood, E.C., Prins, J.B., Bright, N.A., Johnson, D.R., Wolfreys, K., Pober, J.S., O'Rahilly, S., Bradley, J.R., 1998. Tumor necrosis factor is delivered to mitochondria where a tumor necrosis factor-binding protein is localized. *Lab. Invest*. 78, 1583—1589.

Lefrak, E.A., Piťha, J., Rosenheim, S., Gottlieb, J.A., 1973. A clinicopathologic analysis of Adriamycin cardiotoxicity. *Cancer* 32, 302–314.

Legha, S., Benjamin, R., Mackay, B., Ewer, M.S., Wallace, S., Valdivieso, M., Rasmussen, S., Blumenschein, G.R., Freireich, E., 1982. Reduction of Doxorubicin cardiotoxicity by prolonged continuous intravenous infusion. *Ann. Intern. Med*. 96, 133–140.

Leonard, W.J., 2001. Role of Jak kinases and STATs in cytokine signal transduction. *Int. J. Hematol.* 73, 271–277.

Levy, D., Darnell, J.E., 2002. STATS : Transcriptional control and biological impact. *Nat. Rev. Mol. Cell Biol.* 3, 651–662.

Li, H., Zhu, H., Xu, C.J., Yuan, J., 1998. Cleavage of BID by caspase 8 mediates the mitochondrial damage in the Fas pathway of apoptosis. *Cell* 94, 491–501.

Li, K., Sung, R.Y.T., Huang, W.Z., Yang, M., Pong, N.H., Lee, S.M., Chan, W.Y., Zhao, H., To, M.Y., Fok, T.F., Li, C.K., Wong, Y.O., Ng, P.C., 2006. Thrombopoietin protects against in vitro and in vivo cardiotoxicity induced by doxorubicin. *Circulation* 113, 2211–2220.

Li, L., Takemura, G., Li, Y., Miyata, S., Esaki, M., Okada, H., Kanamori, H., Khai, N.C., Maruyama, R., Ogino, A., Minatoguchi, S., Fujiwara, T., Fujiwara, H., 2006. Preventive effect of erythropoietin on cardiac dysfunction in doxorubicin-induced cardiomyopathy. *Circulation* 113, 535–543.

Li, T., Danelisen, I., Singal, P.K., 2002. Early changes in myocardial antioxidant enzymes in rats treated with adriamycin. Mol. Cell. Biochem. 232, 19–26.

Li, X., Luo, R., Jiang, R., Meng, X., Wu, X., Zhang, S., Hua, W., 2013. The role of the Hsp90/Akt pathway in myocardial calpain-induced caspase-3 activation and apoptosis during sepsis. *BMC Cardiovasc. Disord*. 13, 1–8.

Lien, Y.C., Lin, S.M., Nithipongvanitch, R., Oberley, T.D., Noel, T., Zhao, Q., Daosukho, C., St Clair, D.K., 2006. Tumor necrosis factor receptor deficiency exacerbated Adriamycin-induced cardiomyocytes apoptosis: an insight into the Fas connection. *Mol. Cancer Ther*. 5, 261–269.

Lips, D.J., Bueno, O.F., Wilkins, B.J., Purcell, N.H., Kaiser, R., Lorenz, J.N., Voisin, L., Saba-El-Leil, M.K., Meloche, S., Pouysségur, J., Pagès, G., De Windt, L.J., Doevendans, P., Molkentin, J.D., 2004. MEK1-ERK2 signaling pathway protects myocardium from ischemic injury in vivo. *Circulation* 109, 1938–1941.

Lipshultz, S.E., Colan, S.D., Gelber, R.D., Perez-Atayde, A., Sallan, S.E., Sanders, S.P., 1991. Late cardiac effects of Doxorubicin therapy for acute lymphoblastic leukemia in childhood. *N. Engl. J. Med*. 324, 808–815.

Lipshultz, S.E., Rifai, N., Dalton, V.M., Levy, D.E., Silverman, L.B., Lipsitz, S.R., Colan, S.D., Asselin, B.L., Barr, R.D., Clavell, L., Hurwitz, C., Moghrabi, A., Samson, Y., Schorin, M., Gelber, R.D., Sallan, S.E., 2004. The effect of dexrazoxane on myocardial injury in doxorubicin-treated children with acute lymphoblastic leukemia. *N. Engl. J. Med*. 351, 145–153.

Liu, J., Mao, W., Ding, B., Liang, C., 2008. ERKs/p53 signal transduction pathway is involved in doxorubicin-induced apoptosis in H9c2 cells and cardiomyocytes. *Am. J. Physiol. Circ. Physiol.* 295, H1956–H1965.

Liu, X., Chen, Z., Chua, C.H.U.C., Ma, Y., Youngberg, G.A., Hamdy, R., Chua, B.H.L., Chua, C.C., Ma, S., 2002. Melatonin as an effective protector against doxorubicin-induced cardiotoxicity. A*m. J. Physiol. Hear. Circ. Physiol.* 283, 254–263.

Locksley, R.M., Killeen, N., Lenardo, M.J., 2001. The TNF and TNF receptor superfamilies: integrating mammalian biology. *Cell* 104, 487–501.

Lou, H., Danelisen, I., Singal, P.K., 2004. Cytokines are not upregulated in adriamycin-induced cardiomyopathy and heart failure. *J. Mol. Cell. Cardiol*. 36, 683–690.

Lou, H., Danelisen, I., Singal, P.K., 2005. Involvement of mitogen-activated protein kinases in adriamycin-induced cardiomyopathy. *Am. J. Physiol. Hear. Circ. Physiol*. 288, H1925–H1930.

Mann, D.L., 2002. Inflammatory mediators and the failing heart: past, present, and the foreseeable Future. *Circ. Res.* 91, 988–998.

Mann, D.L., 2003. Stress-activated cytokines and the heart: from adaptation to maladaptation. *Annu. Rev. Physiol.* 65, 81–101.

Masella, R., Di Benedetto, R., Varì, R., Filesi, C., Giovannini, C., 2005. Novel mechanisms of natural antioxidant compounds in biological systems: involvement of glutathione and glutathione-related enzymes. *J. Nutr. Biochem*. 16, 577–586.

Mellor, H.R., Bell, A.R., Valentin, J.P., Roberts, R.R., 2011. Cardiotoxicity associated with targeting kinase pathways in cancer. *Toxicol. Sci*. 120, 14–32.

Mercuro, G., Cadeddu, C., Piras, A., Dessì, M., Madeddu, C., Deidda, M., Serpe, R., Massa, E., Mantovani, G., 2007. Early epirubicin-induced myocardial dysfunction revealed by serial tissue Doppler echocardiography: correlation with inflammatory and oxidative stress markers. *Oncologist* 12, 1124–1133.

Meriwether, W.D., Bachur, N.R., 1972. Inhibition of DNA and RNA metabolism by daunorubicin and adriamycin in L1210 mouse leukemia. *Cancer Res*. 32, 1137–1142.

Mimnaugh, E.G., Siddik, Z.H., Drew, R., Sikic, B.I., Gram, T.E., 1979. The effects of α-tocopherol on the toxicity, disposition, and metabolism of adriamycin in mice. *Toxicol. Appl. Pharmacol*. 49, 119–126.

Minotti, G., Menna, P., Salvatorelli, E., Cairo, G., Gianni, L., 2004a. Anthracyclines: molecular advances and pharmacologic developments in antitumor activity and cardiotoxicity. *Pharmacol. Rev.* 56, 185–229.

Minotti, G., Recalcati, S., Menna, P., Salvatorelli, E., Corna, G., Cairo, G., 2004b. Doxorubicin cardiotoxicity and the control of iron metabolism: Quinone-dependent and independent mechanisms. *Methods Enzymol.* 378, 340–361.

Minow, R., Benjamin, R.S., Lee, E.T., Gottlieb, J., 1977. Adriamycin cardiomyopathy--risk factors. *Cancer* 39, 1397–402.

Mitra, M.S., Donthamsetty, S., White, B., Latendresse, J.R., Mehendale, H.M., 2007. Mechanism of protection of moderately diet restricted rats against doxorubicin-induced acute cardiotoxicity. *Toxicol. Appl. Pharmacol*. 225, 90–101.

Mohamed, H.E., Asker, M.E., Ali, S.I., Fattah, T.M., 2004. Protection against Doxorubicin cardiomyopathy in rats: role of phosphodiesterase inhibitors type 4. *J. Pharm. Pharmacol.* 56, 757–768.

Monden, Y., Kubota, T., Inoue, T., Tsutsumi, T., Kawano, S., Ide, T., Tsutsui, H., Sunagawa, K., 2007. Tumor necrosis factor-a is toxic via receptor 1 and protective via receptor 2 in a murine model of myocardial infarction. *Am. J. Physiol. Hear. Circ. Physiol.* 293, 743–753.

Monostori, P., Wittmann, G., Karg, E., Túri, S., 2009. Determination of glutathione and glutathione disulfide in biological samples: an in-depth review. *J. Chromatogr.* B 877, 3331–3346.

Montaigne, D., Hurt, C., Neviere, R., 2012. Mitochondria death/survival signaling pathways in cardiotoxicity induced by anthracyclines and anticancer-targeted therapies. *Biochem. Res. Int.* 2012, 1–12.

Monti, E., Prosperi, E., Supino, R., Bottiroli, G., 1995. Free radical-dependent DNA lesions are involved in the delayed cardiotoxicity induced by adriamycin in the rat. *Anticancer Res.* 15, 193–197.

Mosmann, T., 1983. Rapid colorimetric assay for cellular growth and survival: application to proliferation and cytotoxicity assays. *J. Immunol. Methods* 65, 55–63.

Mross, B.K., Maessen, P., Vijgh, W.J.F. Van Der, Gall, H., Boven, E., Pinedo, H.M., Erba, C., 1988. Pharmacokinetics and metabolism of Epidoxorubicin and Doxorubicin in humans. *J. Clin. Oncol.* 6, 517–526.

Mukherjee, S., Banerjee, S.K., Maulik, M., Dinda, A.K., Talwar, K.K., Maulik, S.K., 2003. Protection against acute adriamycin-induced cardiotoxicity by garlic: Role of endogenous antioxidants and inhibition of TNF-α expression. *BMC Pharmacol.* 3, 1–9.

Muller, C., Chatelut, E., Gualano, V., Forni, M., Huguet, F., Attal, M., Canal, P., Laurent, G., 1993. Cellular pharmacokinetics of doxorubicin in patients with chronic lymphocytic leukemia: comparison of bolus administration and continuous infusion. *Cancer Chemother. Pharmacol.* 32, 379–384.

Murray, D.R., Freeman, G.L., 1996. Tumor necrosis factor-α induces a biphasic effect on myocardial contractility in conscious dogs. *Circ. Res.* 78, 154–160.

Myers, C., Bonow, R., Palmeri, S., Jenkins, J., Corden, B., Locker, G., Doroshow, J., Epstein, S., 1983. A randomized controlled trial assessing the prevention of doxorubicin cardiomyopathy by N-acetylcysteine. *Semin. Oncol*. 10, 53—55.

Myers, C.E., McGuire, W.P., Liss, R.H., Ifrim, I., Grotzinger, K., Young, R.C., 1977. Adriamycin: the role of lipid peroxidation in cardiac toxicity and tumor response. *Science* 197, 165–167.

Nagoshi, T., Matsui, T., Aoyama, T., Leri, A., Anversa, P., Li, L., Ogawa, W., Monte, F., Gwathmey, J.K., Grazette, L., Hemmings, B., Kass, D.A., Champion, H.C., Rosenzweig, A., 2005. PI3K rescues the detrimental effects of chronic Akt activation in the heart during ischemia/reperfusion injury. *J. Clin. Invest.* 115, 2128–2138.

Nakajima, K., Yamanaka, Y., Nakae, K., Kojima, H., Ichiba, M., Kiuchi, N., Kitaoka, T., Fukada, T., Hibi, M., Hirano, T., 1996. A central role for Stat3 in IL-6-induced regulation of growth and differentiation in M1 leukemia cells. *EMBO J*. 15, 3651–3658.

Nakamura, T., Ueda, Y., Juan, Y., Katsuda, S., Takahashi, H., Koh, E., 2000. Fas-mediated apoptosis in Adriamycin-induced cardiomyopathy in rats: in vivo study. *Circulation* 102, 572–578.

Negoro, S., Oh, H., Tone, E., Kunisada, K., Fujio, Y., Walsh, K., Kishimoto, T., Yamauchi-Takihara, K., 2001. Glycoprotein 130 regulates cardiac myocyte survival in Doxorubicin-induced apoptosis through phosphatidylinositol 3-kinase/Akt phosphorylation and Bcl-xL/Caspase-3 interaction. *Circulation* 103, 555–561.

Niedernhofer, L.J., Daniels, J.S., Rouzer, C. a, Greene, R.E., Marnett, L.J., 2003. Malondialdehyde, a product of lipid peroxidation, is mutagenic in human cells. *J. Biol. Chem.* 278, 31426–31433.

Nohl, H., Jordan, W., 1983. OH- generation by Adriamycin semiquinone and H2O2; an explanation for the cardiotoxicity of anthracycline antibiotics. *Biochem. Biophys. Res. Commun*. 114, 197–205.

Oeffinger, K.C., Mertens, A.C., Sklar, C.A., Kawashima, T., Hudson, M.M., Meadows, A.T., Friedman, D.L., Marina, N., Hobbie, W., Kadan-Lottick, N.S., 2006. Chronic health conditions in adult survivors of childhood cancer. *N. Engl. J. Med*. 355, 1572–1582.

Oliver, J.C., Bland, L.A., Oettinger, C.W., Arduino, M.J., McAllister, S.K., Aguero, S.M., Favero, M.S., 1993. Cytokine kinetics in an in vitro whole blood model following an endotoxin challenge. *Lymphokine Cytokine Res*. 12, 115—120.

Olson, H.M., Young, D.M., Prieur, D.J., LeRoy, A.F., Reagan, R.L., 1974. Electrolyte and morphologic alterations of myocardium in adriamycin-treated rabbits. *Am. J. Pathol*. 77, 439–454.

Olson, R.D., Boerth, R.C., Gerber, J.G., Nies, A.S., 1981. Mechanism of Adriamycin cardiotoxicity: evidence for oxidative stress. *Life Sci*. 29, 1393–1401.

Olson, R.D., Mushlin, P.S., 1990. Doxorubicin cardiotoxicity: analysis of prevailing hypotheses. *FASEB J.* 4, 3076–3086.

Ou, B., Hampsch-Woodill, M., Prior, R.L., 2001. Development and validation of an improved Oxygen Radical Absorbance Capacity assay using fluorescein as the fluorescent probe. *J. Agric. Food Chem*. 49, 4619–4626.

Ozes, O.N., Mayo, L.D., Gustin, J.A., Pfeffer, S.R., Pfeffer, L.M., Donner, D.B., 1999. NF-κB activation by tumour necrosis factor requires the Akt serine–threonine kinase. *Nature* 401, 82–85.

Paulson, M., 1999. Stat protein transactivation domains recruit p300/CBP through widely divergent sequences. *J. Biol. Chem*. 274, 25343–25349.

Pfeffer, K., 2003. Biological functions of tumor necrosis factor cytokines and their receptors. *Cytokine Growth Factor Rev*. 14, 185–191.

Pfeffer, L.M., Mullersman, J.E., Pfeffer, S.R., Murti, A., Shi, W., Yang, C.H., 1997. STAT3 as an adapter to couple phosphatidylinositol 3-kinase to the IFNAR1 chain of the type I interferon receptor. *Science* (80-. ). 276, 1418—1420. doi:10.1126/science.276.5317.1418

Phillips, D.R., White, R.J., Cullinane, C., 1989. DNA sequence-specific adducts of adriamycin and mitomycin C. *FEBS Lett*. 246, 233–240.

Podewski, E.K., 2003. Alterations in janus kinase (JAK)-signal transducers and activators of transcription (STAT) signaling in patients with end-stage dilated cardiomyopathy. *Circulation* 107, 798–802.

Rautenbach, F., Faber, M., Laurie, S., Laurie, R., 2010. Antioxidant capacity and antioxidant content in roots of 4 sweetpotato varieties. *J. Food Sci.* 75, C400–C405.

Rawlings, J.S., Rosler, K.M., Harrison, D. a, 2004. The JAK/STAT signaling pathway. *J. Cell Sci.* 117, 1281–1283.

Rébé, C., Végran, F., Berger, H., Ghiringhelli, F., Georges, C., Leclerc, F., Médecine, F. De, Bourgogne, U. De, 2013. STAT3 activation. A key factor in tumor immunoescape. *JAK-STAT 2*, 1–10.

Reil, J.-C., Gilles, S., Zahler, S., Brandl, A., Drexler, H., Hültner, L., Matrisian, L.M., Welsch, U., Becker, B.F., 2007. Insights from knock-out models concerning postischemic release of TNFalpha from isolated mouse hearts. *J. Mol. Cell. Cardiol.* 42, 133–141.

Richter, C., Messerschmidt, S., Holeiter, G., Tepperink, J., Osswald, S., Zappe, A., Branschädel, M., Boschert, V., Mann, D. a, Scheurich, P., Krippner-Heidenreich, A., 2012. The tumor necrosis factor receptor stalk regions define responsiveness to soluble versus membrane-bound ligand. *Mol. Cell. Biol.* 32, 2515–2529.

Ross, W.E., Glaubiger, D.L., Kohn, K.W., 1978. Protein-associated DNA breaks in cells treated with adriamycin or ellipticine. *Biochim. Biophys. Acta (BBA)-Nucleic Acids Protein Synth.* 519, 23–30.

Sack, M.N., Smith, R.M., Opie, L.H., 2000. Tumor necrosis factor in myocardial hypertrophy and ischaemia — an anti-apoptotic perspective. *Cardiovasc. Res.* 45, 688–695.

Safrit, J.T., Bonavida, B., 1992. Sensitivity of resistant human tumor cell lines to tumor necrosis factor and adriamycin used in combination: correlation between down-regulation of tumor necrosis factor-messenger RNA induction and overcoming resistance. *Cancer Res.* 52, 6630–6637.

Sawyer, D.B., Fukazawa, R., Arstall, M. a., Kelly, R. a., 1999. Daunorubicin-induced apoptosis in rat cardiac myocytes is inhibited by Dexrazoxane. *Circ. Res.* 84, 257–265.

Schlame, M., Rua, D., Greenberg, M.L., 2000. The biosynthesis and functional role of cardiolipin 39, 257–288.

Schulz, R., Heusch, G., 2009. Tumor necrosis factor-alpha and its receptors 1 and 2: Yin and Yang in myocardial infarction? *Circulation* 119, 1355–1357.

Seta, Y., Shan, K., Bozkurt, B., Oral, H., Mann, D.L., 1996. Basic mechanisms in heart failure: the cytokine hypothesis. *J. Card. Fail.* 2, 243–249.

Shan, K., Lincoff, M., Young, J.B., 1996. Anthracycline-Induced cardiotoxicity. *Ann. Intern. Med.* 125, 47–58.

Siegel, R., Ma, J., Zou, Z., Jemal, A., 2014. Cancer Statistics 2014. *Cancer J. Clin.* 64, 9–29.

Sies, H., Packer, L., 2004. Quinones and Quinone Enzymes, Part 1, 378th ed. Elsevier Inc.

Simmons, T., Jamall, S., 1989. Relative importance of intracellular glutathione peroxidase and catalase in vivo for prevention of peroxidation to the heart. *Cardiovasc. Res*. 23, 774–779.

Šimùnek, T., Štěrba, M., Popelová, O., Adamcová, M., Hrdina, R., Geršl, V., 2009. Anthracycline-induced cardiotoxicity : Overview of studies examining the roles of oxidative stress and free cellular iron. *Pharmacol Rep* 61, 154–171.

Singal, P.K., Iliskovic, N., 1998. Doxorubicin-induced cardiomyopathy. *N. Engl. J. Med*. 339, 900–905.

Singal, P.K., Iliskovic, N., Li, T., Kumar, D., 1997. Adriamycin cardiomyopathy: pathophysiology and prevention. *FASEB J*. 11, 931–936.

Singal, P.K., Panagia, V., 1984. Direct effects of adriamycin on the rat heart sarcolemma. *Res. Commun. Chem. Pathol. Pharmacol*. 43, 67—77.

Singal, P.K., Pierce, G.N., 1986. Adriamycin stimulates low-affinity Ca2+ binding and lipid peroxidation but depresses myocardial function. *Am. J. Physiol*. 250, H419–425.

Sinha, B.K., 1989. Free radicals in anticancer drug pharmacology. *Chem. Biol. Interact*. 69, 293–317.

Siveski-Iliskovic, N., Kaul, N., Singal, P.K., 1994. Probucol promotes endogenous antioxidants and provides protection against adriamycin-induced cardiomyopathy in rats. *Circulation* 89, 2829–2835.

Somers, S.J., Frias, M., Lacerda, L., Opie, L.H., Lecour, S., 2012. Interplay between SAFE and RISK pathways in sphingosine-1-phosphate-induced cardioprotection. *Cardiovasc. Drugs Ther*. 26, 227–237.

Štěrba, M., Popelová, O., Lenčo, J., Fučíková, A., Brčáková, E., Mazurová, Y., Jirkovský, E., Šimůnek, T., Adamcová, M., Mičuda, S., 2011. Proteomic insights into chronic anthracycline cardiotoxicity. *J. Mol. Cell. Cardiol*. 50, 849–862.

Sugamori, T., Ishibashi, Y., Shimada, T., Takahashi, N., Sakane, T., Ohata, S., Kunizawa, Y., Inoue, S., Nakamura, K., Ohta, Y., Shimizu, H., Katoh, H., Oyake, N., Murakami, Y., Hashimoto, M., 2002. Increased nitric oxide in proportion to the severity of heart failure in patients with dilated cardiomyopathy: close correlation of tumor necrosis factor-alpha with systemic and local production of nitric oxide. *Circ. J*. 66, 627–632.

Sugden, P.H., Clerk, A., 1998. "Stress-Responsive" Mitogen-Activated Protein Kinases (c-Jun N-Terminal Kinases and p38 Mitogen-Activated Protein Kinases) in the Myocardium. *Circ. Res*. 83, 345–352.

Sugimoto, K., Tamayose, K., Sasaki, M., Hayashi, K., Oshimi, K., 2002. Low-dose doxorubicin-induced necrosis in Jurkat cells and its acceleration and conversion to apoptosis by antioxidants. *Br. J. Haematol*. 118, 229–238.

Suleman, N., Somers, S., Smith, R., Opie, L.H., Lecour, S.C., 2008. Dual activation of STAT-3 and Akt is required during the trigger phase of ischaemic preconditioning. *Cardiovasc. Res*. 79, 127–133.

Swain, S.M., Whaley, F.S., Ewer, M.S., 2003. Congestive heart failure in patients treated with doxorubicin: a retrospective analysis of three trials. *Cancer* 97, 2869–2879.

Swain, S.M., Whaley, F.S., Gerber, M.C., Weisberg, S., York, M., Spicer, D., Jones, S.E., Wadler, S., Desai, A., Vogel, C., Speyer, J., Mittelman, A., Reddy, S., Pendergrass, K., Velez-Garcia, E., Ewer, M.S., Bianchine, J.R., Gams, R.A., 1997. Cardioprotection with dexrazoxane for doxorubicin-containing therapy in advanced breast cancer. *J. Clin. Oncol*. 15 , 1318–1332.

Swift, L.P., Rephaeli, A., Nudelman, A., Phillips, D.R., Cutts, S.M., 2006. Doxorubicin-DNA adducts induce a non-topoisomerase II–mediated form of cell death. *Cancer Res*. 66, 4863–4871.

Takemura, G., Fujiwara, H., 2007. Doxorubicin-induced cardiomyopathy. From the cardiotoxic mechanisms to management. *Prog. Cardiovasc. Dis*. 49, 330–352.

Tang, D., Wu, D., Hirao, A., Lahti, J.M., Liu, L., Mazza, B., Kidd, V.J., Mak, T.W., Ingram, A.J., 2002. ERK activation mediates cell cycle arrest and apoptosis after DNA damage independently of p53. *J. Biol. Chem*. 277, 12710–12717.

Taniyama, Y., Walsh, K., 2002. Elevated myocardial Akt signaling ameliorates doxorubicin-induced congestive heart failure and promotes heart growth. *J. Mol. Cell. Cardiol*. 34, 1241–1247.

Tartaglia, L., Goeddel, D. V, 1992. Two TNF receptors. *Immunol. Today* 13, 151–153.

Thomas, X., Le, Q.H., Fiere, D., 2002. Anthracycline-related toxicity requiring cardiac transplantation in long-term disease-free survivors with acute promyelocytic leukemia. *Ann. Hematol*. 81, 504–507.

Tolosa, L., Morlá, M., Iglesias, A., Busquets, X., Lladó, J., Olmos, G., 2005. IFN-γ prevents TNF-α-induced apoptosis in C2C12 myotubes through down-regulation of TNF-R2 and increased NF-κB activity. *Cell. Signal*. 17, 1333–1342.

Torre-Amione, G., Kapadia, S., Lee, J., Durand, J.B., Bies, R.D., Young, J.B., Mann, D.L., 1996. Tumor necrosis factor-alpha and tumor necrosis factor receptors in the failing human heart. *Circulation* 93, 704–711.

Torti, F.M., Bristow, M.L.R., Howes, A.E., Aston, D., Stockdale, F.E., Carter, S.K., Kohler, M., Brown, B.W., Billingham, M.E., 1983. Reduced cardiotoxicity of Doxorubicin delivered on a weekly schedule. *Ann. Intern. Med*. 99, 745–749.

Tracey, K.J., Vlassara, H., Cerami, A., 1989. Cachectin/tumour necrosis factor. *Lancet* 1, 1122–1126.

Ubezio, P., Civoli, F., 1994. Flow cytometric detection of hydrogen peroxide production induced by doxorubicin in cancer cells. *Free Radic. Biol. Med.* 16, 509–516.

Ueno, M., Kakinuma, Y., Yuhki, K., Murakoshi, N., Iemitsu, M., Miyauchi, T., Yamaguchi, I., 2006. Doxorubicin induces apoptosis by activation of caspase-3 in cultured cardiomyocytes in vitro and rat cardiac ventricles in vivo. *J. Pharmacol. Sci*. 101, 151–158.

Unverferth, B.J., Magorien, R.D., Balcerzak, S.P., Leier, C. V, Unverferth, D. V, 1983. Early changes in human myocardial nuclei after doxorubicin. *Cancer* 52, 215–221.

Valko, M., Leibfritz, D., Moncol, J., Cronin, M.T.D., Mazur, M., Telser, J., 2007. Free radicals and antioxidants in normal physiological functions and human disease. *Int. J. Biochem. Cell Biol.* 39, 44–84.

Van Dalen, E., Caron, H., Dickinson, H., Kremer, L., 2011. Cardioprotective interventions for cancer patients receiving anthracyclines. *Cochrane Collab*. 1–74.

Vandenabeele, P., Declercq, W., Beyaert, R., Fiers, W., 1995. Two tumour necrosis factor receptors: structure and function. *Trends Cell Biol*. 5, 392–399.

Vander Heide, R.S., L'Ecuyer, T.J., 2007. Molecular basis of anthracycline- induced cardiotoxicity. *Hear. Metab* 35, 1–4.

Von Hoff, D.D., Layard, M.W., Basa, P., Davis, H.L., Von Hoff, A.L., Rozencweig, M., Muggia, F.M., 1979. Risk factors for Doxorubicin-induced congestive heart failure. *Ann. Intern. Med*. 91, 710–717.

Vorobiof, D., Sitas, F., Vorobiof, G., 2001. Breast cancer incidence in South Africa. *J. Clin. Oncol*. 19, 125S–127S.

Wang, Y.-X., Korth, M., 1995. Effects of Doxorubicin on excitation-contraction coupling in Guinea Pig ventricular myocardium. *Circ. Res*. 76, 645–653.

Ware, C.F., 2003. The TNF Superfamily. *Cytokine Growth Factor Rev*. 14, 181–184.

Watanabe, N., Tsuji, N., Tsuji, Y., Sasaki, H., Okamoto, T., Akiyama, S., Kobayashi, D., Sato, T., Yamauchi, N., Niitsu, Y., 1996. Endogenous tumor necrosis factor inhibits the cytotoxicity of exogenous tumor necrosis factor and adriamycin in pancreatic carcinoma cells. *Pancreas* 13, 395–400.

Weinberg, L.E., Singal, P.K., 1987. Refractory heart failure and age-related differences in adriamycin-induced myocardial changes in rats. *Can. J. Physiol. Pharmacol*. 65, 1957–1965.

Weiss, R.B., 1992. The anthracyclines: will we ever find a better doxorubicin?, in: *Seminars in Oncology*. pp. 670–686.

Widmann, C., 1998. Caspase-dependent cleavage of signaling proteins during apoptosis. A turn-off mechanism for anti-apoptotic signals. *J. Biol. Chem*. 273, 7141–7147.

Wu, W., Lee, W.-L., Wu, Y.Y., Chen, D., Liu, T.-J., Jang, A., Sharma, P.M., Wang, P.H., 2000. Expression of Constitutively Active Phosphatidylinositol 3-Kinase Inhibits Activation of Caspase 3 and Apoptosis of Cardiac Muscle Cells. *J. Biol. Chem*. 275, 40113–40119.

Xiang, P., Deng, H.Y., Li, K., Huang, G.-Y., Chen, Y., Tu, L., Ng, P.C., Pong, N.H., Zhao, H., Zhang, L., 2009. Dexrazoxane protects against doxorubicin-induced cardiomyopathy: upregulation of Akt and Erk phosphorylation in a rat model. *Cancer Chemother. Pharmacol*. 63, 343–349.

Xu, Z., Lin, S., Wu, W., Tan, H., Wang, Z., Cheng, C., Lu, L., Zhang, X., 2008. Ghrelin prevents doxorubicin-induced cardiotoxicity through TNF-alpha/NF-κB pathways and mitochondrial protective mechanisms. *Toxicology* 247, 133–138.

Yang, F., Teves, S.S., Kemp, C.J., Henikoff, S., 2014. Doxorubicin, DNA torsion, and chromatin dynamics. *Biochim. Biophys. Acta* 1845, 84–89.

Yellon, D.M., Hausenloy, D.J., 2007. Myocardial reperfusion injury. *N. Engl. J. Med*. 357, 1121–1135.

Yen, H.C., Oberley, T.D., Vichitbandha, S., Ho, Y.S., St Clair, D.K., 1996. The protective role of manganese superoxide dismutase against adriamycin-induced acute cardiac toxicity in transgenic mice. *J. Clin. Invest*. 98, 1253–1260.

Yi, X., Bekeredjian, R., DeFilippis, N.J., Siddiquee, Z., Fernandez, E., Shohet, R. V, 2006. Transcriptional analysis of doxorubicin-induced cardiotoxicity. *Am. J. Physiol. Heart Circ. Physiol*. 290, H1098–H1102.

Yokoyama, T., Nakano, M., Bednarczyk, J.L., McIntyre, B.W., Entman, M., Mann, D.L., 1997. Tumor necrosis factor-α provokes a hypertrophic growth response in adult cardiac myocytes. *Circulation* 95, 1247–1252.

Zanwar, A.A., Hegde, M. V, Bodhankar, S.L., 2013. Protective role of concomitant administration of flax lignan concentrate and omega-3-fatty acid on myocardial damage in doxorubicin-induced cardiotoxicity. *Food Sci. Hum. Wellness* 2, 29–38.

Zhang, Y., Li, L., Xiang, C., Ma, Z., Ma, T., Zhu, S., 2013. Protective effect of melatonin against Adriamycin-induced cardiotoxicity. *Exp. Ther. Med*. 5, 1496–1500.

Zhang, Y.-W., Shi, J., Li, Y.-J., Wei, L., 2009. Cardiomyocyte death in doxorubicin-induced cardiotoxicity. *Arch. Immunol. Ther. Exp*. (Warsz). 57, 435–445.

Zhang, Z., Oliver, P., Lancaster, J.R., Schwarzenberger, P.O., Joshi, M.S., Cork, J., Kolls, J.K., 2001. Reactive oxygen species mediate tumor necrosis factor alpha-converting, enzyme-dependent ectodomain shedding induced by phorbol myristate acetate. *FASEB J*. 15, 303–305.

Zhao, Y., You, H., Yang, Y., Wei, L., Zhang, X., Yao, L., Fan, D., Yu, Q., 2004. Distinctive regulation and function of PI 3K/Akt and MAPKs in doxorubicin-induced apoptosis of human lung adenocarcinoma cells. *J. Cell. Biochem*. 91, 621–632.

Zhao, Z.-Q., 2004. Oxidative stress-elicited myocardial apoptosis during reperfusion. *Curr. Opin. Pharmacol*. 4, 159–165.

Zhao, Z.-Q., Corvera, J.S., Halkos, M.E., Kerendi, F., Wang, N.-P., Guyton, R. a, Vinten-Johansen, J., 2003. Inhibition of myocardial injury by ischemic postconditioning during reperfusion: comparison with ischemic preconditioning. *Am. J. Physiol. Heart Circ. Physiol*. 285, H579–5788.

Zhou, S., Palmeira, C.M., Wallace, K.B., 2001. Doxorubicin-induced persistent oxidative stress to cardiac myocytes. *Toxicol. Lett.* 121, 151–157.

Zhu, W., Zou, Y., Aikawa, R., Harada, K., Kudoh, S., Uozumi, H., Hayashi, D., Gu, Y., Yamazaki, T., Nagai, R., Yazaki, Y., Komuro, I., 1999. MAPK superfamily plays an important role in Daunomycin-induced apoptosis of cardiac myocytes. *Circulation* 100, 2100–2107.

Zimmermann, R., Flohe, L., Weser, U., Hartmann, H.-J., 1973. Inhibition of lipid peroxidation in isolated inner membrane of rat liver mitochondria by superoxide dismutase. *FEBS Lett*. 29, 117–120.

Zuppinger, C., Timolati, F., Suter, T.M., 2007. Pathophysiology and diagnosis of cancer drug induced cardiomyopathy. *Cardiovasc. Toxicol*. 7, 61–66.

Zweier, J.L., 1988. Measurement of superoxide-derived free radicals in the reperfused heart. *J. Biol. Chem*. 263, 1353–1357.

# APPENDICES

## Appendix A

## Supplementary Results

### TNFR2 protein expression (H9c2 cardiomyocytes)

Figures A1 - 3 depict the three independent experiments of TNFR2 protein expression using three different samples (n1, n2, n3). The same pattern was observed – protein expression was significantly down-regulated after 48 hours.

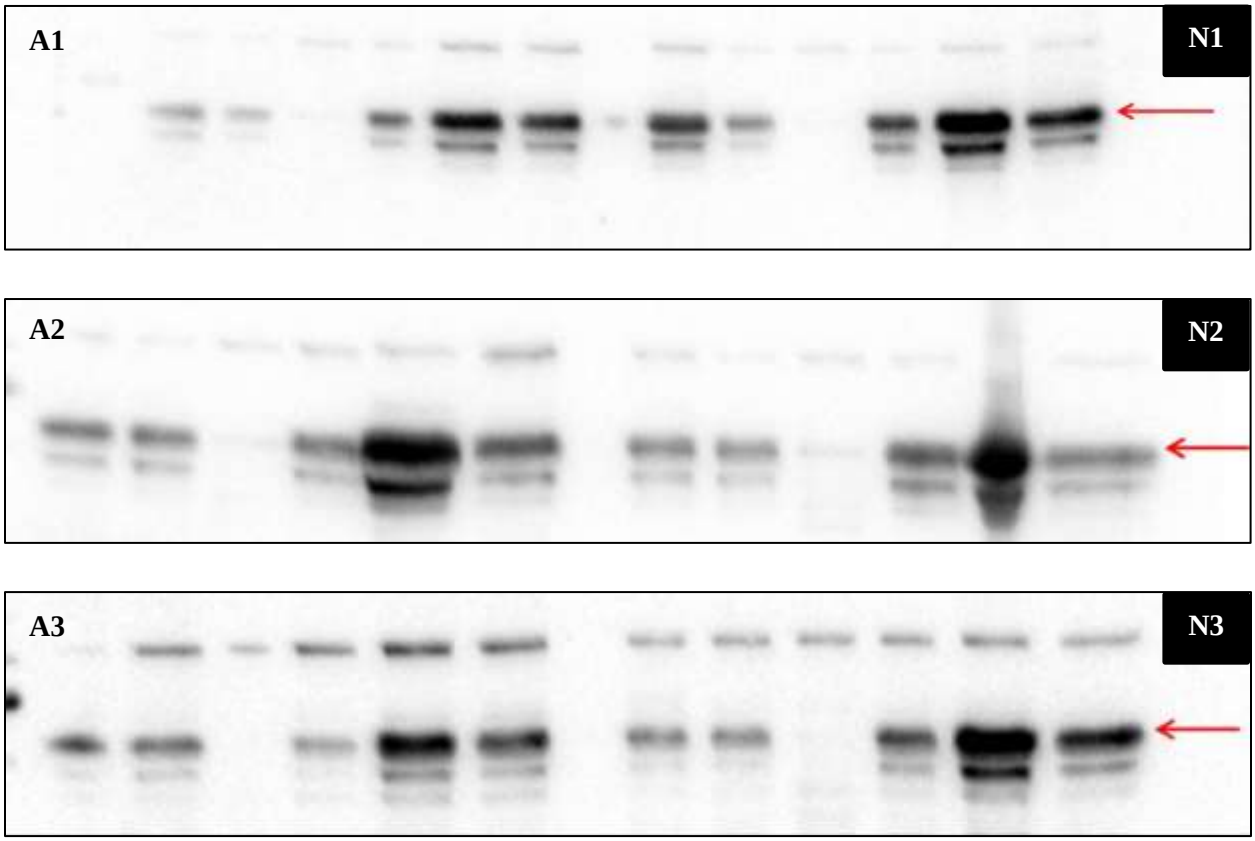


**Figure A1, 2 and 3:** Representative blots of each independent experiment to indicate the same phenomenon in TNFR2 expression after 48 hours of treatment in H9c2 cardiomyocytes.

## The SAFE pathway (Total Jak2 in differentiated C2C12 myotubes)

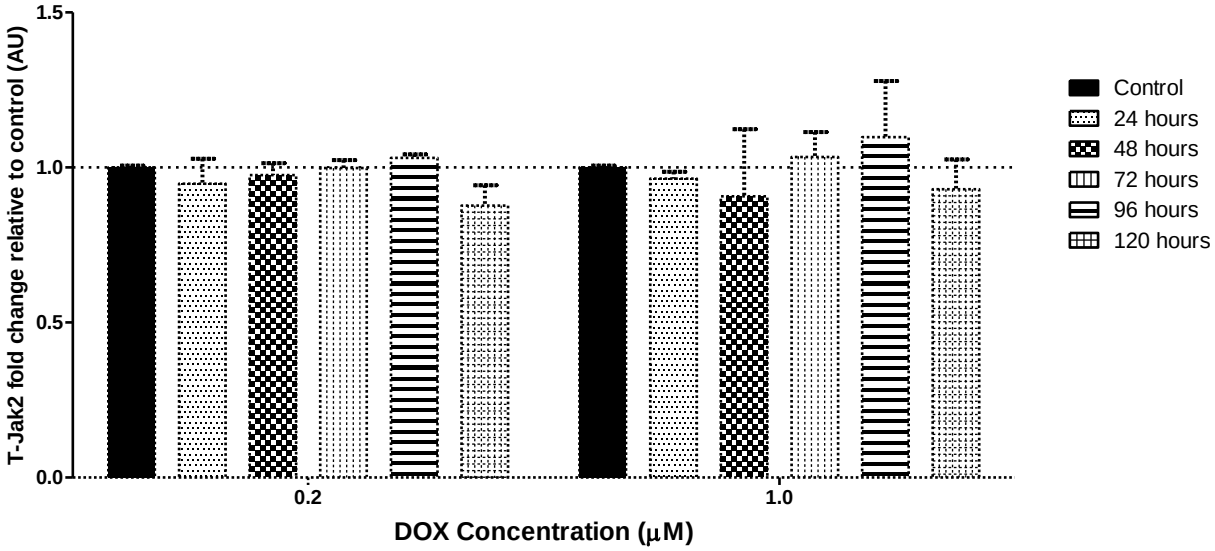


**Figure A4: Analysis of protein expression of T-Jak2 in differentiated C2C12 cells treated with DOX.** The lane profile analysis is presented. The fold change relative to the control was calculated. All values are presented as mean ± SEM, arbitrary units (AU), n = 3, *p< 0.05, **p< 0.01, ***p< 0.001. Ponceau was used to correct for loading discrepancies.

## The SAFE pathway (total-STAT3 in H9c2 cardiomyocytes)

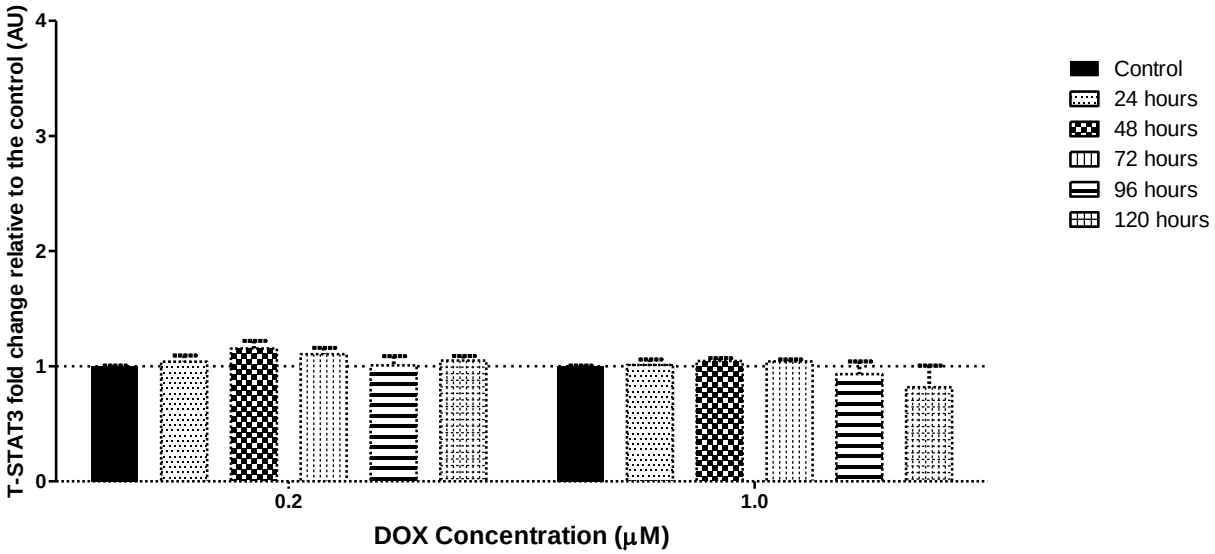


**Figure A5: The analysis of protein expression of total-STAT3 in H9c2 cells.** The lane profile analysis is represented. The fold change relative to the control was calculated. All values are presented as mean ± SEM, arbitrary units (AU), n = 3, *p< 0.05, **p< 0.01, ***p< 0.001. GAPDH was used to correct for any loading discrepancies.

## The SAFE pathway (total STAT3 in differentiated C2C12 myotubes)

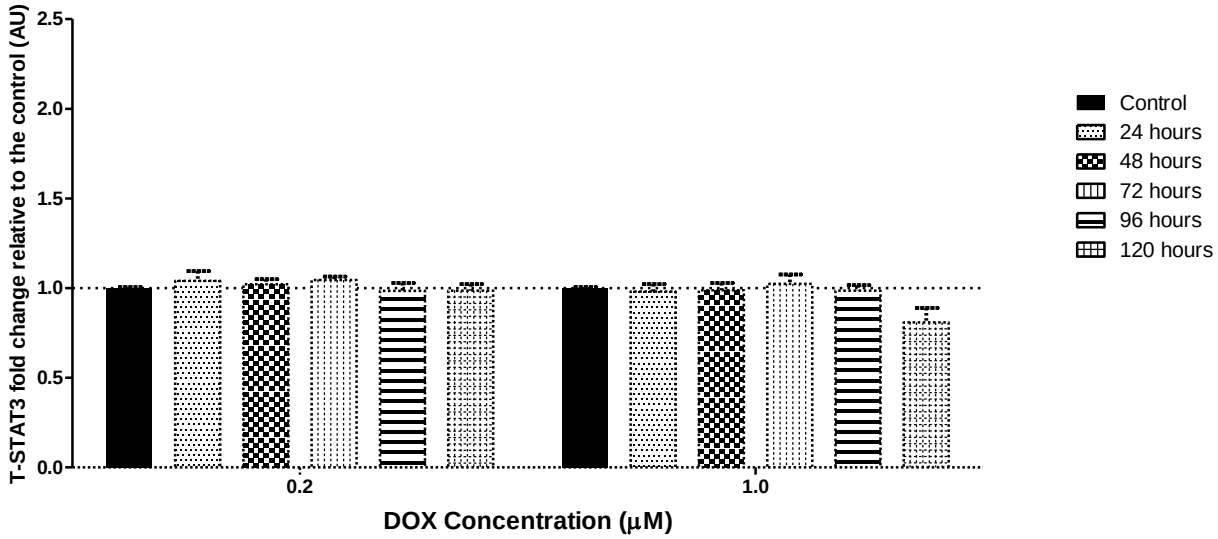


**Figure A6: Analysis of protein expression of T-STAT3 in differentiated C2C12 cells treated with DOX.** The lane profile analysis is represented. The fold change relative to the control was calculated. All values are presented as mean ± SEM, arbitrary units (AU), n = 3, *p< 0.05, **p< 0.01, ***p< 0.001. Ponceau was used as a loading control.

## The RISK pathway (total Akt expression in H9c2 cardiomyocytes)

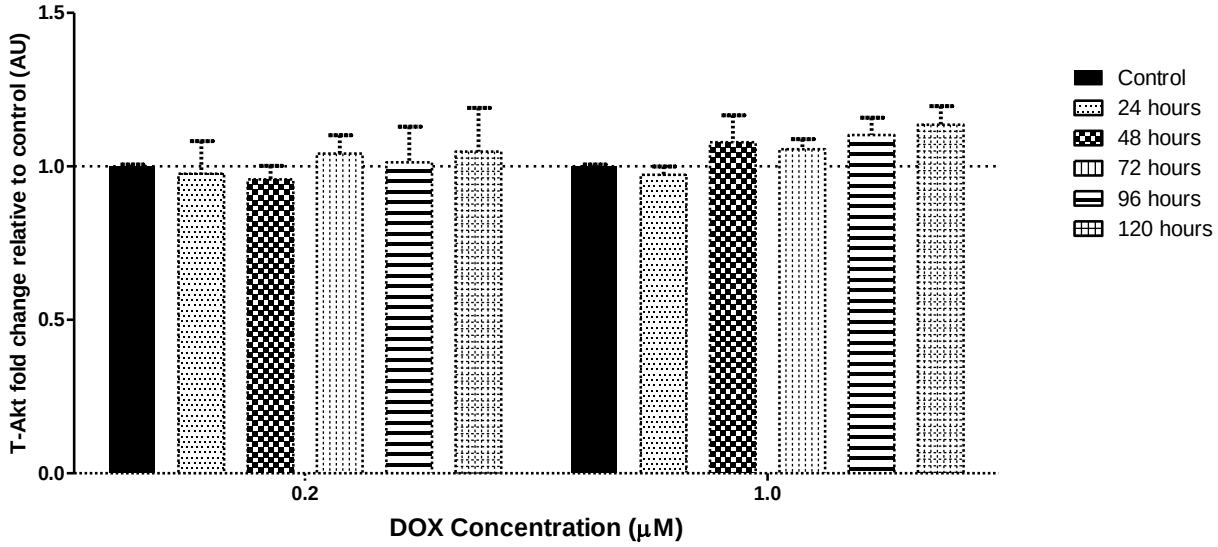


**Figure A7: Protein expression of T-Akt in H9c2 cells in response to treatment with DOX.** The lane profile analysis is presented. The fold change relative to the control was calculated. All values are presented as mean ± SEM, arbitrary units (AU), n = 3, *p< 0.05, **p< 0.01, ***p< 0.001. T-Akt, total-Akt. GAPDH was used to correct for any loading discrepancies.

## The RISK pathway (total Erk1/2 expression in H9c2 cardiomyocytes)

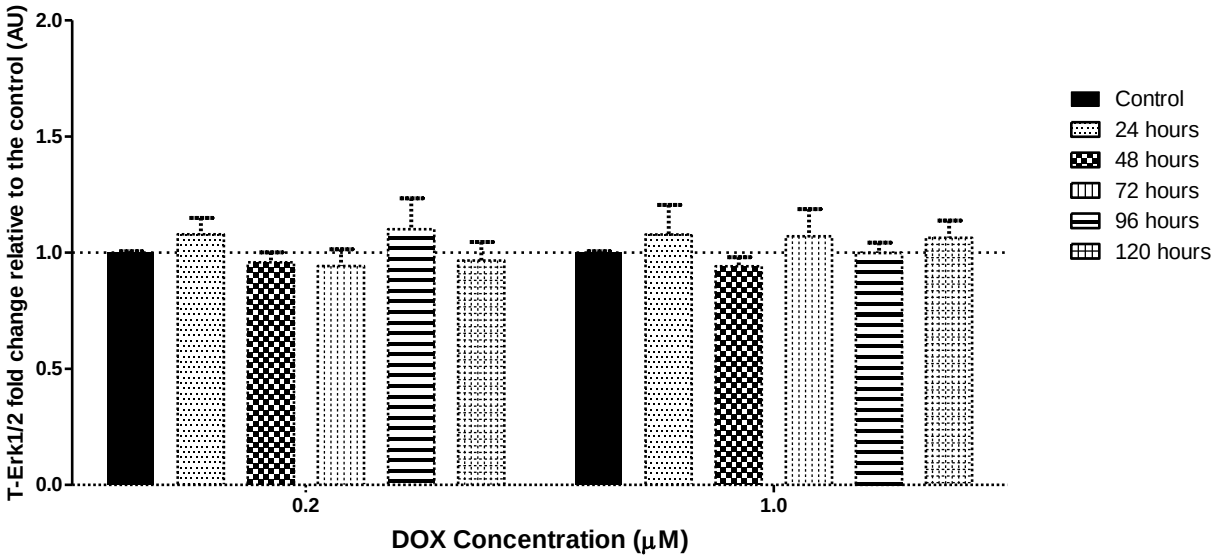


**Figure A8: Protein expression of T-Erk1/2 in H9c2 cells in response to treatment with DOX.** The lane profile analysis is presented. The fold change relative to the control was calculated. All values are presented as mean ± SEM, arbitrary units (AU), n = 3, *p< 0.05, **p< 0.01, ***p< 0.001. T-Erk1/2, total-Erk1/2. GAPDH was used to correct any loading discrepancies.

## The RISK pathway (total Erk1/2 expression in differentiated C2C12 myotubes)

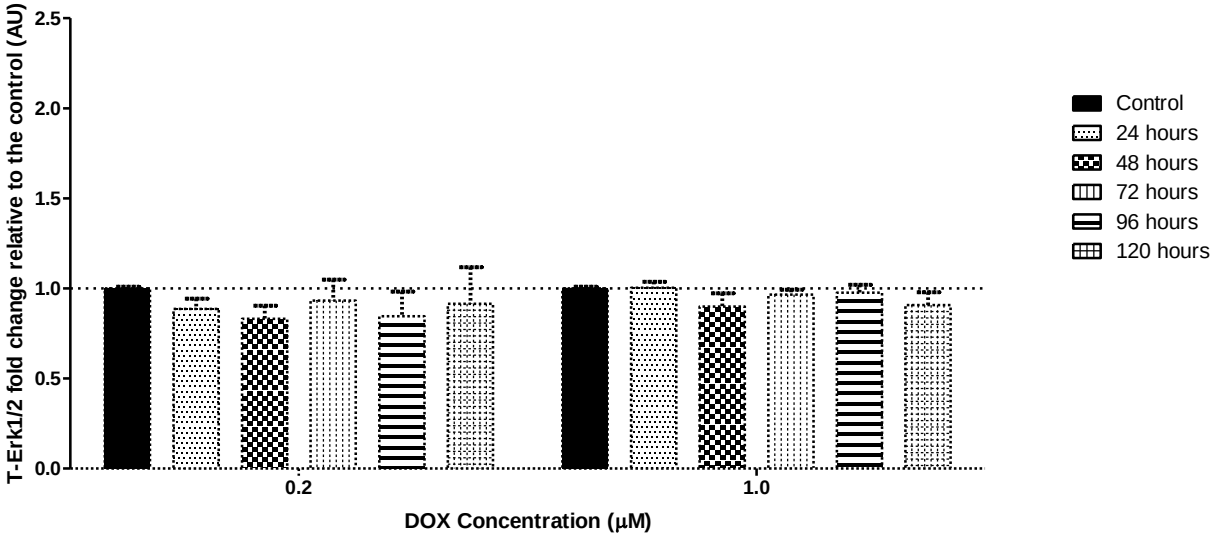


**Figure A9: Protein expression of T-Erk1/2 in C2C12 myotubes in response to treatment with DOX.** The lane profile analysis is presented. The fold change relative to the control was calculated. All values are presented as mean ± SEM, arbitrary units (AU), n = 3, *p< 0.05, **p< 0.01, ***p< 0.001. T-Erk1/2, total-Erk1/2. A Ponceau stain was used to correct any loading discrepancies.

**Ponceau images in their entirety from C2C12 western blots**

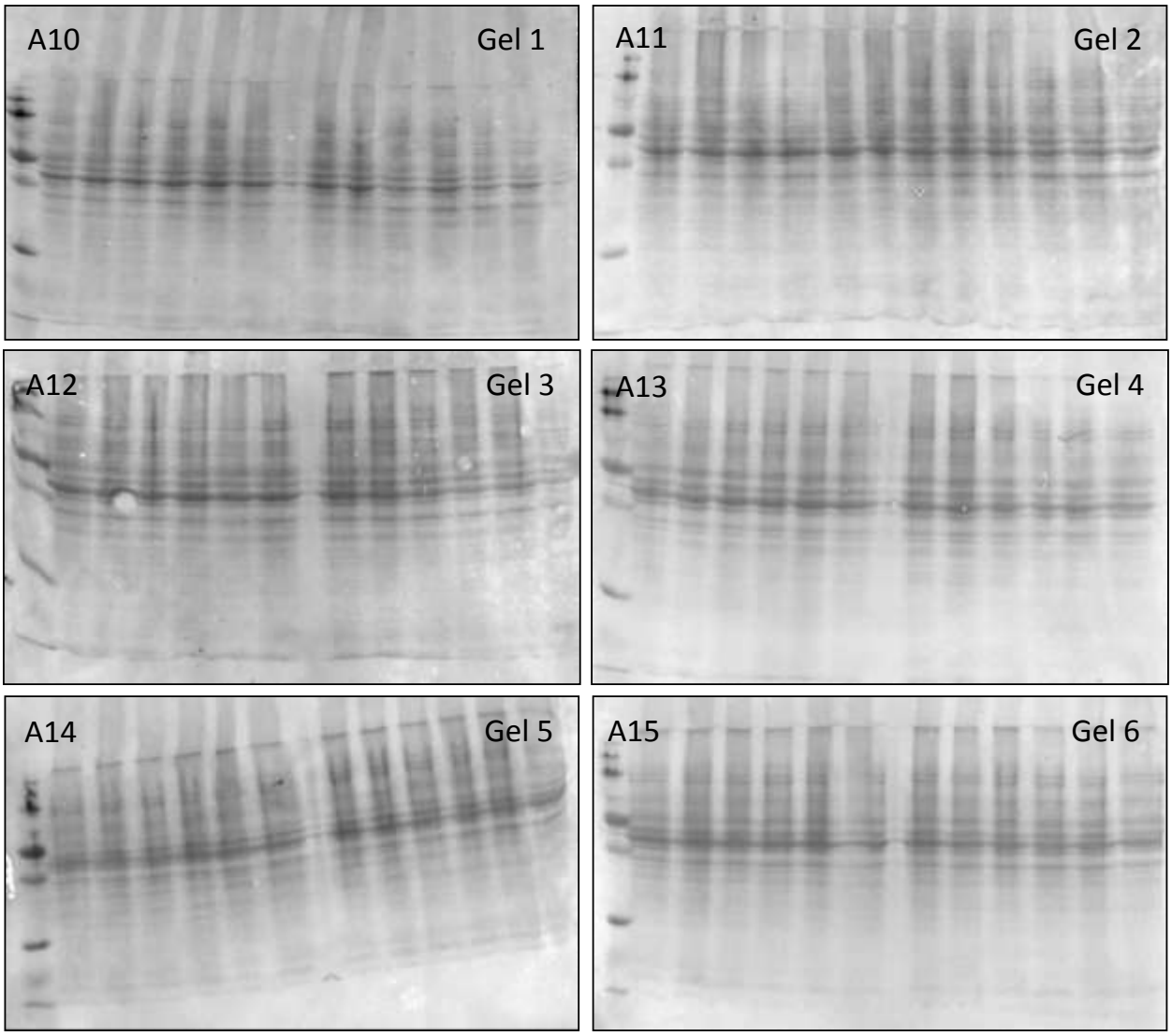

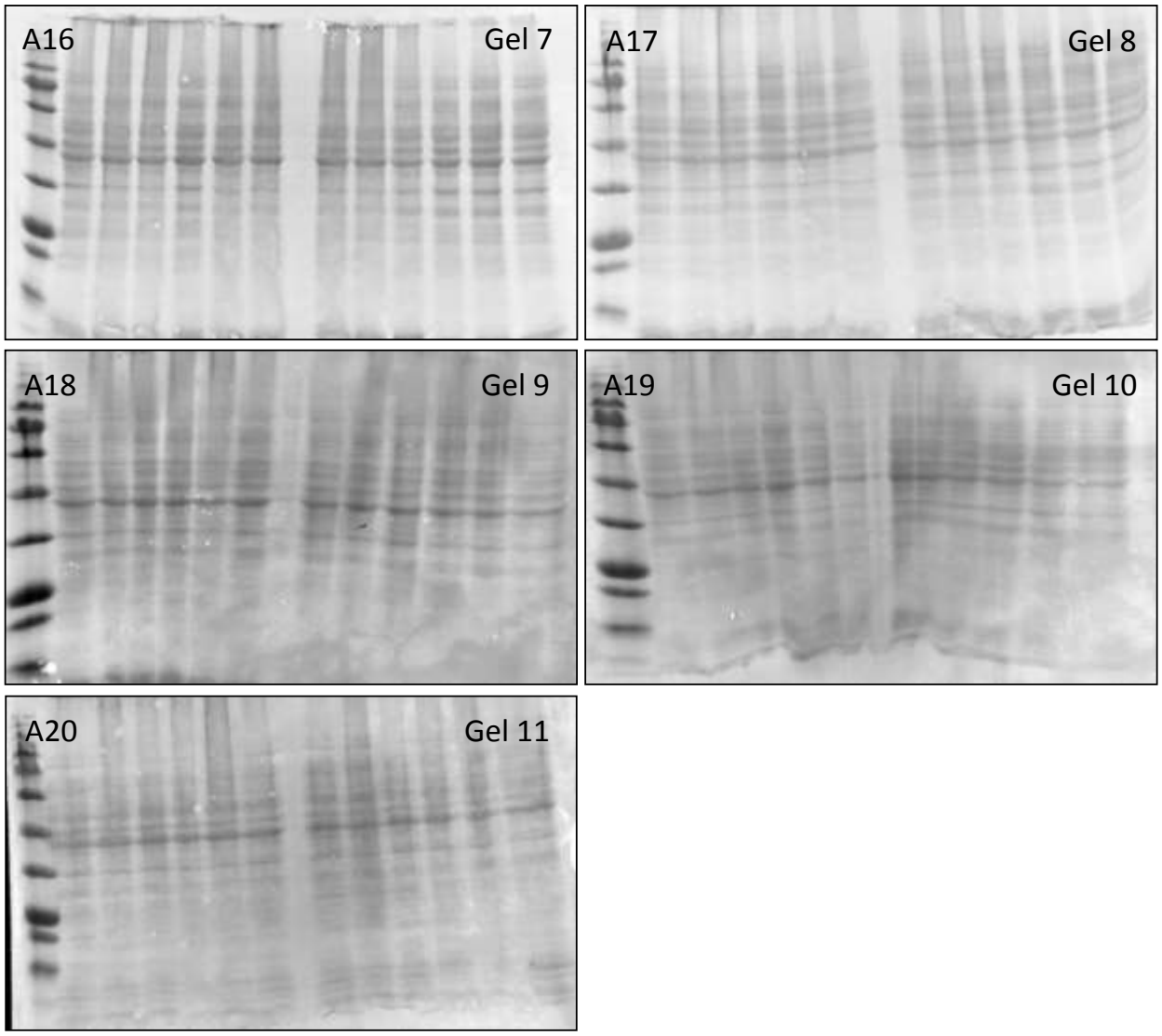


**Figures A10 – A20**: Ponceau stains of the membranes used in the western blotting of C2C12 myotubes.

# Appendix B

# Protocols

### Protocol 1: Cell culture

- Before starting cell culture, hands must be washed, gloved and washed again. Hands must be sprayed with 70% ethanol each time before putting them inside the laminar flow to ensure a sterile environment.
- Laminar flow hoods must be sprayed down with 70% ethanol, and all beakers, test tube racks, reagents and consumables must also be sprayed.

Cracking a vile:

- Remove a vile of cells from the liquid nitrogen tank and thaw at 37 °C.
- Add 6 mL growth medium into a T25 flask
- Transfer the contents of the cryovile into the T25 flask
- Grow cells at 37 °C and 5% CO2 until 70% confluent.

Maintaining cells:

- Remove flask of cells from the incubator and examine under a microscope for signs of infection.
- Sub-culture cells upon reaching 70 – 80% confluence or seed at appropriate densities for experiments.
- Discard old culture medium and gently wash cell monolayer with warm, sterile PBS to remove any remaining medium.
- Loosen cells from the surface of the flask using 4 mL of trypsin.
- Place the flask in a shaking incubator for 2-3 minutes at 37ºC. Check to see if cells have loosened under a microscope. If they have not loosened, tap the bottom of the flask gently to help the process
- Once all the cells are loosened, add warm growth medium (double the amount of trypsin) to neutralize the trypsin
- Transfer the cell/trypsin/medium mixture to a sterile 15 mL falcon tube and centrifuge at 1500 rpm for 3 minutes.

- Discard the supernatant and re-suspend the pellet in 4 mL of fresh medium.
- Count cells by pipetting 20 uL of the cell suspension into each chamber of a haemocytometer (protocol 2)
- Establish the total cell number using a simple calculation (below), where after the desired number of cells can be seeded into new culture flasks or plates, depending on the experiment.

**Protocol 2: Counting cells using a haemocytometer**

- Before use, the haemocytometer must wiped down with 70% ethanol
- Briefly breathe on the haemocytometer in order to create a moist surface for the cover slip to adhere to.
- Pipette 20 µl of the re-suspended cells into each chamber of the haemocytometer, under the cover slip. Be cautious to avoid air bubbles.
- Count the total number of cells by counting blocks 1 to 3 on both sides of the counting chamber (below). Calculate the average number of cells per block (cells/1 µL).
- Multiply the average by 10 000 to obtain the number of cells per milliliter of the original cell suspension

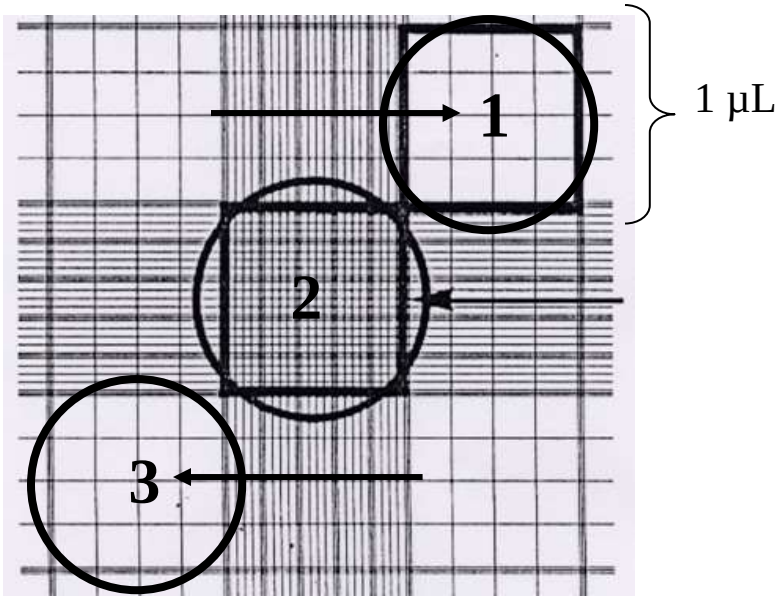


**Figure B1:** haemocytometer counting chamber. Adapted from: www.phe-culturecollections.org.uk

| Experiment | Culture Plate | Seeding density |
|---|---|---|
| MTT Assay | 24-well | 50 000/well |
| Caspase Glo | 96-well | 20 000 |
| LDH | 96-well | 20 000 |
| TBARS Assay | 6-well | 70 000 |
| ORAC Assay | 6-well | 70 000 |
| Western Blotting | 6-well | 100 000 |

Table indicating seeding densities and culture dish for each experiment

**Protocol 3: Cell Freezing**

- Use cells that are approximately 80% confluent
- Discard the old medium and rinse the cell monolayer with sterile PBS
- Discard PBS and add 4 mL trypsin (T75) – place into a shaking incubator for 3 minutes
- Add double the amount of warm medium (8 mL) and transfer the cell suspension to a falcon tube
- Centrifuge at 1500 rpm for 3 minutes
- Carefully discard the supernatant, leaving just the pellet.
- Re-suspend the pellet in FBS at a concentration of 1 – 2 million cells per mL.
- Make up freezing medium (1% DMSO in 1 mL FBS) and add the cells to a cryovile
- Store cryoviles in -80 °C overnight and transfer to liquid nitrogen the next day.

**Protocol 4: Cell Harvesting**

- Discard the old medium and rinse the cell monolayer three times with cold PBS
- Add 50 µl of RIPA buffer (appendix B) to each well of a 6-well plate, on ice.
- Swirl the plate/flask to ensure the whole surface is covered by the RIPA buffer
- Scrape the cells from the surface using a sterile cell scraper
- Transfer the cells to chilled Eppendorf tubes on ice
- The lysates can be stored at -80°C until needed, but no longer than 3 months.

**Protocol 5: MTT assay**

**Preparation of solutions**

1% Isopropanol = 1ml Concentrated HCL added to 99ml Isopropanol

0.1 % Triton = 0.1ml Triton-X-100 in 99 ml distilled water

Isopropanol/ Triton solution (50:1) = 50ml of 1% Isopropanol added to 1mL 0.1% Triton

0.01g MTT/1ml PBS made fresh before use – cover in foil to protect from light, then filter.

- Discard old medium
- Add 1.5ml PBS and 500µl MTT solution to each well.
- Cover the plate in foil and place in the incubator for 2 hours
- Discard the MTT and add 500 µL isopropanol/Triton solution to each well.
- Shake the plates on a belly dancer for 5 minutes to dissolve purple crystals.
- Read the plate at 595 nm.

**Protocol 6: Caspase Glo (Promega Caspase Glo ® 3/7 Assay)**

- Equilibrate the Caspase Glo® 3/7 buffer and substrate to room temperature before use
- Transfer the buffer into the bottle of substrate (brown) to form the caspase glo reagent.
- Mix until thoroughly dissolved, by inverting.
- Equilibrate the 96-well culture plates containing cells to room temperature
- Pipette 100 µL reagent into each well containing 100 µL sample
- Cover the plate with a lid and gently mix on a shaker at 300 – 500 rpm for 30 seconds
- Incubate at room temperature for 1 hour
- Measure the luminescence in a plate-reading luminometer.

**Protocol 7: LDH (Promega CytoTox 96® Non-Radioactive Cytotoxicity Assay)**

5 vials substrate mix

60 mL assay buffer

25 µL LDH Positive Control

5 mL lysis solution (10X)

65 mL Stop solution

- Equilibrate 12 ml of the assay buffer to room temperature

- Prepare an LDH positive control by diluting 2 µl of the Positive Control in 10 mL PBS and 1% BSA (1: 5000)
- Add 50 µl of the LDH positive control to 3 wells that contain no cells
- Add 5 µl lysis solution to each well containing 50 µl medium
- Incubate for 45 minutes in a shaker at 37 °C with 5% $CO_2$
- Add the 12 ml of assay buffer to the bottle of substrate mix (protect from light)
- Invert gently
- Add 50 µl of the substrate mix to each well, cover plate with foil and incubate at room temperature for 30 minutes
- Add 50 µl Stop solution to each well
- Pop any large bubbles with a needle
- Read the absorbance at 490 nm.

**Protocol 8: ELISA (R&D Systems Quantikine® rat and mouse TNF alpha ELISA kits)**

**Contents supplied in the kit (store unopened at 4 °C):**

2 x TNF-α antibody-coated 96-well plates

3 x vials of TNF-α standard

3 x vials of TNF-α control

1 x vial of TNF- α conjugate

1 x vial of assay diluent

2 x vials of calibrator diluent

2 x vials of wash buffer concentrate

1 x vial of colour reagent A

1 x vial of colour reagent B

1 x vial of Stop Solution

8 x plate sealers

**Contents to be supplied by user:**

Microplate reader capable of measuring absorbance at 450 nm (correction wavelength of 540 nm).

Polypropylene tubes for preparing standards and samples

**Sample collection, storage and preparation:**

Remove any particulates by centrifugation.

Assay immediately or store at -80 °C (avoid freeze-thaw cycles)

For the assay, dilute samples for the rat ELISA 3-fold in calibrator diluent (e.g. 50 µL sample in 150 µL diluent).

**Bring all reagents to room temperature before use**

**TNF-α Control:** reconstitute in 1 mL of distilled water.

**Wash buffer:** add 20 mL of wash buffer concentrate to 480 mL distilled water.

**Substrate solution:** Mix A and B together in equal volumes just before use. Protect from light.

***Rat TNF-α standard:** reconstitute in 2 mL calibrator diluent = 800 pg/mL. Allow it to sit for 5 minutes with gentle mixing.

****Mouse TNF-α standard:** reconstitute with 1 mL distilled water = 7000 pg/mL.

**Dilution of standards:** Use polypropylene tubes.

*Pipette 200 µL calibrator diluent into each tube, then perform the dilution series indicated below

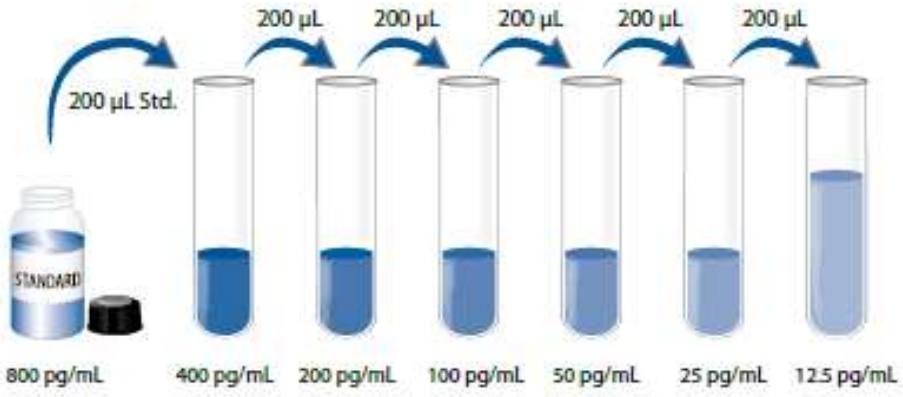


**Figure B2:**

**Rat TNF-α standards**

*The undiluted standard (800 pg/mL) serves as the high standard and the calibrator diluent serves as the zero standard.

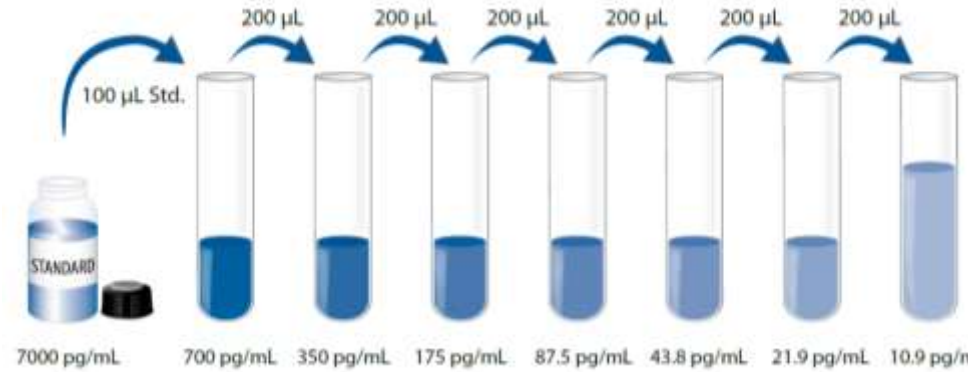


**Figure B3:**

**Mouse TNF-α standards**

**Pipette 900 µL calibrator diluent into the tube for the 700 pg/mL tube. Pipette 200 µL of calibrator diluent into the remaining tubes. Prepare the standards as indicated above. The 700 pg/mL serves as the high standard and the diluent serves as the zero standard.

**Procedure**

1. Prepare all reagents, standards, control and samples as described above
2. Remove a microplate from the foil pouch
3. Add 50 µL assay diluent to each well
4. Add 50 µL standard/control/sample in duplicate to each well. Mix by gentle tapping for 1 minute
5. Cover with an adhesive strip and incubate for 2 hours at room temperature
6. Aspirate each well and wash with wash buffer (400 µL). Repeat four times.
7. Add 100 µL TNF-α conjugate to each well.
8. Cover with a new strip and incubate for 2 hours at room temperature
9. Wash again as in step 6.
10. Add 100 µL substrate solution (A+B) to each well. Incubate for 30 minutes at room temperature (protect from light!)
11. Add 100 µL stop solution. Tap gently to ensure mixing.
12. Read plate at 450 nm with a correction wavelength of 540 nm.
13. Average the duplicate readings for each standard and sample and subtract the average zero optical density
14. Create a standard curve by plotting the mean absorbance for each standard against the concentration.
15. Multiply by the dilution factor.

**Protocol 9: ORAC (Oxygen Radical Antioxidant Capacity) Assay**

Black 96-well plate

**Note: do not use the first two columns and the last column of the plate – inaccurate read

Switch on the plate reader and the Fluoroskan program 30 minutes before read

- Grow and treat cells in 6-well plates.
- Wash cells 3 x with cold PBS
- Add 75 µL PBS to each well and scrape off cells using a cell scraper
- Lyse cells using sonication for 15 seconds
- Centrifuge for 10 minutes at 10 000 x g at 4 °C
- Store the supernatant for future use

**Phosphate buffer 75 mM, pH 7.4:**

Weigh 1.035g sodium di-hydrogen orthophosphate-1-hydrate in 100 mL dd$H_2O$ and mix until dissolved (solution 1).

Weigh 1.335g di-sodium hydrogen orthophosphate dehydrate (Merck #5822880EM) in 100 mL dd$H_2O$ and mix until dissolved (solution 2).

Mix 18 mL of 1$^{st}$ solution with 82 mL 2$^{nd}$ solution

Check pH – adjust with phosphate buffer

Store at 4 °C

**Fluorescein Stock: Sigma #F6377**

Dissolve 0.0225g in 50 mL phosphate buffer (above)

Store at 4 °C in a brown bottle (reused for 1 year)

**Fluorescein Working Solution:**

Take 10 µL of the stock and add it to 2 mL phosphate buffer (epi)

Then take 240 µL of this and dilute in 15 mL phosphate buffer (15 mL falcon)

**Peroxyl radical: Sigma #440914 25 mg/mL**

Weigh 150 mg of AAPH into a 15 mL falcon tube

Only add solute later on

**Trolox (standard): 250 µM stock Sigma # 238831**

Weigh 0.00312 g and add 50 mL phosphate buffer

Mix until dissolved

Should give an absorbance of 0.670 at 289nm

**Procedure:**

Spin down samples – they must not be turbid

Add 6 mL phosphate buffer to the AAPH weighed earlier, mix well.

Put in water bath at 37 °C

Label 6 epi's A – F

Prepare standards as follows:

| | Concentration (uM) | Trolox stock (uL) | Phosphate buffer (uL) | Well |
|---|---|---|---|---|
| A | 0 | 0 | 750 | A1-3 |
| B | 83 | 125 | 625 | A4-6 |
| C | 167 | 250 | 500 | A7-9 |
| D | 250 | 375 | 375 | A10-12 |
| E | 333 | 500 | 250 | B1-3 |
| F | 417 | 625 | 125 | B4-6 |

- Add 12 µL standards to each well
- Add 12 µL of controls per well
- Add 12 µL of samples per well in triplicate
- Add 138 µL of fluorescein working solution to each well using a multichannel
- Add 50 µL of the AAPH solution to each well using a multichannel (AT the plate reader)
- Put the plate into the plate reader
- Read for 2 hours

**Protocol 10: TBARS Assay (Thiobarbituric Acid Reactive Substances)**

- Grow and treat cells in 6-well plates
- Harvest cells in PBS
- Sonicate the cells on ice and store the whole homogenate for use in the assay

Set waterbath to 90/100 °C at 80% water capacity
Use 2 mL epi's and punch holes in their lids

- Put 50 µL of sample into an epi.
- Add 6.25 µL of BHT dissolved in 100% EtOH (to give a concentration of 4mM) to each sample
- Add 50 µL ortho-phosphoric acid (0.2M) to each sample
- Vortex
- Add 6.25 µL TBA reagent to each sample (concentration of 0.11M in 0.1M NaOH)
- Vortex
- Heat at 90 °C for 45 minutes (be strict with time and degrees for each repeat)
- Place samples on ice for 2 minutes (or until needed)
- Add 300 µL butanol to each sample
- Prepare saturated salt by adding NaCl to a tube of water until it no longer dissolves
- Add 50 µL of the saturated salt to each tube.
- Vortex and then centrifuge at 14 000 rpm for 2 minutes.
- Transfer the top phase of each sample to a clear, 96-well plate
- Read at $A_{532} - A_{572}$

**Protocol 11: Glutathione Assay (Antioxidant status)**

**Reagents:**

Buffer A (500 mM $Na_3PO_4$, 1mM EDTA, pH 7.5)

NADPH (1mM, 0.83 mg/mL) in buffer A (add 12 mL directly to vial)* NADPH, disodium salt, Cat nr. N6785 (10 vials) Sigma

M2VP (30 mM in 0.1 M HCL ) measures GSSG Cat nr. 69701 (100mg) Sigma

DTNB (0.3 mM (0.12 mg/mL) in buffer A) (Sigma, D21820)

Standard solution (GSH - 3 µM, Sigma, G4251) in buffer A

Glutathione reductase (16 µL in 984 µL buffer = 1 mL) x5 for one plate Cat nr. G3664 (500 Units) Sigma

**Procedure:**

Prepare standards as follows:

| | **Blank** | **1** | **2** | **3** | **4** | **5** |
|---|---|---|---|---|---|---|
| **GSH (µL)** | 0 | 167 | 333 | 500 | 667 | 833 |
| **Buffer A (µL)** | 1000 | 833 | 667 | 500 | 333 | 167 |

- Split sample into two epi's.
- Add 10 µL M2VP to the samples that will be used for measuring GSSG.
- Sonicate samples for 10 minutes and then centrifuge at 14 000 rpm for 2 minutes.
- Add 50 µL standards/samples (GSSG and GSH) to the wells of a 96-well plate
- Add 50 µL of the DTNB using a multichannel
- Add 50 µL of the glutathione reductase using a multichannel
- Mix briefly and incubate for 5 minutes at 25 °C in a preheated BioTek plate reader
- Add 50 µL NADPH to each well as quickly as possible (30 seconds max)
- Measure absorbance at 412 nm every 30 seconds for 3 minutes
- Use linear slope of the standards to calculate concentration of samples

*10 mg per vial

10 mg/x mL = 0.83 mg/1mL

X = 12 mL

**Protocol 12: Protein extraction from lysates**

- Work on ice at all times to prevent protein degradation
- Thaw lysates (protocol 4) and sonicate at amplitude of 15, for 10 - 15 seconds, in order to rupture cell membranes
- Rinse the tip of the sonicator between each sample.
- After sonication, centrifuge the lysates at 8000rpm for 10 minutes, at 4 °C.

**Protocol 13: Protein determination using the Bradford method**

- Protein determination is carried out on ice to ensure that proteins are not denatured
- Bradford reagent is prepared according to protocol in appendix B.
- Set up a standard curve as follows, using 2 mg/mL BSA:

| Standard | µL of BSA (2 mg/mL) | µL lysis buffer | Final Concentration (µg/mL) |
|---|---|---|---|
| #1 | 0 | 1000 | 0 (blank) |
| #2 | 125 | 875 | 5 |
| #3 | 250 | 750 | 10 |
| #4 | 375 | 625 | 15 |
| #5 | 500 | 500 | 20 |
| #6 | 625 | 375 | 25 |
| #7 | 750 | 250 | 30 |
| #8 | 1000 | 0 | 40 |

- Pipette 5 µL of each standard (1 – 8) and samples into the wells of a 96-well plate.
- Add 250 µL Bradford reagent to each well and read immediately at 595 nm.
- Enter values into an Excel sheet to produce a standard curve (see example below).

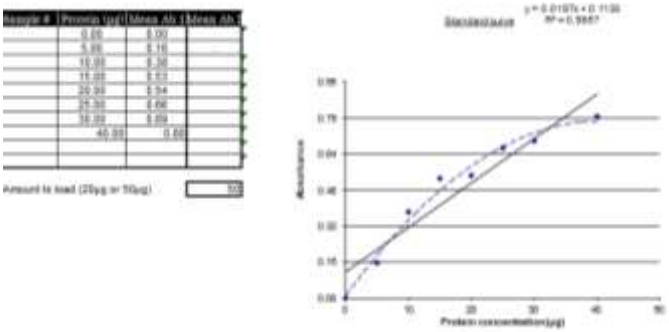

- The formulae will generate the concentration of protein in each sample
- Choose desired protein concentration (20 or 50 µg).
- Pipette the calculated volumes of each sample into new eppendorf tubes
- Add the Laemlli's loading buffer (appendix B)
- Pierce Eppendorf tubes with a teasing needle and boil at 95 °C for 5 minutes
- Samples can be stored at – 80 °C until needed

**Protocol 14: Western Blotting**

**Preparation of assembly and gels**

- Clean glass plates with 70% alcohol and place into casting frames
- Clean rubber with 70% alcohol to remove any debris
- Place the frames with rubber gaskets into casting stands and firmly clip into place.
- Check for leaks with distilled water, then discard water
- Make up the separating gel (% determined by size of proteins) (Appendix B)
- Using a Pasteur pipette, pour the separating gel between the glass plates, to the top of the green door - avoid making bubbles by pipetting into the corner of the plate
- Pour a layer of iso-butanol onto the gel to prevent oxidation and to ensure a straight line
- Allow the gel to set (+- 30 minutes)
- Wash off the iso-butanol using distilled water
- Prepare the 4% stacking gel (Appendix B)
- Using a Pasteur pipette, pour the stacking gel onto the top on the separating gel
- Immediately insert the appropriate comb (10- or 15-well)
- Allow to set for +-30 minutes.
- Denature samples by boiling at 95 °C for 5 minutes (punch a hole in the eppi).
- Centrifuge samples briefly.
- Carefully remove combs from the set gel.
- Place gels into the U-shaped adaptor.
- Place the apparatus into a tank and add running buffer (Appendix B) into the middle compartment until it overflows into the wells

**Loading samples**

- Pipette 10 µL BLUeye Prestained protein ladder into the first well of the gel
- Pipette samples in the rest of the wells using a new tip for each one.
- Once all samples are loaded, pour running buffer into the outer compartments
- Place a lid onto the tank and ensure the electrodes are correctly orientated – red to red and black to black
- Run samples for 10 minutes at 400mA and 100V (constant)
- Then run samples at 400 mA, 120V for about 50 minutes

**Membrane transfer**

- Open a "transfer pack" and place the blotting paper marked 'bottom' onto the cassette.
- Roll out any air bubbles
- Carefully place the gel on top of the membrane.
- Again roll out any bubbles
- Place the blotting paper marked 'top' on top of the gel
- Roll out any bubbles
- Put the lid back on and lock into place.
- Set the transfer for 7 – 12 minutes.
- Once the transfer is complete, put the membrane into blocking solution (Appendix B)

**Antibodies**

- Wash the membrane 3 x 3 minutes with TBS-T (Appendix B).
- Make up the primary antibody solution (Appendix B) in a 50 mL falcon tube and roll the membrane inside the tube
- Rotate in a 4 °C fridge overnight.
- Wash 3 x 3 minutes with TBS-T.
- Make up secondary antibody solution (Appdenix B) in a 50 mL falcon tube and roll the membrane inside the tube
- Leave on roller for 1 hour at room temperature

**Exposure**

- Wash membrane 3x 3 minutes with TBS-T

- Prepare a 1:1 solution of Pierce ECL substrate (must be room temperature)
- Evenly pipette the ECL over the membrane
- Expose in the ChemiDoc until desired bands appear.

**Stripping membranes**

- Wash membrane for 5 minutes in distilled water
- Wash for 5 minutes in NaOH
- Wash for 5 minutes in distilled water.

OR

- Wash membrane in stripping buffer for 2 x 5 minutes (Appendix C)
- Wash for 2 x 10 minutes in distilled water
- Block in milk solution

# Appendix C

# Reagent Preparation

**Protocol 1: Growth Medium**

500 mL DMEM

50 mL FBS (10%)

5 mL PenStrep (1%)

- All components must be thawed in the waterbath at 37 °C.
- Under sterile conditions, remove 55 mL of DMEM from the bottle.
- Add the FBS and PenStrep and invert to mix.
- Aliquot into 50 mL tubes and store at 4 °C.

**Protocol 2: Differentiation Medium**

500 mL DMEM

10 mL horse serum (2%)

5 mL PenStrep (1%)

- All components must be thawed in the waterbath at 37 °C.
- Under sterile conditions, remove 15 mL of DMEM from the bottle.
- Add the HS and PenStrep and invert to mix.
- Aliquot into 50 mL tubes and store at 4 °C.

**Protocol 3: Doxorubicin stock**

Doxorubicin Hydrochloride ($M_R$ = 579.98 g/mol) 3.4 mM

- Under sterile conditions, dissolve 10 mg Doxorubicin in exactly 5.071 mL medium.
- Vortex, filter-sterilize, protect from light and store in aliquots at -20 °C.

**Protocol 4: Phosphate Buffer Saline 1X (PBS)**

Dissolve the following in 1L of distilled water:

16 g NaCl

0.4 g KCl

2.88 g $Na_2HPO_4$

0.48 g $KH_2PO_4$

- Adjust the pH to 7.4
- Fill up to the 2L mark with distilled water
- Autoclave

**Protocol 5: 95% alcohol (1L)**

- Dilute 950 mL 100% ethanol in 50 mL distilled water

**Protocol 6: 70% alcohol (1L)**

- Dilute 700 mL 100% ethanol in 300 mL distilled water

**Protocol 7: RIPA Buffer (100 mL)**

- Prepare 50 mM Tris-HCl: add 790 mg Tris to 75 mL distilled water. Add 900 mg NaCl and stir. Adjust pH to 7.4 using HCl. Pour the prepared Tris-HCl into a 100 mL beaker.
- Add the following in the same order that they appear:

| | **Volume** | **Final Concentration** |
|---|---|---|
| **NP-40** | 10 mL | 1% |
| **Na-deoxycholate** | 2.5 mL | 0.25% |
| **EDTA** | 1 mL | 1 mM |
| **Phenylmethylsulponyl Fluoride (PMSF)** | 1 mL | 1 mM |
| **Leupeptin** | 1 µL | 1 µg/mL |
| **SBTI-1** | 80 µL | 4 µg/mL |
| **Benzamidine** | 100 µL | 1 mM |
| **$Na_3VO_4$** | 1 mL | 1 mM |
| **NaF** | 500 µL | 1 mM |

- Add 1000 µL Triton-X-1000 to the solution and fill up to the mL mark with distilled water.
- Mix thoroughly.
- Aliquot the RIPA into 1 mL Eppendorf tubes and store at -20 ° C.

**Protocol 8: Bovine serum albumin (BSA)**

- To prepare a 2 mg/mL stock of BSA, weigh off 20 mg and mix thoroughly in 10 mL distilled water.
- Freeze in aliquots of 1 mL.

**Protocol 9: Bradford Reagent**

- Weigh off 200 mg Coomassie Brilliant Blue G250 and add to 100 mL 95% EtOH (95 mL ETOH, 5 mL water)
- Mix on the magnetic stirrer
- Add 200 mL 85% O-phosphoric acid (170 mL O-phosphoric acid, 30 mL water)
- Put into a brown bottle
- Add 1.7L distilled water
- Filter until reddish-brown (+- 7 times)

**Protocol 10: Laemmli's Sample Buffer (stock)**

- 3.8 mL distilled water
- 1 mL 0.5M Tris-HCl, pH 6.8
- 0.8 mL glycerol
- 1.6 mL 10% (w/v) SDS
- 0.4 mL 0.05% (w/v) Bromophenol blue

Note: For use in western blotting, make a working solution by adding 150 µL $\beta$-mercaptoethanol to 850 µL Laemmli's stock solution.

**Protocol 11: 10% Sodium dodecyl sulphate (SDS)**

- Weigh out 50 g SDS and add 500 mL distilled water

**Protocol 12: 10X Running Buffer**

- Weigh off 60.6 g Tris
- Weigh off 288 g glycine
- Add to $\pm$ 1.5L distilled water
- Add 20 g SDS

- Adjust the pH to 8.6
- Fill up to the 2L mark with distilled water.

**Protocol 13: 10X TBS**

- Dissolve 24.2g Tris and 80g NaCl in 600 mL distilled water.
- Adjust pH to 7.6 with HCl
- Fill up to 1L mark with distilled water.

- For use in Western Blotting, make up 1X TBS-T by thoroughly mixing 100 mL TBS in 900 mL distilled water, with 1mL Tween

**Protocol 14: 10% Ammonium persulphate**

- Weigh out 0.1 g APS into an Eppendorf tube and add 1000 µL distilled water

**Protocol 15: Tris pH 8.8**

- Weigh out 68.1 g Tris (1.124M) and 1.5 g SDS (0.3%) and place into a beaker
- Add 400 mL distilled water, mix and then adjust pH to 8.8 using HCl
- Make the final volume up to 500 mL

**Protocol 16: Tris pH 6.8**

- Weigh out 30.3 g (0.5M) Tris and 2 g SDS (0.4%) and place into a beaker
- Add 400 mL distilled water, mix and adjust pH to 6.8 with HCl
- Make final volume up to 500 mL

**Protocol 17: Tris pH 6.7**

- Weigh out 6.057 g Tris (100 mM) and place in a beaker
- Add 400 mL distilled water, mix and adjust the pH to 6.7 using HCl
- Make final volume up to 500 mL

**Protocol 18: Acrylamide Resolving Gels (makes enough for 2 gels)**

| **Gel Constituent** | **6%** | **8%** | **10%** | **12%** | **15%** |
|---|---|---|---|---|---|
| **$dH_2O$** | 5.88 mL | 7.84 mL | 9.8 mL | 11.76 mL | 14.70 mL |
| **30% Acrylamide** | 3 mL | 4 mL | 5 mL | 6 mL | 7.5 mL |

| | | | | | |
|---|---|---|---|---|---|
| **1.5M Tris-HCl, pH 8.8** | 3 mL | 4 mL | 5 mL | 6 mL | 7.5 mL |
| **20% w/v SDS** | 60 µL | 80 µL | 100 µL | 120 µL | 150 µL |
| **10% w/v APS** | 60 µL | 80 µL | 100 µL | 120 µL | 150 µL |
| **TEMED (last!!)** | 24 µL | 32 µL | 40 µL | 48 µL | 60 µL |

**Protocol 19: 4% Acrylamide Stacking Gel (makes enough for 2 gels)**

| **Gel Constituent** | |
|---|---|
| **$dH_2O$** | 7.5 mL |
| **30% Acrylamide** | 1.5 mL |
| **0.5M Tris-HCl, pH 6.8** | 3 mL |
| **20% w/v SDS** | 60 µL |
| **10% w/v APS** | 80 µL |
| **TEMED (last!!)** | 40 µL |

**Protocol 20: Milk blocking solution**

- Weigh out 5 g fat-free instant milk powder and add 100 mL of TBS-T
- Mix well on a magnetic stirrer
- This is enough for one membrane

**Protocol 21: Primary (1°) Antibody**

- Pipette 5 µL of the primary antibody into a falcon tube containing 5 mL TBS-T.
- Prepare just before use

**Protocol 22: Secondary (2°) Antibody**

- Pipette 0.5 µL secondary antibody into a falcon tube containing 5 mL TBS-T.

**Protocol 23: Stripping Buffer**

- 7.5 g glycine
- 0.5 g SDS
- 5 mL Tween
- Dissolve in +- 300 mL distilled water
- Adjust pH to 2.2

- Fill up to the 500 mL mark with $dH_2O$

# Appendix D

## Reagents

| Reagents | Catalogue # | Company |
|---|---|---|
| 2-Propanol | UN1219 | Merck |
| 32% Hydrochloric acid | UN1789 | Merck |
| 2,2'-Azobis (2-methylpropionamidine) dihydrochloride (AAPH) | 440914 | Sigma-Aldrich |
| Absolute alcohol | 32221 | Riedel deHaën |
| Acrylamide | UN3426 | Merck |
| Acrylamide | A3699 | Sigma-Aldrich |
| Ammonium Persulphate (APS) | UN1444 | Merck |
| Antibiotic antimycotic (AA) | 15240-062 | Gibco |
| Bovine Serum Albumin | A4503 | Sigma-Aldrich |
| Bromophenol Blue | 32400A | UnivAR |
| Caspase Glo 3/7 | G8091 | Promega |
| Coomassie Brilliant Blue G | 27815 | Fluka |
| D-(+)-Glucose | G7021 | Sigma-Aldrich |
| Di-sodium hydrogen orthophosphate dehydrate | 5822880EM | Merck |
| Doxorubicin | D1515 | Sigma-Aldrich |
| DTNB | D21820 | Sigma-Aldrich |
| Dulbecco's Modified Eagles Medium (DMEM) | D5796 | Sigma-Aldrich |
| Fetal Bovine Serum | 10270-106 | Invitrogen Gibco |
| Fluorescein sodium salt | F6377 | Sigma-Aldrich |
| Glutathione standard | G4251 | Sigma-Aldrich |
| Glutathione reductase (GR) | G3664 | Sigma-Aldrich |
| Glycerol | G5516 | UnivAR |
| Glycine | G8898 | Sigma-Aldrich |
| Horse Serum | S9133 | Biochrom |
| Iso-butanol | UN1212 | Merck |
| LDH Cytoxicity Kit | G1780 | Promega |
| Malondialdehyde | 805797 | Merck |
| Methanol | UN1250 | Merck |

| | | |
|---|---|---|
| Mouse Quantikine TNF-$\alpha$ ELISA Kit | MTA00B | R&D Systems |
| MTT (Thiazolyl Blue Tetrazolium Bromide | M2128 | Sigma-Aldrich |
| M2VP | 69701 | Sigma-Aldrich |
| NADPH disodium salt | N6785 | Sigma-Aldrich |
| Ortho-phosphoric acid | UN1805 | Merck |
| PenStrep | 15140-122 | Invitrogen Gibco |
| Pierce® ECL Western Blotting Substrate | 32106 | Thermo Scientific |
| Ponceau S Solution | P7170 | Sigma-Aldrich |
| Rat Quantikine TNF $\alpha$ ELISA Kit | RTA00 | R&D Systems |
| Sodium Dodecyl Sulphate (SDS) | L3771 | Sigma-Aldrich |
| Thiobarbituric acid | T5500 | Sigma-Aldrich |
| TEMED | T9281 | Sigma-Aldrich |
| TNF-$\alpha$ | 400-14 | PeproTech Inc. |
| Trolox | 238831 | Sigma-Aldrich |
| Triton-X-100 | BB306324 | BDH |
| Trizma-Base | 93304 | Fluka |
| Trypsin EDTA | 25200-012 | Invitrogen Gibco |
| Tween®20 | P1379 | Sigma-Aldrich |
| $\beta$-Mercaptoethanol | M3148 | Sigma-Aldrich |

| **Antibody** | **Size** | **Species** | **Catalogue #** | **Company** |
|---|---|---|---|---|
| Cleaved caspase 3 | 17/19 | Rabbit | 9661S | Cell Signaling |
| Cleaved PARP | 89/25 | Rabbit | Ab32064 | Abcam |
| GAPDH | 37 | Rabbit | Ab37168 | Abcam |
| IgG, HRP-linked | | Anti-Rabbit | 7074S | Cell Signaling |
| LC3 | 14/16 | Rabbit | 4108S | Cell Signaling |
| P62 | 62 | Rabbit | Ab91526 | Abcam |
| P-Akt | 60 | Rabbit | 9271S | Cell Signaling |
| P-Erk | 42/44 | Rabbit | 4370S | Cell Signaling |
| P-Stat 705 | 79/86 | Rabbit | 9131S | Cell Signaling |
| P-Stat 727 | 86 | Rabbit | 9134S | Cell Signaling |

| | | | | |
|---|---|---|---|---|
| T-Akt | 60 | Rabbit | 9272S | Cell Signaling |
| T-Erk | 42/44 | Rabbit | 4695S | Cell Signalling |
| TNF-a | 17/25/28 | Rabbit | 11948S | Cell Signalling |
| TNFR1 | 55 | Mouse | SC-8436 | Santa Cruz |
| TNFR2 | 75 | Rabbit | 3727S | Cell Signalling |
| T-Stat3 | 79/86 | Mouse | 9139S | Cell Signalling |